



**Investigating the cellular and anti-cancer effects of REST and
HDAC inhibition in Daoy medulloblastoma cells**

Abdulelah Saleh Alshawli

Submitted in accordance with the requirements of
Doctor of Philosophy

The University of Leeds
Faculty of Biological Sciences
School of Biomedical Sciences

March 2019

The candidate confirms that the work submitted is his own and that appropriate credit has been given where reference has been made to the work of others.

This copy has been supplied on the understanding that it is copyright material and that no quotation from the thesis may be published without proper acknowledgement.

The right of Abdulelah Saleh Alshawli to be identified as Author of this work has been asserted by him in accordance with the Copyright, Designs and Patents Act 1988.

Acknowledgements

This work and all my life would not have been possible unless Allah's support.

Thank you, Allah, for everything

I would like to express my deep gratitude to my supervisor Professor John Ladbury for his continuous support, insightful comments, and vital encouragement. He was extremely helpful in formulating my written work in a more comprehensive way. I am extremely thankful to him for giving such a nice support, although he had busy schedule managing the faculty.

Also, my sincere thanks go to Dr Heiko Wurdak who took keen interest in my project work and guided me all along providing all the necessary information for developing a good research. Thank you for your guidance, enthusiastic, and encouraging me to publish my work.

I would like to thank Dr Ian Wood and Dr Dan Donnelly for their guidance and support which had major impact on my progress. Dr Steven Clapcote, Dr Ronaldo Ichiyam and Lucy Parker for their kind help, support, and standing by my side during the hard time.

Also, my thanks are extended to Dr Sally Boxall for her help in running the flow cytometry analysis, Dr Jessica Kwok for her advice and assistance in growing human neurons, Dr Lin-Hua Jiang for his assistance in selecting an appropriate experimental model, Dr Neil Ashley (Oxford, MRC Weatherall Institute of Molecular Medicine) for his support in running the 10X Genomics analysis.

I wish to thank my mother for her prayers support and encouragement throughout my study. Of utmost importance, I dedicate this thesis to my wonderful wife, Wafa, and to my precious daughters, Ghadi, Raghad and Leen who have been a source of great support throughout every aspect of my life, including my thesis experience. Their constant love and encouragement provided a lot of hope and support during the tribulation time of my PhD. Words cannot express the gratitude and love I have for all of them.

Finally, I would like to thank my government who have supported me financially throughout my doctoral years.

Abstract

REST is a transcriptional repressor protein and has been suggested to maintain the self-renewal potential of several brain tumours including medulloblastoma. REST represses transcription by recruiting several chromatin modifiers, including histone deacetylase (HDAC) enzymes to gene promoters which have been associated with several cancers. Nevertheless, HDAC inhibitors (HDACis) have shown promising results in targeting specifically tumour cells. Interestingly, REST expressing cells showed higher sensitivity to HDACis yet, it is not known if they induce their action through the HDACs recruited in REST repression complexes. Also, it is not fully understood how HDACis specifically inhibit the growth of tumour cells, and in what way normal cells protect themselves from the hyperacetylation effect of these drugs.

In this study, I examined the contribution of REST in the medulloblastoma Daoy cell line by modulating its expression using CRISPR/Cas9. To explore the HDACis anti-cancer molecular mechanism, I profiled the gene expression of HDACis-treated tumour and normal cells at a single cell level using the next generation sequencing analysis.

The results showed that disrupting REST expression induced upregulation of neuronal genes, slightly (~6 %) reduced the cell growth, prolonged the cell cycle, and reduced the migration ability of the tumour cells. However, it did not stimulate apoptosis or reduce the sensitivity of the cell to the HDACis. Treating the tumour cells with HDACis resulted in activating the TNF α signalling via NF κ B pathway and modulating the expression of the cell cycle and Myc pathways. Whereas, exposing the normal cells to HDACis caused considerable changes on the transcriptome level.

Collectively, the data of this study showed that blocking REST expression did not lead to tumour cell death. It also showed the ability of HDACis to induce their action independent of HDACs recruited in REST complexes. Treating with HDACis caused global gene expression changes in tumour and normal cells which activate a defined signalling pathways however, this raises concerns regarding the toxic side effects of HDACis in normal cells. Hence, the use of HDACis should be revised carefully even with their minimal side-effect in clinical trials.

Table of Contents

Acknowledgements	I
Table of Contents	II
1 Introduction.....	1
The Road Map	1
1.1 REST.....	2
1.1.1 REST Gene Structure.....	3
1.1.2 REST Protein	5
1.1.3 REST DNA Binding Site	6
1.1.4 REST Expression	7
1.1.5 Regulation of REST Expression	8
1.1.6 REST Transcriptional Repression Mechanism.....	9
1.2 REST Involvement in Medulloblastoma	12
1.2.1 Medulloblastoma	12
1.2.2 REST Contribution in Medulloblastoma	15
1.3 HDACs as a Potential Target for Cancer Therapy	16
1.3.1 Acetylation and Deacetylation of Histone Lysine Residue	16
1.3.2 HDACs Classes.....	18
1.3.3 HDACs and their Involvement in Cancer	19
1.3.3.1 Class I HDACs and its Involvement in Cancer.....	19
1.3.3.2 HDAC Class IIa and its Involvement in Cancer	19
1.3.3.3 Class IIb HDACs and its Involvement in Cancer	20
1.3.3.4 Class IV HDAC and its Involvement in Cancer	20
1.4 HDACs As Anticancer Drugs.....	22

1.5	The Therapeutic Action of HDAC Inhibitors	22
1.5.1	HDACis Induce Apoptosis	23
1.5.2	HDACis Induce DNA damage	24
1.5.3	HDACis Anti-Angiogenesis Effect	25
1.5.4	HDACis Interfere with Cell Cycle.....	25
1.6	The HDACis used in this study	25
1.6.1	SAHA (Vorinostat)	26
1.6.2	MS-275 (Entinostat)	27
1.6.3	MI-192	27
1.6.4	Apicidin	27
1.6.5	Valproic Acid.....	28
1.7	HDACis Side-Effects.....	28
1.8	The Research Background and Questions	29
1.8.1	REST Contribution in Medulloblastoma	29
1.8.2	HDACis Molecular Action in Tumour and Normal Cells.....	29
1.8.3	The Research Hypothesis and Questions.....	30
Chapter 2	31
2	Material and Methods	31
2.1	Introduction.....	31
2.1.1	The Experimental Model	31
2.1.2	Modulating REST Expression using CRISPR/Cas9 and shRNA..	32
2.1.2.1	CRISPR/Cas9 to Knockout REST Expression	33
2.1.2.2	shRNA to Knockdown REST Expression.....	34
2.1.3	Profiling the Gene Expression at Single Cell Level using the 10x Genomics Chromium Single Cell 3'	36

2.1.3.1	Selecting the HDACis	38
2.1.3.2	The Cell Number and the Sequencing Depth of the scNGS 39	
2.2	The Methods	40
2.2.1	Standard Cell Culture.....	40
2.2.2	Culturing the Human Neurons	41
2.2.3	Identifying a Suitable Daoy Seeding Density for HDACi Treatment 41	
2.2.4	HDACis Preparation	42
2.2.5	Generating the Dose Response Curves, and Measuring the Cells Proliferation Rate and the Sensitivity to HDACis	42
2.2.6	The MTT Assay	43
2.2.7	Calculating the Doubling Time.....	44
2.2.8	Modulation of REST Expression	44
2.2.8.1	Knockout REST Expression Using the CRISPR/Cas9 System.....	44
2.2.8.2	Knockdown REST Expression using the shRNA System	45
2.2.8.2.1	The shRNA Sequence Annealing	45
2.2.8.2.2	The pSUPER-Puro Plasmids Preparation and Linearization	46
2.2.8.2.3	The shREST-pSUPER Plasmid Construction.....	46
2.2.8.2.4	The shREST-pSUPER Plasmid Transformation	46
2.2.8.2.5	The shREST-pSUPER Plasmid Isolation	47
2.2.8.3	The shRNA Transfection Reactions.....	48
2.2.8.3.1	Transfection Optimisation	48
2.2.8.3.2	Transfection with the shREST-pSUPER and Establishing the Stable Cell Clones	49

2.2.9	Study the Effect of REST-Modulation on the Daoy Cells Migration Using Wound Healing Assay.....	49
2.2.10	The Flow Cytometer Analysis	50
2.2.10.1	Cell Cycle Analysis using Propidium Iodide	50
2.2.10.2	Apoptosis Detection using Annexin V and PI	51
2.2.11	The Single Cell Next Generation Sequencing (scNGS)	52
2.2.11.1	Cell Treatment and Cryopreservation	52
2.2.11.2	The scNGS Sample Preparation.....	52
2.2.11.3	The scNGS GEMs Preparation and RT-PCR.....	53
2.2.11.4	Post GEMs-RT Clean-up	54
2.2.11.5	The cDNA Amplification, Purification and Quality Check	54
2.2.11.6	The cDNA Fragmentation, End Repair and A-tailing ..	55
2.2.11.7	Adaptor Ligation	55
2.2.11.8	Sample Indexing (i7).....	55
2.2.12	Sequencing Data Demultiplexing	56
2.2.12.1	Installing the required Software	56
2.2.12.2	Running the CellRanger mkfastq Pipeline.....	56
2.2.12.3	Running the CellRanger count Pipeline.....	57
2.2.12.4	Running the CellRanger aggr Pipeline.....	58
2.2.12.5	Visualising the Data using Loupe Cell Browser	58
2.2.12.6	Analysing the scNGS Gene Expression using Seurat...	58
2.2.12.7	Gene Functional Annotation and Gene Set Enrichment Analysis	60
2.2.12.8	Pathway Analysis	61
2.2.13	Basic Molecular Biology Procedures	61

2.2.13.1	Extracting DNA from 6-Well Culture Plates	61
2.2.13.2	DNA Extraction from 96-Well Culture Plates	62
2.2.13.3	Extracting Total RNA from Cultured Cells	62
2.2.13.4	The Nuclear Protein Extraction from Cultured Cells....	63
2.2.13.5	Polymerase Chain Reaction (PCR)	64
2.2.13.6	Quantitative Polymerase Chain Reaction (qPCR)	64
2.2.13.7	Agarose Gel Electrophoresis.....	66
2.2.13.8	Western Blot Analysis.....	66
2.2.14	Evaluating Gene Expression using the GEO-NCBI Data Sets	67
2.2.15	The Statistical Analysis and Visualization	68
Chapter 3	69
3	Results I	69
3.1	Preface	69
3.1.1	The aim and the Objectives of the Study	69
3.1.2	The objectives of the study	69
3.1.3	The Roadmap	69
3.2	The Results	72
3.2.1	Investigate REST Expression using Published Microarray Gene Expression Data	72
3.2.1.1	REST Expression is Higher in Medulloblastoma Tumours Compared to Normal Cerebellum.....	72
3.2.1.2	REST Expression is Elevated in the Daoy Medulloblastoma Cells Compared to Normal Cerebellum...	75
3.2.2	The Experimental Optimization to Examining REST contribution in Medulloblastoma	76
3.2.2.1	Daoy Seeding Density of 3.5×10^4 cell/mL Reaches ~100% Confluence by 72 Hours.....	76

3.2.2.2	Generating the Cell Dose-Response Curve for HDACis	78
3.2.2.3	HDACis Showed Variable Anticancer Activity and a Time-dependent Effect	80
3.2.2.4	HDACis Induced a Prolonged Cell Cycle Delay and not a Complete Cell Cycle Arrest.....	83
3.2.2.5	Optimizing the Transfection of the Daoy Cell.....	87
3.2.3	Modulating REST Expression in the Daoy Cell.....	88
3.2.3.1	Modulating REST Expression Using CRISPR/Cas9	88
3.2.3.2	Modulating REST Expression Using the shRNA Knockdown System	92
3.2.4	Confirm the Modulation of REST Expression	93
3.2.4.1	Modulating REST Expression Resulted in a Significant Reduction in REST mRNA and Protein levels.....	93
3.2.4.2	Modulation of REST Expression Derepresses the Expression of the RE1-Containing Genes	95
3.2.5	Study the Effect of REST Modulation on the Daoy Cell	98
3.2.5.1	REST Deficiency does not Strongly Inhibit the Cell Proliferation Rate.....	98
3.2.5.2	Modulating REST Expression Increased Cells Accumulation in G1 Phase of the Cell Cycle	101
3.2.5.3	Knockout REST Expression Significantly Reduced Cells Migration	103
3.2.5.4	Disrupting REST Expression did Not Reduce the Sensitivity of the Cells to HDACis.....	107
3.2.6	The Daoy Cells Express REST4 Isoform	109
3.2.7	HDAC Inhibitors Decrease Cell Viability Independent of DNA Fragmentation	110
3.3	Discussion.....	112
3.3.1	WNT Medulloblastoma Subtype Exhibits the Highest REST Expression.....	114

3.3.2 REST Repression of the RE1-containing Genes is not Equivalent between the Subtypes.....	116
3.3.3 Medulloblastoma Daoy Cell Showed High Sensitivity to HDACis	117
3.3.3.1 MI-192 Induced a Significant Cell Death within 12 Hours from the Treatment	117
3.3.3.2 Apicidin Induced a Progressive Cell Death	118
3.3.3.3 MS-275 Showed a Delay in Inducing Cell Death.....	119
3.3.3.4 SAHA Did not Completely Eradicate the Daoy Cells ..	121
3.3.3.5 The Daoy Cells Showed Concentration-Dependent Sensitivity to VPA	122
3.3.4 HDACis Induced a Prolonged Cell Cycle Delay and not a Complete Arrest	123
3.3.5 Blocking REST Expression in Medulloblastoma did not Stimulate Apoptosis Mechanism.....	126
3.3.6 Modulating REST Expression Slightly Reduced Cell Proliferation and Increased the Accumulation of the Cells in G1 Phase	127
3.3.7 Modulation of REST Expression Significantly Reduced Cell Migration	128
3.3.8 HDACs Recruited in REST Repression Complexes are not the Primary Element for HDACis to Induce Their Action	129
3.3.9 Daoy Medulloblastoma REST4 Expression	130
3.4 Conclusion	131
Chapter 4	132
4 Results II.....	132
4.1 Introduction.....	132
4.2 The Results	133
4.2.1 Assessing the Apoptosis Level in SAHA and MS-275 Treated Daoy Cells	133
4.2.2 Estimating the Treatment Length Based on the MTT and FACS Analysis	135

4.2.3	The scNGS Samples Preparation	137
4.2.4	scNGS data Demultiplexing	139
4.2.4.1	The Initial Visualization of the 10x scNGS Data.....	142
4.2.5	Improving the Quality of the 10x scNGS Generated Data	145
4.2.6	Daoy scNGS Data analysis	147
4.2.6.1	SAHA and MS-275 Affected the Expression of the Daoy Cell Cycle-Specific Markers.....	147
4.2.6.2	Merging the D.Vehicle, D.SAHA, and D.MS-275 Data Sets.....	154
4.2.6.3	Dissecting the Molecular Regulation of the Daoy Untreated and Treated Cells	158
4.2.6.4	Study the Differential Expression between the HDACis Untreated and Treated Daoy Cells.....	163
4.2.6.4.1	TNF α Signalling via NF κ B Molecular Pathways.....	164
4.2.6.4.2	Treating with SAHA and MS-275 Deactivated Myc Signalling Pathway	166
4.2.6.5	Treating with SAHA and MS-275 Decreased the Expression of Cell Cycle Specific Genes	168
4.2.6.6	The expression of the Apoptosis Genes	170
4.2.7	Normal Human Neurons scNGS Data Analysis	173
4.2.7.1	Clustering the Neurons Based on their Type	175
4.2.7.2	Exploring the Effect of HDACis on the Normal Neurons	179
4.2.7.2.1	The Effect of HDACis on Myc Signalling Pathways.....	182
4.2.7.2.2	The Effect of HDACis on Cell Cycle Pathway	184
4.2.8	The Expression of HDAC and HAT Genes.....	186
4.2.9	Pathway Analysis of the Untreated and Treated Samples	191
4.3	Discussion.....	195

4.3.1	Assessing the Quality of the scNGS	196
4.3.1.1	Assessing the Quality Based on the Number of the Analysed Cells	196
4.3.1.2	Assessing the Quality Based on the Sequencing Saturation and Depth	197
4.3.1.3	Assessing the Quality Based on the Q30 and the Background Noise.....	198
4.3.1.4	The Analytical Approach used to Process the Data	198
4.3.2	HDACis Affected the Expression of Several Cellular Pathways	200
4.3.2.1	HDACis Disrupted the Expression of Cell Cycle-Specific Genes	201
4.3.2.2	HDACis Disrupted the Expression of Myc Pathway	203
4.3.2.3	HDACi Disrupted the Expression of TNF α signalling via NF κ B Pathway	204
4.3.3	The Expression of HDAC and HAT Genes	205
4.3.4	The limitation of the scNGS	207
5	General Discussion.....	210
5.1	Summary of the Research Aims and Methodology	210
5.2	Knockout REST did not Induce Medulloblastoma Cell Death.....	210
5.3	HDACis Effected the Cell Cycle Regulation in Tumour and Normal Cells	212
5.4	Future Work.....	218
5.5	Final Conclusion	220
6	Bibliography	221
7	Appendices.....	243

List of Tables

Table 1: Summary of HDACs contribution in medulloblastoma.....	21
Table 2: Summary table of HDACis targets and their IC₅₀.....	28
Table 3:HDACis concentrations used to produce the dose-response curves	43
Table 4: SDS-PAGE Preparation.....	67
Table 5: Single cell samples identification Acronym.....	137
Table 6: Summary of the GO terms that were more frequent for each cluster	153
Table 7: GSEA results of the highly enriched gene sets of the Daoy cells.....	162
Table 8: GSEA results for some of the highly enriched gene sets of the neurons	181
Table 9: The DGE of the genes that were annotated as cell cycle arrest.....	184
Table 10: Gene information	213
Table 11: Summary of the four studies.....	215

List of Figures

Figure 1: Schematic representation of REST gene exons	4
Figure 2: Schematic illustration of human REST protein and its alterative isoforms.....	6
Figure 3: REST repression mechanism	11
Figure 4: Acetylation and deacetylation of a lysine residue.....	18
Figure 5: Role of HDAC Inhibitors in regulating apoptosis.....	24
Figure 6: Representation of HDACis blocking the catalytic domain of a HDAC enzyme	26
Figure 7: The map of the pCas-Guide Vector	34
Figure 8: pSUPER-Puro vector map and the shRNA knockdown concept	35
Figure 9: 10x Genomic Single Cell Generation and Library Construction	38
Figure 10: Schematic representation of the research workflow.....	71
Figure 11: The expression of REST and some selected RE1-containing genes in medulloblastoma and normal cerebellum tissue samples	74
Figure 12: The expression of REST and RE1-containing genes in the Daoy cell and normal cerebellum.....	75
Figure 13: Identifying the Daoy cell count that yield 90 – 100% confluence after 72 hours from culturing	77
Figure 14: The Daoy cell dose-response curves showed a concentration-dependent effect of HDACis on the cell growth.....	79
Figure 15: HDACis induce a time-dependent antiproliferative effect.....	82
Figure 16: HDACis induced a prolonged cell cycle delay though, it did not arrest the cell cycle.....	86
Figure 17: Daoy Cell Transfection optimization.....	87
Figure 18: CRISPR/Cas9 induced mono-allelic genome editing	89
Figure 19: CRISPR/Cas9 has induced homologous recombination genome editing.....	90

Figure 20: CRISPR/Cas9 induced bi-allelic genome editing in the KO cell clone	91
Figure 21: 5 µg/mL of Puromycin was used to select for stable expression of the shRNA	93
Figure 22: REST modulation has induced a significant reduction in REST protein	94
Figure 23: The shRNA resulted in a significant reduction in the KD REST-mRNA level	95
Figure 24: Modulation of REST expression resulted in increasing the expression of the RE1-containing genes	97
Figure 25: Modulating REST expression slightly reduced the proliferation rate in the KO and KD cells	99
Figure 26: The doubling time of the KO and KD cells was slightly longer than REST expressing cells	100
Figure 27: Modulating REST expression increased the KO and KD cells accumulation in G1 phase	102
Figure 28: The effect of 1% FBS on the wound healing assay results	104
Figure 29: Modulating REST expression resulted in reducing the cells migration ability	106
Figure 30: Disrupting REST expression did not affect response of the Daoy cells to HDACis	108
Figure 31: Daoy medulloblastoma cells expresses REST4	110
Figure 32: HDACis induced Daoy cell death independent of DNA fragmentation	111
Figure 33: Evaluating the apoptosis level in SAHA and MS-275 treated cells	134
Figure 34: Estimating the scNGS treatment duration length using the MTT and FACS results	136
Figure 35: Microscopic images for SAHA and MS-275 (-/+) Daoy and neurons at 36 hours	138
Figure 36: Schematic representation of the scNGS analysis workflow	139
Figure 37: Statistical summary of the 10x scNGS data quality measures	141

Figure 38: Schematic representation of the data analysis workflow 143

Figure 39: Visualization of the untreated and treated Daoy cell and neurons 144

Figure 40: Exploring the scNGS Data to improve the quality..... 147

Figure 41: The clustering of the Daoy treated cells was independent of the cell cycle phase 149

Figure 42: Visualization of the cell cycle markers in D.Vehicle, D.SAHA, and D.MS-275 151

Figure 43: Illustration of the number of detected D.Vehicle, D.SAHA, and D.MS-275 genes..... 154

Figure 44: Merging the three conditions into one Seurat object to study the DGE 155

Figure 45: The differential expression of the highly variable genes across the Daoy untreated and treated cells..... 157

Figure 46: GSEA enrichment plots of the highly enriched molecular regulations 161

Figure 47: Representation of the genes that showed high enrichment scores across the identified pathways..... 163

Figure 48: Illustration of the DGE with high enrichment scores in TNF α Signalling via NF κ B pathway 164

Figure 49: Fold change expression of the TNF α Signalling via NF κ B pathway165

Figure 50: Illustration of the DGE with high enrichment scores in Myc Signalling pathway..... 166

Figure 51: Fold change expression of the Myc signalling pathway 167

Figure 52: Illustration of the DGE with high enrichment scores in cell cycle signalling pathway 168

Figure 53: Fold change expression of the cell cycle regulating genes 169

Figure 54: Illustration of the DGE with high enrichment scores in cell apoptosis signalling pathway 170

Figure 55: Fold change expression of the D.Vehicle positive and negative phenotype apoptotic genes 171

Figure 56: Fold change expression of the apoptotic genes 172

Figure 57: t-SNE plots of the untreated and treated neurons	174
Figure 58: t-SNE plots of the merged Cortex.1, Cortex.2, and Striatum.1 data set.....	176
Figure 59 : The expression differences between the three neurons samples and across the different cell types.....	178
Figure 60: GSEA enrichment plots of the highly enriched gene sets of the neurons.....	180
Figure 61: Fold change expression of Myc Pathway across the different neuron cells	183
Figure 62: Fold change expression of the cell cycle component genes across the different neuron cells.....	185
Figure 63: t-SNE plots of the HDAC genes in the Daoy untreated and treated cells	187
Figure 64: t-SNE plots of HATs genes in the Daoy untreated and treated cells.....	188
Figure 65: t-SNE plots of HDAC genes in the untreated and treated human neurons.....	189
Figure 66: t-SNE plots of HATs genes in the untreated and treated neurons	190
Figure 67: Pathway analysis of the differentially expressed genes	194

List of Appendixes

Appendix 1: Partial list of non-histone protein substrates of HDACs..... 243

Appendix 2: The chemical information about the used HDACis..... 245

Appendix 3: The proposed plan for gene expression analysis using bulk NGS247

Appendix 4: NGS Experimental Considerations 248

Appendix 5: The Suggested Time-points for the Bulk NGS analysis and how they could be used to address the molecular mechanisms 249

Appendix 6: Western blot of REST protein (Complete image)..... 252

Appendix 7: REST mRNA expression in the KO cell clone 253

Appendix 8: Cell migration assay analysis images 254

Appendix 9: shRNA and TUNEL Assay Images of Kamal et al, 2012 Study . 255

Appendix 10: scNGS Cell Sorting (BD FACSDiva)..... 256

Appendix 11: The neurons gene list that were used to identify the cells identity258

Abbreviation Term

a.a	Amino Acid
AS	Alternative Splicing
Bak	BCL2 Antagonist/Killer 1
Bax	BCL2 Associated X Protein
Bcl-1	B-Cell Lymphoma 1 Protein
BCL2	B-Cell CLL/Lymphoma 2
BCL2L11	BCL2 Like 11
BDNF	Brain-Derived neurotrophic factor
BrdU	Bromodeoxyuridine
BRG1	Brahma-related gene 1
CDK	Cyclin Dependent Kinases
CDKN1A	Cyclin Dependent Kinase Inhibitor 1A - also known as p21 ^{WAF1}
ChAT	Choline Acetyltransferase
CRISPR	Clustered regularly interspaced short palindromic repeats
CTCL	Cutaneous T-cell lymphoma
CTD	C-terminal domain
CTNNB1	Cadherin-associated protein
DBD	DNA binding domain
DGE	Differential Gene Expression
DMEM	Dulbecco's Modified Eagle's Medium
dNTPs	Deoxynucleotide Triphosphates
DR4	Death Receptor 4
DR5	Death Receptor 5

Abbreviation Term

E2F1	E2F Transcription Factor 1
EDTA	Ethylenediaminetetraacetic acid
EGFR	Epidermal Growth Factor Receptor
EmpVec	pSUPER Empty Vector
ERK1/2	Extracellular Signal-regulated Kinase
ES	Enrichment Score
Fas	apoptosis antigen 1
FasL	Fas ligand-a TNF family member
FBS	Fetal Bovine Serum
FDRq	False Discovery Rate q-value
FPKM	Fragments Per Kilobase Million
FSC-A	Forward Scatter-Area
FSC-H	Forward Scatter-Hight
g	Relative Centrifugal Force
GDE	Gene Differential Expression
GES	GenClip Enrichment Score
GO	Gene Ontology
gRNA	guide RNA
h	Hour
H2BK5	Acetyl-Histone H2B Lys5
H3K4	Histone H3 lysine 4
H4K12	Acetyl-Histone H4 Lys12
HDAC	Histone deacetylases
HDACis	Histone deacetylases inhibitor/s

Abbreviation Term

HEPES	4-(2-hydroxyethyl)-1-piperazineethanesulfonic acid
HIF-1 α	Hypoxia-inducible factor -1 α
HR	Homologous Recombination
IL-6	Interleukin 6
KAI1	Kangai
KD	REST Knockdown Daoy Cell Clone
kDa	Kilodalton
KO	REST Knockout Daoy Cell Clone
Ku70	X-Ray Repair Cross Complementing 6
LCA	Large-cell anaplastic
miR-RNA	microRNA
MMPs	Matrix Metalloproteinases
MMuLV	Murine leukaemia virus
MMuLV RT	Moloney Murine Leukaemia Virus Reverse Transcriptase
MS-275	Entinostat
MTT Assay	3-(4,5-dimethylthiazol-2-yl)-2,5-diphenyltetrazolium bromide
Myc	v-myc Avian Myelocytomatosis Viral Oncogene Homolog
NF2	Neurofibromin 2
NF κ B	Factor kappa-light-chain-Enhancer of Activated B Cells
nGene	Number of Genes
NHEJ	non-homologous end joining
NRSF	Neuron-Restrictive Silencing Factor
NSCs	Neuronal Stem Cells
NTD	N-terminal domain

Abbreviation Term

nUMI	Number of Unique Molecular Identifier
NuRD	Nucleosome Remodelling Deacetylase
OTX	Orthodenticle homeobox 2
p21WAF1	Cyclin Dependent Kinase Inhibitor 1A
PAM	Protospacer Adjacent Motif
PCA	Principal Component Analysis
percent.mito	Percentage of the Mitochondrial Genes
pGL3	pGL3-CMV-LUC
PI	Propidium iodide
Pin1	peptidylprolyl cis/trans isomerase
pRB	Retinoblastoma Tumour Suppressor Protein
PRC2	Polycomb Repressive Complex 2
PS	Phosphatidylserine
PTCH1	Patched 1
RAD51	RAD51 Recombinase
RbAp4	46 Retinoblastoma-associated proteins
RE1	Repressor Element 1
RE1-LUC	pASTA-RE1s-CMV-LUC
RECK	Reversion-Inducing-Cysteine-Rich Protein with Kazal Motifs
REST	Repressor Element 1-Silencing Transcription Factor
RhoB	Ras Homologue Gene Family, Member B
RNAi	RNA interference
RNase A	Ribonuclease A
RPKM	Reads Per Kilobase Million

Abbreviation Term

SAHA	Suberoylanilidehydroxamic acid
SCF	Skp/Cullin/F box
SCF- β TRCP	Skp/Cullin/F box binds to β -transducin repeat containing gene
SCG10	Super cervical ganglion-10
scNGS	Single Cell Next Generation Sequencing
SCP1	Small C-terminal domain phosphatase
SD	Standard Deviation
SDS	Sodium dodecyl sulfate
SHH	Sonic hedgehog
shREST	Short hairpin REST
shRNA	Short hairpin RNA
SOC medium	Super Optimal Broth
SRRM4	Serine/Arginine Repetitive Matrix 4
SSC-A	Side Scatter-Area
SUFU	Suppressor of fused homologue
SYN1	Synapsin I
TBP-2	Thioredoxin-binding protein-2
TIMP-1	Tissue Inhibitor of Metalloproteinases-1
TNF	Tumour Necrosis Factor
TP53	Tumour protein p53
TPM	Transcripts Per Kilobase Million
TRAIL	TNF-related apoptosis-inducing ligand
TSA	Trichostatin A
t-SNE	T-distributed Stochastic Neighbour Embedding

Abbreviation Term

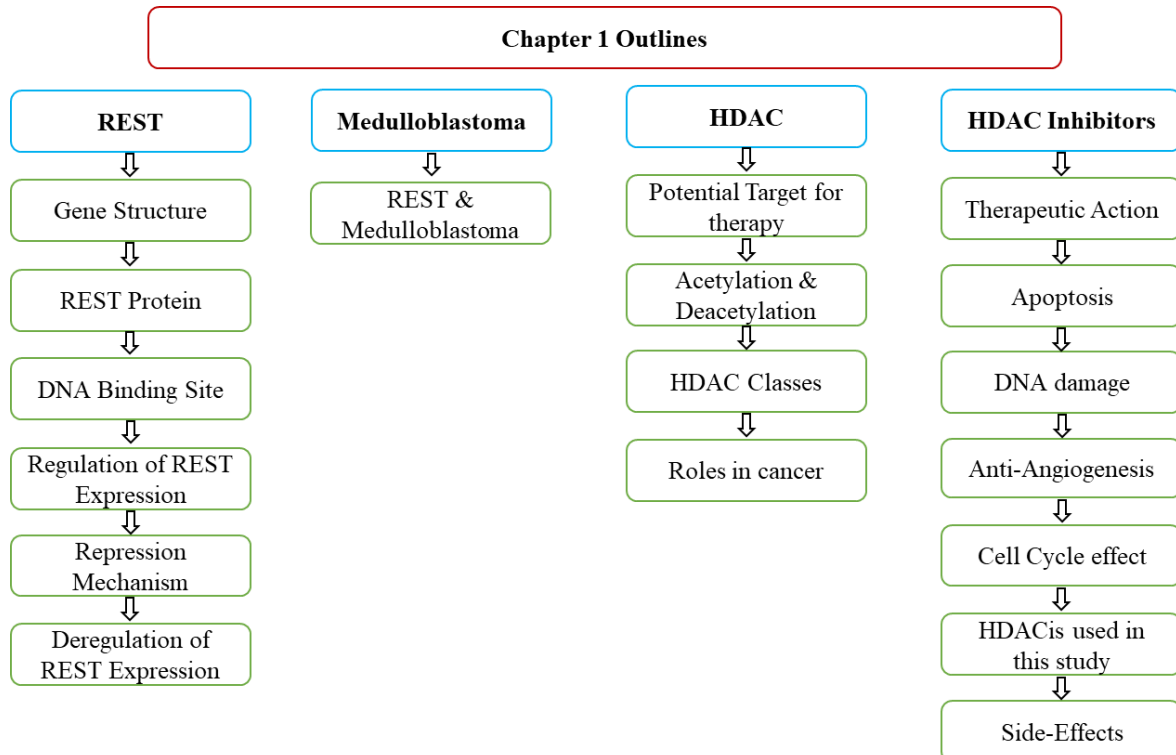
TSP1	Thrombospondin-1
TUBB3	Tubulin Beta 3 Class III
UMI	Unique Molecular Identifier
VACHT	Vesicular Acetylcholine Transporter
VEGF	Vascular Endothelial Growth Factor Receptor-2
VHL	von Hippel–Lindau Tumour Suppressor
VPA	Valproic acid
WNT	Wingless-Type Signalling Pathway
ZMYM3	Zinc Finger MYM-Type Containing 3
β-TrCP	Beta-transducing repeats-containing proteins

Chapter 1

1 Introduction

The Road Map

This thesis aimed to study the contribution of Repressor Element 1-Silencing Transcription Factor (REST), HDAC and HDAC inhibitors in the Daoy medulloblastoma cells growth and treatment response. Also, it aimed to uncover the molecular regulation of HDACs anticancer effect and how normal cells protect themselves from the hyperacetylation induced by these drugs. This chapter begins with a literature review of four main elements (REST, HDAC, HDACs, and medulloblastoma) and then will move to talk in more details about the research hypothesis, goals, and the used methodology. Chapter 3 Results I: presents the findings of REST modulation on the Daoy medulloblastoma cells. Whereas, Chapter 4 (Results II) presents the findings of the gene profiling of the HDACs treated and untreated cells at single cell level.



1.1 REST

REST [also known as Neuron-Restrictive Silencing Factor (NRSF)] is a DNA-binding protein that binds to a DNA sequence known as Repressor Element 1 (RE1) located in the promoter region of some genes where it is able to recruit several protein complexes. In 1995, REST was originally described as a transcriptional silencer of neuronal genes in non-neuronal cells ¹. Though, this view was reformed after observing the repression activity of REST on actively transcribed genes rather than a silencer for all RE1-containing genes ².

The main function of REST is to repress gene transcription through engaging several chromatin modifiers and histone alteration factors at gene promoter, which leads to chromatin condensation and blocks the binding of transcriptional machinery. In humans there are more than 2000 REST-target genes, the majority of them are neuronal differentiation genes ³. Hence, REST has a major role in regulating neurogenesis and prevents the neuronal phenotype in non-neuronal cells. However, REST function is not limited to neuronal genes and it extends to regulate the tumour necrosis factor superfamily, complement genes, cadherins, synaptotagmins, immune responses, olfactory receptors, voltage-dependent calcium and potassium channels, and microRNA genes ^{3, 4}. Lately, REST has been reported to regulate the differentiation of stem cells by regulating pluripotent genes such as Oct4, Sox2, and Nanog ⁵.

Deregulation of REST expression has considerable implications on the differentiation of neuronal stem cells (NSCs), proliferation of non-neuronal cells, and on tumour cells. REST plays a dual function in cancer; as a tumour suppressor in non-neuronal tumours, and as an oncogene in neuronal tumours. In some non-neuronal tumours such as colon carcinoma and breast cancer the loss of REST expression, as a result of REST locus deletion, has been suggested to contribute to tumour formation ^{6, 7, 8}. In contrast, in neuronal cells, overexpression of REST induces oncogenic activity, which blocks cells differentiation and maintains the self-renewal potential of NSCs, and ultimately contributes to tumour formation ^{9, 10}. Hence, downregulating REST activity in medulloblastoma and glioblastoma has been suggested to block tumour cell proliferation and initiate apoptosis ^{9, 11, 12, 13}.

There is a considerable volume of published studies that associate– medulloblastoma with REST expression ^{11, 14, 15}. The most reasonable explanation for REST linkage with medulloblastoma is that the continuous REST expression in tumour stem cells prevents the expression of neuronal differentiation genes which maintains cell multiplication. Conversely, blocking REST expression has been suggested to release neuronal genes expression and produce the stimulation of tumour cell death ^{11, 14, 15}.

In order to provide a better understanding about the relation of REST with medulloblastoma, the following sections will present more information about REST gene structure, REST protein, its repression mechanism, and what it has been known about its contribution in medulloblastoma.

1.1.1 REST Gene Structure

REST gene is located on chromosome 4q12, spans 24 kilo base-pairs of genomic DNA, and encodes REST protein and its isoforms. As with most human multiexon genes, the REST mRNA transcript undergoes extensive alternative splicing sites (AS) which could be due to the nature of the neuronal cells that show the most complex repertoires of splice variant. The REST gene is composed of four constitutive coding exons; Exon1 with four AS (1a, 1b, N1 and 1c), Exon2 has 12 AS (2a to 2k), Exon3 contains 4 AS (AS3; a neuronal specific AS located between the third and the fourth exons, N3a, N3b and N3c), and Exon4 which includes 12 AS (Figure 1). In addition to the previous four exons, a new exon (Exon5) has been found approximately 30kb downstream of exon4 ^{16, 17, 18} (Figure 1). At least, 45 variants of REST alternative splices have been reported most of them are expressed at low levels in a cell-type and in a tissue-specific manner, yet REST Isoform1 was the most common among all tissues and cell lines that were tested ¹⁸.

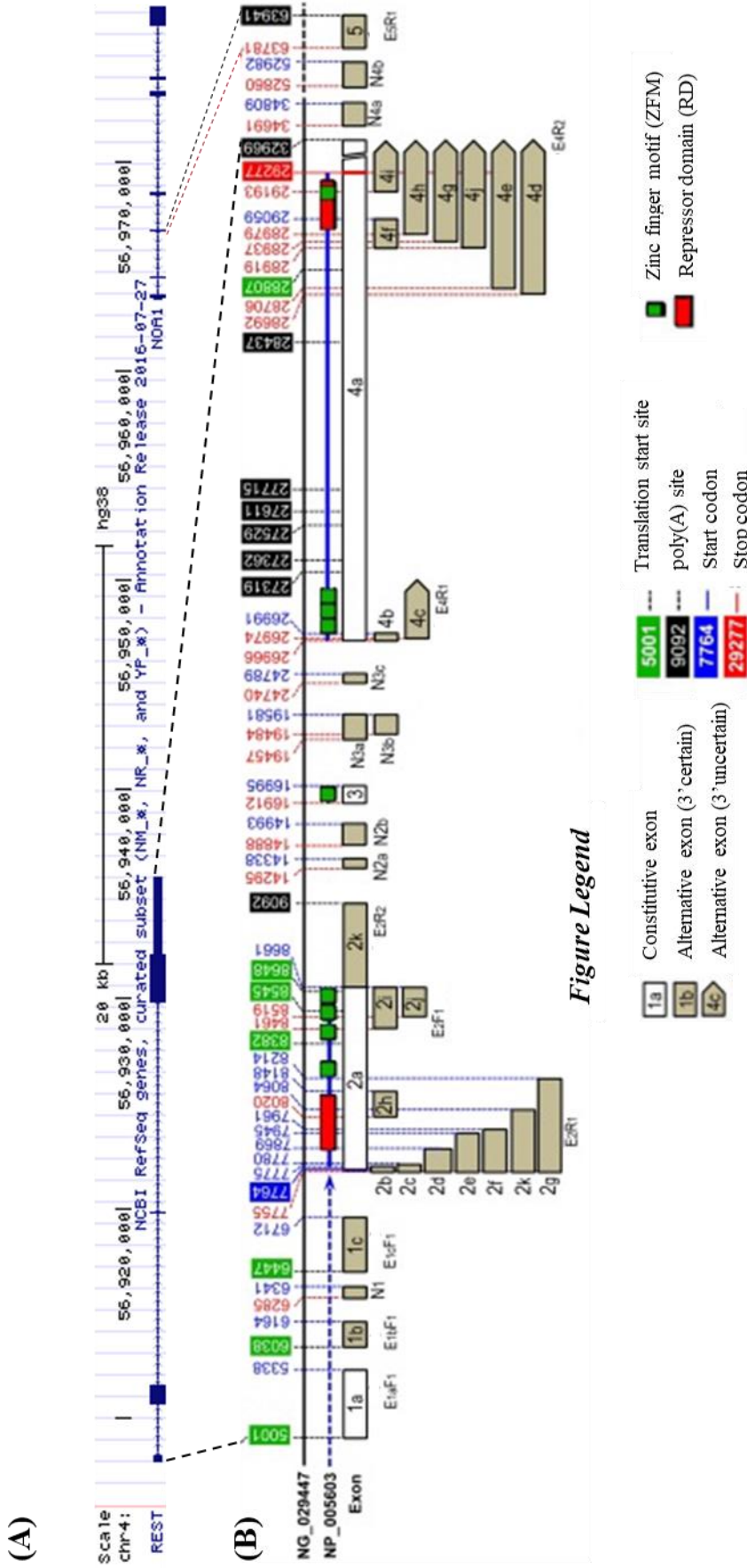


Figure 1: Schematic representation of REST gene exons

The diagram is a schematic representation of REST gene exons and their alternative splices. The UCSC gene tracker (A) was used to show REST gene locus and the exons positions based on genomic sequence (NG_029447). (B) is the NP_005603 REST protein reference sequence and was used to show the major REST protein domains parallel to the corresponding coding regions. The alternative splice exons are colour coded and the vertical numbers represent the position on the REST. The figure was adapted from (Chen et al., 2013)¹⁸.

1.1.2 REST Protein

There are at least four REST proteins have been reported; REST full length protein, also known as Isoform1, is 122 kilodalton (kDa) zinc finger, structured from three domains: The DNA binding domain (DBD) which consist of eight Cysteine and Histamine zinc fingers flanked by amino or N-terminal domain (NTD) and carboxy or C-terminal domain (CTD) (Figure 2) ¹⁹. Isoform2 which mainly localized in the cytoplasm and retains the NTD and four zinc fingers ¹⁹. Isoform3, also known as REST4, localized in the nucleus and retains the NTD five zinc fingers (Figure 2). The REST4 isoform has been suggested to be a posttranscriptional regulator of REST expression. REST4 is generated from the inclusion of a neuronal-specific exon (known as exon N) located between the third and the fourth exons of REST. The formed transcript has a frameshift sequence which contains a stop codon at the beginning of exon 4 which causes a premature termination of REST transcription and the formation of REST4 ¹⁷. REST4 protein has a stable structure that retains five of the eight zinc fingers present in REST but does not have the CTD. Hence, it does not efficiently recruit the repression complexes which results in upregulating REST target genes expression in neuronal cells ⁷. Interestingly, high expression of REST4 has been associated with several cancers such as neuroblastoma, breast cancer, and small cell lung cancers ⁷. Isoform4 is similar to REST full-length though, it has a selective deletion of zinc finger 5 ¹⁸ (Figure 2). Not much are known about REST isoform 2 and 4 and their contribution in cancer may warrant further investigation.

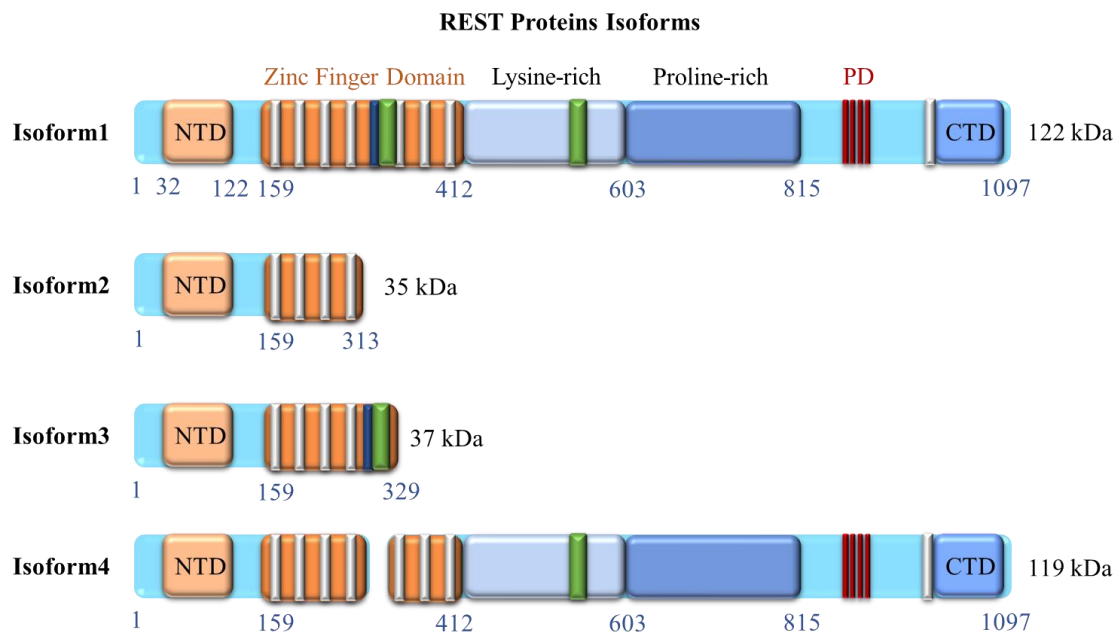


Figure 2: Schematic illustration of human REST protein and its alterative isoforms

Four isoforms of REST have been identified. **Isoform 1** (REST full-length, 1097 amino acid (a.a), and 122 kDa protein) produced by skipping off the neuronal-specific alternative splice exon between exon 3 and 4, has two repressing domains (NTD and CTD), a DNA binding domain (159-412) which contains eight zinc fingers and the ninth zinc finger is located in the C-terminal (1006-1082), lysine-rich domain (400-603), proline-rich domain (595-815), two nuclear localization signals (shown in green), a phosphodegron (E1009/S1013 or S1027/S1030). **Isoform 2** (313 a.a, 35 kDa protein) is a truncated protein, and retains from 1 to 4 zinc fingers only. **Isoform 3** (also known as REST4) (329 a.a, 37 kDa protein) is a truncated protein, and retains zinc fingers from 1 to 5. **Isoform 4** (1074 a.a, 119 kDa protein) is similar to isoform 1 though, it has a deletion of zinc finger 5. The figure was adapted from (Faronato et al., 2010) ¹⁶.

1.1.3 REST DNA Binding Site

REST transcriptional repression complexes are mainly recruited to a Repressor Element 1 (RE1) DNA sequence (also known as NRSE) which works as a regulator for gene transcription ⁴. RE1 is a group of highly conserved 21 to 23 bp DNA sequences that exist in the promoter region of a large number of neuronal genes and several of non-neuronal multigene families and microRNA genes ³. These sequences represent the sole binding

site of REST, to which it recruits various chromatin remodelling and histone modifying factors²⁰.

The number of functional RE1 sites in human has been estimated to reach to more than 2000 sites most of them are located in neuronal genes²⁰. The majority of RE1 sites are occupied by REST repression complexes, in particular, the sites in REST expressing cells such as embryonic and NSCs^{3,5,21,22}. In contrast, the expression of RE1-containing genes is higher in cells with low developmental potential as is the case with differentiated neurons⁵. In addition, the RE1 sites have been found in more than 300 non-neuronal genes that are commonly downregulated by the pluripotency factors such as Oct4, Sox2 and Nanog. Interestingly, several pluripotency controlling genes, such as Nanog, Wingless signalling pathway, ZF206, ZF281, Lin28, and some neurosecretory genes have been reported to have RE1 sites in their promoters which may demonstrate the broad function of REST^{5,22}.

1.1.4 REST Expression

Regulated REST expression is vital for cell development and neurogenesis and it has specific expression patterns based on the stage of the cell cycle and the tissue type. During embryonic brain development REST expression is up-regulated in neuronal cells which induces a transient repression of most neuronal genes and drives cellular proliferation. As neuronal progenitors differentiate into mature neurons REST and its corepressor disperse from the RE1 sites resulting in the expression of neuronal genes to the default level which stimulates neuronal cells differentiation²³. In animal models, mice with blocked REST expression appear normal until embryonic day 9 and they die by day 11 due to the widespread of apoptosis^{1,24}.

In mature cells, REST mediates long term silencing and transient repression for specific genes based on the stage of cell differentiation and the developmental context. During neural stem-cell differentiation, the CoREST complex remains bound and continues to repress the RE1-containing genes despite the cleavage of REST from the RE1 sites²⁵. In normal developed neurons, REST expression is downregulated resulting in the expression of neuronal genes and increases the synaptic activity.

In non-neuronal cells, the expression of REST remains high which mediates a long-term silencing of most neuronal-specific genes. However, during cellular multiplication, REST repression complexes transiently dissociate from most the RE1-containing genes and re-established following mitosis ²⁵.

On the level of REST corepressors, REST has been found to selectively recruit part of its corepressor complexes at certain genes and not all complexes are recruited at all genes ²⁵. This could explain the mechanism of short-term repression and long-term silencing and illustrate why certain chromatin markers are consistently associated with a particular cellular context. However, the molecular mechanism that regulates the binding of a particular corepressor is not known. It has been suggested that the sequence of the RE1 site and certain sub-nuclear organization could play a significant part in defining which cofactors are recruited ⁵.

1.1.5 Regulation of REST Expression

Despite the extensive studies aimed at understanding REST involvement in normal and disease states, little has been done to identify how the REST expression level is regulated. However, what is known about the regulation of REST expression suggests that it may occur at the REST gene transcriptional level, Rest mRNA, and posttranscriptional level.

Analysis of REST gene structure has identified the presence of three alternative exons (1a,1b and 1c) located at exon1, each of which works as a transcription initiation point. The abundance of specific transcripts mainly depends on the initiating exon, for instance the transcripts that initiated from exon1a have the highest abundance compared to the 1b and 1c transcripts however, none of these transcripts is cell-specific as they were found in all tested cells ²⁵. Also, it has been reported that some of the main pluripotent transcription factors such as Oct4 and Nanog may play a significant role in regulating REST transcriptional expression ⁹.

Also, miRNAs have been found to play a significant role in regulating the Rest mRNA level. miRNA is an endogenous noncoding RNA sequence that regulates the expression of specific protein based on the complementarity of its sequence to the protein mRNA. For example, *miR-153* has been reported to target Rest mRNA expression and represses its

transcription²¹. Accordingly, ectopic induction of *miR-153* to medulloblastoma cell lines showed a significant reduction in cell proliferation²⁶.

With respect to posttranscriptional regulation, REST has been found to have conserved phosphodegron sites at serine 861 and 864 which are located in the proline-rich domain. Also another two phosphorylatable sites were found as part of a second phosphodegron motif at serines 1027 and 1030 which are present in the CTD of REST^{27,28}. Serine 861/864 have been identified to work as substrates for the Peptidylprolyl cis/trans isomerase (Pin1) enzyme, which induces protein conformational changes leading to REST protein cleavage. It has also been reported that both serine 861/864 work as targets for ERK1/2 (an extracellular signal-regulated kinase) kinases which catalyse their phosphorylation²⁷. The serine 1027/1030 phosphodegrons are associated with REST downregulation in particular during neuronal cell differentiation. Both of these phosphodegrons are recognised by Beta-transducing repeat-containing proteins (β -TrCP) which work as a recognition site for Skp/Cullin/F box (SCF). Interaction of the β -TrCP with the SCF protein forms the SCF $^{\beta$ -TrCP complex which attracts E3 ubiquitin ligase and degrades REST^{29, 30}. Likewise, overexpression of β -TrCP results in excessive REST degradation as reported in mammary epithelial cancer²⁸.

1.1.6 REST Transcriptional Repression Mechanism

The mechanism of REST transcriptional repression is not entirely known however, it is initiated when the REST zinc finger domain recognises an RE1 site (Figure 3 A). The interaction of REST with DNA is then increased by the bromodomain of Brahma-related gene 1 (BRG1, an ATP-dependent dependent helicase also known as SMARCA4) protein, which increases REST occupancy through increasing the acetylation of histone H4 lysine 8 (H4K8) resulting in reducing the chromatin condensation around REST target site and allowing REST to form more stable binding with the RE1 site DNA^{5,31} (Figure 3 B).

Then Both of REST terminal domains work as hubs to recruit several chromatin-modifying enzymes that cannot directly bind to DNA. The NTD recruits mSin3 complex, which contains interaction domains for the histone deacetylases (HDAC1 and HDAC2). The CTD recruits several transcriptional repression complexes including the CoREST (REST corepressor 1) complex, which incorporates HDAC1, HDAC2, LSD1 (a H3K8 demethylase) and G9a (a H3K9 methylase)^{25, 32} (Figure 3 C). Once REST is attached to

its connate site on DNA, the HDAC enzymes that are recruited by mSin3 and CoREST catalyse the removal of acetyl groups from lysine amino acids on H3 and H4 tails and promote the electrostatic binding between histone tails and surrounding DNA allowing histones to wrap the DNA more tightly³². Deacetylation of H3K9 stimulates LSD1 (a histone H3K4 demethylase) and G9a methyltransferase activity which removes the methyl group of H3K4 and di-methylate H3K9, respectively leading to chromatin condensation¹². Methylated H3K9 can recruit heterochromatin protein 1 (HP1) which interacts with adjacent nucleosomes resulting in long term silencing of an RE1-containing gene²⁵ (Figure 3 D).

These alterations cause DNA condensation and mobilize the nucleosomes with respect to the DNA allowing the nucleosomes to bind the DNA more tightly, which imposes a spatial control and constrains the access of the transcription machinery²⁵. The ability of REST to recruit several chromatin alteration factors may also explain the ability of REST to induce long-term repression of RE1-containing genes, even when its expression is downregulated. Hence, removing REST from the promoter of an RE1-containing gene may not be adequate to restore gene expression due to the chromatin modifications that are induced by the REST complexes³³.

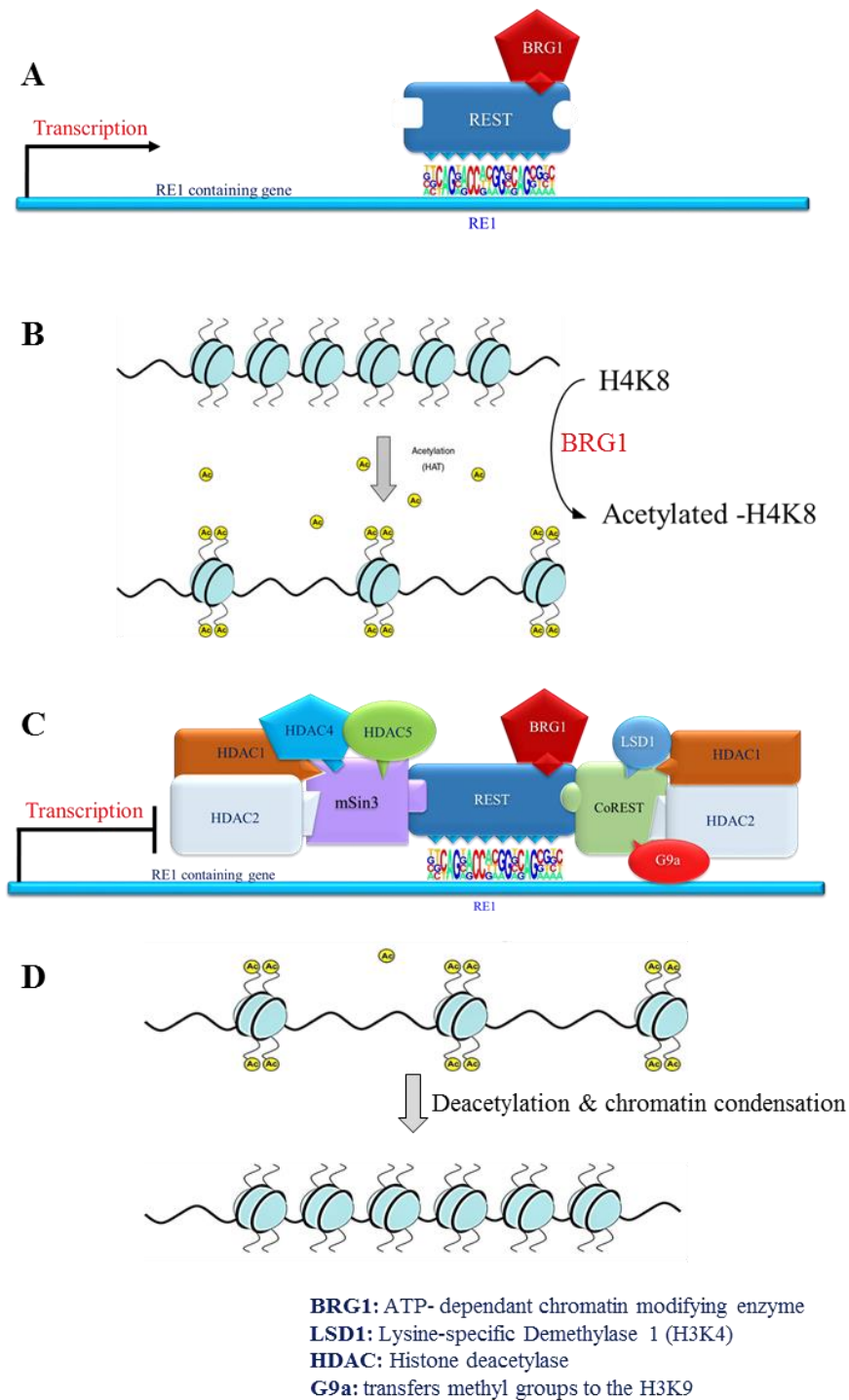


Figure 3: REST repression mechanism

REST transcriptional repression starts when *REST* zinc fingers recognise an *RE1* site (**A**). The bromodomain of *BRG1* then acetylates *H4K8*, which reduces the chromatin condensation around the *RE1* site (**B**) and facilitates the recruitment of *REST* corepressors complexes (**C**). *REST* corepressors contain several histone modifiers and chromatin modulators that induce spatiotemporal control of gene transcription (**D**).

1.2 REST Involvement in Medulloblastoma

1.2.1 Medulloblastoma

Medulloblastoma is the most common and aggressive form of embryonal and childhood brain tumour. It develops in both adults and children with a peak incidence between age 4 and 7 years though it has a rare occurrence in adults. The exact aetiology of medulloblastoma formation is not well known however, both genetic and epigenetic alterations have been reported to be involved in medulloblastoma development and treatment response³⁴. As medulloblastoma is an embryonic tumour, the number of the tumour stem cells has been reported to be very low and they involved in cancer initiation, propagation, metastasis, and recurrence³⁵. These cells characterized by expression of stem cell markers including CD133, regulate stemness pathways such as Wingless-Type signalling pathway (WNT) and Sonic hedgehog (SHH), and they have the ability to differentiate into multiple tumour cell types which contributes in the intratumoral heterogeneity³⁶. The cells are also have high capability of DNA repair which contributes in tumour resistance to therapy³⁵. The tumour stem cells have also been found to be tightly associated with medulloblastoma dissemination along the cerebrospinal fluid pathway in approximately 30% of cases especially in late stages yet, the dissemination outside the central nervous system is very rare^{36,37}. Hence, understanding the molecular regulation of stem cells in medulloblastoma will contribute to the discovery of more efficient anticancer agents and helps in improving the survival rate.

Based on the genetic profiling analysis the medulloblastoma tumours were classified into four subgroups that vary in clinical outcome, age, gender, and molecular genetics and epigenetic signatures³⁸. WNT subgroup, represents about 10% of medulloblastomas and shows wingless signalling pathway activation. The majority of WNT medulloblastomas have been found to harbour Catenin Beta 1 (CTNNB1) mutations and are characterized by Tumour Protein P53 (TP53) mutation³⁹. WNT subgroup has the best prognosis among the other subgroups even when metastasize and shows more than 5 years survival in more than 95% of cases under the current treatment regime⁴⁰. Recently, two WNT subtypes have been identified WNT α and WNT β . WNT α is enriched with monosomy of chromosome 6 and mostly observed in children. WNT β has a high frequency of diploid chromosome 6 and mainly affects adults⁴¹.

SHH subgroup, which represents 30% of medulloblastoma tumours, displays sonic hedgehog pathway activation and is dominated by mutations in MYCN Proto-Oncogene (MYCN, a transcription Factor), GLI Family Zinc Finger 2 (GLI2), Patched 1 (PTCH1) or Suppressor of fused homologue (SUFU)⁴². Four SHH subtypes have been reported. In affected children SHH α shows the worst prognosis. SHH β is more dominant among infants, frequently results in metastatic outcome, and has worse overall survival rate. SHH γ mainly affects infants and it is enriched for medulloblastoma with extensive nodularity. SHH δ primarily affects adults and shows more favourable prognosis⁴¹. Generally, the SHH subgroup has an intermediate prognosis and around 64% of cases reach 5 years survival however, cases with TP53 mutations showed poor prognosis⁴³. Both WNT and SHH medulloblastomas have been found to be driven from embryonic cell types.

Group 3 and Group 4 medulloblastoma have the generic name as not much is known about their genetic origin however, they are significantly different. Group 3 represents 20% of medulloblastomas, occurs exclusively in children, frequently metastatic, and represents the worse prognosis of all subgroups. Three subtypes of Group 3 have been identified; Group 3 α represents around 60% of cases with a favourable outcome. Group 3 β shows a favourable outcome with low frequency of dissemination and mainly affects the over 3 years old. Group 3 γ has the worse prognosis and is enriched with isochromosome 17 q arm (iso17q) and MYC expression⁴¹.

Group 4 is the most common medulloblastoma subgroup and represents 40% of cases though it is the least understood of the subgroups and often exhibits iso17q. Lately three subtypes of Group 4 have been identified; Group 4 α which is enriched by MYCN amplification, chromosome 8p loss and 7q gain. Group 4 β enriched for Cyclin Dependent Kinase 6 (CDK6) amplification and shows a high level of neurodegeneration. Group 4 γ is enriched for chromosome 8p loss and 7q gain and CDK6 amplification⁴¹. Both of Group 3 and 4 medulloblastomas do not have a specific therapy target, present unfavourable clinical prognosis and have been proposed to initiate from a foetal cell type⁴⁴.

Approximately 87 % of medulloblastoma cases were diagnosed as Group 4, Group 3 or SHH, which show the unfavourable clinical outcome of most medulloblastoma cases⁴⁴. Based on the research findings it can be clearly seen that medulloblastomas display a considerable intertumoral and intratumoral heterogeneity which increases the difficulty of developing targeted treatments. Also, the genetic signature of medulloblastoma metastases

is considerably different to their parent primary tumours which has important implications on medulloblastoma treatment as the vast majority of the research focuses on primary tumours.

Molecular analysis of medulloblastoma has revealed the presence of somatic copy number aberrations and mutations in histone lysine methyltransferases, demethylases, acetyltransferases and deacetylases, and in some members of the polycomb transcriptional repressor complexes such as PRC1 and PRC2. However, the frequency of the reported mutation is relatively low across the medulloblastoma subtypes ⁴⁵.

Current medulloblastoma treatment strategies mainly depend on patient stratification into Low-risk, High-risk, and Standard-risk groups, based on the clinical features and outcome. The Low risk is characterized by positive β -catenin (cell adhesion protein), presence of large-cell anaplastic (LCA), or it shows MYC amplification, though it does not metastasise. The High-risk is defined as metastatic disease with LCA, or demonstrates MYC amplification. Whereas, the Standard-risk are the cases that lacks the high and low risks discriminating features ⁴⁶. This classification, in general has improved the treatment response and the overall survival to more than 70% ⁴⁶. Unfortunately, nearly 30 % of patients demonstrate the High-risk form of the disease and they experience the recurrence of the tumour ¹⁴. Apart from SHH pathway, targetable therapy such as Vismodegib (a smoothed inhibitor) and Sonidegib (a SHH inhibitor that blocks SHH through PTCH and Orthodenticle homeobox 2 (OTX2) genes) there are no targetable genes or pathways for the other medulloblastoma subgroups ^{7, 47}. Existing medulloblastoma treatment is mainly based on chemotherapy, radiotherapy and surgery however, they have serious and long-lasting side effects. Clinical trial of children with medulloblastoma receiving radiotherapy plus chemotherapy showed more than 75% event-free survivals and 80% overall survival rate in five- and 10-years ⁴⁸. Unfortunately, many of the recovered cases develop severe late toxicity which severely affects the growth, endocrine function, neurocognitive development. It also could result in cardiac, pulmonary, and gynecological toxicity ⁴⁹.

Elevated REST expression has been reported in approximately 80% of the medulloblastoma tumours and it is associated with elevation in Myc pathway expression ^{11, 14, 50, 51}. It has been proposed that elevated REST expression may sustain the

proliferation of the NSCs and prevent their differentiation which may propose REST as an attractive therapeutic target due to its reversible nature ^{11, 14, 51}.

1.2.2 REST Contribution in Medulloblastoma

The majority of REST expressing medulloblastoma cells do not express neuronal differentiation genes such as Synapsin I, Tubulin Beta 3 Class III (TUBB3), and Superior Cervical Ganglion-10 Protein (SCG10, also known as Stathmin 2 (STMN2)), which indicates the direct repression effect of REST ⁵². Based on immunohistochemistry, western blot, and quantitative PCR analysis around 80 % of medulloblastoma cases show high REST expression and poor cellular differentiation ^{11, 14, 50}. It has also been reported that patients with high REST-expressing tumours exhibit worse overall survival, have higher occurrence of metastasis, and demonstrate the poorest prognostic indicator compared to REST-low and negative tumours ^{14, 37}. Knocking down REST in human medulloblastoma cell lines such as Daoy and D283 has been reported to repeal the tumorigenic potential of these cells, upregulate neuronal genes expression, and trigger apoptosis ^{9, 11, 14, 50}. Exogenous induction of REST in normal neuronal progenitor cells has been claimed to stimulate tumour formation and maintain the self-renewal potential of NSCs ⁵³. Hence, REST has been suggested as a promising target for neuronal and non-neuronal cancer however, there is no accessible drug to target REST expression. Nevertheless, targeting REST repression complexes, in particular recruited HDACs, has been an area of enormous research interest. Some medulloblastoma subgroups such as SHH, Group 3 and Group 4 have been found to overexpress HDACs. Hence, targeting HDACs has been suggested to reduce the viability of cells, especially in those expressing MYC ⁵⁴.

Several HDACis have been approved as anticancer drugs due to their ability to activate the transcription of silenced genes, arrest cell proliferation, induce differentiation, promote apoptosis, intensify host immune response to cancer cells and impair angiogenesis ⁵⁵. Remarkably, HDACis have shown the most tolerable side effect profile compared to the traditional chemotherapy.

As HDACs are one of the elements of this study, the following sections will introduce HDACs, their classes, deacetylation function and their role in cancer. They also will give a summary about HDACis pharmaceutical properties and actions.

1.3 HDACs as a Potential Target for Cancer Therapy

The genetic mutations have been considered as primary factors for cancer initiation and formation as they induce a dramatic effect on activating oncogenes and blocking the expression of tumour suppressor genes. However, epigenetic changes such as methylation, acetylation, deacetylation and phosphorylation also play major roles in cancer cell growth, invasion, metastasis, and treatment response^{44,56}. A typical picture of human cancer shows a disruption in most of epigenetic regulators, including the balance between the acetylation and deacetylation (which has major implications in cancer cell growth), metastasis, heterogeneity and drug resistance. Thus far there is no conclusive evidence about the mechanisms that cause the disruption in this balance. However it has been widely observed that the irregular Histone acetyltransferases (HATs) expression in leukaemia, colorectal, gastric and, breast cancers is a result of overexpression, genetic mutations, or chromosome translocations of HAT genes⁶. Also, mutations in HATs binding complex such as p300 and CBP, which function as tumour suppressor-like genes, have been found to stop HAT transcriptional coactivation⁵⁷. However, mutations in HDACs genes were mainly reported in leukaemia cancers.

1.3.1 Acetylation and Deacetylation of Histone Lysine Residue

Acetylation and deacetylation are the most common histone modifications that regulate chromatin structural remodelling through adding or removing the epsilon group of lysine (K) amino acid⁵⁸. The histone is an octameric structure assembled from a histone H3 and H4 tetramer and two H2 and H2B dimers. Histone tails contain a large number of positively and negatively charged amino acids which dictate the binding affinity between histones and DNA.

Lysine is one of the amino acids in the histone tail that has a major role in regulating genes expression. The lysine residue is an α -amino acid that includes an ϵ -amino group (NH_2) attached to the fifth carbon atom and has a positive charge at the physiological pH. The ϵ -amino group on histone tails works as a substrate for a variety of enzymatic activity and post-transcriptional modification; including acetylation and deacetylation, methylation, phosphorylation and ubiquitination. The collective effect of these modifications generates an epigenetic coding system that regulates genes expression.

Acetylation of a lysine residue neutralizes the positive charge on the amino acid via HATs enzymes resulting in the transference of an acetyl moiety from acetyl-Coenzyme A to the ϵ -group of a lysine (Figure 4). The acetylation process reduces the interaction between histones and the negatively charged DNA, resulting in more relaxed chromatin and the formation of euchromatin which holds the most active genes ⁵⁹. The acetylation mechanism can affect a single factor in several ways. For instance, acetylation of transcription factors can change protein stability, protein-protein interactions, protein localization and DNA binding. Also, the acetylation location of an acetyl group may enhance or repress DNA binding ability. In addition, it may enhance the binding of non-histone proteins such as p53, NF- κ B, and several of other proteins, or reduce the binding of other factors such as FOXO1 (works as myogenic growth and differentiation), HMGA1 (regulates gene transcription), and p65 (NF- κ B Subunit) ⁶⁰.

Conversely, deacetylation is an antagonist process of acetylation, catalysed by HDACs, and results in the removal of acetyl group from acetylated lysine, adding a charge, and generating a free acetate (Figure 4). Adding a positive charge to histone tails increases histone interaction with the negatively charged DNA backbone resulting in increasing the condensation of the surrounding chromatin (heterochromatin, inactive genes), and blocking the access of the transcriptional machinery ⁵⁸. Deacetylation of histone H3 and H4 is generally associated with gene transcriptional repression. The machinery of lysine acetylation and deacetylation is a reversible post-transcriptional modification process that induces spatiotemporal control on gene expression. Over the years it has become evident that histone deacetylase is a misnomer as HDAC enzymes targets many of non-histone proteins.

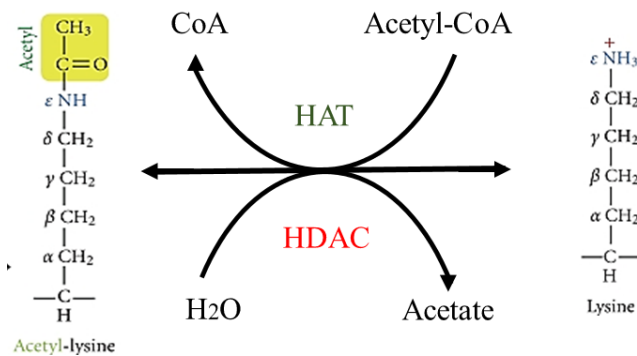


Figure 4: Acetylation and deacetylation of a lysine residue

Acetylation of a lysine residue is the process that neutralize the positive charge of lysine, using HATs enzymes and results in transferring an acetyl moiety from acetyl-Coenzyme A to the ϵ -group of a lysine. Conversely, deacetylation is an antagonist process of acetylation, catalysed by HDACs, and results in the removal of acetyl group from acetylated lysine, adding a charge and generating a free acetate.

1.3.2 HDACs Classes

Human HDACs are a family of 18 enzymes grouped into four classes (I, IIa, IIb and IV) based on the sequence homology of their catalytic domains to yeast (*Saccharomyces cerevisiae*) deacetylases. The HDAC enzymes are different in their molecular structure, enzymatic function, expression level and subcellular localization⁵⁸. These enzymes cannot solely bind to DNA and they are recruited to a target gene by association with a transcriptional activator or repressor protein, or through incorporation with multiprotein complexes such as Co-REST, mSin3, SMART/N-CoR, Polycomb Repressive Complex 2P (RC2), Nucleosome Remodeling Deacetylase (NuRD), and Zinc Finger MYM-Type Containing 3 (ZMYM3) complexes⁴⁵.

HDAC classes I, IIa, IIb and IV are predominantly expressed in nucleus and they depend on zinc as a cofactor to deacetylate lysine residues⁵⁹. HDAC Class III or (Sirtuins) is a specific group of nicotinamide adenine dinucleotide (NADs⁺) dependent HDACs that deacetylate histone and non-histone proteins. There are more than 50 of non-histone proteins that are regulated by HDACs and they have different cellular function ranging from tumour suppressor, transcription factor, signalling mediator, oncoprotein, steroid hormone receptors, and DNA-repair protein⁵⁸ (Appendix 1).

1.3.3 HDACs and their Involvement in Cancer

In cancer the expression of HDAC enzymes is widely variable between various types of tumours and within the tumour cells of the same entity. However, the elevated HDACs level is mostly accompanied with a severe disease condition and poor survival ⁶¹. It has also been reported that the expression of class I HDAC is frequently upregulated in cancers whereas, the class II HDAC is often downregulated and its high expression is associated with a better prognosis ⁶². The following 4 subsections will introduce the HDACs subclasses and their involvement in cancers.

1.3.3.1 Class I HDACs and its Involvement in Cancer

Class I HDACs is a family of four members (HDAC1, 2, 3, 8) that show a high enzymatic activity to histone 3 and 4. All the members are localized predominantly within the nucleus apart from HDAC8 which is found both in nucleus and cytoplasm. HDAC1 and HDAC2 are very similar and generally found together in most repression complexes such as mSin3, CoREST, PRC2 and NuRD complexes ⁵⁸. Cells with blocked HDAC1 and HDAC2 expression have been reported to show high sensitivity to DNA damaging agents. This could be due to the ability of HDAC1 and HDAC2 to repress the transcription at DNA damaging sites which allows DNA repair mechanism to take place ⁶³. In medulloblastoma elevated expression of HDAC2 has been reported in SHH, Group 3 and Group 4 subgroups and it is connected with poor prognosis ⁵⁴. Modulating HDAC2 expression resulted in reducing the metabolic activity, cell growth and viability, and stimulated cell death ⁵⁴. HDAC3 shows a considerable role in DNA repair regulation, which may suggest the significant therapeutic benefits of targeting HDAC3 in cancer treatment ⁶⁴. HDAC8 has the ability to deacetylate histone and non-histone proteins though its protein complex is not clearly known ⁵⁸. Recently HDAC8 has been reported to play an important part in regulating the transcription of wild-type and mutant p53 protein, suggesting that inhibiting HDAC8 could be a tool to block mutant p53 expression ⁶⁵.

1.3.3.2 HDAC Class IIa and its Involvement in Cancer

HDAC Class IIa consists of a family of four members (HDAC4, 5, 6 and 9) that have approximately 40% sequence homology. They exhibit the lowest deacetylation activity among all HDACs and are primarily implicated in muscle cell differentiation and

development⁵⁹. They are present either in the nucleus or the cytoplasm, bind to C-terminal-binding protein (CtBP) and HP1 complexes, and display tissue-specific expression pattern⁶⁶. They have also been reported to assist in recruiting Class I HDACs to a repression complex through their NTD, which probably accounts for a part of their repression function⁵⁸. High expression of Class IIa HDACs members has been reported in cancer and they showed cancer-dependent expression. For example, the expression of HDAC4 is higher in breast cancer compared to colorectal, bladder, and renal cancers⁶⁷. Overexpression of HDAC5 and HDAC9 has also been associated with a high-risk medulloblastoma group, and they were proposed as markers for poor survival⁶⁸. HDAC7 overexpression has mainly been reported in pancreatic cancer⁵⁹.

1.3.3.3 Class IIb HDACs and its Involvement in Cancer

Class IIb is (HDAC6 and 10) a unique HDAC isoform as it has two homologous catalytic domains, is mainly expressed in cytoplasm, and has been reported to regulate cell cycle, cell migration, apoptosis, and metastasis of cancer cells⁶⁹. Overexpression of HDAC6 has been reported to promote cancer cell proliferation through acetylating cancer-related pathways such as Heat Shock Protein 90 (Hsp90), cortactin (rearranges the actin cytoskeleton) and α -tubulin. It also reduces the sensitivity of HDACs through stabilizing Epidermal Growth Factor Receptor (EGFR). Inhibiting HDAC6 expression in lung adenocarcinoma and glioblastoma has been found to reduce the EGFR level resulting in diminishing the associated signalling pathway and initiation of apoptosis⁶⁹. Not much is known about HDAC10 though it has been found to be overexpressed in high-risk neuroblastomas and ovarian cancer.

1.3.3.4 Class IV HDAC and its Involvement in Cancer

HDAC11 is the only isoform of Class IV and the depletion of its expression does not affect cell metabolic activity and viability⁷⁰. Overexpression of HDAC11 has been suggested to suppress Bone Morphogenetic Protein 4 (BMP4) expression, which increases cancer malignancy in colon, prostate, breast, and ovarian cancers. Inhibiting HDAC11 expression has been reported to induce apoptosis and inhibit the metabolic activity of some of non-neuronal cancers⁷⁰. See (Table 1) more information about the HDACs contribution in medulloblastoma.

Table 1: Summary of HDACs contribution in medulloblastoma

HDACs	The activity of HDACs in medulloblastomas
HDAC1	Selective inhibition of HDAC1 in Med1-MB mouse cell line and reported to affect the SHH medulloblastoma cell growth ⁷¹ . In human, its expression is downregulated in the prognostically unfavourable medulloblastoma groups ⁶⁸ .
HDAC2	Showed elevated expression in SHH, Group 3, and group 4 and has been associated with medulloblastoma unfavourable outcome. Depletion of HDAC2 in Myc amplified cells such as MED8A, UW228-2, ONS76 and DAOY increased the acetylation of Histone 4 and induced cell death ⁵⁴ .
HDAC3	Did not show high expression in medulloblastoma and its contribution in medulloblastoma tumorigenesis and treatment has not been investigated ⁶⁸ .
HDAC4	Downregulated in the prognostically unfavourable medulloblastoma groups yet, not much are known about its role in medulloblastoma ⁶⁸ .
HDAC5 HDAC9	Showed the high expression in primary medulloblastomas and prognostically poor subgroups and they are significantly associated with poor overall survival. Knockdown their expression in medulloblastoma cells such as Daoy, UW228-2, UW228-3, ONS76, and Med8A resulted in decreased the cells growth and viability ⁶⁸ .
HDAC6	Upregulated in SHH-MB mouse cell line and knocking down its expression lead to cell death ⁷¹ .
HDAC7	Its contribution in medulloblastoma tumorigenesis and treatment has not been investigated.
HDAC8	Slightly elevated in medulloblastoma cell lines such as UW-288-2, DAOY, and ONS76 yet, its contribution in medulloblastoma tumorigenesis and treatment has not been investigated ⁷² .
HDAC10	Elevated HDAC10 expression is associated with poor outcome of treated medulloblastoma patients ⁷³ .
HDAC11	Showed reduced expression in Smo/Smo medulloblastoma mouse model ⁷⁴ .

1.4 HDACis As Anticancer Drugs

HDACis are a group of epigenetic molecular drugs that interact with the catalytic domain of HDAC enzymes and block their activity. The principle of the epigenetic cancer therapy mainly depends on reversing epigenetics abnormalities that support the disease formation which often results in loss or gain of function of many cellular regulators including proliferation, differentiation, cell cycle, angiogenesis and apoptosis mechanisms⁷⁵. These simultaneous actions on multiple factors represent a major advantage of HDACis as anticancer therapeutics, and it explains their ability to treat different cancers. Currently, a large number of HDACis are in clinical trials, and to date five were approved for clinical use (four drugs approved by the US Food and Drug Administration, namely Vorinostat, Romidepsin, Panobinostat and Belinostat, while Chidamide is approved in China)⁷⁶.

Clinically the inhibitors have shown potent anticancer activity with remarkable specificity to tumour cells and the side-effects were favourable in small set of patients with selected diseases⁷⁶. Also, they showed several advantages over the classical anticancer drugs. One of their major advantages is that they showed high selectivity to transformed cells and they have not shown damaging effects on normal cells⁶⁰.

Most transformed cells showed high sensitivity to HDACis compared to normal cells however, this sensitivity mainly depends on cancer type, inhibitor structure, concentration and exposure length⁶. The exact mechanism of the effect of HDACis on tumour cells and not normal cells is unclear.

1.5 The Therapeutic Action of HDAC Inhibitors

In recent years the list of the HDACis has grown and the research work to uncover their biological and chemical mechanisms has become one major research theme in cancer treatment⁷⁷. A large number of studies have tried to decipher the therapeutic mechanisms of HDACis though this regulation is too intricate and often embedded in a network of molecular interactions that occur simultaneously. Generally, the findings of these studies have pointed out several of cellular mechanisms that collectively resulted in a lethal effect on the tumour cell. These mechanisms result in cell differentiation and cell cycle effect, DNA damage, deregulation of non-coding RNA, autophagy, deregulation of cellular signalling pathways, and affect angiogenesis (blood vessels formation). They also

modulate the immune response and stimulate apoptosis⁷⁸. However, the onset and the regulation of these mechanisms are relatively different between cancers and they are mainly shaped by; the tumorigenesis regulation, the inhibitor selectivity, and the dosage and the duration of the treatment. Interestingly, much of the crosstalk between these mechanisms is poorly understood and their initiation factors remain unclear.

Current understanding of HDACis molecular action has outlined several important cellular and molecular mechanisms of HDACis anticancer effects including stimulation of apoptosis, DNA damage, anti-angiogenesis effect, and the effect on cell cycle.

1.5.1 HDACis Induce Apoptosis

HDACis have been reported to stimulate both the extrinsic and the intrinsic (mitochondrial) apoptotic pathways (Figure 5). The stimulation of the intrinsic pathway has been reported to be through decreasing the expression of the anti-apoptotic proteins such as B-Cell Lymphoma 1 Protein (Bcl-1) and B-Cell CLL/Lymphoma 2 (BCL2) and upregulating the proapoptotic proteins such as BCL2 Associated X Protein (Bax), BCL2 Antagonist/Killer 1 (Bak) and BCL2 Like 11 (BCL2L11) which initiate the intrinsic pathway^{60, 79, 80}. It has also been found that the hyperacetylation effect of HDACis in medulloblastoma initiates p53-dependent Bax activation, which delays the progression in cell-cycle and activates the proapoptotic genes⁸¹. HDACis stimulate the extrinsic pathway through activating death receptors such as Death Receptor 5 (DR5), Apoptosis Antigen 1 (Fas), Fas Ligand (FasL, a TNF family member) and TNF-related Apoptosis-inducing Ligand (TRAIL)^{34, 82}. It has been reported that Blockade of these factors resulted in decreasing the efficacy of HDACis in preclinical settings⁸³.

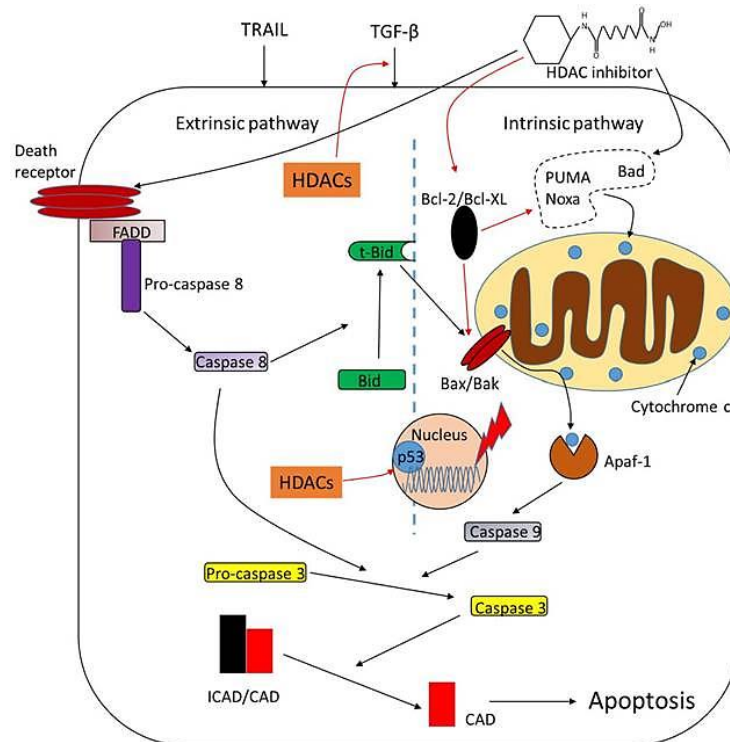


Figure 5: Role of HDAC Inhibitors in regulating apoptosis

In cancer, HDACs function as apoptotic repressors factors therefore, treatment with HDACis has been suggested to release the repression effect and upregulate the expression of the pro-apoptotic proteins and downregulate the expression of the anti-apoptotic proteins. HDACis activate apoptosis in cancer cells through both the extrinsic and intrinsic pathways. Note: Black arrows mean activate, while red arrows mean downregulate. This figure was adapted from Li et al., 2014⁷⁵.

1.5.2 HDACis Induce DNA damage

HDACis have been suggested to promote DNA damage response though increasing the acetylation level leading to relaxation of the chromatin⁷⁸. Consequently the DNA becomes more susceptible to damaging agents such as Reactive Oxygen Species (ROS), DNA damaging drugs, or radiation which eventually lead to caspase-independent cell death⁷⁸. HDACis have also been reported to downregulate the expression of homologous recombination DNA-repair genes through decreasing the expression of E2F Transcription Factor 1 (E2F1), RAD51 Recombinase (RAD51), HDAC1 and HDAC2 which are known through their role in regulating the expression of DNA-repair proteins^{78, 84}.

1.5.3 HDACis Anti-Angiogenesis Effect

In most transformed cells, HDACis have been found to block blood vessels formation by blocking the expression of angiogenesis-related genes such as Hypoxia-inducible factor - 1 α (HIF-1 α) and its target Vascular Endothelial Growth Factor Receptor-2 (VEGF) gene. They also upregulate genes that are known by their angiogenesis suppressing role such as p53, von Hippel–Lindau (VHL, a tumour suppressor), Neurofibromin 2 (NF2), and Thrombospondin-1 (TSP1) ⁸⁵.

1.5.4 HDACis Interfere with Cell Cycle

In cancer HDAC 1, 2, 3, 4 and 6, have been reported to have a considerable involvement in cell cycle progression and proliferation ⁷⁸. For example, the lack of HDAC1 and HDAC2 expression stops cell progression to G1 phase both in normal and cancer cells therefore, selective inhibition of these HDACs has been proposed to inhibit cancer proliferation ⁸⁶. Also, it has been found that diminishing HDAC4 expression is associated with an increase in Cyclin Dependent Kinase Inhibitor 1A (p21^{WAF1}) expression in some cancer cells which contributes to inhibiting tumour cell growth and stimulates apoptosis ⁸⁷.

1.6 The HDACis used in this study

HDACis are a family of large and diverse naturally occurring and synthetic compounds that have different structures, function and specificity. Generally, HDACis can be classified into four structural groups; hydroxamic acid, cyclic peptides, bibenzimides, and short-chain fatty acids. Each HDAC inhibitor comprises three domains; a zinc-binding domain which chelates the zinc cofactor of a HDAC and inactivates its enzymatic activity, a surface binding domain that blocks the entrance of a HDAC channel to the active site, and a linker which connects the previous two domains and fills the hydrophobic channel leading to the HDAC catalytic site ⁶⁰ (Figure 6). In this study, five HDACis were used and the following sections will give a brief overview about each inhibitor. See Appendix 2 for more information about the chemical properties of these inhibitors.

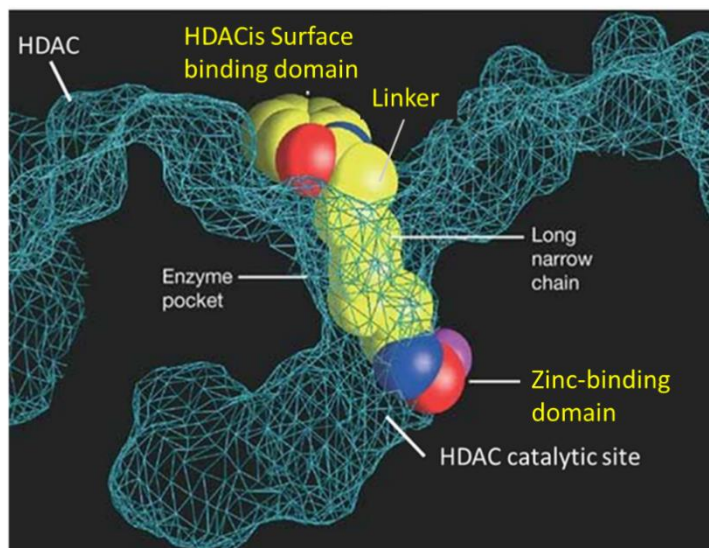


Figure 6: Representation of HDACis blocking the catalytic domain of a HDAC enzyme

HDAC inhibitor comprises of three domains; a zinc-binding domain which chelates the zinc cofactor of a HDAC, a surface binding domain, and a linker. Adapted from Kevin et al., 2005⁸⁸.

1.6.1 SAHA (Vorinostat)

SAHA is a hydroxamic acid class HDACi and it is the first HDAC inhibitor approved by FDA-approved to treat Cutaneous T-cell lymphoma, non-Hodgkin's lymphoma and mantle-cell lymphoma^{60, 89}. In solid cancers, using SAHA as single treatment was ineffective in most clinical trials and it has been strongly recommended to use SAHA either in combination with other treatment or prior using conventional cancer treatments⁹⁰. SAHA shows a high effectiveness in inhibiting class I and class IIb in a sub-micromolar range⁹¹. *In vitro* analysis showed that SAHA exhibits rapid kinetic binding rate and it induces rapid acetylation, in particular with Acetyl-Histone H2B Lys5 (H2BK5) and Acetyl-Histone H4 Lys12 (H4K12). Washout of SAHA induces a rapid dissociation of SAHA kinetic binding followed by decrease in acetylation to the basal level⁹¹. SAHA stimulates cellular apoptosis through activating TRAIL expression in breast cancer and ROS in leukaemia⁷⁸.

1.6.2 MS-275 (Entinostat)

MS-275 is a benzamide class HDAC inhibitor characterized by its slow binding and dissociation properties which has been attributed to the need to disrupt the hydrogen bonds that connect a protein structure in order to accommodate MS-275 lipophilic aromatic rings⁹¹. MS-275 demonstrates a broad anticancer activity and well-tolerated side effects in the Phase I clinical trials of acute myeloid leukaemia and refractory solid tumour⁹². On the molecular level MS-275 exhibits a greater HDAC isoform selectivity to class I HDACs with sub-micromolar effectiveness to HDAC1 and 3⁹³.

MS-275 has been found to display dose-dependent effect on cells. For example, at low concentration (1 μ M) MS-275 acts as an antiproliferative agent through increasing the expression of p21^{waf1} growth arresting protein, hypo-phosphorylate Retinoblastoma Tumour Suppressor Protein (pRB), and downregulates the expression of most cell cycle-related proteins including cyclin D1⁹⁴. However, at higher concentrations (5 μ M) it induces early increase in ROS, followed by loss of mitochondrial membrane, cytosolic release of cytochrome *c*, and ultimately triggers apoptosis⁹⁴.

1.6.3 MI-192

MI-192 is benzamide HDAC inhibitor, characterized by its inhibition selectivity to class I HDACs with high affinity to HDAC3 (> 60-fold effective than MS-275) and limited affinity to HDAC2⁹⁵. In Leukaemia, MI-192 has been reported to inhibit TNF and Interleukin 6 (IL-6) production and induced cellular differentiation and apoptosis with no observed effect on normal bone marrow cells⁹⁶.

1.6.4 Apicidin

Apicidin is fungal metabolite that has cyclic tetrapeptide structure and exhibits HDAC inhibiting activity against class I HDAC with a higher affinity to HDAC2 and HDAC3⁹³. Apicidin has been reported to display anti-proliferative activity in many cancers through altering the expression of p21^{WAF1}, cyclin A and E-cadherin⁹⁷. Also, it showed apoptotic activity in leukaemia through Fas/Fas ligand, and activation of mitochondria-dependent caspase⁹⁸.

1.6.5 Valproic Acid

VPA is a short chain fatty acid HDACi with more affinity to class I (HDAC1, 2, 3 and 8) than class IIa (HDAC4, 5, 7 and 9). Clinically VPA was exclusively tested as a monotherapy and it showed improvement in 24% of acute myeloid leukaemia and myelodysplastic syndrome patients ⁹⁹. It has also been approved to treat epilepsy and depression. Combination treatment of VPA with other anticancer drugs appears to be more efficient and less toxic ⁹⁹. VPA has been found to act as a radioprotection for normal hippocampal neurones in radiation therapy through increasing the expression of the anti-apoptotic proteins and downregulating the pro-apoptotic proteins. It has also been found to act as a radio-sensitizer with glioblastoma cells through inducing cell cycle arrest ¹⁰⁰. From more information about the HDACis targets and their effective inhibitory concentrations see table (Table 2).

Table 2: Summary table of HDACis targets and their IC₅₀

HDACis	HDACs Target	IC ₅₀
SAHA	Classes I, II and IV marked decrease in HDAC1 ⁷⁵	10 nM ¹⁰¹
MS275	Strongly inhibits HDAC1, HDAC2, and HDAC3 ⁵⁴	HDAC1 (300 nM) ¹⁰¹ HDAC2 (130 nM) ¹⁰¹ HDAC3 (720 nM) ¹⁰¹
MI192	HDAC2 and HDAC3 ⁹⁵	HDAC2 (16 nM) ⁹⁵ HDAC3 (30 nM) ⁹⁵
Apicidin	HDAC2 and HDAC3 ⁹³	HDAC2 (1 nM) ¹⁰¹ HDAC3 (2 nM) ¹⁰¹
VAP	Class I and II HDAC inhibitor with a high potency for HDAC1 ⁹⁹	0.4 - 20 mM ¹⁰¹

1.7 HDACis Side-Effects

Despite the HDACis favourable outcomes in clinical trials their chronic administration is possibly associated with risk of increasing the side effects and cytotoxicity which could bring fatigue, dehydration, diarrhoea, and moderate thrombocytopenia ⁶¹. In addition, the effect of HDACis on normal neuronal and non-neuronal growing cells and stem cells has not been well addressed yet. In several studies depletion of HDAC1 and HDAC2 in mice has been reported to cause sever structural abnormalities in brain cerebellum and

hippocampus which results in a lethal effect ¹⁰². Depletion of HDAC3 also causes an imbalance between carbohydrate and lipid metabolism and leads to embryonic death ⁶¹. Therefore, using non-selective HDACis to treat cancer could unnecessarily block some HDACs that are required for normal cells function and may result in unfavourable side-effects. This may suggest the importance of understanding the pharmacodynamics of HDACis in tumour and normal cells.

1.8 The Research Background and Questions

1.8.1 REST Contribution in Medulloblastoma

The contribution of REST in medulloblastoma has been an area of disagreement in literature. For example, some studies have suggested elevated REST expression as oncogene due to its ability to blockade the differentiation of cancer stem cells and retain their self-renewal potential, which ultimately contributes to tumour cell proliferation ^{9,10}. Knocking down REST expression in medulloblastoma cell lines such as Daoy and D283 has been claimed to abrogate the tumorigenic potential of the cells and stimulates apoptosis ^{11,14,50}. Whereas, the exogenous induction of REST into normal neuronal progenitors cells has been claimed to stimulate tumour formation and maintain the self-renewal potential of neuronal stem cells ⁵³.

In contrast, the gene expression studies of medulloblastoma have not proposed REST involvement, or at least its exclusive repression of the RE1-containing genes, in medulloblastoma tumorigenesis ^{39,41,44,103}. Also none of the medulloblastoma genome sequencing studies have identified any direct or indirect genetic mutations that could contribute to increasing REST expression ^{42,104}. These conclusions are further supported by a recent study which revealed that knocking down REST using an shRNA system resulted in inhibiting glioblastoma cells migration yet, it did not stimulate cell death or reduce tumour size ¹². Therefore, this research was set out to obtain more knowledge about the contribution of REST in the Daoy medulloblastoma cells growth and treatment.

1.8.2 HDACis Molecular Action in Tumour and Normal Cells

Treating with HDACis results in increasing the acetylation level both in normal and transformed cells ^{105,106,107,108}. However, it is not known how HDACis induce their anticancer effect in tumour cells and what are the consequences of the HDACis treatment

on the normal cell gene expression. This study aimed to investigate the anticancer mechanism of HDACis in the Daoy medulloblastoma cells and explore their effect on normal neurons.

1.8.3 The Research Hypothesis and Questions

In this study I hypothesized that:

- Elevated REST expression in medulloblastoma cells sustains tumour cell growth.
- HDACis induce their anticancer effect through the HDACs recruited in REST repression complexes
- The study also explored the HDACis molecular regulation in Daoy medulloblastoma cells and examined their effect on normal neurons

This study aimed to address the following research questions:

- Is REST expression elevated in all medulloblastoma subgroups?
- Does REST expression have a main contribution in sustaining the growth of the medulloblastoma?
- What is the effect of HDACis on the cell cycle?
- What is the effect of modulating REST on the expression of RE1-containing genes?
- Does REST expression play a role in tumour cell migration ability?
- Do HDACis induce their action through the HDACs recruited in REST repression complexes?
- What molecular mechanisms and pathways are mainly targeted by the HDACis?
- What is the effect of HDACis on normal neuronal cells?

Chapter 2

2 Material and Methods

2.1 Introduction

2.1.1 The Experimental Model

Studying brain tumours in general, and medulloblastoma in specific, has been an area of hindrance due to; the intertumoral and intratumoral genetic variations, limited primary tumour samples, and the tissue samples are often contaminated with a mixture of genetically variant cancerous and non-cancerous cells. Hence, the cancer cell lines could be the ideal model to understand the molecular regulations prior examining the therapeutic potential on animal model and eventually in clinical trials.

Cancer cell lines have been the foundation of cancer treatment research as they are easy to expand, comparatively uniform, and their research outcomes can be reproduced. Though, they have been an area of criticism as not always known from what type or subtype of cancer a particular cell line was generated from, or to what extent a specific cell line resembles the original cancer after years in culture⁴³. The established cell lines are selected from specific tumour subsets that grow under *in vitro* culture conditions and this selection does not represent the diversity of human tumours¹⁰⁹. Therefore, cell lines do not completely mimic the primary cells and they usually used in the absence of their local environment which often contains many interactions with other cell types¹¹⁰. The culture conditions and the infections with mycoplasma can also affect the morphology, the gene expression, the cellular pathways, and the response of a cell line toward tested drugs could be different from patient response. Hence, with many studies, what it has been therapeutically promising in cell lines and animal models comes back negative in clinical trials¹¹¹. This may express the importance of identifying a cell line that best mirrors a particular medulloblastoma condition, which will considerably help in generating more accurate disease picture both in primary and preclinical research.

Comparing to other tumours, medulloblastoma has relatively less cell lines which it could be due to the rarity of the tumour and the difficulty of establishing a continuous cell line from paediatric brain tumour. Currently, there are around 44 medulloblastoma cell lines have been produced over a period of four decades⁴³. Eighteen of these cell lines have only

been classified into the current medulloblastoma subgroups; eleven cell lines grouped under Group 3, four cell lines sub-grouped with SHH, two cell lines under Group 4, and one cell lines represents the WNT medulloblastoma¹⁵. Among these cell lines, Daoy has been the most frequently used cell in literature to study medulloblastoma¹⁵.

The Daoy cell line was established in 1985 from a biopsy taken from a posterior fossa tumour of four-years-old boy¹¹². The cell has a polygonal shape with irregular shaped-nucleus, prominent nuclei, multiple nucleoli, and the cytoplasm contains a large number of rough endoplasmic reticulum, Golgi apparatus and many small mitochondrial aggregates¹¹². On the chromosome level, the cell is hypertetraploid with 93 to 99 chromosomes and two normal X chromosomes however, the Y chromosome is not detectable¹¹². The Daoy cell expresses a mutated non-functional form of p53 protein as the *TP53* gene has a single point mutation at base 725, which results in substituting the phenylalanine at amino acid 242 by a cysteine¹¹³. The original tumour of the cell reported to show both of neuronal and glial phenotypes though, the cell line dose not retain these phenotypes and it has been reported to contain a mixture of CD133⁻ and CD133⁺ side population^{43,114}. Based on the current molecular profiling of medulloblastoma, Daoy was classified as SHH subgroup with mutant *p53*⁴³. Elevated REST expression in Daoy has been reported in a large number of literatures which brands the cell as an ideal modal to study the effect of REST modulation on tumour cell growth and to study its functional effect on the RE1-containing genes^{11, 14, 52, 115}. Hence, Daoy was used in this research as an experimental model for medulloblastoma.

To study the effect of hyperacetylation on normal cells, the cerebellum cells are possibly the most appropriate counterpart of medulloblastoma however, due to the unavailability of such cells the analysis was performed using primary human neurons (ScienCell, 1520). The neurons were isolated from a male donor and they are categorized as neurons with highly communication networks. As a result of limited amount of the neurons they were exclusively used for the analysis and their sensitivity to the used HDACis was not examined.

2.1.2 Modulating REST Expression using CRISPR/Cas9 and shRNA

In most of the earlier studies, the shRNA and the REST-VP16 knockdown approaches were the tool of choice to uncover the contribution of REST in medulloblastoma,^{14, 50, 53,}

^{116, 117, 119}. However, these approaches showed some limitations as the efficiency of the knockdown is highly variable between studies and they do not completely block the expression of REST, which may affect the interpretation of REST contribution in cancer. Therefore, in this study the CRISPR/Cas9 system was used to completely knockout REST expression. As the CRISPR/Cas9 system has not been used before to modulate REST expression, the shRNA knockdown approach was used to further confirmed the results of the knockout.

2.1.2.1 CRISPR/Cas9 to Knockout REST Expression

CRISPR/Cas9 is one of the tools that has a high degree of accuracy to modify DNA sequence and interrupt gene translation. CRISPR (or Clustered Regularly Interspaced Short Palindromic Repeats) is a pre-designed sequence of around 20 RNA bases known as guide RNA (gRNA) designed to target a unique complementary sequence in genome. Also, it contains a recognition component for CRISPR associated protein 9 (Cas9) endonuclease enzyme known as Protospacer Adjacent Motif (PAM) and located at the 3' end. Both the gRNA and PAM sequences are integrated within a longer RNA scaffold which encompasses a sequence-code that activates Cas9. Cas9 is a *Streptococcus pyogenes* immunity system used with CRISPR to cleave the DNA at the PAM site which could result in activating either the non-homologous end joining (NHEJ) or the homologous recombination (HR) DNA repair systems ¹¹⁸. The NHEJ repair pathway is the most dynamic mechanism and it frequently causes small nucleotide insertions or deletions (indels) at the double-strand break site which leads to disrupting the open reading frame of a gene. Whereas, the HR repair pathway can be utilized to insert specific homologous nucleotide sequence immediately upstream or downstream of the target sequence. In this study, I used pCas-Guide system (Origene) which characterized by its ability to produce both of the gRNA and the Cas9 expression sequences (Figure 7).

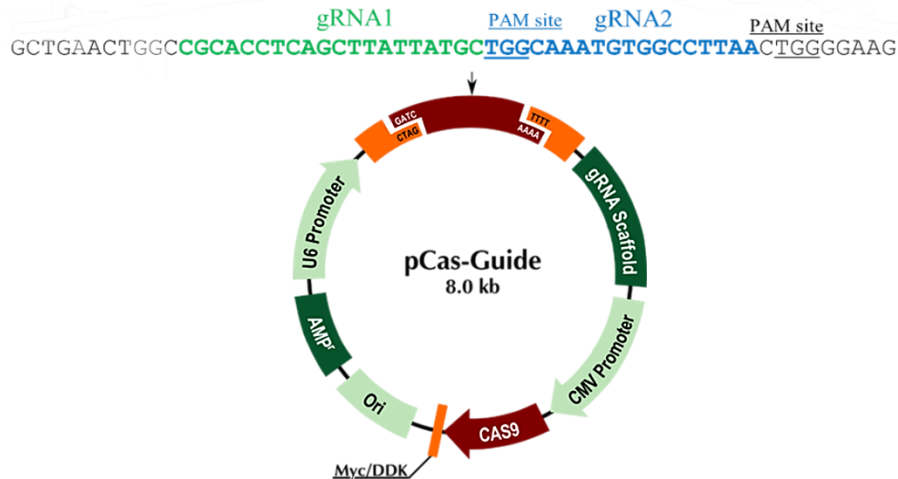


Figure 7: The map of the pCas-Guide Vector

The pCas-Guide is an 8-kb vector, designed for cloning a gRNA insert between a U6 promoter and gRNA scaffold. The vector contains a Cas9 cassette driven by a CMV-optimized codon and an ampicillin resistance gene for *E. coli* transformation selection. The sequence above shows the gRNA1 (green) and its PAM site (black), and the gRNA2 (blue) and its PAM site (black).

2.1.2.2 shRNA to Knockdown REST Expression

short hairpin RNA (shRNA) is an artificial double-stranded RNA molecule used to cleave mRNA and knockdown the expression of gene. In this study, the shRNA was delivered into the Daoy cell through an expression vector (pSUPER-Puro) which has a Phosphoglycerate Kinase promoter (PKG) promoter sequence located before the cloning site and it helps in achieving a robust expression of the shRNA (Figure 8 A). Also, the plasmid contains a puromycin resistance *PUR* gene which protects the cell from the lethal effect of the puromycin selective treatment.

Once the vector is integrated into a cell genome, the transcription of the shRNA starts by producing a *pre-miRNA* (a hairpin RNA) which then processed by Nuclear RNase III enzyme (Drosha) into approximately 70 base pairs long known as small hairpin RNA (*shRNA*). The resulted *shRNA* is exported by Exportin 5 into the cytoplasm where the connection loop is further processed by ribonucleases (Dicer). The antisense (guide) strand is then loaded into a ribonucleoprotein known as RNA-induced silencing complex

(RISC) and when the sequence of the guide-strand perfectly matches a complementary mRNA sequence, the enzymatic activity of the RISC is activated and results in degrading the mRNA and silencing the transcription ¹¹⁹ (Figure 8 B).

In small proportion of the transfected cell, the pSUPER-Puro plasmid is integrated into the cell genome and passed into the cell progeny. This causes a stable expression of the *shRNA* which sustains the knockdown of REST expression. The selection for the stable expression can be achieved by exposing the cells to Puromycin (an amino-nucleoside antibiotic) which acts by covalently binding to the elongated polypeptide chains on ribosomes resulting in terminating protein synthesis and cell death. Though, cells that express the puromycin resistance gene (*puro*) inactivates the cytotoxic effect of puromycin ¹²⁰.

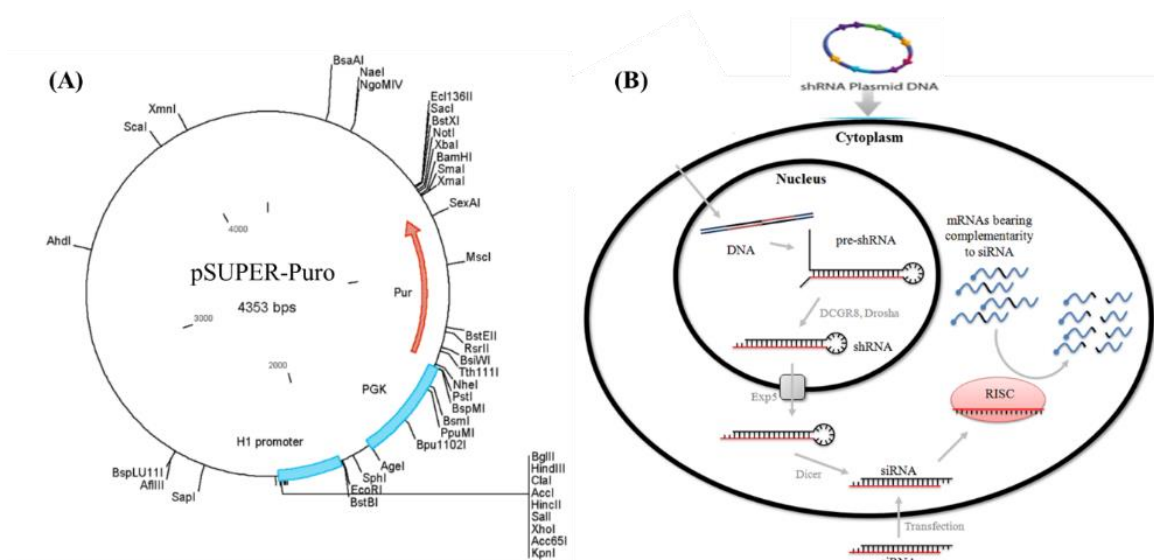


Figure 8: pSUPER-Puro vector map and the shRNA knockdown concept

(A) *pSUPER-Puro* is 4.3 kb mRNA expression vector contains an mRNA cloning site driven by polymerase-III H1-RNA gene promoter. Also, it contains a puromycin resistance *Pur* gene cassette driving by the PGK promoter. This vector produces a small RNA transcript missing the polyadenosine tail though, it contains five thymidine bases (T5) signal at the start of the transcription and at the termination site. The termination site is after two uridine bases, which yields a transcript that has similar ends to the synthetic shRNA. (B) An illustration for the shRNA knockdown mechanism.

2.1.3 Profiling the Gene Expression at Single Cell Level using the 10x Genomics Chromium Single Cell 3'

One of the aims of this study is to investigate the molecular regulations of the HDACs and the HDACis in tumour and normal cells at the transcriptome level. Until recently, the method of choice to address such research question was profiling gene expression using microarray analysis yet, the sensitivity and the accuracy of this approach tend to be relatively low especially with gene that show low expression. Also, the microarray results should be used for screening only and the findings should be conformed using qPCR analysis. With the advance in Next Generation Sequencing (NGS), the bulk gene expression profiling by the RNA-seq has been the preferable alternative due to its high analytical sensitivity and accuracy. This research work was originally designed to be performed using the bulk NGS analysis (see Appendix 3 and Appendix 4 for more information about the suggested NGS plan). However, with the advance in the NGS analysis, the single cell NGS (scNGS) has become the method of choice to avoid the effect of cells heterogeneity especially, and it provides a higher statistical power data to dissect the molecular regulation of an individual cell in a diverse population of cells. With the single cell analysis approach measuring the gene expression at a single time point could be sufficient to uncover the molecular regulation and understand the differences between the cells. For example, at an early time point of treatment, there will be a mixture of cells at their early and late stages of apoptosis, cells that have not initiate the apoptosis mechanism and they will die during the late hours of the treatment. These cells are also distributed among each phase of cell cycle.

The scNGS is a gene expression profiling technique that measure the expression at an individual cell level. The main concept of the scNGS is relying on barcoding the mRNA with specific DNA sequence during the reverse-transcription step and measuring the transcripts using the NGS. The barcodes were then used to index the transcripts back to their original cell. Currently, there are several platforms of scNGS all share the previous concept but, they are mainly different in; the way of partitioning the cells into a single cell reaction, and in their ability to target few hundreds to several thousands of single cells at a time. In this study, the scNGS analysis was performed using the 10x Genomics Chromium platform.

This platform mainly depends on partitioning a single cell suspension into nanolitre-scale reaction vesicles known as Gel Bead in Emulsions (GEMs). The GEMs are formed on a microfluidic chip by combining; gel beads containing barcoded oligonucleotides, in parallel with the single cell suspension within an oil vesicle (Figure 9). This allows producing hundreds to tens of thousands of single cells reaction vesicles in less than 7 minutes using the Chromium Instrument. The gel beads contain an Illumina R1 sequencing primer, a 10x barcode of 16 nucleotides (used to associate the individual reads back to the individual cells), a unique molecular identifier (UMI) of 10 nucleotides (10X Barcode, used to; count the number of reads of specific sequence, identifies transcriptomes from individual cells also, helps in reducing the bias and the noise created during the cDNA amplification), and a poly-dT primer. Whereas, the single cell suspension contains a mixture of RT primers and enzymes mix. Within each GEM reaction vesicle, the poly-adenylated mRNA was reverse-transcribed and used to generate a barcoded full-length cDNA containing the Illumina Read 1 (a primer site for sequencing read 1 and used to encode UMI), the 10x Barcode, and the UMI. After lysing the GEMs, the contents of the gel beads are mixed with; the cell lysate, and the master mix. Due to the small amount of the mammalian transcriptome (10 picograms (pg) of the RNA and 0.1 pg the mRNA in a typical cell) the full-length cDNA is amplified first. Simultaneously, the Illumina P5 primer, the Read 2, the sample index (i7), and the P7 primer (used for Illumina paired-end sequencing) are incorporated in the cDNA library. The Read 1 is used to sequence the 10x barcode and the UMI whereas, the Read 2 is utilized to sequence the cDNA fragment. Next the library is sequenced on Illumina sequencers using paired-end sequencing with single indexing.

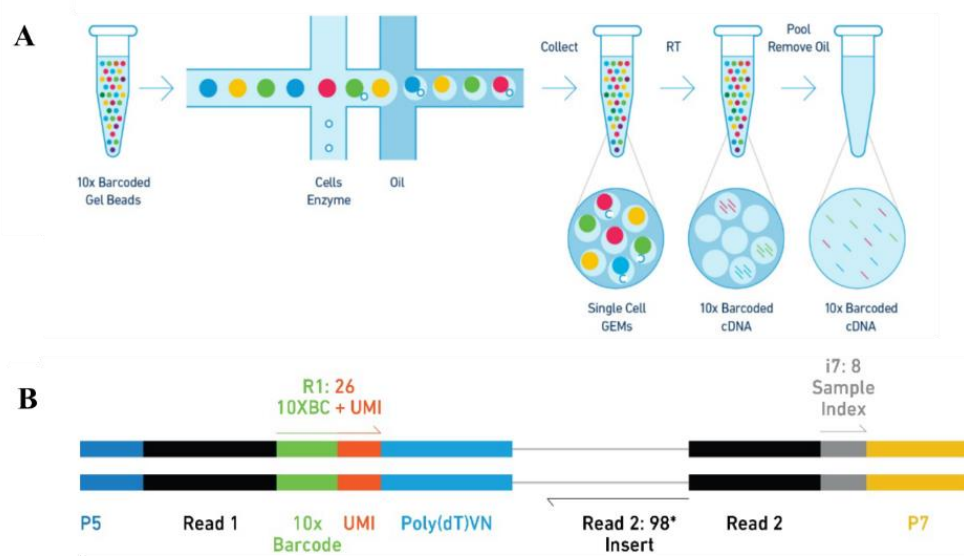


Figure 9: 10x Genomic Single Cell Generation and Library Construction

The 10x Genomics platform uses emulsion-tagging to generate single cell reaction vesicles or GEMs. The generation of GEMs is performed on a microfluidic chip by encapsulating gel beads and a single cell suspension within an oil vesicle (A). When dissolution the mixture, the reaction generates full-length cDNA from poly-adenylated mRNA containing Read 1, 10x Barcode, and UMI. The cDNA is then amplified and the Illumina P5 primer, the Read 2, the sample index (i7), and the P7 primer are incorporated into the cDNA library (B). Next, the library is sequenced on Illumina sequencers using paired-end sequencing with single indexing. Read 1 is used to sequence the 10x barcode and the UMI, where Read 2 is utilized to sequence the cDNA fragment. (The images above were adapted from the 10x Genomics website (<https://www.10xgenomics.com/>)).

2.1.3.1 Selecting the HDACis

In this study, five HDACis (SAHA, MS-275, MI-192, Apicidin, and VPA) were used in studying the contribution of REST in medulloblastoma. Yet, due to the high cost of the scNGS analysis, the gene expression profiling was performed using SAHA and MS-275. The selection criteria for these two inhibitors were based on the inhibitor potency, selectivity, and if the inhibitor has been in clinical trials. In the Daoy cell analysis, all the five inhibitors showed high anticancer activity apart from the VPA hence, it was excluded.

MI-192 and Apicidin showed high affinity to HDAC3 and HDAC2 and HDAC3, respectively. MI-192 was not selected as it has not been thoroughly investigated, and both of MI-192 and Apicidin have not been in clinical trials. SAHA is a pan-inhibitors and was approved for clinical used whereas, MS-275 showed higher selectivity to HDAC 3 and 2 and it has been in phase II clinical trial ⁶⁰. Both of SAHA and MS-275 showed differences in the onset of their anticancer activity which attract research interest. Hence, the scNGS analysis was performed using SAHA and MS-275.

2.1.3.2 The Cell Number and the Sequencing Depth of the scNGS

The number of targeted cells and the transcript sequencing depth are important factor for the scNGS analysis. There are no specific criteria for targeting a specific cell number yet, the required number increases with the increase in the heterogeneity of the cells. Undoubtedly, it is difficult to predict the degree of the heterogeneity however, the required number might be estimated based on the flowcytometry data. As mentioned earlier, the Daoy cell-line has been reported to contain a mixture of CD133⁻ and CD133⁺ side population whereas, the human neurons is a mixture of neurons and glia cells ^{43, 114}. It should be considered that with the Chromium technology there is an increasing chance of multiplets (two or more cells within a GEM) rate with the increase in the number of loaded cells. Also, the presence of dead cells in the cell suspension could reduce the number of the observed cells. Once the library prepared, the number of the successfully targeted cells can be estimated using the UMI. Generally, the more cells the greater the statistical power, and in this study, we aimed to target 2000 cell for each sample.

The sequencing depth (Coverage) with the scNGS analysis represents the number of the detected transcripts for each cell and can be estimated by normalizing the library as per the recommendations of the Illumina sequencing platforms. The recommended sequencing depth for the 10x scNGS is ranged from 50.000 to 100.000 reads/cell whereas, the deeper sequencing often leads to saturation and does not improve the number of the detected genes ¹²¹. In this study, we aimed to reach to a read depth of 100.000 reads/cell.

2.2 The Methods

2.2.1 Standard Cell Culture

The human medulloblastoma Daoy cell-line was purchased from ATCC (HTB-186). The SH-SY5Y and HeLa cells were obtained from Dr I. C. Wood. The cells were cultured in Dulbecco's Modified Eagle's Medium (DMEM, Life Technologies) supplemented with 10 % (v/v) Fetal Bovine Serum (FBS, PAA Cell Culture Company) and 1% (v/v) Penicillin & Streptomycin (Sigma). The cells were grown at 37°C humidified incubator in 5% CO₂ air. Subculturing of the cells was performed every fourth day or when they reached a confluency of approximately 80-90%. The subculturing was carried out by removing the old culture media and washing the cells with 10 mL of room temperature phosphate buffer saline (PBS, Oxoid [Dulbecco A, 10 mM phosphate buffer, 2.7 mM potassium chloride and 137 mM sodium chloride, pH 7.4, at 25 °C], 1 tablet in 100 mL of ddH₂O, solution was autoclaved) for one time. The cells were treated with 1 mL of Trypsin-EDTA (Sigma) to dislodge the cells from the bottom of the culture plate and incubated at 37 °C incubator for 5 minutes. The cells were then examined under a microscope to check for their detachment and rounded appearance. Around 9 mL of complete culture media was used to deactivate the trypsin, and the cells were released by pipetting the media up and down for 3 times. The cell suspension was transferred into 15 mL sterile conical tube. The cells were pelleted by centrifuging the tube at 400 g for 5 minutes, and the supernatant was removed by aspiration without disrupting the cell pellet. The pelleted cells were re-suspended in 5 mL complete culture media by gently pipetting the cells up and down to break up the clumps using a 10 mL serological pipette. New subculture plates were prepared by using 1 mL of the resuspended cells with 9 mL of complete media and incubated at 37°C in a humidified incubator at 5% CO₂ air. All experiments were conducted on cells with fewer than 15 passages.

The confluency of the cell was determined qualitatively using an inverted microscope and the confluence was defined as the proportion of the culture surface that was covered by the cells at the time of measurement (a confluency of 50 % means half of the culture surface was covered by cells).

2.2.2 Culturing the Human Neurons

Neurons from human brain (P0) were purchased from ScienCell (#1520) in a cryopreserved form. Prior culturing, the surface of a 6-well culture plate was coated using 2 μL of poly-L-lysine (10 mg/mL, ScienCell) in 2 mL of sterile water and the plate was left in a 37°C incubator overnight. The wells were washed twice with sterile water prior to use and the neurons were seeded using complete Neurons Medium (NM, contains neuronal growth supplement and penicillin/streptomycin solution, ScienCell) at a seeding density of $\sim 2.5 \times 10^4$ cells/well. The plate was incubated at 37°C humidified incubator in 5% CO₂ air for 16 hours and the media was replaced with 2 mL fresh culture medium. The neurons were left in culture for 48 hours before treating them with the HDACis.

Harvesting the neurons was carried out by removing the old culture media and washing the cells for 3 times with 2 mL of cold phosphate buffer saline (ScienCell). The culture plate was then rocked back and forth for a few times and the PBS was drawn out by aspiration. The cells were overlaid with 300 μL of Tryple Express (Gibco) to dislodge the cells from the bottom of the culture plate and incubated at 37 °C incubator of 7 minutes. The cells were then examined under a microscope to check for their detachment and rounded appearance and 1 mL of the NM was used to deactivate the Tryple Express, the cells were released by pipetting the media up and down for 3 times, and the cells suspension was transferred into 15 mL sterile conical tube. The cells were pelleted by centrifugation at 400 g for 2 minutes and the supernatant was removed by aspiration without disrupting the cell pellet.

2.2.3 Identifying a Suitable Daoy Seeding Density for HDACi Treatment

The Daoy cells were seeded into 24-well culture plates (Nunc Cell-Culture Plate) using following concentrations: 1×10^4 , 2×10^4 , 5×10^4 , and 1×10^5 cell/mL. The cells were harvested at 24, 48, and 72 hours post seeding using Trypsin-EDTA as described above. Post Trypan Blue staining (0.4%, Sigma), the cells were gently mixed and 25 μL of the stained cells were loaded underneath the coverslip of a cleaned haemocytometer allowing the cell suspension to be drawn out by capillary action. The count was performed using Neubauer haemocytometer under an inverted microscope. The cells with a dark blue staining were considered dead and excluded from the count. The total number of viable cells was calculated by dividing the cell count by 4 (the average), multiplying by (10^4) and

then by 2 to correct for trypan blue addition. To measure the sensitivity of the cells to HDACis, the cells were seeded at 3.5×10^4 cell/mL in 6-well culture plates and treated with HDACis (Table 3). The cells were harvested (at 24, 48, and 72 hours) and counted as described in section 2.2.3).

2.2.4 HDACis Preparation

The HDACis SAHA(10009929); MS-275(13284); MI-192(18288); Apicidin(10575) were purchased from Cayman and were dissolved in DMSO. Hence, a DMSO cell-treated control was included in all experiments. VPA was purchased from Sigma (P4543) and was prepared in water.

2.2.5 Generating the Dose Response Curves, and Measuring the Cells Proliferation Rate and the Sensitivity to HDACis

To generate the HDACis dose-response curves and to study the proliferation rate and the sensitivity of the cells to the inhibitors, the Daoy cells were harvested and counted as described previously (section 2.2.1) and a cell concentration of 3.5×10^4 cell/mL was used to seed 96-well culture plates (Greiner). The plates were left at room temperature for 30 minutes to allow even distribution of the cells throughout the wells and then the plates were incubated at 37°C in 5% CO₂ air for 24 hours. HDACis treatment was carried out by carefully replacing the culture media with complete media containing the required concentration of the drugs (Table 3). The plates were re-incubated at 37°C in 5% CO₂ air and the viability of the cells was measured after 72 hours from the treatment for the ‘dose response analysis’ and at 24, 48, and 72 hours for the ‘sensitivity’ experiment. The proliferation rate was measured at 24, 48, 72 and 96 hours or every 24 hours over a period of 7 days. All the measurements were performed using the colorimetric MTT assay (section 2.2.6).

Table 3:HDACis concentrations used to produce the dose-response curves

SAHA (μM)	MS-275 (μM)	MI-192 (μM)	Apicidin (μM)	VPA (mM)
0.003	0.01	0.003	0.003	0.3
0.01	0.03	0.01	0.01	1
0.03	0.1	0.03	0.03	3
0.1	0.3	0.1	0.1	4
0.3	1	0.3	0.3	5
1	2	1	1	10
2	3	2	2	12
3	4	3	3	13
4	5	4	4	14
5	6	5	5	15
Concentrations used to study the effect of REST expression modulation				
5 μM	5 μM	3 μM	3 μM	10 mM

2.2.6 The MTT Assay

The principle of this assay depends on the activity of mitochondria in viable cells to convert tetrazolium MTT (3-(4,5-dimethylthiazol-2-yl)-2,5-diphenyl-tetrazolium bromide) dye to formazan colour by Nicotinamide Adenine Dinucleotide Phosphate (NADPH) oxidoreductase enzyme. The MTT stock solution was prepared by dissolving 5 mg of the MTT powder (Sigma, M5655) in 1 mL of PBS. The solution was then stored in 500 μL aliquots at -20°C . The MTT working solution (0.5 mg/mL MTT) was prepared by 1:9 dilution using culture media. The MTT assay was performed by gently aspirating the culture media using a multichannel pipette and adding 50 μL of the 0.5 mg/mL MTT working solution. Subsequently, the plates were re-incubated for 90 minutes at 37°C in dark. The solution was then replaced with 100 μL of acidified isopropanol solution (0.04 M HCL) and the plates were covered with foil and placed on an orbital shaker (~ 300 rpm, Stuart SSM1) at room temperature for 15 minutes. The absorbance of the MTT was measured at 590 nm wavelength with a reference filter of 720 nm using a spectrophotometer plate reader (FLUOstar Omega, BMG Labtech).

The cellular viability was calculated by subtracting the blank value (720 nm) from the formazan absorbance (590 nm). At least, 6 biological repeats with 3 technical replicates

were performed for each condition and the average of all the biological replicates was used to represent the cells responses.

2.2.7 Calculating the Doubling Time

The doubling time of the Daoy wildtype, REST knockout and knockdown cells was estimated using the results of the MTT assay. The calculation was performed by subtracting the time value of the 0.8 MTT absorbance on the proliferation curve from the time value of the 0.4 MTT absorbance.

2.2.8 Modulation of REST Expression

2.2.8.1 Knockout REST Expression Using the CRISPR/Cas9 System

The CRISPR/Cas9 system was used to disrupt *REST* gene expression. Two guide RNA sequences (gRNA) were designed using the OriGene Technologies CRISPR/Cas9 tool, (**gRNA1**: 5'- CGCACCTCAGCTTATTATGC-3', and **gRNA2**: 5'- TGGCAAATGTGGCCTTAACT-3')¹²². Both sequences were followed by (TGG) PAM sequence and cloned into pCas-Guide vector (pCas-Guide1 [OriGene, KN211570G1], pCas-Guide2 – [OriGene, KN211570G2]) in addition to the antisense strand of the later gRNAs sequences. A negative scramble-targeting (control) vector (OriGene, GE100003) of 20 bp sequence, which does not target any sequence, was included in the transfection reactions.

The transfection reactions were performed in 6-well culture plates (Nunc Cell-Culture Plate) with a cell confluence of 50-70%. The transfection solution was prepared by gently pipetting up and down 6 µL of Lipofectamine 2000 transfection reagents (Invitrogen, Life Technology) in 250 µL of the Opti-MEN media and the tubes were incubated at room temperature for 20 minutes. The vectors (pCas-Guide1, pCas-Guide2, and Scramble control) mixtures were prepared by diluting 2 µg of vector in 250 µL of a pre-warmed Opti-MEN serum reduced medium (Gibco, 31985062) and left at room temperature for 5 minutes. The diluted DNA was then added into the lipofectamine solution using a 1:1 ratio. Prior the transfection, the cells were washed with sterile PBS for two times and 1 mL of basal DMEM media was added into each well. The transfection mixture was added in a dropwise manner and the plate was gently rocked back and forth and incubated at 37°C incubator in 5% CO₂ air. After 4 hours, the transfection media was replaced with 2 mL complete DMEM media and the plate was re-incubated for 48 hours.

Monoclonal cell culture was established by seeding 96-well plates with a cell concentration of 1 cell/100 μL of the CRISPR/Cas9 transfected cells. After 5 days from the seeding, wells with monoclonal cell growth were identified microscopically and left to grow for two weeks with replacing the media every 7 days. After 14 days from the seeding, a daughter plate was prepared by harvesting the cells as described previously (see section 2.2.1) using 25 μL of Trypsin-EDTA, and 70 μL of the culture media was pipetted up and down to detach the cells. From each well, 30 μL of the cells was then transferred into a new 96-well culture plate containing 70 μL of complete media and the cells were re-grown to 90-100% confluency.

The screening for the genome editing was performed by sequencing REST exon 2 using the DNA Sanger sequencing facility at Beckman Coulter Genomics service (Stortford). The efficiency of the knockout was verified using Western blot and SYBR green qPCR analysis and the cells with genome editing were propagated for further analysis.

2.2.8.2 Knockdown REST Expression using the shRNA System

To knockdown *REST* expression, two shRNA sequences were designed using human homologue sequences of previously used mouse shRNA sequences (Gao et al., 2011)²³. The homologous human sequences were; 5'-AGTGTAATCTACAGTATCAC-3' which targets *REST* exon4; and 5'-AGCAGAATCTGAAGAACAGT-3' which targets exon2. The designed sequences were; **shREST1**: 5'-AGCTAAAAACAGTGTAATCTACAGT ATCACTTCTCTTGAAAGTGATACTGTAGATTACACT-3', and **shREST2**: 5'-AGC TAA AAAAGCAGAATCTGAAGAACAGTTTCTCTTGAAAACACTGTTCTTCAGATT CTGCT-3'.

2.2.8.2.1 The shRNA Sequence Annealing

Annealing the forward and reverse sequences of the two shRNA was performed by mixing 1 μL of the forward and the reverse sequences (100 μM) with 48 μL of annealing buffer (100 mM NaCl, and 50 mM HEPES pH7.4). The mixture was incubated at 95°C in a heating block to denature the oligoes and after 5 minutes the heating block was turned off and left to cool down at room temperature in order to allow the oligo to anneal. When the block temperature reached 40°C the tubes were transferred into ice and 100 μL of sterile

distilled water was added into each tube. The oligos were either used directly in ligation reactions or stored at -20°C.

2.2.8.2.2 The pSUPER-Puro Plasmids Preparation and Linearization

pSUPER-Puro plasmid was prepared by streaking a loop-full suspension from glycerol stocks on ampicillin LB agar plates (2 % of LB Broth [Sigma] in H₂O supplemented with 1.5 % agar [Melford] and 100 µg/mL ampicillin [Sigma]) and incubated at 37°C. After 24 hours, a single colony was cultured in 100 mL LB broth (2 % of LB Broth [Sigma] in H₂O, supplemented with 100 µg/mL ampicillin) and incubated at 37°C in a shaker incubator. The plasmid was extracted after 24 hours using HiSpeed plasmid midi kit (Qiagen; 12663) and processed according the manufacturer's instructions.

pSUPER plasmid was linearized using HindIII and BamHI restriction digestion enzymes. All restriction digestions were carried out in a reaction mix of 10 µL containing; 5 units of the restriction enzymes (New England BioLabs), 1 µL of 10x restriction enzyme buffer, 1 % BSA (supplied by the enzyme manufacturer), 5 µL of the pSUPER-Puro DNA, and the volume was brought up to 10 µL using ddH₂O. The reactions were incubated at 37°C for one hour and then stored on ice. The restriction digestion products were analysed on a 1.2% agarose gel via electrophoresis.

2.2.8.2.3 The shREST-pSUPER Plasmid Construction

The annealed shREST1 and shREST2 molecules were cloned into the linearized pSUPER plasmid using; 1 µL of T4 DNA ligase enzyme (New England BioLabs), 1 µL of 10X ligation buffer (supplied by the enzyme manufacturer), 2 µL of the annealed oligonucleotides (~ 40 nM), 1 µL of the linearized pSUPER, and 5 µL of sterile distilled water. The cloning reactions were performed by incubating the tubes at room temperature overnight. A negative control containing the linearized vector and no insert was included with each ligation reaction.

2.2.8.2.4 The shREST-pSUPER Plasmid Transformation

Transformation into *E. coli* competent bacteria was performed using a heat-shock transformation reaction. The reaction was performed by thawing competent cells (XL1-Blue Subcloning-Grade, Agilent Technologies) on ice for 10-15 minutes and 50 µL of the

bacteria were transferred into a pre-chilled 14 mL BD Falcon tube and kept on ice. A volume of 2 μ L of the cloning products were gently mixed with the cells by pipetting up and down for few times and the tube was incubated on ice for 20 minutes. The cells were then heat-shocked at 42°C for 45 seconds and immediately incubated on ice for 2 minutes. A volume of 900 μ L preheated (42°C) SOC medium (Thermo-Fisher) was added into each tube, and the cells were then revived at 37°C in a shaker incubator (~230 rpm, Sanyo orbital incubator MIR-220RU) for one hour. The transformed bacteria were then grown on pre-warmed ampicillin (100 μ g/mL) LB agar (5g Tryptone, 2.5g Yeast extract, 2.5g NaCl, 1.5% Agar, ddH₂O to 500 mL, media was autoclaved and stored in 4°C, the mixture was autoclaved, supplemented with 100 μ g/mL ampicillin and poured into plates) plates by spreading all the transformation mixture evenly around the surface of the agar and the plate was left upright to dry with the lid was slightly off. After 10 minutes, the plate was incubated upside down at 37°C for overnight.

In the following day, six random colonies from the LB culture plate were picked up using 200 μ L pipette tip and cultured into in 5 mL LB broth (5g Tryptone, 2.5g Yeast extract, 2.5g NaCl and ddH₂O to 500 mL, media was autoclaved and stored in 4°C) medium supplemented with ampicillin (100 μ g/mL) and incubated at 37°C in a shaker incubator (~230 rpm, Sanyo orbital incubator) for overnight.

2.2.8.2.5 The shREST-pSUPER Plasmid Isolation

After the overnight incubation, 1.4 mL of the LB broth cultured cells were transferred into 1.5 mL tube and the cells were pelleted by centrifugation at 28000 g for 1 minute, whereas, the remaining volume of the LB broth was stored at 4°C. After removing the LB culture media, the cells were lysed in 100 μ L lysis buffer (50 mM Tris-HCl, 10 mM EDTA, and 100 μ g/mL RNase A pH 8.0 (Sigma, Ribonuclease A from bovine pancreas, R4875). The DNA was released and isolated by adding 200 μ L of (1% SDS, and 0.2 M NaOH) buffer and then 50 μ L of pre-chilled potassium acetate buffer (3.0 M, pH 5.5) was added. After 5 minutes of incubating the tubes on ice, a 400 μ L of isopropanol was added into each tube to precipitate the DNA, and the tubes were incubated for 2 minutes at room temperature and centrifuged at 28000 g for 3 minutes. The isopropanol was removed and 200 μ L of 70 % ethanol was added to remove the salt. The tubes were further centrifuged at 28000 g for 3 minutes, the ethanol was removed, and the pellet was air dried at room temperature for

5 minutes. After complete drying of the pellet, the DNA was suspended in 30 μ L of TE buffer (10 mM Tris-HCL, 1 mM EDTA, pH 8.0). Enzymes restriction digestion was used to screen for successful cloning and it was performed as described previously (2.2.8.2.2). The products of the restriction digestion reaction were separated by electrophoresis in 1.2 % agarose gels at 100 volts. Constructs that showed the correct digestion product size were sequenced using Sanger sequencing facility at Beckman Coulter Genomics service. Plasmid with correct cloning sequence was then propagated in 50 mL LB broth for overnight and the plasmid isolation was performed using QIAprep Miniprep (QIAGEN) according to the manufacturer's instructions.

2.2.8.3 The shRNA Transfection Reactions

2.2.8.3.1 Transfection Optimisation

The amount of the DNA needed to induce an optimal transfection level of the Daoy cells was established by transfecting the cells with the pCMV-Beta plasmid expressing β -galactosidase. This plasmid contains *LacZ* gene upstream a CMV promoter which produces β -galactosidase enzyme. When lactose (X-gal) is added, the β -galactosidase enzyme catalyses the X-gal and produce blue colour (5-bromo-4-chloro-3-hydroxyindole) which can be used to represents the transfection efficiency. The effect of the transfection on the cell survival was evaluated microscopically and the transfection efficiency was measured by calculating the ratio of the stained to non-stained cells.

The analysis was performed by transfecting the Daoy cells (80-100 % confluency) with the pCMV-Beta plasmid at concentrations of 125, 250 and 500 ng, using Lipofectamine 2000 transfection reagents (Invitrogen, 11668-027) at ratios of 1:2, 1:3, and 1:4. Both of the DNA and the transfection reagents were suspended in 1X Opti-MEM media (Gibco, 31985062) and the transfection mixture was incubated at room temperature for 20 minutes. The cultured cells were washed with sterile PBS for two times and each transfection reaction was prepared by adding one part of the transfection mixture and 4 parts of Opti-MEM media. Culture plates were incubated at 37 °C in a 5% CO₂ air incubator for 4 hours before replacing the transfection media with complete DMEM media.

After 48 hours from transfection, the cells were washed three times in PBS and fixed in 100 μ l X-Gal Fixative Solution (2% v/v formaldehyde, 0.2% v/v glutaraldehyde) for 5 minutes. The cells were washed in PBS for three times and then overlaid with 150 μ L of

X-Gal solution (5mM Potassium ferricyanide, 5mM Potassium ferrocyanide, 2mM MgCl₂ in PBS). X-Gal [1mg/mL] was added freshly. The efficiency of the cell transfection was analysed using a bright field microscope after an overnight incubation at 37 °C.

2.2.8.3.2 Transfection with the shREST-pSUPER and Establishing the Stable Cell Clones

The transfection with the shREST-pSUPER vectors was performed as described previously (section 2.2.8.1) using 2.25 µL of Lipofectamine 2000 with 750 ng of the DNA vectors. After 48 hours from the transfection, the culture media was replaced with complete DMEM media supplemented with 5 µg/mL of puromycin. A non-transfected (wild type Daoy) control was included in the selection assay and treated with puromycin. The culture was then incubated at 37°C and the media was replaced every 3 days with fresh media containing the puromycin. The cells were examined microscopically on a daily basis and the selection for stable expression of the vector was assumed to be completed when all the cells in the non-transfected control had been killed. REST knockdown monoclonal cell clones were then established as described earlier in the knockout approach (2.2.8.1).

2.2.9 Study the Effect of REST-Modulation on the Daoy Cells Migration Using Wound Healing Assay

The Daoy cells were cultured in 6-well plates using complete DMEM culture media at a cell density of 1×10^5 cell/mL and incubated at 37°C in 5% CO₂ air. After 24 hours the growth was examined under an inverted microscope and the cells monolayer (90 - 100% confluency) was scratched by passing a sterile 200-µL pipette tip across the middle of the well in a vertical and horizontal directions. The well was then gently washed for two times with PBS, fed with either 1% FBS-media or FBS-free media, and imaged at the intersection between the vertical and horizontal scratches. A second image was taken 24 hours from wounding and the wound closure was analysed using TScratch software (CSElab, Zurich, Switzerland) (<http://www.cse-lab.ethz.ch>)¹²³.

2.2.10 The Flow Cytometer Analysis

2.2.10.1 Cell Cycle Analysis using Propidium Iodide

The samples for cell cycle analysis on flow cytometry (FACS) were prepared by harvesting the cultured cells when they reached 80 - 90 % confluency for single time-point analysis or at 24, 48, 72 hours (time-courses analysis) using trypsin-EDTA as described in section (2.2.1). The cells were fixed in 9 mL of 70% cold ethanol with gentle vortex while adding the ethanol dropwise and the tubes were stored at -20°C for at least 24 hours. Prior the flowcytometry analysis, the ethanol was removed by centrifuging the cells at 400 g for 5 minutes and the pellet was washed twice with ice cold PBS. The cells were then resuspended in 250 μ L PBS supplemented with 12.5 μ L of RNase A (0.5 mg/mL) and incubated at 37°C for 1 hour. To each tube, a 12.5 μ L of Propidium iodide (PI) (50 μ g/mL, Sigma, P4170) was added and the samples were kept on ice in dark until the analysis.

The cells were analysed on a flow cytometer (FACSAria II, Becton Dickinson Biosciences) using low-flow rate mode and the PI fluorescein was detected using 488 nm excitation. The parameters of signal detection were; Forward Scatter-Area (FSC-A), Side Scatter-Area (SSC-A), SSC-H (Hight), and Phycoerythrin (PE-A, has an excitation wavelength (488 nm) similar to Propidium iodide). The 'gating' was performed using FSC-A vs SSC-A (to exclude debris), PE-A vs. FSC-A (shows cellular material stained by PI), and PE-A vs. PE-H (to discriminate between singlets and doublets).

The results were presented as DNA content frequency histograms, and the percentages of the cells (represented by peaks) were estimated by deconvoluting the histograms using ModFit LT DNA analysis software (Verity Software House, version 3.2). The percentage in G1, S and G2 phases was calculated using Sync-Wizard mode of the ModFit, which models the actual number of the events after filtering out cell aggregates and debris. The G0-G1 marker in the synchronization wizard was adjusted to align the most frequent part of the peak with SD between 1.5 and 2.0; the G2-M marker was adjusted to face the highest part of the second visible peak; whereas, the G2/G1 ratio was adjusted automatically between 1.7 and 2.0. These values were then used to generate PI histogram plot which was used to quantitate the percentage of the cells in each cell cycle phase. The accuracy of the DNA measurements was assessed by evaluating the coefficient of variation (CV) of the G1 mean and the results were accepted when their CV value is

less than 6% ¹²⁴. The average of the biological replicates was used to calculate the percentages of cells within each cell cycle phase.

2.2.10.2 Apoptosis Detection using Annexin V and PI

The Daoy cells were cultured at 3.5×10^4 cell/mL in 6-well plates using complete DMEM culture media and the wells were labelled as 42, 36, and 30 and the plates were incubated at 37°C in 5% CO₂ air. Prior harvesting the cells by 42, 36, and 30 hours, the cells were treated with a single dose of the HDACis by carefully replacing the culture media with a complete media containing the required concentration of the drug (Table 3). The cells were harvested by collecting both floating and attached cells as described in section 2.2.1, and kept on ice.

The apoptosis analysis was performed using FITC Annexin V Apoptosis Detection Kit I (BD Pharmingen, 556547) according to the manufacturer's recommendations. Briefly, the cells were washed twice in 1 mL of PBS and once in 600 µL of 1X Annexin V Binding Buffer and the cells were pelleted by centrifugation (400 g for 5 min). For each sample, four tubes (Eppendorf, 1.5 mL) were prepared (labelled as Annexin V-/PI-, Annexin V+/PI-, Annexin V-/PI+, and Annexin V+/PI+) and a cell number of $\sim 1 \times 10^5$ was transferred into each tube. The cell staining was performed by adding 5 µL of Annexin V-FITC and 5 µL of PI and the tubes were gently vortexed and incubated for 15 min at room temperature in the dark.

The flowcytometry analysis was performed on CytoFLEX S (Flow Cytometry, Beckman Coulter) and the acquisition settings were customised to acquire FSC, SSC, FITC-green and PI red fluorescence. The compensation algorithm was performed using cells treated with HDACis for 36 hours and stained with Annexin V-/PI-, Annexin V+/PI-, or Annexin V-/PI+. The 'gating' for the apoptotic analysis was performed by using (FSC-A vs. SSC-A) to remove debris (lower left corner of the plot), (SSC-A vs. SSC-H) to sort-out doublets (the cells off the diagonal population). The percentages of the viable, necrotic, apoptotic (early/late) cells were interrogated using CytExpert 2.2 software (Beckman Coulter) using FITC vs. PE plot and applying a quadrant gate. The quadrant location on the plot was adjusted using Annexin V-/PI-, Annexin V+/PI-, Annexin V-/PI+ controls and the cells percentages were represented by bar diagram.

2.2.11 The Single Cell Next Generation Sequencing (scNGS)

2.2.11.1 Cell Treatment and Cryopreservation

The Daoy cell (Passage 1) and the human neurons were seeded into 6-well culture plates at a cell density of 1.5×10^5 cell/mL and $\sim 2.5 \times 10^5$ cells/well, respectively. The culture was performed as described in section (2.2.1 and 2.2.2). The cells were then treated with by replacing the culture media with fresh media containing 5 μ M of SAHA and MS-275 and DMSO controls were included with each cell line. The plates were incubated in 5% CO₂ air incubator at 37°C for 36 hours. The cells were harvested as described in section (2.2.1 and 2.2.2), resuspended in 1 mL of cryopreservation media (Daoy: 10% DMSO, 20% FBS in DMEM media, the neurons: 10% DMSO in NM medium) and transferred into 1.8 mL cryogenic vials (nunc). The vials were placed in Mr Frosty freezing container (Thermo Scientific) and the container was stored at – 80°C for 8 hours and then the vials were stored in liquid nitrogen. The vials were transferred to the MRC Weatherall Institute of Molecular Medicine (University of Oxford) in liquid nitrogen where the scNGS analysis was performed. Within the facility, the vials were stored on dry ice until the cells were processed.

2.2.11.2 The scNGS Sample Preparation

The samples for the scNGS analysis were rapidly thawed in a 37°C water bath for ~ 2 minutes. A small volume of the untreated neurons was transferred to a sterile microscope culture flask and they were checked microscopically for clumps. Due to the presence of clumps, the neurons were centrifuged at 250 g for 3 minutes and the supernatant was removed without disrupting the cell pellet. The neurons were resuspended in 200 μ L of TrypLE Express and incubated in 37°C water bath. After 2 minutes, the cells were gently mixed with a pipette and re-incubated at 37°C for another 2 minutes. During the incubation time, the Daoy cells were thawed in a 37°C water bath at for 2 – 3 minutes. To each neurons tube, 1 mL of the neuron media was added, the cells were gently pipette mix for 5 times and both the neurons and Daoy cells were pelleted by centrifugation at 250 g for 3 min. The supernatant was removed, and the neurons were washed twice using cold NM whereas, the Daoy cells were washed twice in cold PBS supplemented with 0.04% (w/v) BSA. The supernatants were removed, and the neurons were suspended in 500 μ L of NM by gentle pipetting for 10 – 15 times. The Daoy cells were suspended in 500 μ L PBS

containing 0.04% (w/v) BSA. The cells were then stained with DAPI (5%) and stored on ice for cell sorting.

Sorting and isolation of viable cells was performed using FACSAria II SORP (Becton Dickinson Biosciences) at the MRC Weatherall Institute of Molecular Medicine (University of Oxford) using BD FACSDiva (8.0.1) software. The sorting was performed using the FSC-A vs. DAPI to gate for the viable cell population 1 (P1) (located in the lower part of the plot). The P1 was then further deconvoluted using a FSC-A vs. SSC.A plot to minimize cellular debris and to gate for the cells of interest (P2). The doublets in P2 were excluded using FSC-A vs. FSC-H plot and the singlets (P3) were isolated. For each sample at least 2000 events from P3 were sorted out into 1.5 mL tube containing 2 μ L of 10% (w/v) BSA for the Daoy cell or NM for the neurons and the tubes were stored on ice.

2.2.11.3 The scNGS GEMs Preparation and RT-PCR

The single cell next generation sequencing was performed using the 10x Genomics technology (Chromium Single Cell 3' Reagent Kits v2) and the work was performed by the 10x team of the MRC Weatherall Institute of Molecular Medicine (University of Oxford). Briefly, the single cell master mix for loading the cells into a Chip A Single Cell was prepared by mixing the contents of the Chromium Single Cell 3' Library & Gel Bead Kit v2, 4 rxns (PN-120267 (Per sample; 50 μ L of RT Reagent Mix, 3.8 μ L of RT Primer, 2.4 μ L of Additive A, and 10 μ L of RT Enzyme Mix) and approximately most of the sorted cells were transferred into the master mix tubes. The unused wells of the chip were filled with 50% glycerol solution apart from the recovery wells and 90 μ L of the master mix was transferred into row #1 of the chip. Row #2 of the chip was filled with 40 μ L of Single Cell 3' Gel Beads whereas the row #3 was filled with 270 μ L of Partitioning Oil. The chip was then assembled using a 10x Chip Holder and the 10x Gasket was placed on the 10x tray. The GEMs were generated using Chromium Controller for 6.5 minutes. A volume of 100 μ L of the GEMs was transferred into an emulsion-safe plate and the plate was heat sealed with pierceable foil at 185°C for 6 seconds. The plated was loaded into a thermal cycler (Proflex Veriti MiniAmp, Applied Bio System, Thermo Fisher) and the GEM-RT was performed at 53°C for 45 minutes, 85°C for 5 minutes and the reaction was terminated at 4°C.

2.2.11.4 Post GEMs-RT Clean-up

Post GEM-RT clean-up was performed by adding 125 μL of Recovery Agent (P/N 220016) into each well and the entire volume transferred into an 8-tube strip and centrifuged at 250 g for 30 seconds. A volume of 125 μL of the Recovery Agent/Partitioning Oil (pink) was removed from the bottom of the tube and discard. Into each well, 200 μL of Dynabeads Cleanup Mix (182 μL of Buffer Sample Clean Up, 4 μL of Dynabeads MyOne SILANE, 9 μL of Additive A, and 9 μL of nuclease-free water) was added and the tubes were incubated at room temperature for 10 minutes. A volume of 100 μL of Elution Solution was added (98 μL of Buffer EB, 1 μL of 10% Tween 20, and 1 μL of Additive A) and the tubes were then placed on 10x Magnetic Separator in the High position until the supernatant is clear. The supernatant was then discarded and a total volume of 300 μL of freshly prepared 80% ethanol was added to the pellet while on the magnet and stood for 1 minute. The ethanol was then carefully discarded and 200 μL of 80% ethanol was added and carefully removed after 30 seconds. The tubes were centrifuged and returned to a 10x Magnetic Separator in the low position and the samples were air dried for 1 minute. The tubes were then removed from the magnet and the beads were resuspended in 35.5 μL of Elution Solution I and incubated at room temperature for 1 minute. The tubes were then placed in a 10x Magnetic Separator in the low position until the solution is clear and 35 μL of the purified GEM-RT product were transferred into a new tube strip.

2.2.11.5 The cDNA Amplification, Purification and Quality Check

The cDNA amplification was prepared by adding 65 μL of cDNA Amplification Reaction Mix (50 μL of Amplification Master Mix, 5 μL of cDNA Additive, and 2 μL of cDNA Primer Mix) to the 35 μL of purified GEM-RT product and the cDNA was amplified on Proflex Veriti MiniAmp cycler using 90°C for 3 min, and 12 cycle of 98°C for 15 sec, 67°C for 20 sec, 72°C for 1 min, and a final extension step of 72°C for 1 min.

The amplified cDNA was cleaned up using 60 μL of SPRIselect Reagent to each sample and the tubes were incubated at room temperature for 5 minutes. The tubes were then placed in a 10x Magnetic Separator in the high position until the solution is clear, and the supernatant was carefully discarded. The pellet was then washed three times using 200 μL of 80% ethanol and the samples were air dried for 2 minutes. The tubes were then removed from the separator and 40.5 μL of Buffer EB was added and left for 2 minutes at room

temperature. The tubes were then placed in a 10x Magnetic Separator in the high position until the solution is clear and 40 μL of sample was transferred into a new tube. The quality of the cDNA amplification was evaluated using the Agilent Bioanalyzer D5000 ScreenTape High Sensitivity chip (5067-5592).

2.2.11.6 The cDNA Fragmentation, End Repair and A-tailing

The fragmentation of the amplified cDNA was performed by mixing 15 μL of the Fragmentation Mix (5 μL of Fragmentation Buffer, and 10 μL of Fragmentation Enzyme Blend) with 35 μL of the purified cDNA. The fragmentation reaction was performed on Proflex Veriti MiniAmp cycler at 32°C for 5 minutes. The reaction was then followed by end repair & A-tailing step thus, the temperature was increased to 65°C for 30 minutes and the reaction was stopped at 4°C.

The products of the fragmentation reaction were isolated by adding 30 μL of SPRIselect Reagent to each sample and the mixtures were incubated at room temperature. After 5 minutes, the tubes were placed in a 10x Magnetic Separator in the high position until the solution is clear. A volume of 75 μL of the supernatant was transferred to new tubes and 10 μL of SPRIselect was added to each tube. The tubes were placed in a 10x magnetic separator in the high position until the solution is clear and then 80 μL of the supernatant was removed and discarded. The pellets were then washed as described in the previous step using 125 μL of 80% ethanol and 50.5 μL of Buffer EB.

2.2.11.7 Adaptor Ligation

The ligation reaction was performed by mixing 50 μL of the purified fragments with 50 μL Adaptor Ligation Mix (20 μL Ligation Buffer, 10 μL DNA Ligase, and 2.5 μL of Adaptor Mix). The reaction was incubated at 20°C for 15 minutes, and the products were cleaned using SPRIselect as described in the previous step using 200 μL of 80% ethanol and 30.5 μL of Buffer EB.

2.2.11.8 Sample Indexing (i7)

Sample indexing was performed by mixing 60 μL of the Sample Index PCR Mix (50 μL of Amplification Master Mix, 2 μL of SI-PCR Primer, and 8 μL of nuclease-free water) with 30 μL of the ligation-reaction purified samples and 10 μL of Chromium i7 Sample

Index was added into each sample mix. The indexing reaction was performed on the Proflex Veriti MiniAmp cycler (98°C for 45 sec, and then 12 cycles of 98°C for 20 sec, 54°C for 30 sec, and 72°C for 1 minutes, the reaction was followed by an elongation step of 72°C for 1 minute). The reaction products were clean using SPRIselect as described previously using 200 µl of 80% ethanol and 35.5 µL of Buffer EB. A volume of 35 µL of sample was transferred into a new tube and the quality of the library construction was evaluated using Agilent Bioanalyzer High Sensitivity chip. The samples were sequenced using Illumina NextSeq 500/550 High Output Kit v2. The sequencing analysis was carried out at the MRC Weatherall Institute of Molecular Medicine (University of Oxford) using the following run parameters: Read 1-26 cycles, Read 2 - 98 cycles, Index 1-8 cycles. A sequencing depth of approximately 50,000 reads/cell was aimed for each sample.

2.2.12 Sequencing Data Demultiplexing

2.2.12.1 Installing the required Software

The data demultiplexing was performed on Advanced Research Computing 3 (ARC3), part of the High-Performance Computing facilities at the University of Leeds, UK (<http://www.arc.leeds.ac.uk>). The access to ARC3 was through using the MobaXterm software (<https://mobaxterm.mobatek.net/download.html>) and secure remote login (Secure Shell protocol). The CellRanger V3.0 software was installed as per the 10x genomics instructions (<https://support.10xgenomics.com/>). Into the same directory, the Human reference (GRCh38) data set was downloaded and the successful installation of CellRanger was verified and the site-checked file was uploaded to 10x support for future support. Further the Illumina bcl2fastq2 Conversion Software (v.20.0) was installed on the ARC3 server.

2.2.12.2 Running the CellRanger mkfastq Pipeline

The 10x scNGS Illumina sequencing data (Illumina raw base call (bcl) files format) were demultiplexed to FASTq (text files containing sequence data with a quality score for each base) files format using the CellRanger mkfastq pipeline. The data demultiplexing was carried out by uploading the data files to the ARC3 with the sample-index-set of each

sample (csv.format). The mkfastq pipeline was ran by defining the path to the CellRanger and the bcl2fasq files location using the following commands:

Note: the texts in grey font are the variables where the italic texts are the description of the command

```
export PATH=/directory path/bcl2fastq2-v20.0.x/bin:$PATH
export PATH=/directory path/cellranger-3.0.0:$PATH
```

The bcl data files were then converted to fastq format using:

```
cellranger mkfastq --id=directory_name \
--id= (creates a directory and call it as the defined after the = sign, the name should not be exist in the directory)
--run=/nobackup/bsasa/rawdata/seq1/ \
--run= (the path to the location of the seq data)
--csv=samplesheet.csv
--csv= (the sample sheet ended with .csv, no need to include the path of the directory).
```

2.2.12.3 Running the CellRanger count Pipeline

The generated files were aligned to GRCh38 reference genome, de-duplicated, filtered, and the UMIs were counted using the CellRanger count. The pipeline was run using the following commands:

```
cellranger count --id=sample_number \
--transcriptome=/path_to_ref_genome/refdata-cellranger-GRCh38-3.0.0 \
--transcriptome= (Path to the Cell Ranger compatible transcriptome reference)
--fastqs=/path_to_fastq_files/outs/fastq_path \
--fastqs= (Path to the fastq_path folder generated by mkfastq)
--sample=sample_no \
--sample= (Sample name as specified in the sample sheet)
--chemistry=SC3Pv2 \
--chemistry= (Assay configuration)
--expect-cells=3000
--expect-cells= (Expected number of recovered cells)
```

The commands were re-run for each sample and the output summary files were used to evaluate the quality of the 10x analysis and to generate a digital gene expression matrix. Upon the cell quantification, single-cell specific quality control measures were

examined including the sequencing depth, the total read per cell, and the total number of genes detected per cell.

2.2.12.4 Running the CellRanger aggr Pipeline

The generated data of all samples were aggregated and normalized using CellRanger count. The pipeline requires a (csv) format file which specify the list of the CellRanger count output files path (molecule_h5) and the library ID in order to label the output files. The csv file was uploaded to the analysis directory and the pipeline analysis was performed using:

```
cellranger aggr --id=cellaggr \  
--id=(creates a directory and call it as the defined after the = sign)  
--csv=cellaggr.csv \  
--csv=(Path to the csv file which contains a list of cellranger count)  
--normalize=mapped  
--normalize=(equalizes the read depth between samples before merging until all the samples have an equal number of mapped reads per cell)
```

2.2.12.5 Visualising the Data using Loupe Cell Browser

The data generated by the CellRanger aggr were visualized using Loupe Cell Browser (V.3.0.1) on Windows environment. The browser was used to visualize the cell dimensional reduction on t-distributed Stochastic Neighbour Embedding of the principal components (t-SNE) projector.

2.2.12.6 Analysing the scNGS Gene Expression using Seurat

Seurat scNGS R Package (version 3.0) was used to filter out the dead, empty droplets, mitochondrial genes, and doublets from the data sets of the CellRanger count matrix files¹²⁵. The analysis was performed by uploading the raw data matrix files into Seurat using the (Read10X) function, and the (CreateSeuratObject) function was used to include all the genes that were detected in at least 3 cells. Next, the gene numbers (nGene), the UMI counts (nUMI), and the percentage of the mitochondrial genes (percent.mito) of each sample were counted and the results were visualized on violin and scatter plots. The plots were then used to identify the cells with a clear outlier number of genes and they were assumed as potential multiplets. The cells with fewer than 300 genes were

also assumed as dead, or empty droplets and they were filtered out using (FilterCells) function. Next, the gene expression values of each cell were normalized to the total expression using (LogNormalize) function which multiplies the values by a scaling factor of (1×10^4) and the values were then log-transformed. Further, the cell to cell variations, the nUMI, and the percent.mito expression were regressed out using (ScaleData) function.

To find the correlations between the genes and the cellular phenotypes, the genes with high variance were identified using Seurat (FindVariableGenes) function. In Seurat, the highly variable genes were defined as significantly expressed genes with greater than zero at a false discovery rate (FDR) of 5% (i.e. getting false positive) and they were calculated based on the gene average expression and the dispersion level ¹²⁶. These genes were proposed to drive the heterogeneity across cells in a population and were used to cluster the cells ¹²⁶. The data were scaled to regress out cell to cell variations in the gene expression which they could be generated from the technical noise, the reagent batch, the nUMI, and the percent.mito. Further, the data were dimensionally reduced using the principal component analysis (PCA, statistical procedure used to convert a set of correlated variables into a set of linearly uncorrelated variables) of the highly variable genes and the results of the cells and the genes clustering were visualized on heatmap and JackStraw plots ¹²⁷. The plots were used to determine the number of the principal components that were included in the subsequent steps.

The cells were then clustered using Seurat (FindClusters) function and the number of the included PCs was determined based on the JackStraw plots significant *P*-values. The (FindClusters) function mainly implements the graph-based clustering approach (construct a graph and then apply a clustering algorithm to partition the graph) based on the similarity of gene expression patterns between the cells ¹²⁵. The data sets were dimensionally reduced using the (RunTSNE) function, and the clusters were visualized on t-SNE plots. The differential expression analysis was performed using Seurat (FindAllMarkers) function which identifies the positive and the negative markers of each cluster by comparing genes in a cluster of cells against genes in all other cells. The genes that were; differentially expressed in at least 10% of cells within a cluster, and with more than 0.25 log fold change and *P*-value of less than 0.01 were considered as marker genes.

With the tumour cell only, as the phase of the cell cycle has a major impact on the gene expression, each cell was subjected to cell cycle gene expression classification using Seurat (CellCycleScoring) function. This function calculates the S and G2/M phase scores for each cell using a pre-set of genes that showed significant cell cycle-dependent expression¹²⁸. The selection of these genes was based on their anticorrelated expression thus, the cells expressing these markers should not be in G1 or quiescent (G0) phases. The clusters of each sample were renamed based on the cell cycle phase and displayed on t-SNE projectors. As HDACi induced a significant effect on the expression of cell cycle genes, the analysis was conducted by merging the three Daoy conditions in one Seurat object using (MergeSeurat) function.

With the human neurons only, the identified markers were loaded into the Cell-type Specific Expression Analysis (CSEA) website manning server (<http://genetics.wustl.edu/jdlab/csea-tool-2/>) in order to identify the cell-type of each cluster¹²⁹. The cell-type of the neurons was determined based on the expression of specific neuronal markers and the identity of the cells was assigned based on the significance of the *P*-value (Appendix 11). The clusters of the neurons in each sample were renamed based on the cell identity and displayed on t-SNE plots. Further, to study the effect of SAHA and MS-275 on the normal neurons, the analysis was carried out by extracting the data sets of each cell type cluster and the clusters of the same identity were merged in a single Seurat object.

The Daoy and the neurons Seurat objects were normalized, dimensionally reduced, and the new dimensional reduction was visualized on non-linear t-SNE plots. Further, the merged objects were subjected to the Seurat (FindClusters) function which cluster the cells based on their new PCA values. The data were then subjected to Seurat (FindAllMarkers) function which calculates the average log expression of a gene in a single cluster and compared it to all other cells. Also, it calculates the percentage of the cells in each group and uses these values to calculate the *P*-values.

2.2.12.7 Gene Functional Annotation and Gene Set Enrichment Analysis

The functional annotations of the differentially expressed genes were investigated using the online GenCLiP v2.0 web-based text-mining server (<http://ci.smu.edu.cn/GenCLiP2/analysis.php>)¹³⁰. The enquiries were made by

uploading a list of genes IDs and the enrichment of the Gene Ontology (GO) were evaluated based on the GenClip enrichment scores.

The gene set enrichment analysis was performed using java Desktop Gene Set Enrichment Analysis (GSEA) Application (v3.0) of the Broad Institute¹³¹. The analysis was carried out by ranking the upregulated and downregulated genes as per the decrease in their fold change values and the ranked lists were analysed using the Run-GSEA-Preranked tool. The analysis was performed using the gene sets databases of Hallmark (gene symbols v.6.2), BioCarta (gene symbols v6.2), KEGG (gene symbols v6.2), and Reactome (gene symbols v6.2). The gene sets with less than 15 genes and more than 500 genes were excluded and the statistical significance of the enrichment score (ES) was estimated by a permutation test with 1000 replications. The pathways with a false discovery rate (FDR) q -value <0.25 and nominal P -value <0.01 were chosen as significantly enriched. The upregulated pathways were defined by a positive normalized ES and described as positive phenotype and the downregulated pathways were defined by a negative normalized ES and described as negative phenotype.

2.2.12.8 Pathway Analysis

The PathVisio (version 3.3.0) pathway visualisation and analysis software (<http://www.pathvisio.org>) was used to examine the over-representation of the differentially expressed genes and visualized the pathway¹³². The homo sapiens pathways were downloaded from the WikiPath and were used for searching the overrepresentation of the genes¹³³. The search for the pathway was performed by defining the a criterion that select all the differently expressed genes in a pathway (e.g. $\log_2FC > 0.2$ AND $\log_2FC < -0.2$) and the pathway was selected based on the highly significance of the P-Value and the results of the GSEA analysis.

2.2.13 Basic Molecular Biology Procedures

2.2.13.1 Extracting DNA from 6-Well Culture Plates

The DNA extraction was performed using cells cultured in 6-well culture plates. After removing the culture media, the cells were washed in sterile PBS buffer and scrapped into a 1 mL sterile PBS. With the DNA fragmentation assay, both of floating and attached cells were used for the DNA extraction. The cells were pelleted by centrifugation (12000 g for

5 min) and re-suspended in 400 μ L of TE buffer (10 mM Tris pH 7.6, and 0.5 mM EDTA pH 8.0), 100 μ L of 10% SDS (10 g of sodium dodecyl sulfate in 100 mL H₂O), and 20 μ L of Proteinase-K (Sigma, 10 mg/mL). The tubes were mixed by gentle inversion for 3 minutes and were incubated at 55 °C for overnight. To precipitate the DNA, 50 μ L of 2.5 M NaCl solution was added into each mixture followed by adding 400 μ L of 100% ethanol, and the tubes were incubated with rotation for 10 minutes at room temperature. The DNA was picked by pipet tip (when it is contact) and transferred into 1.5 mL tube contains 400 μ L of 70% ethanol. The DNA that is not condense and not observable was precipitated by centrifugation at 28000 g for 10 minutes. Next, the DNA was washed for two times in 400 μ L of 70% ethanol, the ethanol was removed by centrifugation at 28000 g for 3 minutes, and the pellet was air-dried at room temperature for 5 minutes. The DNA was then dissolved in 50 μ L TE buffer and the DNA concentration was measured using NanoDrop 2000c (ThermoScientific) at 260 nm. The purity of the total DNA was evaluated by the ratio of A₂₆₀/A₂₈₀ (between 1.8 and 2.0).

2.2.13.2 DNA Extraction from 96-Well Culture Plates

The DNA extraction from 96-well plate was performed by removing the culture media by flipping the plate, and the wells were washed once with PBS. A volume of 50 μ L of (40 μ L TE, 10 μ L of 10% SDS, and 2 μ L Proteinase K [10 mg/mL] stock solution) buffer was added into each well and the plate was mixed on a plate mixture for 1 minute and incubated at 60 °C for overnight in humidified chamber. Next, a 20 μ L of NaCl was added into each well using a multichannel pipette followed by 130 μ L of 100% ethanol, and the plate was mixed on a horizontal rotator for 5 minutes and incubate at room temperature. After 30 minutes, the plate was centrifuged at 2400 g (Eppendorf Centrifuge 5810R) for 15 minutes and the supernatant was removed using a multichannel pipette. The precipitated DNA was washed with 150 μ L of 70% ethanol, centrifuged for 3 minutes at 2400 g, and the ethanol was removed with a multichannel pipette. The precipitated DNA was left to dry at room temperature for around 15 minutes and was suspended in 30 μ L of TE buffer and stored at -20 °C.

2.2.13.3 Extracting Total RNA from Cultured Cells

The RNA was extracted from cells cultured in 6-well culture plates. The cultured cells were washed in sterile PBS buffer and harvested using trypsin-EDTA for 5 minutes. The

cells were then washed off the plate using 1 mL ice-cold PBS, transferred into a sterile 1.5 mL tube, and pelleted by centrifugation at 12000 g for 3 min at 4 °C (Heraeus Fresco centrifuge). The RNA extraction was performed by suspending the pellet in 1 mL of cold TRI-reagent (Sigma-Aldrich, 93289) and the cells were homogenized by passing the lysate several times through a 1 mL pipette tip, then vortexed for 1 minute and incubated on ice for 10 minutes. Into each tube, 200 μ L Chloroform (Arcos Organics, 158210250) was added and the suspension was vortexed for 1 minute and incubated on ice for another 10 minutes. The mixture was centrifuged at 28000 g for 10 minutes at 4 °C and the upper aqueous phase was transferred into a fresh 1 mL tube. Total RNA was precipitated by adding 600 μ L of isopropanol (Sigma, 59300-M) and the suspension was kept at – 80 °C for at least 1 hour. The samples were then thawed on ice and centrifuged at 24000 g for 20 minutes at 4 °C. The supernatant was removed, and the pellet was washed with 200 μ L of 70 % ethanol, centrifuged at 28000 g for 5 minutes, and the ethanol was removed. The pellet was air dried at room temperature for 5 minutes and the RNA was dissolved in 50 μ L TE buffer. The RNA concentration was measured using NanoDrop 2000c (ThermoScientific) at 260 nm, and the purity of the total RNA was evaluated by the ratio of A260/A280 (between 1.8 and 2.0).

2.2.13.4 The Nuclear Protein Extraction from Cultured Cells

Cultured cells in 6-well plates were washed in sterile PBS buffer and harvested using trypsin-EDTA for 5 minutes. The cells were then washed off the plate using 1 mL ice-cold PBS and transferred into a sterile 1.5 mL tube. The cell suspension was then pelleted by centrifugation at 12000 g for 3 minutes at 4°C and washed twice with cold PBS. After removing the supernatant, the pelleted cells were resuspended in 1 mL of ice-cold Triton Extraction Buffer (TEB, consists of PBS containing 0.5% Triton X100 (v/v), 0.02% (w/v) NaN₃, the buffer was sterilized by filtration and supplemented with 1 mM Phenylmethanesulfonyl Fluoride (PMSF) (Cell Signal, 8553S) dissolved in isopropanol) using up and down pipetting for at least 10 times. The lysate was incubated on ice for 30 minutes with vortex every 10 minutes and clarified by centrifugation at 12000 g for 10 minutes at 4 °C. After removing the supernatant, the nuclei were resuspended in 100 μ L of Nuclear Lysis Buffer (NLB; 20 mM HEPES-KOH pH 7.9, 25% glycerol, 420 mM NaCl, 1.5 mM MgCl₂, 0.2 mM EDTA, 0.5 mM dithiothreitol, 0.2 mM PMSF, Protease Inhibitor Cocktail powder (Sigma, P8465) [prepared by suspending the powder in NLB

buffer and aliquoted in 100 μ L], dithiothreitol, PMSF and the inhibitor was added freshly) and incubated on ice. After 20 minutes, the mixture was centrifuge at 28000 g for 2 minutes at 4 °C, and the supernatant, which contains the proteins, was transferred into a new a 1.5 mL tube and stored at -20 °C until further analysis.

The concentration of the protein was measured using Pierce BCA Protein Assay Kit (ThermoScientific, 23221) as per the manufacturers' instructions for 96-well plates. Briefly, 10 μ L of; samples, BSA standards, and blank were mix with 200 μ L of BCA Working Reagent (50 parts of BCA Reagent A with 1 part of BCA Reagent B). The plate was mixed for 30 seconds and incubated at 37°C for 30 minutes. The plate was then cooled down to room temperature and the absorbance was measured at 562nm wavelength (FLUOstar Omega, BMG Labtech). Protein concentration was determined by plotting the average blank-corrected 562nm measurement for each BSA standard against its concentration in μ g/mL.

2.2.13.5 Polymerase Chain Reaction (PCR)

The DNA was amplified using 1 μ L of the DNA, 0.5 μ L of 10 mM dNTPs (Bioline, 39028), 0.5 μ L of 10 μ M forward and reverse primers (NHEJ-FWD:5'-GCGATGTG GTTTTAAGCCAGT-3', NHEJ-REV: 5'-GTTATCCCCAACCGGCATCA-3'), 0.2 unit of Taq DNA Polymerase and 2 μ L of 5X PCR reaction buffer (Thermo Fisher Scientific, M7122). The volume was completed to 10 μ L with sterile distilled water.

The DNA amplification was performed on Eppendorf PCR machine (Mastercycler EP Gradient 5341) under the following conditions: denaturation at 95 °C for 2 minutes, followed by 30 cycles of 95 °C for 30 seconds, annealing at 60 °C for 30 seconds, extension at 72 °C for 1 minute. A post-PCR incubation step of 10 minutes at 72 °C was performed to complete the synthesis of the PCR products. The extension temperature was adjusted according to the primers melting time and the PCR efficiency, and all the reactions included positive and negative controls.

2.2.13.6 Quantitative Polymerase Chain Reaction (qPCR)

The total RNA was reverse-transcribed using 1 μ g of the total RNA, 0.1 μ g Oligo (dT) 15 Primer (Promega, C1101), and 0.2 μ g of Random Primers (Promega, C1181). The volume

was then completed to 15 μ L with sterile distilled water and incubated at 65 °C for 5 min and quenched on ice for 1 minute. Next, each reaction mixture was supplemented with 4 μ L of MMuLV RT 5x Buffer (Promega, M1701), 8 units of RNasin inhibitor (Promega, N2111), 1mM dNTPs (Bioline, 39028), and 40 units of MMuLV RT (Promega, M1701) in a final volume of 20 μ L. The reaction was incubated at 37 °C for 1 hour, and then at 4 °C for 10 minutes and a volume of 30 μ L of sterile distilled water was added into the reaction.

The Sybr Green quantitative PCR was performed in Rotor Gene 6000 (Corbett series) using 2X SensiMix SYBR & Fluorescein reagent (Florescencein kit, BioLine, QT615-05). The reactions were performed in 10 μ L volume containing 2.5 μ L of the reverse transcribed product, 5 μ L of the 2X SensiMix SYBR & Fluorescein, 1.9 μ L distilled water, and 0.3 μ L of forward and reverse primers (10 mM) :(REST; FWD: 5'-ACTTTGTCCTTACTC AAGTTCTCAG-3', REV: 5'-ATGGCGGGTTACTTCATGTT-3', SNAP25; FWD: 5'-CGTCGTATGCTGCAACTGGTTG-3', REV: 5'-GGTTCATGCCTTCTTCG ACACG-3', Synapsin FWD: 5'-AGATTTTTGGGGGACTGGAC-3', REV: 5'-TGTCTT CATCCTGGTGGTCA-3', SCG10 FWD: 5'-TGAAGTCGTTTCTCCCAAC-3', REV: 5'-TCACAGCTTGCTCACAATGA-3', GluR2 FWD: 5'-TTGACTTCTCAAAGCCCTT CA-3', REV: 5'-GGCTAAAGGATCAAGAAAGGAA-3', REST Bi-allelic genome editing FWD: 5'-GCAACATTGGAATGGCCCTG-3', REV 5'-ATGGCGGGTTACTTC ATGTT-3', REST4 FWD: 5' ACTTTGTCCTTACTCAAGTTCTCAG 3', REV: 5' GGTATGGATAACCATTTGGTAATA 3'). Each gene expression reaction was performed in duplicate and the cDNA amplification was performed under the following real-time PCR conditions: Taq polymerase activation at 95 °C for 10 minutes, followed by 40 cycles of 95 °C for 10 seconds, annealing at 60 °C for 15 seconds, and extension at 72 °C for 20 seconds. The reaction was followed by a melting step ramping from 72 °C to 95 °C with 1 °C increment and 5 seconds wait for each step which was later used to confirm the specificity of the amplification. The expression of the RNU6 (RNA, U6 Small Nuclear 1) housekeeping gene (FWD:5'-CTCGCTTCGGCAGCACA-3', REV: 5'-AACGCTTCAC GAATTTGCG T-3') was measured for each sample and was used to normalize the expression level of the measured gene/s. The qPCR expression analysis was performed using the Rotor Gene 6000 Series Software, and the expression level was presented by calculating the power of two exponent.

2.2.13.7 Agarose Gel Electrophoresis

The agarose solution was prepared by dissolving 1.2 % (w/v) of agarose (Sigma, A9539) in a volume of Tris-acetate-EDTA (TAE: 2M Tris base, 5M EDTA, and 5.71 % glacial acetic acid, pH8.0) and the agarose mixture was melted in a microwave oven. The agarose gel was prepared by pouring the agarose solution into an electrophoresis chamber. The PCR products were mixed with loading dye and 12 μ L were loaded into the gel alongside of a pre-stained DNA ladder (New England, BioLabs, N3236). The DNA was electrophoresed at 100 volts in 1X TAE buffer until the first migrating band had reached the end of the gel. The DNA was stained with ethidium bromide (Sigma, E1510) and imaged using the Bio-Rad ChemiDoc XR system.

2.2.13.8 Western Blot Analysis

To study protein expression, 30 μ g of the total protein were mixed with 10 μ L of 2X SDS loading buffer (Tris-HCL 0.5M pH 6.8, 20% glycerol, 4 % SDS, and 0.1% bromophenol blue, and 0.2 M DTT was added freshly), denatured at 95 °C for 10 minutes, and incubated on ice. SDS polyacrylamide gel electrophoresis was prepared by pouring a (5%) stacking gel over a pre-casted (8%) resolving gels in a 1.5 mm thickness vertical casting plates (SDS-PAGE, Mini-PROTEIN Tetra Cell, Bio-Rad) (Table 4). The samples were loaded into the gel using 80 ng of the protein alongside a colour-coded prestained protein Marker (Cell Signal, 14208). The electrophoresis was performed using 40 mA constant current in electrophoresis buffer (25 mM Tris, 192 mM glycine, 0.1 % SDS, and dH₂O) until the fast migrating band (~ 10 kDa) had migrated off the gel, and the resolving gel was separated from the staking gel prior western blotting.

The protein was wet transferred to a Hybond-P PVDF 0.45 μ m membrane (Amersham, GE10600100). Before the transfer, the membrane was hydrated in 100 % methanol for 1 minute, rinsed in H₂O for 5 minutes and then equilibrated in transfer buffer (25 mM Tris, 192 mM Glycine, and 20 % methanol) for 10 minutes. The wet transfer of the protein was performed in XCell II Blot Module (Invitrogen) electrophoresis chamber by sandwiching the membrane between the SDS-PAGE gel, filter papers, and support pads with keeping the transfer membrane facing the node. The XCell chamber was filled with the transfer buffer and the transfer was performed at 30 V (Start: at ~170 mA, and End: ~110 mA, and ~ 5W) for 1 hour and 15 minutes. The Membrane was blocked with 5 % milk (prepared

in 1 X PBS, and 0.1 % Tween 20) at room temperature for 1 hour on a roller mixer. Immunoblotting with primary antibody was carried out at 4 °C overnight on a mixer using 1:500 rabbit anti-REST antibody (OriGene, TA330562) and mouse anti- β -actin (1:10000, Sigma, A1978) antibody. The membrane was washed three times in (1 X PBS and 0.1 % Tween 20) for 15 minutes on a roller mixer. The detection with the secondary HRP-conjugated antibodies was performed at room temperature for 1 hour using a mixer of anti-rabbit (1:20000) and anti-mouse (1:40000) (Cell Signalling Technology, 7074 and 7076, respectively). The membrane was washed three times in (1 X PBS and 0.1 % Tween 20) for 15 minutes. The immunoreactive bands were visualized using 1 mL of Amersham ECL Western Blotting Detection reagent (RPN2209) and the membrane was scanned using LAS-3000 intelligent dark-box (Fujifilm).

Table 4: SDS-PAGE Preparation

Constituents	8% Resolving	5% stacking gel
Water	3.33 mL	3.3 mL
30% Acrylamide/Bis-acrylamide (Severn Biotech, 29:1)	2.7 mL	1.02 mL
1M Tris pH 8.8	3.8 mL	-
0.5M Tris pH 6.8	-	1.5 mL
10% SDS	100 μ L	60 μ L
10% Ammonium persulfate	100 μ L	60 μ L
TEMED (Tetramethylethylenediamine)	8 μ L	6 μ L
Total volume	10 mL	~ 6 mL

2.2.14 Evaluating Gene Expression using the GEO-NCBI Data Sets

To explore the expression of REST, Synapsin, Synaptosome Associated Protein 25 (SNAP25), Superior Cervical Ganglion-10 Protein (SCG10) and glutamate Ionotropic Receptor AMPA Type Subunit 2 (GluR2 also, known as GRIA2) in human medulloblastoma and normal cerebellum, I used the Gene Expression Omnibus (GEO, NCBI) data sets; [GSE85217 for medulloblastoma ⁴¹, GSE109403 ¹³⁴, GSE13162 ¹³⁵, GSE42658 ¹³⁶, GSE68776 ¹³⁷, and GSE86574 ¹³⁸ were used for normal human cerebellum, and GSE34101 ¹³⁹, GSE20492 ¹⁴⁰, GSE77947 ¹⁴¹ for the Daoy cell gene expression]¹⁴². The data were downloaded and analysed using ExAtlas software (<https://lgsun.irp.nia.nih.gov/exatlas/>)¹⁴³. The analysis was performed by transforming the

values into log₂ and the correlation between the selected samples data was performed by normalizing the values using a set of pre-selected housekeeping genes. The quality of the normalized samples were assessed by the standard deviation (SD) and ANOVA with error variance adjustment (also, known as empirical error variance) ¹⁴³.

2.2.15 The Statistical Analysis and Visualization

The normal distribution of the data was examined using Shapiro–Wilk test and *P*-values of >0.05 was used to show that the data may follow a normal distribution. Significant differences between the means were evaluated using the Unpaired t-test and the One-Way ANOVA, and the two tailed and the *P*-values of <0.05 were considered significant and the measures were presented as means ± standard error of the mean (SEM). Statistical analysis was performed using the GraphPad Prism version 8.0.1 for Windows, GraphPad Software, La Jolla California USA, (www.graphpad.com).

The heatmaps were generated using the Heatmapper web server tool (<http://www2.heatmapper.ca/expression/>) ¹⁴⁴ or the Seurat R function of heatmap.3. The violin plots were generated using the ggplot2 R package, and the t-SNE plots were generated using the Seurat (TSNEPlot) function. The Venn diagrams were produced using Venny online tool (v.2.1) (<http://bioinfogp.cnb.csic.es/tools/venny/index.html>).

Chapter 3

3 Results I

(Investigating the contribution of REST in Medulloblastoma)

3.1 Preface

3.1.1 The aim and the Objectives of the Study

This study aimed to investigate the contribution of REST in the medulloblastoma Daoy cell proliferation, cell cycle, migration, and to identify if HDACis induce their therapeutic action through the HDACs that are recruited in REST repression complexes.

3.1.2 The objectives of the study

- Identifying the difference in REST expression between the medulloblastoma tumours and the normal brain tissue and across the medulloblastoma subgroups and subtypes
- Modulating REST expression in the Daoy medulloblastoma cell line using both CRISPR/Cas9 and shRNA systems, and investigate the effect of REST depletion on the expression of the RE1-containing genes, on the cell proliferation, and on the migration ability
- Investigating whether the HDACis induce their therapeutic action through the HDACs that are recruited in REST repression complexes

3.1.3 The Roadmap

To address the research questions, the expression of REST in the Daoy cell line was modulated using the CRISPR/Cas9 and the shRNA systems to knockout and knockdown REST expression, respectively. The effect of REST modulation was then examined; on the expression of the cell proliferation, the cell cycle, and on the migration ability of the cell. Also, the sensitivity of the cells to HDACis was examined before and after REST modulation. Additionally, the study used the GEO-NCBI gene profiling data of medulloblastoma patients' tissue samples to explore the expression difference of REST

between the medulloblastoma tumours and normal cerebellum, and between the medulloblastoma classes (Figure 10).

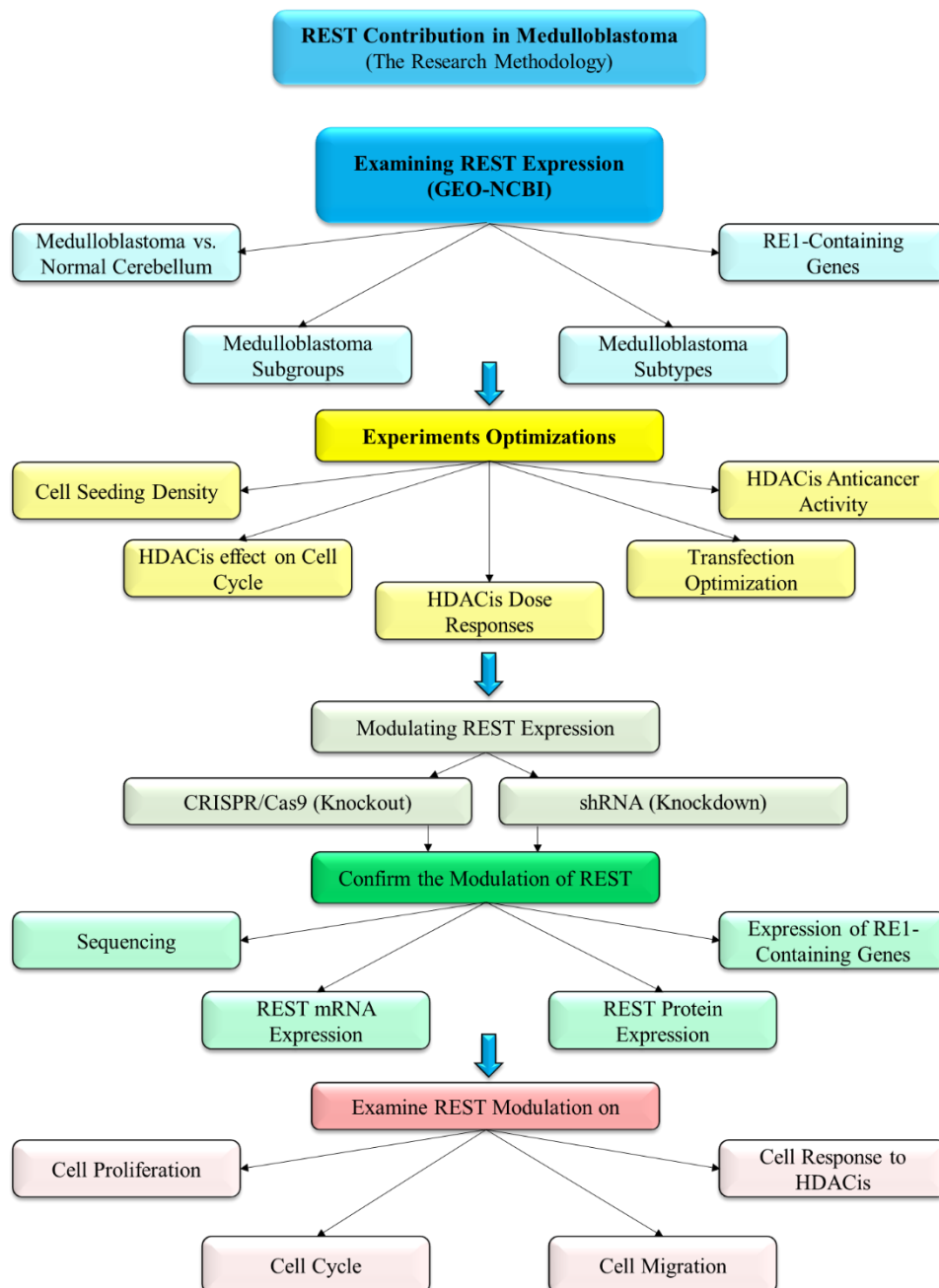


Figure 10: Schematic representation of the research workflow

The research started by optimizing the experimental condition of the cell seeding density, the HDACis dose response curves, Daoy transfection optimization, and measuring the effect of HDACis on the cell growth and the cell cycle. REST expression was then modulated using the CRISPR/Cas9 and the shRNA systems. The conformation of REST modulation was carried out by the DNA sequencing, measuring REST mRNA and protein expression, and the expression of some RE1-containing genes. The contribution of REST modulation on the Daoy cell growth, the cell cycle, the cell migration, and the cell response to HDACis was then examined.

3.2 The Results

3.2.1 Investigate REST Expression using Published Microarray Gene Expression Data

Elevated REST expression has been reported in approximately 80% of the medulloblastoma tumours^{11, 14, 50}. However, it is not known if all the subgroups and the subtypes display an elevated REST expression. In this analysis, the Gene Expression Omnibus (GEO, NCBI) microarray database was used to examine the variations in REST expression between the medulloblastoma tumours and normal brain cerebellum¹⁴². Also, the expression of REST and its functional effect on the RE1-containing genes was evaluated in the Daoy cell line.

3.2.1.1 REST Expression is Higher in Medulloblastoma Tumours Compared to Normal Cerebellum

To examine the difference in REST expression between the medulloblastoma tumours and normal cerebellum, the GSE85217 data set was compared to normal cerebellum samples using the ExAtlas tool⁴¹. This data set contains 763 fresh-frozen primary medulloblastoma tissue samples which were originally classified according to their genetic and the methylation signature into the 4 subgroups and the 12 subtypes of the medulloblastoma classes⁴¹. The analysis was performed using the ExAtlas tool which normalizes the values between the data sets using a set of pre-selected housekeeping genes¹⁴³.

Comparison of REST expression between the medulloblastoma groups and the normal cerebellum showed a significant ($P < 0.0001$) increase in REST level in the tumour samples by 0.3-fold change (Figure 11 A). On the level of the medulloblastoma subgroups, the expression of REST showed some differences between the subgroups. For example, the WNT subgroup showed the highest expression of REST whereas, the Group 3 and the SHH subgroups showed relatively equivalent expression with an extensive variation between the samples of the SHH subgroup. In contrast, the mean of REST expression of the Group 4 was the lowest among all the subgroups however, around 50% of the samples displayed a relatively similar REST expression to the SHH and Group 3 (Figure 11 A).

Further, I clustered the samples according to the proposed medulloblastoma twelve subtypes in order to demonstrate the expression difference of REST between and within the subtypes⁴¹. The analysis revealed that the WNT β subtype displayed the highest REST expression though, the difference in the mean between WNT β and α was not significant ($P=0.531$). Also, the results revealed a statistically significant difference between the means of the SHH subtypes as determined by one-way ANOVA ($p<0.0001$) (Figure 11 B). Both of the SHH α and β subtypes displayed an elevated REST expression compared to γ and δ subtypes. Whereas, the expression of REST was comparable between Group 3 subtypes as determined by one-way ANOVA ($P=0.0539$). Group 4 showed a significant difference between the means of the α and β subtypes compared to the γ subtype (ANOVA $P<0.0001$) and they demonstrated the lowest expression of REST in all medulloblastoma classes (Figure 11 B).

In order to evaluate the effect of REST expression, I extracted the expression values of some REST-regulated genes that are known by their high sensitivity to the modulation in REST expression and the high occupancy of REST to their RE1 sites (Synapsin (regulates synaptogenesis), SNAP25 (is a membrane fusion and involved in neurotransmitter release), SCG10 (helps in regulate the microtubule dynamic and stability) and GluR2 (is a neurotransmitter receptors))¹⁴⁵. The expression of Synapsin and SNAP25 was low ($P<0.0001$) in the medulloblastoma subtypes compared to the normal cerebellum. Also, it was lower in the subtypes that display elevated REST expression such as the WNT subtypes when compared to the subtypes with low REST expression such as the Group 4 subtypes (Figure 11 C and D). Unexpectedly, the expression of SCG10 and GLuR2 was high in the medulloblastoma subtypes compared to the normal cerebellum apart from the GLuR2 ($P<0.001$) in the WNT and Group 3 subtypes (Figure 11 E and F).

Taken together, the expression of REST in the medulloblastoma tumours is variable between the subtypes and within each subtype and it showed an elevated expression with the WNT and SHH pathways. The WNT subgroups showed the highest REST expression whereas, the Group 4 α and β subtypes exhibited the lowest expression among all subtypes. These findings may indicate that the contribution of REST in medulloblastoma could be different between the subgroups.

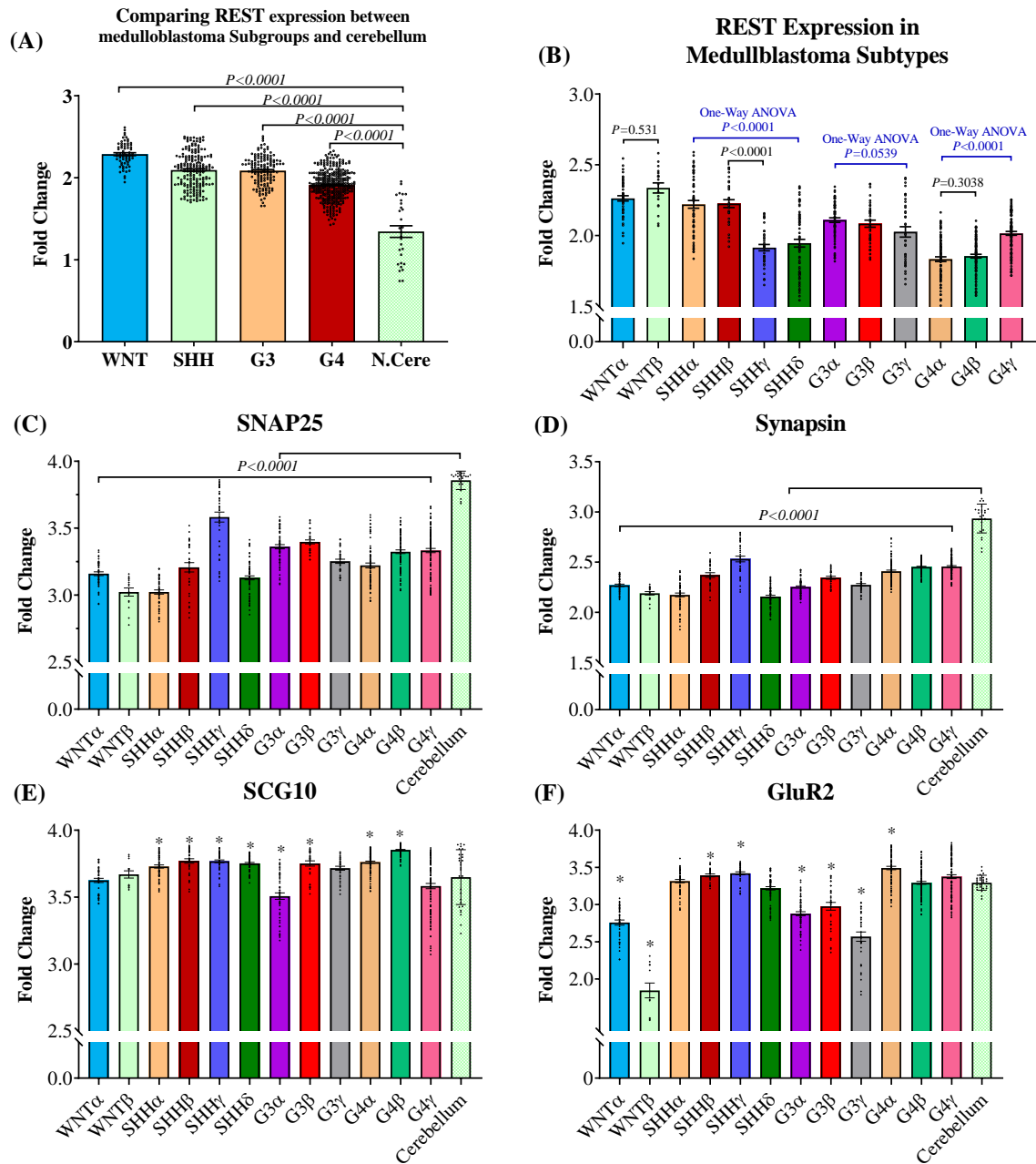


Figure 11: The expression of REST and some selected RE1-containing genes in medulloblastoma and normal cerebellum tissue samples

The expression of REST in the medulloblastoma subgroups (A) and the subtypes (B), and expression of SNAP25 (C), Synapsin (D), SCG10 (E), and GluR2 (F) was extracted from the GEO NCBI database using ExAtlas tool. The expression values were represented by the circular dots and the difference between the means was calculated using the two tailed Student's *t*-test (the * in E and F is $P < 0.001$) and the One-Way ANOVA (SHH subtypes ($F(3, 143) = 29.61, P < 0.0001$), Group3 ($F(2, 102) = 6.305, P = 0.003$), and Group4 ($F(2, 221) = 75.07, P < 0.0001$)), and the error bars are SEM.

3.2.1.2 REST Expression is Elevated in the Daoy Medulloblastoma Cells Compared to Normal Cerebellum

Elevated REST expression in the Daoy cell has been reported previously in several studies^{11, 14, 115}. In this study, I used the GEO gene expression data to identify the expression difference of REST between the Daoy cell and normal cerebellum. The result showed that the expression of REST was almost 1.8-fold change ($P < 0.0001$) higher in the Daoy cell compared to the normal cerebellum (Figure 12 A). To evaluate if the increase in REST expression has a significant functional effect on the RE1-containing genes, I compared the expression of the aforementioned genes between the Daoy cell and the normal cerebellum. The results showed that the expression of the genes in the Daoy is at least one-fold ($P < 0.0001$) less compared to the normal cerebellum (Figure 12 B).

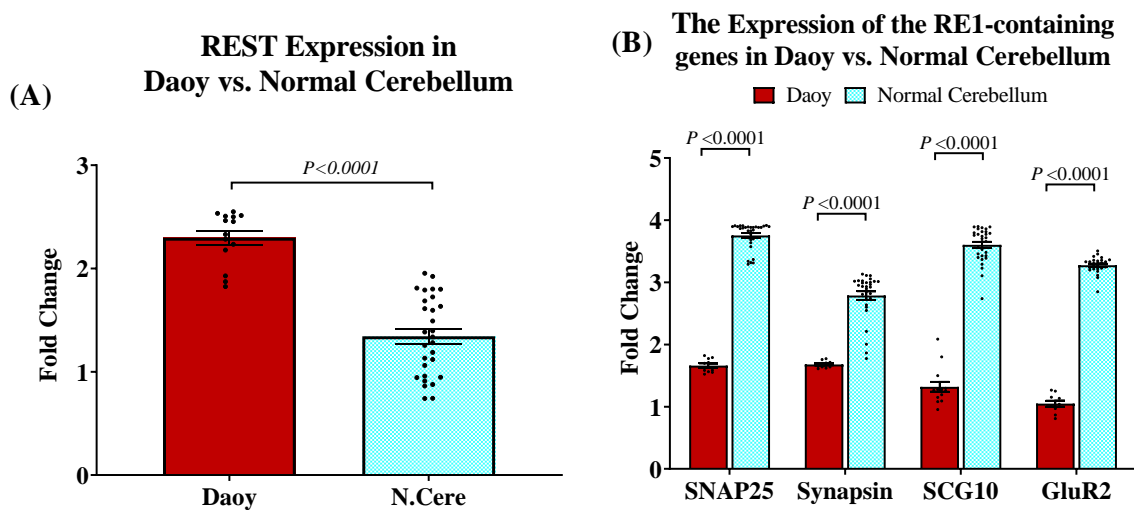


Figure 12: The expression of REST and RE1-containing genes in the Daoy cell and normal cerebellum

(A) Shows the expression of REST in the Daoy cell and the normal brain cerebellum. (B) Shows the functional effect of REST expression on the expression of the RE1-containing genes. The expression values are represented by the circular dots and the differences between the means was calculated using *t*-test and the error bars are SEM.

3.2.2 The Experimental Optimization to Examining REST contribution in Medulloblastoma

3.2.2.1 Daoy Seeding Density of 3.5×10^4 cell/mL Reaches ~100% Confluence by 72 Hours

Daoy is a highly proliferative cell with a population doubling time of around 29.8 hours⁷. Generally, the confluency of the cells could have a major impact on the cell response to the treatment which may affect the comparison between the biological replicates. Hence, I started by identifying the cell count that yields 90 to 100 % confluency by 72 hours. This experimental condition was selected in order to study the sensitivity of the cell to HDACis. The confluency was defined as the proportion of the culture surface that was covered by the cells at the time of measurement thus, a confluency of 50 % means half of the culture surface was covered by cells.

To identify the seeding density that gives the former experimental condition, several dilutions (1×10^4 , 2×10^4 , 5×10^4 , and 1×10^5 cell/mL) of the Daoy cell were prepared in volumes of complete culture media and cultured in 6-well culture plates. The confluence of the cells was assessed at 24, 48, and 72 hours using an inverted microscope and the cells at each time point were also counted using haemocytometer cell counter.

During the first 24 hour, both the 5×10^4 and 1×10^5 densities showed an increase in the cell count in comparison to the seeding time by more than 40% and 20%, respectively. Microscopically, the 5×10^4 cells started to show high confluency by the 48 hours, and at the 72 hours they showed an increase in the number of the detached cells and a decline in the number of the living cells by around 20%. This outcome could be due to the high cell number which led to the consumption of the media nutrients and possibly affected the other cell functions. In contrast, the 2×10^4 and 1×10^4 densities have reached a confluence of 50% and 20% at 72 hours and their count increased by 30% and 15%, respectively (Figure 13 B). As the 1×10^5 and 5×10^4 showed high confluence after 48 hours whereas, the 2×10^4 did not reach the required confluence, I used a cellular density of 3.5×10^4 cell/mL for all the subsequent experiments.

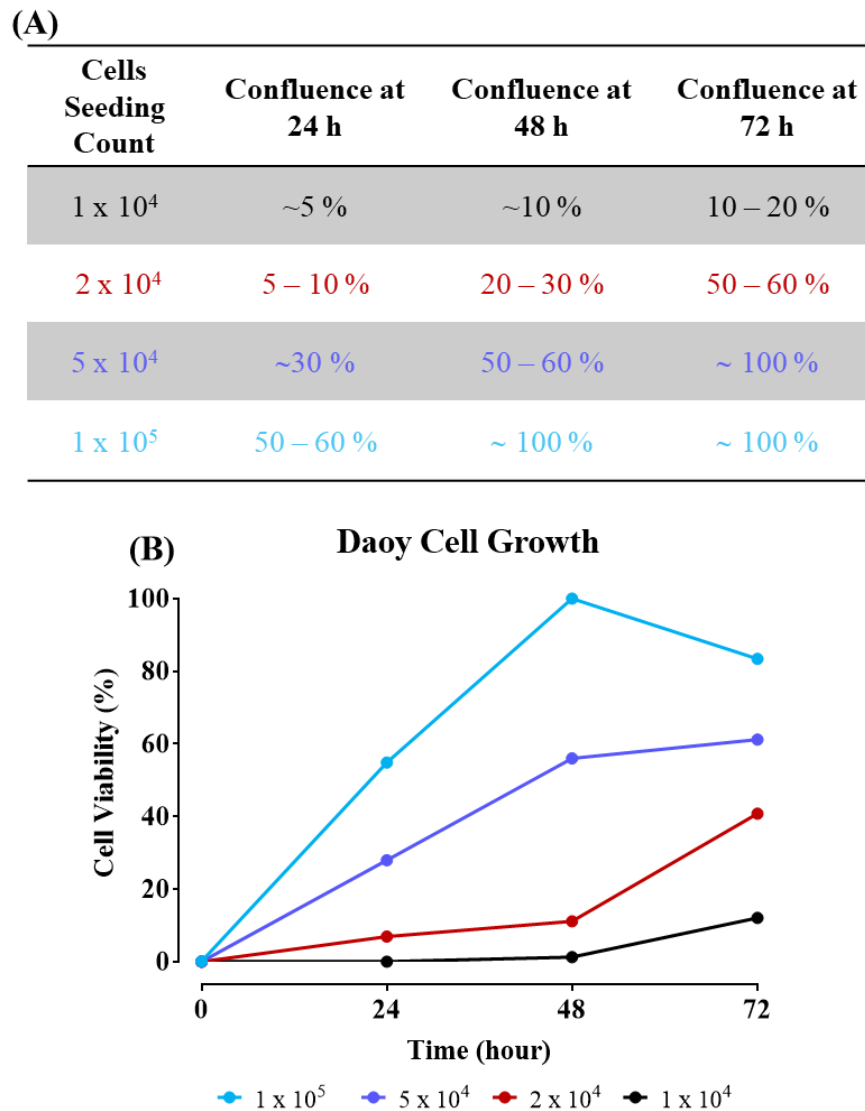


Figure 13: Identifying the Daoy cell count that yield 90 – 100% confluence after 72 hours from culturing

Different densities (1×10^4 , 2×10^4 , 5×10^4 , and 1×10^5 cell/mL) of the Daoy cell were prepared in a complete culture media and seeded into 6-well culture plates. The confluence of the cell (A) was evaluated microscopically every 24 hours from the seeding by assuming a confluency of 50% as half of the culture surface is covered by the cells. The cells at each time-point were counted and the percentage of the growth was calculated by assuming the concentration of 1×10^5 cell/mL at 48 hours (the highest reading) as 100% and the other readings were proportioned to its value (B).

3.2.2.2 Generating the Cell Dose-Response Curve for HDACis

HDACis are a family of anticancer drugs that inhibit the deacetylation of the histone and non-histone proteins leading to change the gene expression, the cell metabolic activity, and the cell cycle which ultimately result in stimulating apoptosis⁸¹. Both the *in vivo* and *in vitro* analysis demonstrated the high sensitivity of the transformed cells to HDACis compared to normal cells^{75, 146}. Based on the distinct chemical structure of the HDACis, they have been grouped into four main classes. In this study, I examined, at least, a drug from each of the four structural groups (SAHA is hydroxamic acid structural groups, MS-275 and MI-192 are bibenzimidides, Apicidin is cyclic tetrapeptide, and VPA is classified under the Short-chain fatty acids group).

The analysis was started by generating Daoy cell dose-response curve for each inhibitor. The dose-response analysis was performed by seeding the cell at 3.5×10^4 cell/mL in 96-well culture plates and after 24 hours from the culturing, the media was replaced with ranges of the inhibitor's concentrations. Untreated and DMSO controls were included with each measurement and the anticancer effect of the drugs was measured after 72 hours from the exposure using the MTT assay. The colorimetric results of this assay were presented as percentage by assuming the value of the Daoy untreated control at 72 hours as 100% and the values of the other reading were proportioned to its value.

The absorbance of the untreated Daoy control showed robust growth and reached a plateau at 72 hours. The DMSO control did not show any significant cytotoxicity and the cell continued to grow with very minimal difference to the untreated cell. In contrast, the HDACis treated cells showed a progressive reduction in the cell viability in a concentration-dependent manner (Figure 14). SAHA, MS-275, MI-192 and Apicidin have induced their antiproliferative effect in sub-micromolar concentrations with complete cell death at the highest concentrations apart from SAHA which showed some viable cells at 10 μ M. In contrast, VPA induced a slight increase in the cell proliferation rate at the 0.03mM concentration. With higher concentrations, VPA showed a concentration-dependent effect and exhibited more than 95% cell death with the 15 mM concentration.

The generated dose-response curves were also used to estimate the IC₅₀ (half maximal inhibitory concentration) of the cell at 72 hours (Figure 14). The subsequent analysis were carried out using [SAHA (5 μ M), MS275 (5 μ M), MI192 (3 μ M), APICIDIN (3 μ M), and

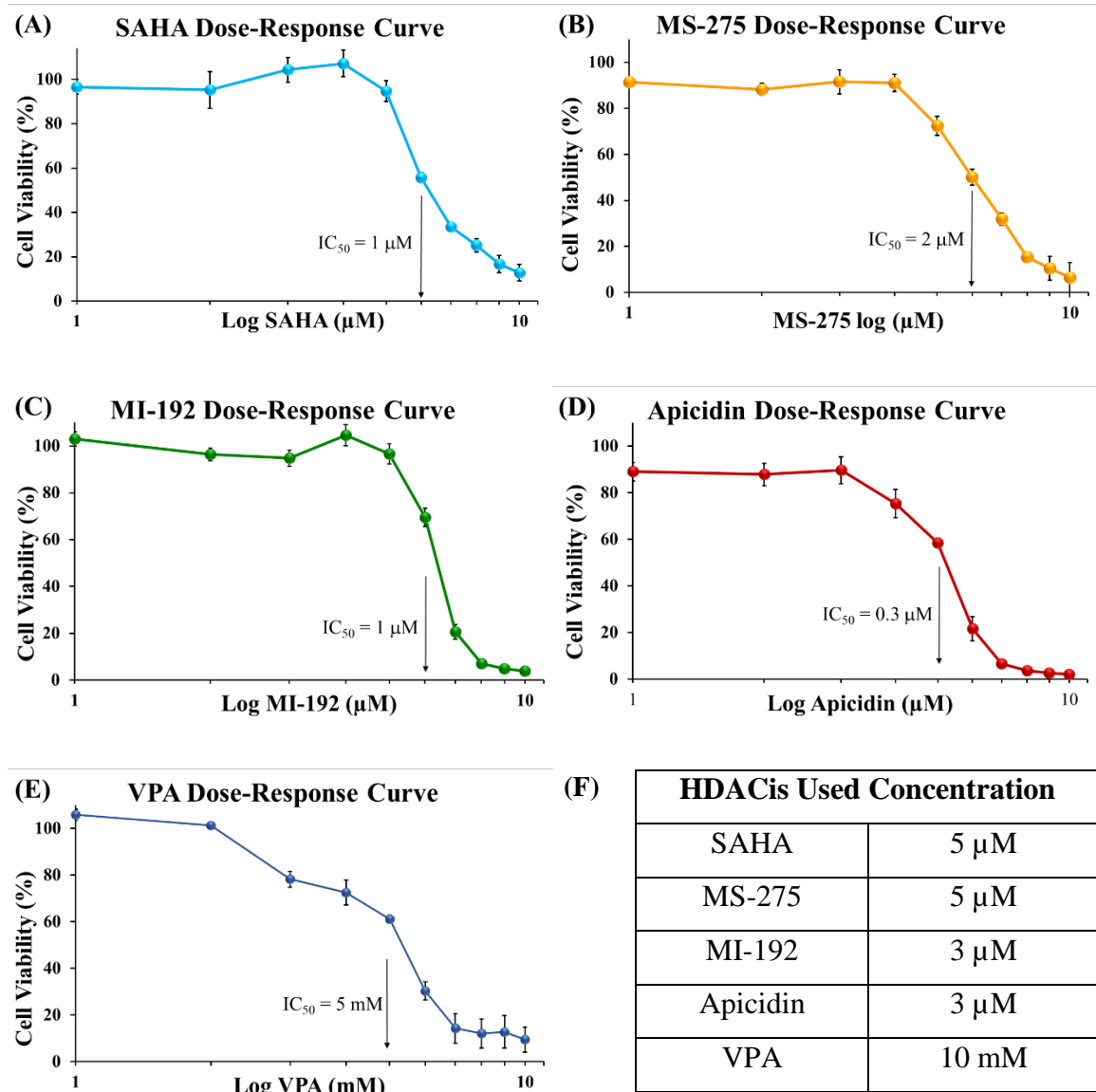


Figure 14: The Daoy cell dose-response curves showed a concentration-dependent effect of HDACis on the cell growth

The Daoy cells were seeded at 3.5×10^4 cell/mL into 96-well plates, and after 24 hours incubation the media was replaced with ranges of the HDACis concentrations; SAHA (0.003 μ M to 5 μ M) (A), MS-275 (0.01 μ M to 6 μ M) (B), MI-192 (0.003 μ M to 5 μ M) (C), and VPA (0.03 mM to 15 mM) (D). The viability of the cells was measured after 72 hours from the treatment using the MTT assay. The results are the average of three independent replicates and presented in percentage by assuming the value of the vehicle control at 72 hours as 100% and the values of the other reading were proportioned to its value. The error bars are SEM. Table (F) shows the used concentrations in the subsequent analysis.

VPA at (10 mM)] concentrations which induce a significant cell death at 72 hours. These concentrations have been reported to induce tumour cell death though, they do not affect the viability of normal cells ^{147, 148, 149}.

3.2.2.3 HDACis Showed Variable Anticancer Activity and a Time-dependent Effect

As most anticancer drugs, HDACis have been reported to reduce the tumour cell growth and stimulate apoptosis in a time-dependent manner ^{65, 150}. In this study, the difference in the anticancer activity between the used inhibitors was investigated in a time-course manner. The analysis was performed by treating the cell with a single concentration of SAHA (5 μ M), MS-275 (5 μ M), MI-192 (3 μ M), Apicidin (3 μ M), and VPA (10 mM) and the viability of the cell was measured at 0, 12, 24, 36, 48, 60 and 72 hours from the exposure using the MTT assay. Untreated controls were included with each time-point which were used later to normalize the results of the treated cells.

The MTT results exhibited the ability of HDACis to induce a progressive reduction in the cells count in a time-dependent manner yet, the anticancer activity was slightly different between the drugs (Figure 15). For instance, the viability results of MI-192 showed a rapid and statistically significant ($P \leq 0.05$) decline in the total number of the cells by more than 15% at the 12-hours measurement and it continued to eradicate the cell by around 50% between a time-point and the subsequent time-point ($P \leq 0.001$) (Figure 15 C). Whereas, the effect of SAHA, Apicidin and VPA started at the 24-hours with more than 20% reduction ($P \leq 0.001$) in the total count of the cells. The Apicidin effect was more progressive and it reduced the cell number by more than 60% at the 36-hour ($P \leq 0.001$). The SAHA effect was gradual with around 20% reduction between the time-points whereas, the VPA effect was slightly low compared to the other inhibitors and it showed around 15% reduction between a time-point and the subsequent point ($P \leq 0.001$). In contrast, MS-275 did not show any significant anticancer effect during the first 24 hours of the exposure though, at the 36-hours it started to show a significant reduction ($P \leq 0.001$) in the cell number by more than 20% and it eradicated most the cells at the 72 hours.

The results were further used to measure the amount of the dead cells at each time point by calculating the difference between the value of a time point and the time point before it. These investigations may appear as an inverse to the above cells viability results though,

it was used to show the anticancer effect of HDACis from two sides (Figure 15 F). The results of the dead cells clearly showed that all the inhibitors induce their anticancer effect after the first twelve hours, apart from MI-192 which showed a rapid increase in the dead cell at the 12-hours reading by around 13% and it reached to more than 30% at the 36-hours. SAHA and Apicidin showed more than 20% dead cell at the 24-hour time point though, the Apicidin anticancer effect continued to increase and reached to 40% at the 36-hours (Figure 15 F). The anticancer activity of 10 mM VPA concentration was relatively equivalent to the micromolar-concentration of the other inhibitors yet, its anticancer activity during the first 48-hours was lower in comparison with the other inhibitors (Figure 15 F).

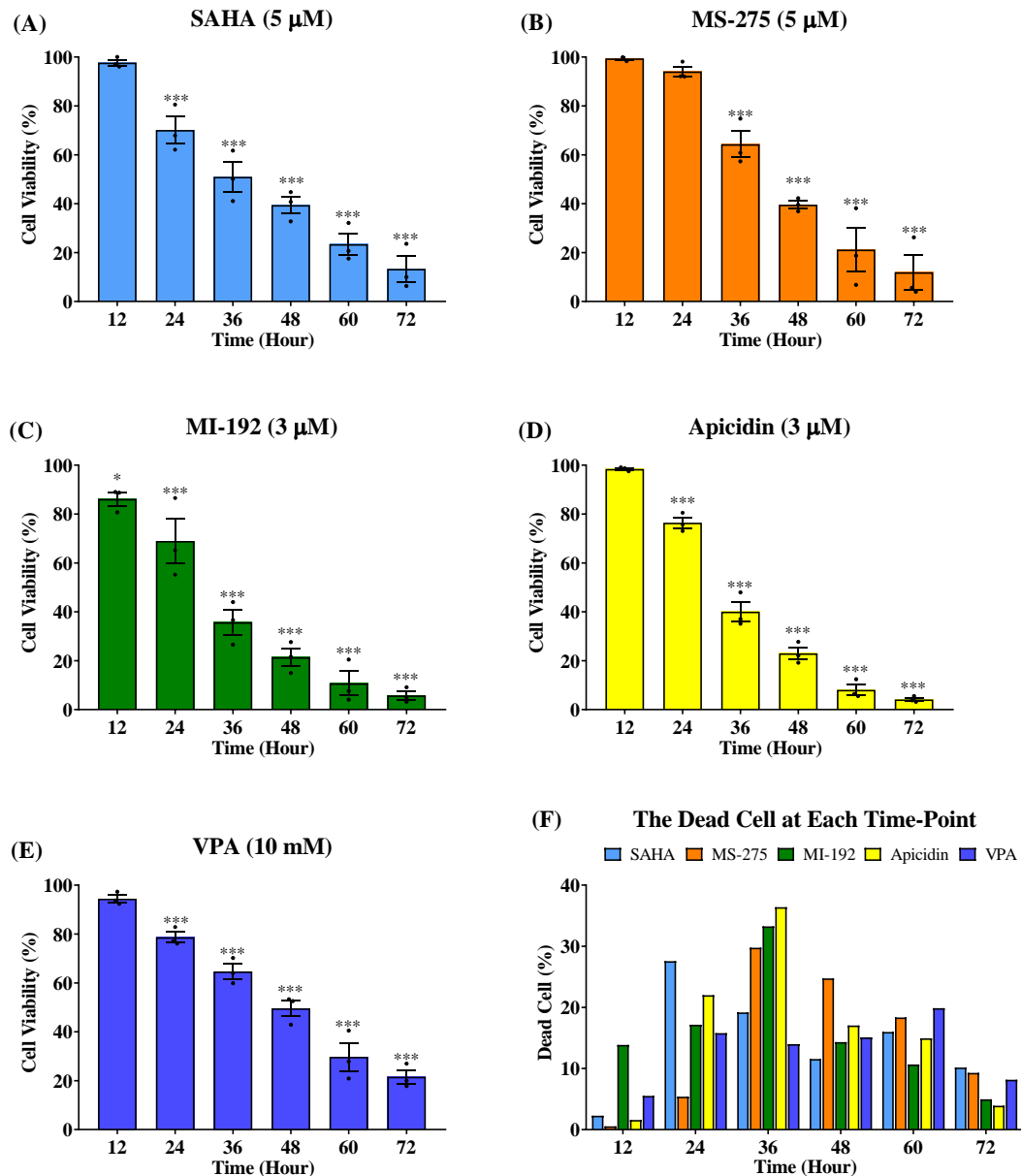


Figure 15: HDACis induce a time-dependent antiproliferative effect

A time course analysis of the HDACis anticancer effect. The Daoy cells were seeded at 3.5×10^4 cell/mL into 96-well plates and after 24 hours the cells were treated with a single dose of SAHA (5 μ M) (A), MS-275 (5 μ M) (B), MI-192 (3 μ M) (C), Apicidin (3 μ M) (D), and VPA (10 mM) (E). Untreated controls were included with each time point. The viability of the cell was measured at 12, 24, 36, 48, 60, and 72 hours using the MTT assay and the results of each time point was normalized to the untreated control (not displayed in the graphs). The dots represent the values and the P-value was calculated using the two tailed Student's t-test (* $P \leq 0.05$, *** $P \leq 0.001$) by comparing the values of a time point

to the untreated control of the same time-point which was considered as 100%. The error bars are SEM. The amount of the dead cell (F) for each time point was measured by calculating the difference in the MTT absorbance between a time point and the time point before it. The results are the average of three independent replicates and represented in percentage.

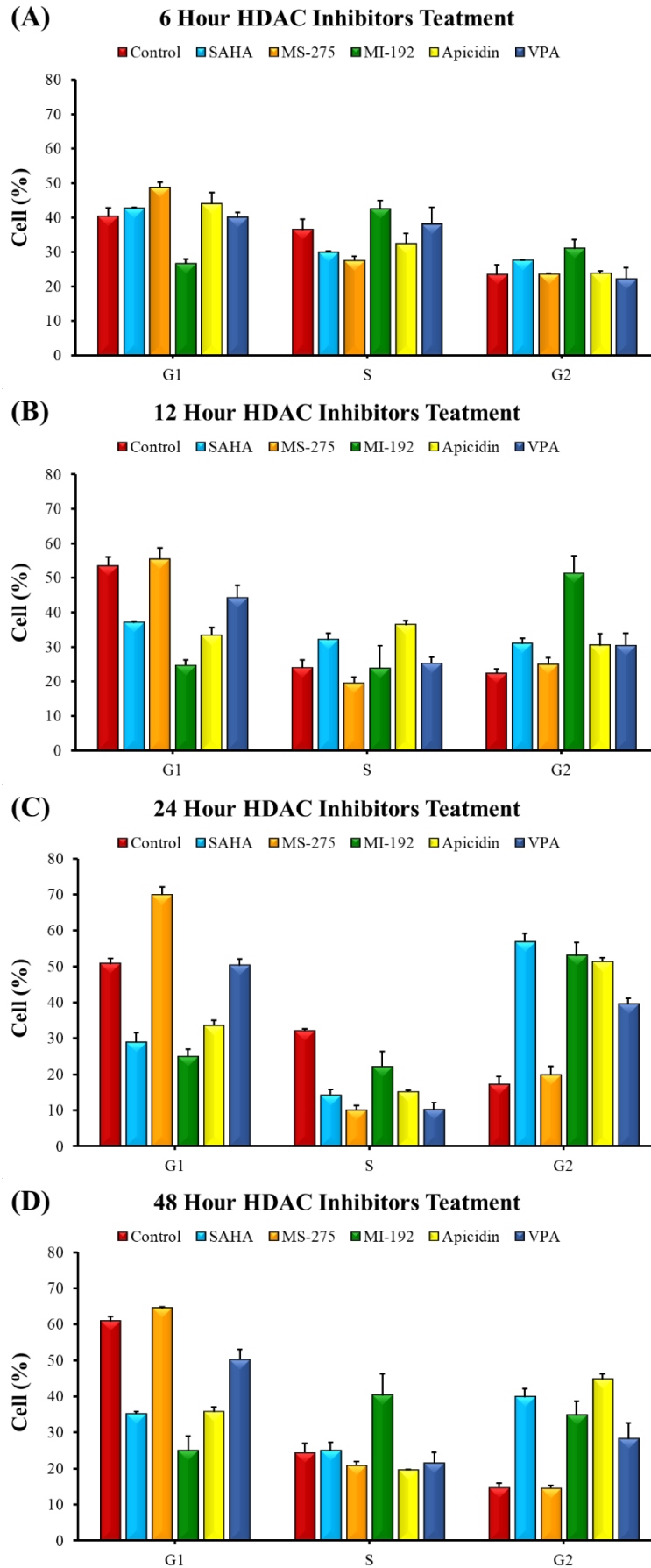
3.2.2.4 HDACis Induced a Prolonged Cell Cycle Delay and not a Complete Cell Cycle Arrest

HDAC enzymes have a considerable role in regulating several cellular functions including the cell cycle. In several studies, HDACis have been claimed to cause cell cycle arrest at G2 phase yet, this conclusion was based on the results of a single time-point analysis^{151, 152, 153, 154}. In this study, the effect of HDACis on the Daoy cell cycle was investigated by treating the cell with HDACis in a time-course manner (at 6, 12, 24, 48 and 54 hours from culture). This approach helps in showing the dynamic and the duration of each phase and aids in revealing if HDACis induce a complete cell cycle arrest.

The distribution of the cells in each phase can be assessed by staining the cells with PI and assay them on FACS¹⁵⁵. The concept of this analysis depends on the amount of the DNA in each phase, and the fluorescence intensity of the PI is presumed to be stoichiometric relationship to the DNA content¹⁵⁵. For example, in G1 and G2 phases the DNA is uniform and it is equivalent to the DNA ploidy index (DI) of 1.0 for G1 and 2.0 for G2/M, where the DI in S phase is between 1.0 and 2.0¹⁵⁶.

The results of this analysis displayed that the untreated cell have an active cell cycle profile (Figure 16). Whereas, the results of the treated cells showed a non-stopping cell cycle with a prolonged delay in the progression between the phases however, there was no evidence for the cell cycle arrest. The results of SAHA and Apicidin showed a relatively similar pattern. For instance, they show more than 30% increase in the cells of the G2 phase at the 24-hours however, the accumulation slightly decreased at the 48 and the 54-hours (Figure 16). MS-275 showed different pattern of cell cycle delay. At the 6-hours, it showed ~10% increase in G1 phase accumulation and it reached to more than 70% at the 24-hours. This accumulation was associated with a decrease in S and G2 phases cell count (Figure 16). Similarly, MI-192 also showed different pattern of

cell cycle delay however, its effect started at the 6-hours with ~15% accumulation in G1 phase. At the 24-hours, it induced an increase in cells accumulation in G2 by ~30% yet, at the 54-hours it increased the accumulation in S phase by more than 40% compared to the untreated cell (Figure 16). The effect of the VPA started at the 24-hours with around 20% increase in G2 phase though, it did not last for long and the distribution of the cell in the S phase started to increase at the 48-hours (Figure 16).



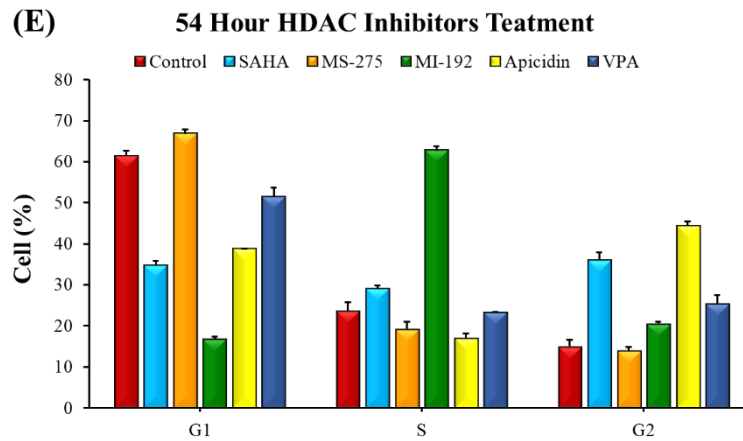


Figure 16: HDACis induced a prolonged cell cycle delay though, it did not arrest the cell cycle

The effect of HDACis on the distribution of the cells in the cell cycle phases. The cells were treated with the HDACis and harvested at 6h (A), 12h (B), 24h (C), 48h (D), and 54h (E) from the treatment. The cells were fixed in 70% ethanol and stored at -20 °C for at least 24 hours. Before the analysis, the cells were treated with RNase A, stained with PI, and analysed on FACS. The cell distribution results are the average of 3 biological replicates and the accuracy of the DNA measurements was assessed by the CV value of the G1 mean (≤ 6)¹⁵⁷. The error bars are SEM.

3.2.2.5 Optimizing the Transfection of the Daoy Cell

In order to identify the optimal ratio between the Lipofectamine transfection reagent and the plasmid DNA concentration, I used three concentrations (125, 250 and 500 ng) of the pCMV- β -gal plasmid with a Lipofectamine reagent ratio of 1:2, 1:3, and 1:4 to transfect the Daoy cell. The results showed that the transfection ratio of 1:2 DNA to Lipofectamine was not enough to introduce the DNA into the cells and it did not cause any noticeable cell death. Whereas, the 1:4 ratio showed more than 40% efficiency with all the DNA concentrations, but it induced more than 60% cell death. The 1:3 ratio showed more than 20% transfection efficiency with the 125 and 250 ng of the DNA, with the 500 ng the transfection efficiency reached to around 30% and the cell death was less than 30% (Figure 17). As the 1:3 ratio showed the lowest cell death and generated around 30% transfection efficiency with the 500 ng hence, the transfection reactions of the shRNA knockdown were prepared using 1:3 ratio with 750 ng of the DNA.

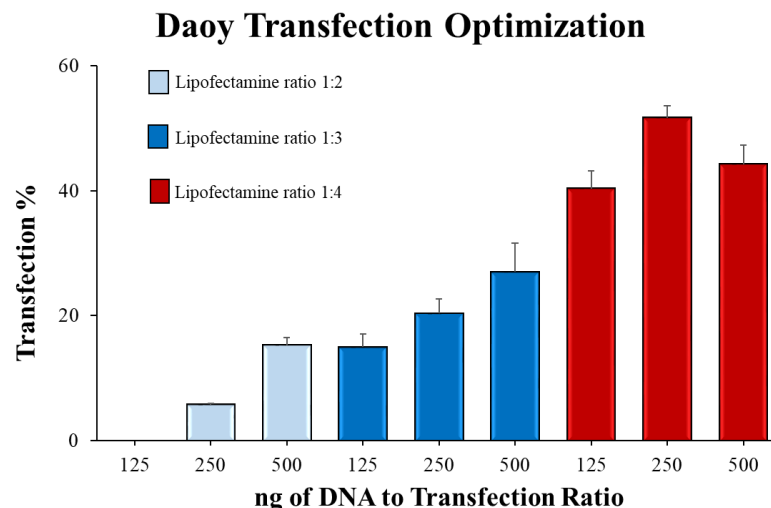


Figure 17: Daoy Cell Transfection optimization

The X-Gal assay was used to optimize the lipofectamine transfection reaction. The Daoy cell with 60 - 80% confluency was transfected with the pCMV- β -gal plasmid using 125, 250 and 500 ng of the plasmid DNA to Lipofectamine reagent at ratios of 1:2, 1:3, and 1:4. After 48 hours from the transfection, the cells were exposed to X-gal solution and incubated overnight for colour development. The effect of the transfection on the cell viability was evaluated under inverted microscope, and the transfection efficiency was measured by identifying the proportion of the stained to non-stained cells.

3.2.3 Modulating REST Expression in the Daoy Cell

To study the effect of REST ‘loss-of-function’ on the Daoy cell and to investigate whether HDACs induce their action through the HDACs recruited in the REST repression complexes, I disrupted REST expression using the CRISPR/Cas9 and shRNA systems.

3.2.3.1 Modulating REST Expression Using CRISPR/Cas9

With the CRISPR/Cas9 system, two guide RNA (gRNA) sequences were used to selectively target the sense and the anti-sense strand of REST exon 2 (Figure 18 A). The off-target effect for each gRNAs was examined using NCBI-blast and the analysis displayed the 100% sequence identity and covary of the gRNAs to the human REST mRNA transcription variant 1 and 2 (NCBI Reference Sequence: NM_005612.4 and NM_001193508.1). The E value, which represents the number of hits that is expected to be found in the NCBI blast search, was 0.017 (the closer to zero the more significant the match is). The shortest sequence compatible with other genomic sites is 18 bp for gRNA1 and 16 bp for gRNA2 and they aligned to ZNF91 (a zinc finger protein of the KRAB (Kruppel-associated box) and NEAT1 (a long non-coding RNA), respectively. The shortest sequence of the scramble control that is compatible with other genomic sites was 15 bp with E-value of 9.1. These results demonstrate the low probability of the two gRNA sequences to induce off-target effect. In order to isolate cells with complete knockout of REST expression, the CRISPR/Cas9 transfected cells were grown as a single cell per culture to produce a monoclonal cell growth. The cells were screened for the genome editing by amplifying the editing sites and the products were analysed using Sanger sequencing. The sequencing results of 140 monoclonal cell growths showed the presence of 6% of the cells with mono-allelic genome editing in forms of a single nucleotide deletion and/or insertion in REST exon 2 (Figure 18 B).

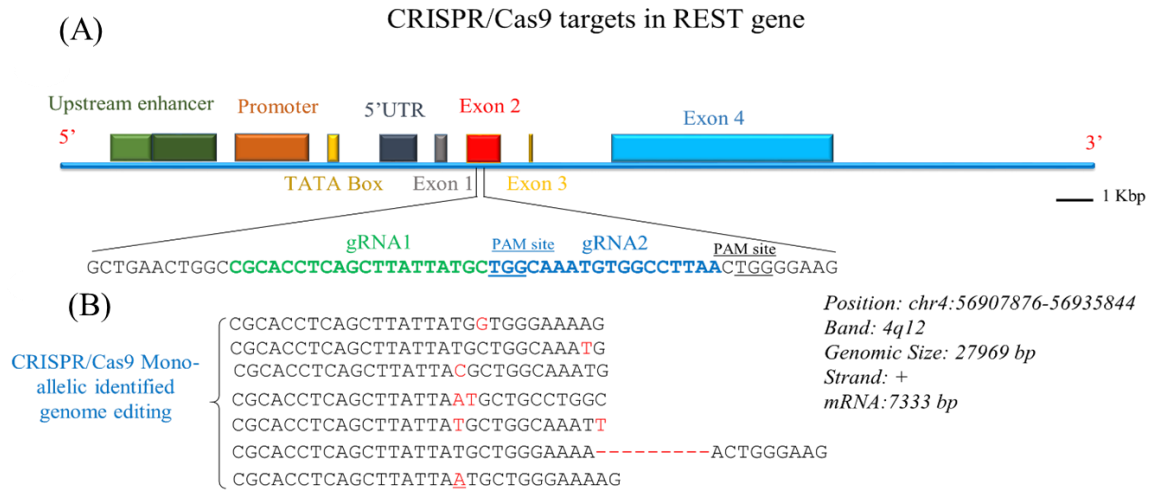


Figure 18: CRISPR/Cas9 induced mono-allelic genome editing

(A) A schematic diagram of the REST gene regulatory regions, the exons, the genome target site of gRNA1 (green) and gRNA2 (blue) at exon 2, and the PAM sites (TGG) which are located immediately following the gRNA sequence. (B) Examples of the mono-allelic genome editing in form of insertion (AT, T, C, or GAAAA) or deletion (TGTGGCCTTA).

Interestingly, the PCR screening revealed a cell clone (hereinafter referred to as KO) with a single PCR product of more than 1500 bp and no amplification product at 326 bp (the expected product size) which may suggest that the genomic editing in this clone could involve all REST alleles (Figure 19). Sequencing of the KO cell clone has identified a homologous recombination of more than 1500 bp DNA insert at the editing site. The NCBI blast analysis of the insert referred the sequence to a highly conserved E. coli enzyme, known as triphosphoribosyl-dephospho-CoA synthase (citrate fermentation enzyme).

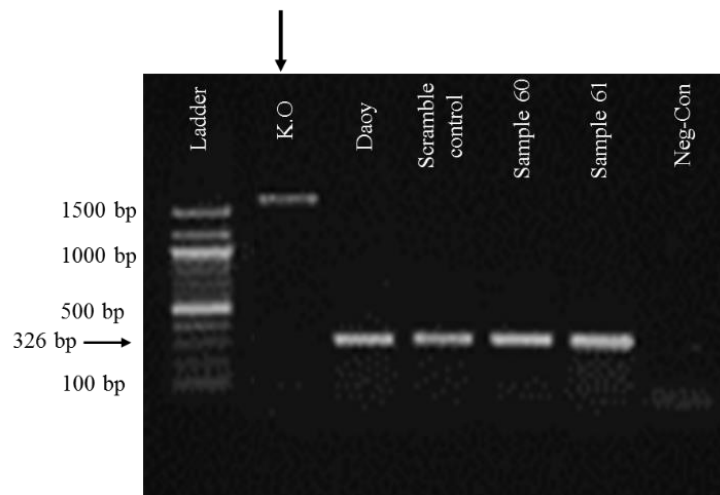


Figure 19: CRISPR/Cas9 has induced homologous recombination genome editing

Agarose gel electrophoresis (1.2%) shows the PCR amplification products of the CRISPR/Cas9 editing sites. REST exon 2 was amplified using specific primers to amplify the editing sites. The cell clone KO showed a single PCR product of more than 1500 bp and did not show the expected product size (~ 326 bp).

With the knockout approach, to achieve functional knockout both copies of a gene should be mutated (biallelic mutation). Hence, to confirm the biallelic editing of REST in the KO cell, the editing site was amplified using SYBR green qPCR. For efficient SYBR green amplification signal, the recommended amplicon length should be between 50-150 bp. Amplifying longer fragments of cDNA mostly leads to loss of the qPCR efficiency in detecting the fluorescence signal which it could be due to the inability of the reaction to produce completed PCR products that can be used as templates in further cycles¹⁵⁸. Accordingly, this reaction is expected to show amplification with the wildtype and if the editing in the KO cell involved one allele (monoallelic editing) as the size of the product is 188 bp. If all the REST alleles in the KO cell were edited the qPCR should show no amplification due to the long fragment of the insert (~1500 bp). As this reaction generates negative results (no amplification), a positive control that amplifies REST exon1 (known here as E1) was included. In this study, I used U6 Small Nuclear 1 RNA (RNU6, also known as RNU6-1) as an endogenous control to normalize the qPCR results. This gene has been widely used to normalize the qPCR results due to its consistent high expression in transformed cells compared to healthy controls also, it characterized by its narrow standard deviation^{159, 160, 161}.

The qPCR results showed an amplification with the Daoy, the scramble control, and the E1 control. The KO reaction did not show any amplification signal, which could confirm the genome editing of all REST alleles in the KO cell (Figure 20). Further, the expression of REST protein in the KO cell clone was examined using western blot analysis (section 3.2.2.4). Also, the expression of the RE-1 containing genes was examined using the qPCR analysis (section 3.2.4.2).

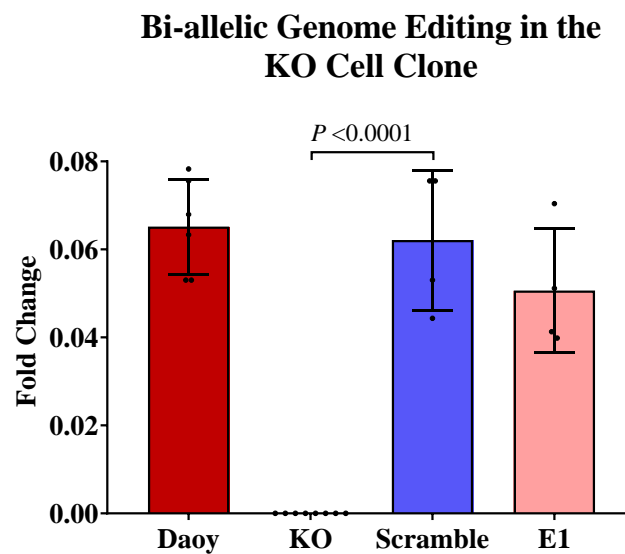


Figure 20: CRISPR/Cas9 induced bi-allelic genome editing in the KO cell clone

qPCR amplification of the REST editing site. The qPCR was performed by reverse-transcribing 1.0 µg of the total RNA and the SYBR green qPCR reactions were performed using a pair of primers that specifically amplifies the CRISPR/Cas9 editing site (188 bp). A positive control that amplified REST exon 1 (E1) was included to verify the no-amplification of the KO reaction and the qPCR was performed using the standard amplification conditions. The measurements were performed in duplicate and the results are the average of 6 repeats normalized to RNU6 housekeeping gene. The expression values are log₂ transformed and represented by the circular dots, the P-value was calculated using the two tailed Student's t-test, and the error bars are SEM.

3.2.3.2 Modulating REST Expression Using the shRNA Knockdown System

As CRISPR/Cas9 has not been used previously to knockout REST expression, the shRNA knockdown approach was used to validate the knockout results. With the knockdown, two shRNA sequences were used to target REST exon 2 and exon 4. The selection for stable shRNA-expression cells was performed by culturing the cells in puromycin selective medium.

Ahead of this work, the puromycin killing curve was generated by treating the Daoy cell with various concentrations of puromycin and the viability of the cells was evaluated using the MTT assay at day 4 and day 7 from the start of the treatment (Figure 21). The result of this analysis showed that the puromycin concentration of 5 $\mu\text{g}/\text{mL}$ was sufficient to eradicate the Daoy cell within 7 days of treatment.

To select for the stable shRNA expression, the transfected cells were treated with 5 $\mu\text{g}/\text{mL}$ of puromycin and the selection was completed when all the cells in the non-transfected control had been killed. The survived cells were then grown as a single cell per culture to produce a monoclonal cell growth. Screening for the pSUPER-puro genomic integration was performed using the PCR amplification and the clones that showed shRNA plasmid integration were further analysed with western blot analysis.

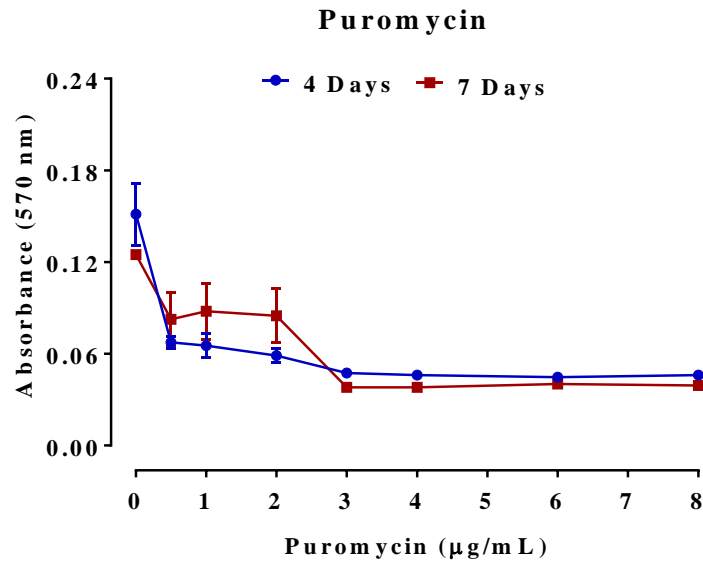


Figure 21: 5 µg/mL of Puromycin was used to select for stable expression of the shRNA

Puromycin kill curve for the Daoy cell. The cell was seeded at 3.5×10^4 cell/mL and after 24 hours the media was replaced with range of puromycin concentrations (0, 1, 0.5, 1, 2, 3, 4, 6, and 8 ug/mL). The viability of the cell was measured after 4 days and 7 days from the treatment using the MTT assay. The results are the average of three independent replicates and presented in percentage by assuming the value of the untreated control at 72 hours as 100% and the values of the other reading were proportioned to its value. The error bars are SEM.

3.2.4 Confirm the Modulation of REST Expression

3.2.4.1 Modulating REST Expression Resulted in a Significant Reduction in REST mRNA and Protein levels

To further confirm the modulation of REST, Western blot with anti-REST polyclonal antibody was used to examine the KO cell clone and to screen the stable shRNA cell clones for REST expression. The immunoblotting analysis of the KO cell did not show the expression of REST protein (122 kDa) (Figure 22 A). With the shRNA knockdown system, I found a cell clone (hereinafter referred to as KD) showed approximately 80% reduction in the REST protein expression compared to the wild type cell (Figure 22 A and B). It should be noted that the other immunoreactive bands may be incompletely reflecting the different REST isoforms due to: the specificity of the anti-REST antibody, not all REST

protein isoforms have been experimentally verified, and the post-translational modifications of the isoforms can substantially alter their apparent molecular weight when resolved on western blots¹⁶². These factors make difficult to determine whether an unknown immunoreactive band is non-specific or a REST isoform. See (Appendix 6) for more information.

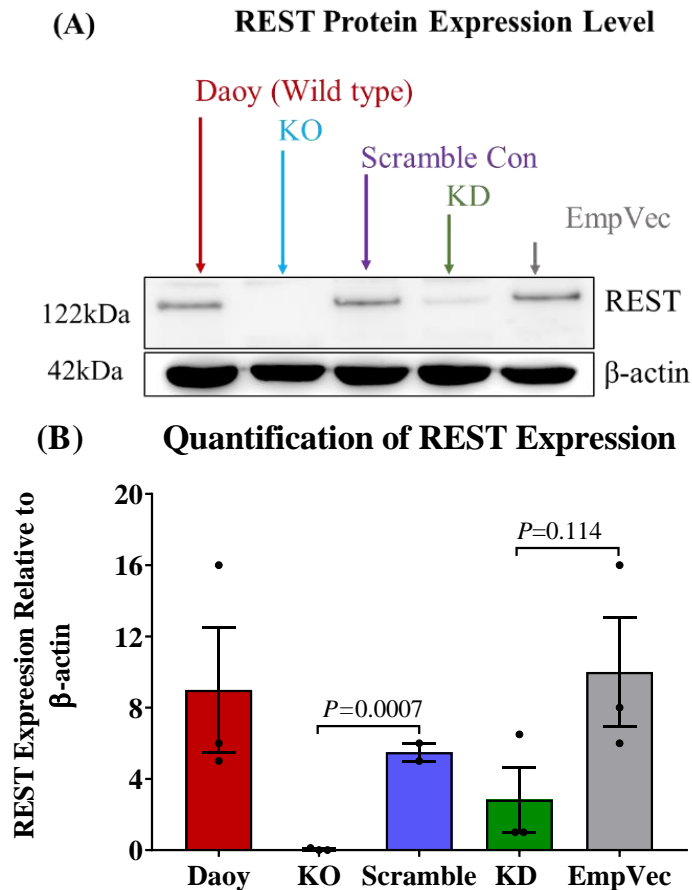


Figure 22: REST modulation has induced a significant reduction in REST protein

Western blot analysis of REST protein expression in the KO and KD cells. The nuclear protein was immunoblotted with anti-REST polyclonal antibody (1:1000) and anti- β -actin antibody (1:20000) (A). The Bar chart (B) is the densitometric quantification of the western blot membrane using Image J. The dots represent the REST expression relative to β -actin value and the P-value was calculated using the two tailed Student's t-test and the error bars are SEM. See (Appendix 6) for complete western blot image and comment.

The mechanism of the shRNA knockdown is based on the sequence-specific degradation of the host mRNA which results in decreasing the mRNA level and accordingly the REST protein expression. To study the functional effect of the shRNA, the expression of REST mRNA was examined using a qPCR reaction that amplifies part of exon 3 and 4. The

results of the KD cell showed a significant reduction ($P < 0.0001$) in the REST mRNA level by more than 50% compared to the control (Figure 23).

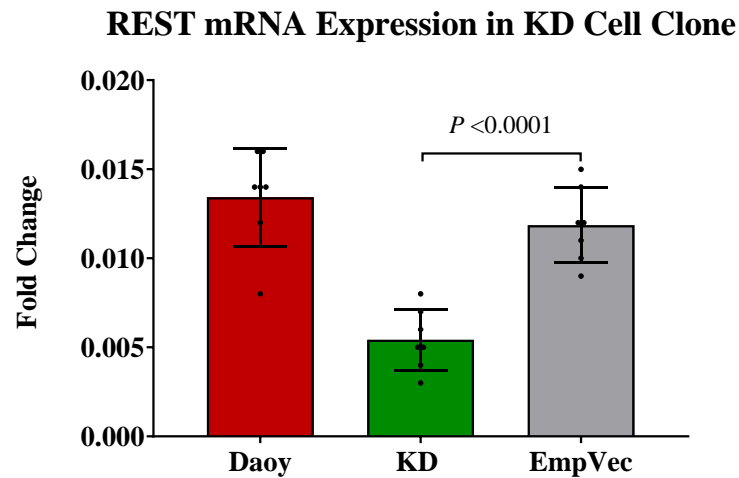


Figure 23: The shRNA resulted in a significant reduction in the KD REST-mRNA level

The qPCR amplification of REST-mRNA in the KD cells. The mRNA (1.0 μ g) was reverse-transcribed and amplified using a pair of primers that specifically amplifies part of REST exon 3 and 4. The measurements were performed in duplicate and the results are the average of seven repeats normalized to the RNU6 housekeeping gene. The expression values are log2 transformed and represented by the circular dots, the P-value was calculated using the two tailed Student's t-test, and the error bars are SEM.

3.2.4.2 Modulation of REST Expression Derepresses the Expression of the RE1-Containing Genes

REST expression is typically associated with repressing the expression of the RE1-containing genes conversely, depletion of REST expression results in the derepression of the REST-regulated genes²³. To study the impact of REST modulation, I measured the expression of the four RE1-containing neuronal genes (Synapsin, SNAP25, SCG10 and GluR2) that are known by the high occupancy of REST to their RE1 sites and showed sensitivity to the modulation in REST expression¹⁴⁵.

The qPCR results revealed a significant upregulation in the expression of these genes by more than 5-fold change in the KO and KD cells compared to the wild type (Figure 24). The expression in the KO cell was almost 2-fold higher than the KD, apart from SCG10, which showed a higher expression in the KD cell (Figure 24 C). It is not clear why the SCG10 expression is elevated in the KD cell however, it could be due to the SCG10 function in regulating neurite outgrowth and branching during the neuronal cell maturation. This may suggest that despite the general repression effect of REST on most RE1-containing genes however, there could be concomitant regulations that precisely adjust the expression of a gene according to the internal regulations. Collectively, these results confirmed that REST expression is elevated in the Daoy medulloblastoma cells and demonstrated its functional impact on the expression of the RE1-containing genes. The results also verify the efficiency of the knockout and knockdown systems to modulate REST expression.

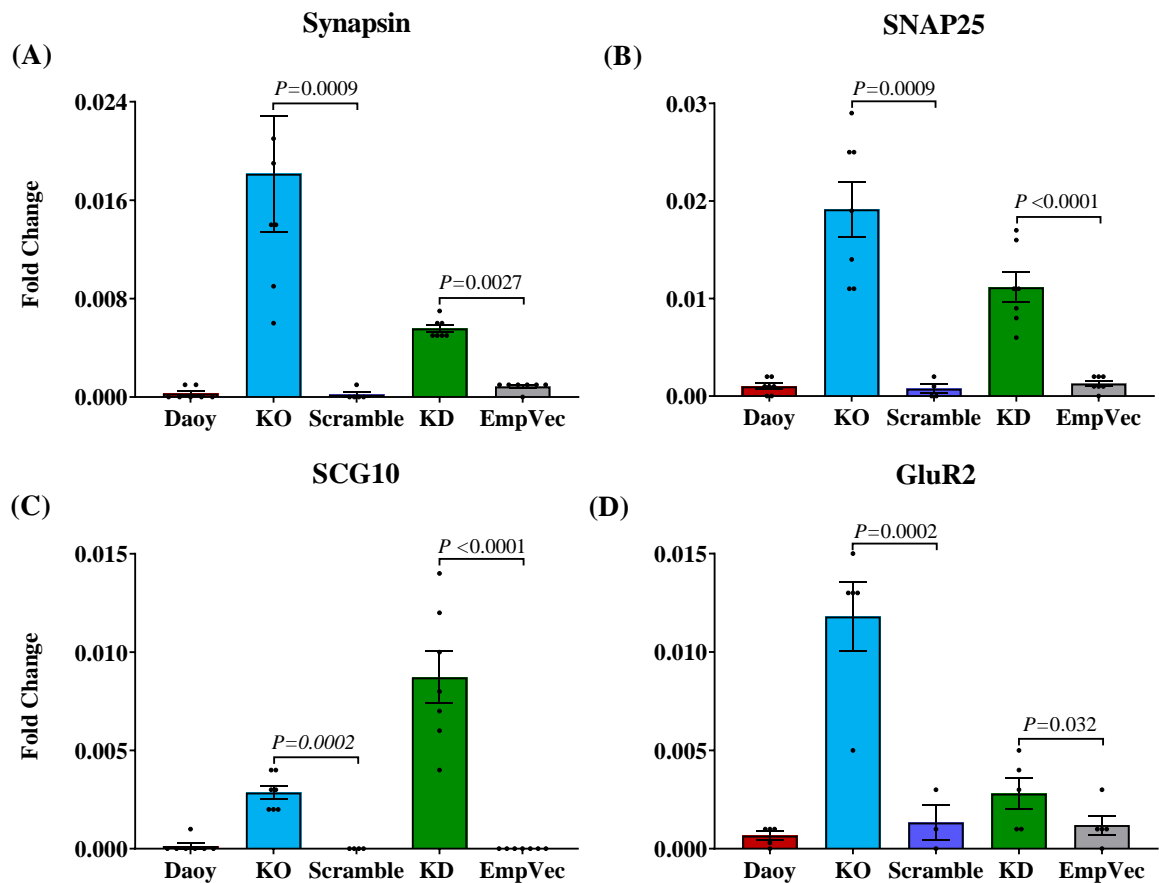


Figure 24: Modulation of REST expression resulted in increasing the expression of the RE1-containing genes

The expression of Synapsin (A) SNAP25 (B) SCG10 (C) and GluR2 (D) in the KO and KD cell clones. The total RNA was (1.0 μ g) was reverse-transcribed to cDNA and amplified using SYBR green qPCR. The measurements were performed in duplicate and the results are the average of seven repeats normalized to the RNU6 housekeeping gene. The expression values are represented by the circular dots, the P-value was calculated using the two tailed Student's t-test, and the error bars are SEM.

3.2.5 Study the Effect of REST Modulation on the Daoy Cell

In brain cancers, REST has been proposed as an oncogene due to its ability to govern the expression of the neuronal differentiation genes. In a number of previous studies, the oncogenic property of REST was investigated through knockdown REST expression. Such studies have claimed the direct involvement of REST in reducing the tumour cells growth and stimulating apoptosis^{4, 11, 12, 13, 14}. However, this study has moved further to examine REST contribution in cancer through using the knockout approach as the partial expression of REST in the knockdown approaches may maintain some repression on different subsets of the neuronal genes.

The following sections will present the functional effect of REST modulation on the Daoy cell proliferation rate, cell cycle, and the cell migration ability, and if HDACs induce their action through the HDAC recruited in REST repression complexes.

3.2.5.1 REST Deficiency does not Strongly Inhibit the Cell Proliferation Rate

In cancer, unrestrained cell proliferation depends mostly on bypassing at least, a checkpoint pathway however, there is a large number of oncogenic factors that may contribute in maintaining the self-renewal potential of tumour cells. To study the effect of REST knockout on the cell growth, the MTT assay was used to measure the viability of the cells at 24, 48 and 72 hours from seeding.

The analysis showed that blocking REST expression did not induce a significant effect on the self-renewal potential of the KO and KD cells though, it slightly decreased their proliferation rate compared to REST expressing cells (Figure 25 A & B). However, due to the small difference in the KO and KD growth to the control cells, the MTT analysis was performed over a period of 7 days. The results of the 7 days culture showed a decrease in the KO and the KD cells growth by around 20% compared to the REST expressing cell (Figure 25 C).

In addition, the proliferation curves were used to calculate the doubling time of the cells by subtracting the time value of 0.8 MTT absorbance from 0.4. The calculated doubling time for the Daoy cells was around 27.9 hours, and for the KO cell it was 29.5 hours, and the KD cell was 29 hours (Figure 26).

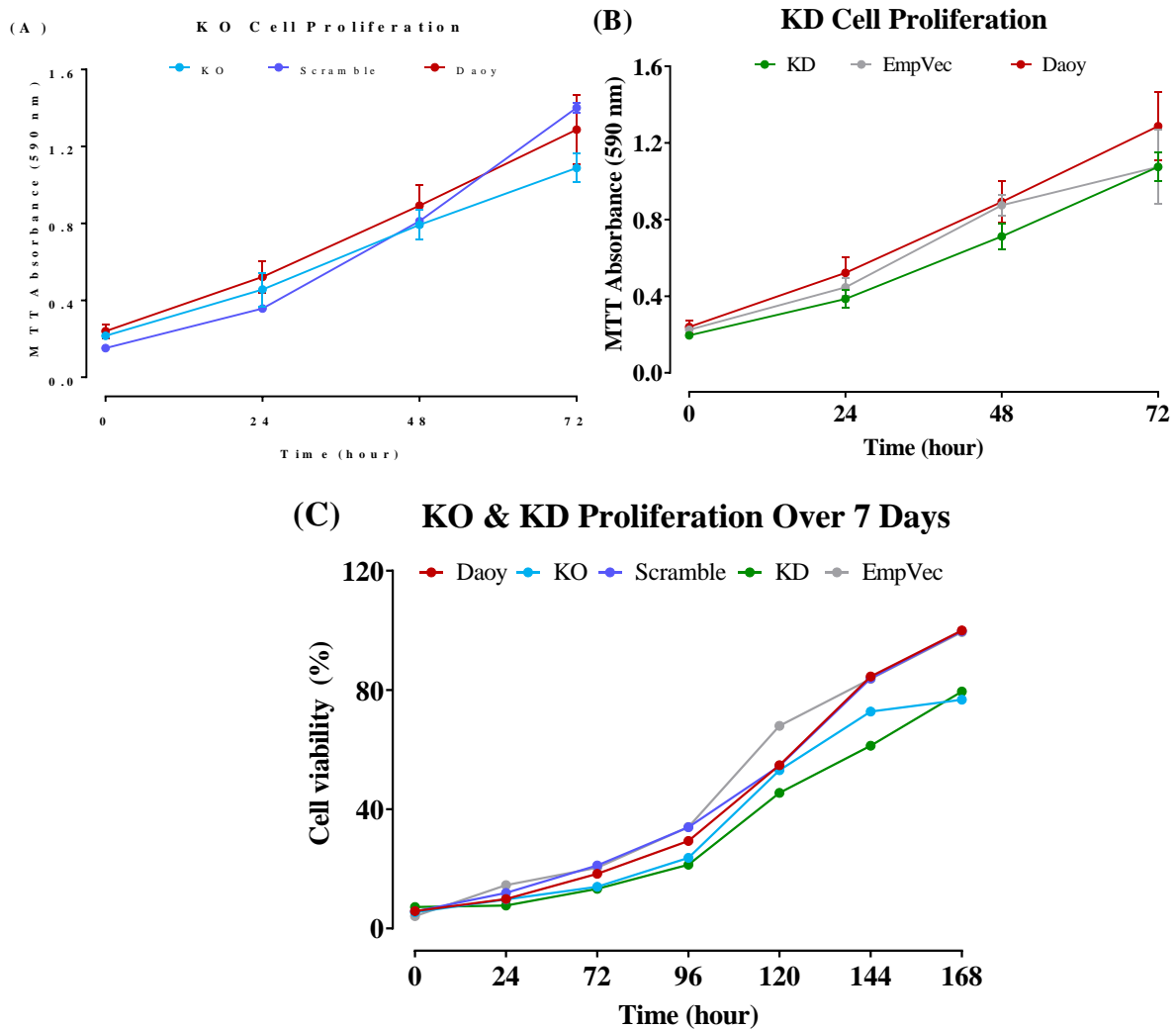


Figure 25: Modulating REST expression slightly reduced the proliferation rate in the KO and KD cells

The proliferation rate of the KO and KD cells. The Daoy cells were seeded at 3.5×10^4 cell/mL in complete culture media and the growth was measured using the MTT assay at 24, 48 and 72 hours (A & B) and at day 7 (C). The results are the average of three replicates and the percentage in the graph (C) was calculated by assuming the control value (the highest reading) at 72-hour and 7 days as 100% and the other readings were proportioned to it. The error bars SEM. Further experiments are required to establish the effect of REST on the proliferation of the Daoy cells.

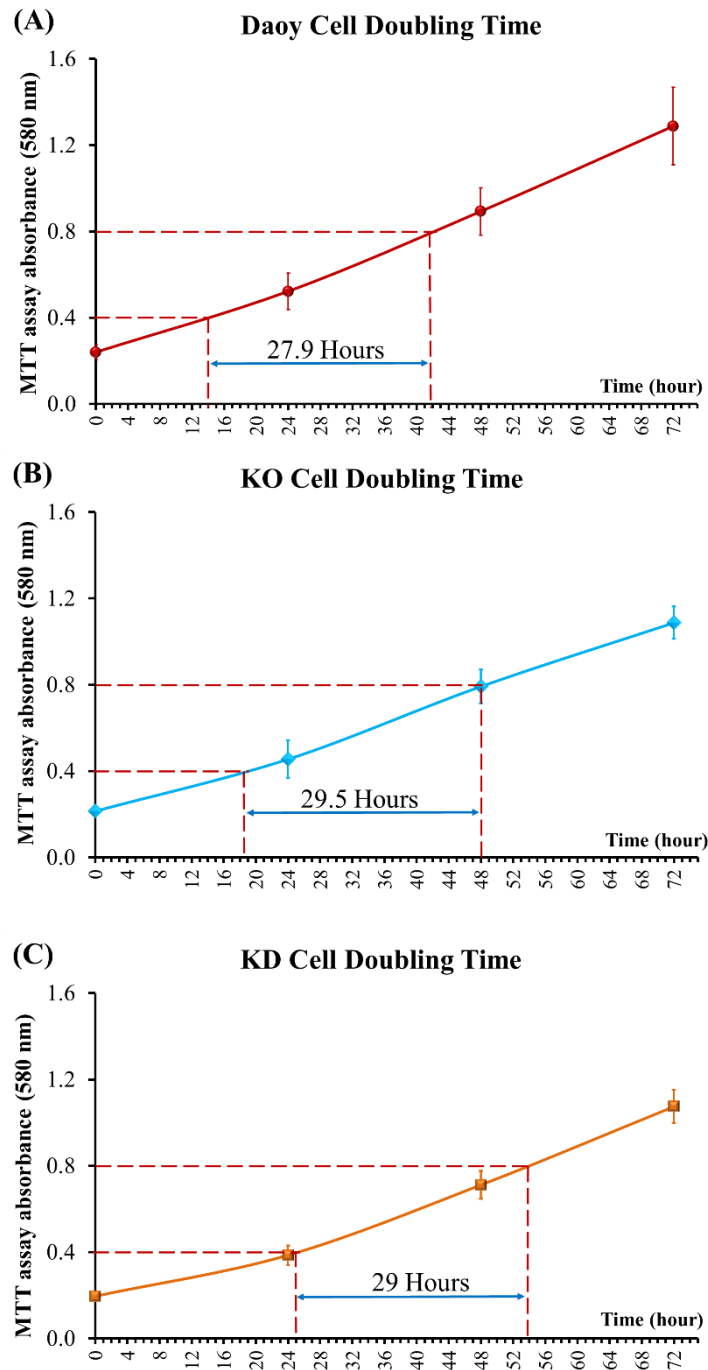


Figure 26: The doubling time of the KO and KD cells was slightly longer than REST expressing cells

The doubling time was calculated from the proliferation curves by subtracting the time value of 0.8 MTT absorbance from 0.4. (A) Daoy doubling time (DT) ~ 27.9 Hour, (B) the KO DT~ 29.5 Hour, and (C) the KD DT~ 29 Hour. Further experiments are required to establish the effect of REST on the doubling time of the Daoy cells.

3.2.5.2 Modulating REST Expression Increased Cells Accumulation in G1 Phase of the Cell Cycle

The proliferative advantage of a tumour cell arises from its ability to bypass the quiescent state of the parent G1 phase as a result of alterations in the cell molecular regulations. These changes generally disturb the mitogenic signalling and affect the cell cycle regulation. In tumour cell, there is a large number of factors that may contribute in evading the quiescent state.

In this study, the effect of REST modulation on the KO and KD cell cycle was investigated by isolating the cells in two conditions: when their growth reached 80-100% confluency (single time-point), and in a time-course manner (at 24, 48 and 72 hours from culture). The single time-point analysis helped in giving an overall view about the percentage of the cells in each phase of cell cycle, but it does not show the kinetic of the cell cycle. Whereas, the time-course method helped in revealing the dynamic of each phase.

The results of the single time-point showed the active cell cycle profile of the Daoy cells wildtype with progression throughout the phases of the cell cycle. However, the KO and KD cells displayed about 10% accumulation ($P < 0.0001$) at G1 phase with a concomitant reduction in the cells proportion at S phase compared to the control cell (Figure 27 A). The time-course analysis revealed that the accumulation of the KO cells at G1 phase continued for 48 hours before the progression of the cell cycle became moderately similar to the control cells at the 72-hour time point. With the KD cell, the progression in the cell cycle was relatively comparable to the KO cell at the 24-hour time point yet, at the 48-hour the proportion of the cells within each phase became similar to the control cells (Figure 27 B, C, and D).

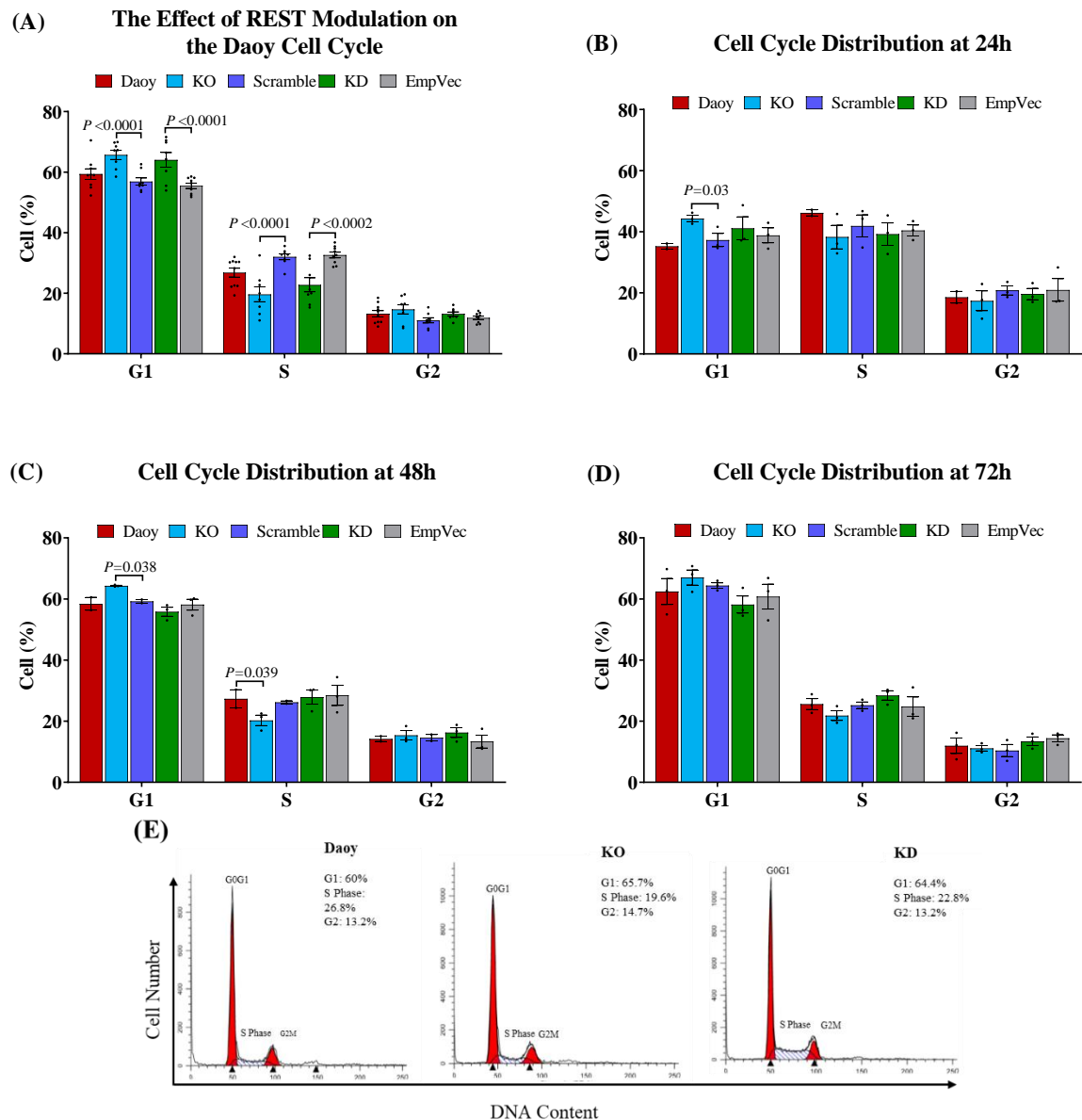


Figure 27: Modulating REST expression increased the KO and KD cells accumulation in G1 phase

The effect of REST modulation on the distribution of the cells in the cell cycle. The cells were grown in standard culture conditions and harvested when they reached 80-100% cell confluence (A) or at 24h (B), 48h (C), and 72h (D) from the seeding. The cells were treated with RNase A, stained with PI, and subjected to flow-cytometry analysis (10.000 events were recorded for each sample). The distribution of the cells was presented as frequency histograms of the DNA content (E). The results are the average of 3 biological replicates and the accuracy of the DNA measurements was assessed by the CV value of the G1 mean (≤ 6). The dots represent the values and the P-values were calculated using the two tailed Student's t-test and the error bars are SEM.

3.2.5.3 Knockout REST Expression Significantly Reduced Cells Migration

Migration of cancer cells represents a major challenge in medulloblastoma treatment and has been associated with poor clinical prognosis and outcome^{163, 164}. In this study, the wound healing assay was used to investigate the effect of REST modulation on the KO and KD cells migration ability. The concept of this assay depends on creating a scratch in a confluent cell monolayer which allows the migration of the cells in the edge of the gap toward the opening until the cells contact is re-established again. This assay has been widely adapted to study the cell migration ability under several experimental conditions, including the modulation of gene expression¹⁶⁵.

The analysis was performed, initially, by culturing the cells after creating the scratch in 1% FBS-containing media. In order to ensure the acquisition of reliable and reproducible results, the assay was evaluated by measuring the difference between several biological repeats. The results showed a considerable difference between the repeats and within the results of the same cell clone which resulted in high standard deviation values (Figure 28). These variations could be due to the 1% FBS which could induce some effect on the cell growth. Hence, in order to minimize the cell growth effect on the analysis, the experiment was carried out using FBS-free media. Microscopically, growing the cells in FBS-free media did not show any observable cell death during the first 24 hours and the number of dead cells started to show a noticeable increase after 72 hours from the culture (Figure 28A). The results of the biological repeats of this work showed more consistent results with relatively low SD. The migration results showed a significant difference between the means of the Daoy to the Scramble and EmpVec controls. However, the difference between the KO and KD cells and their controls was also statistically significant ($P < 0.0001$) and the cells were less efficient in migration and closing the gap by around 40% compared to the controls (Figure 28 B and C).

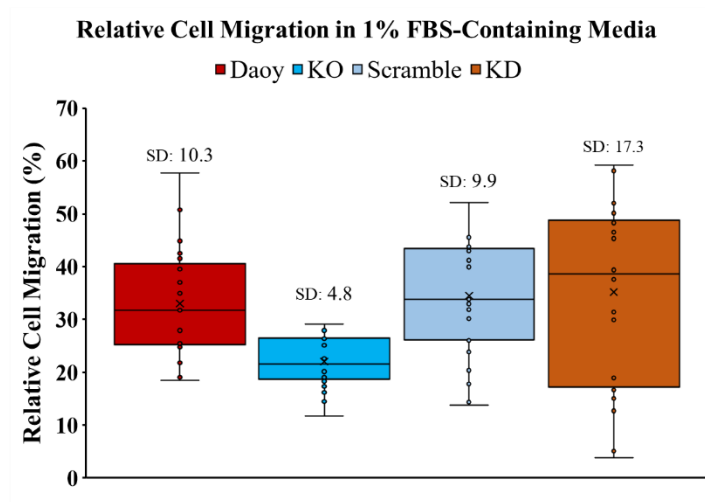
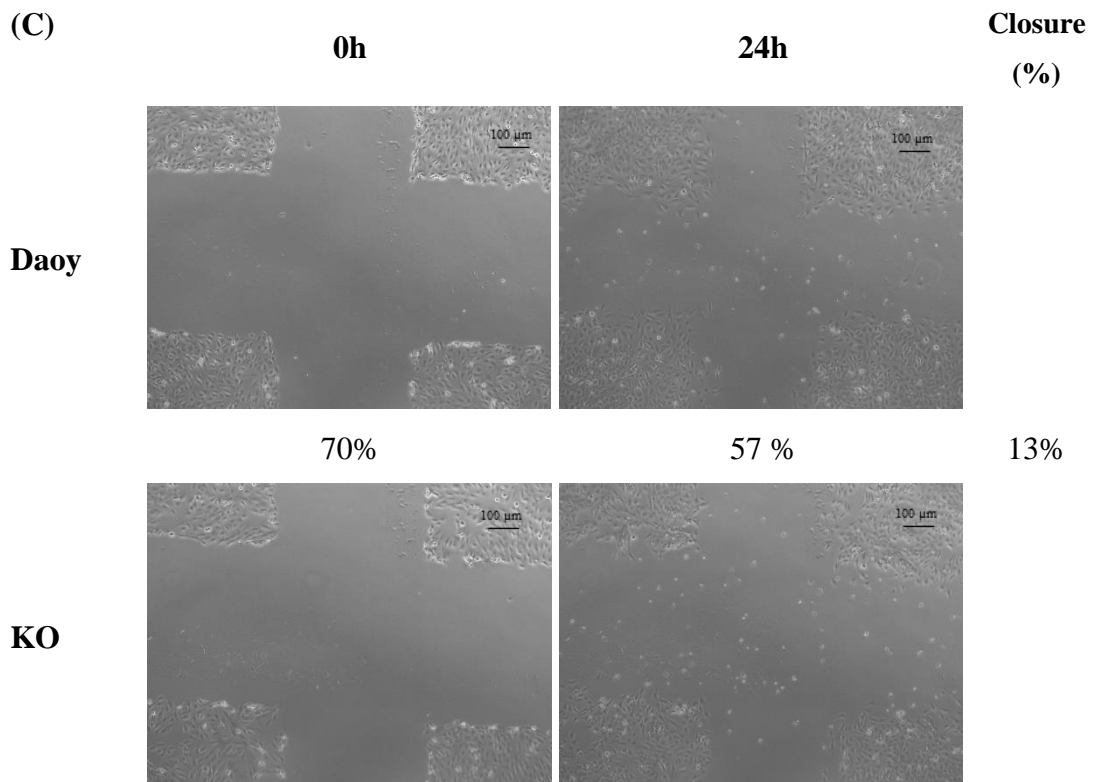
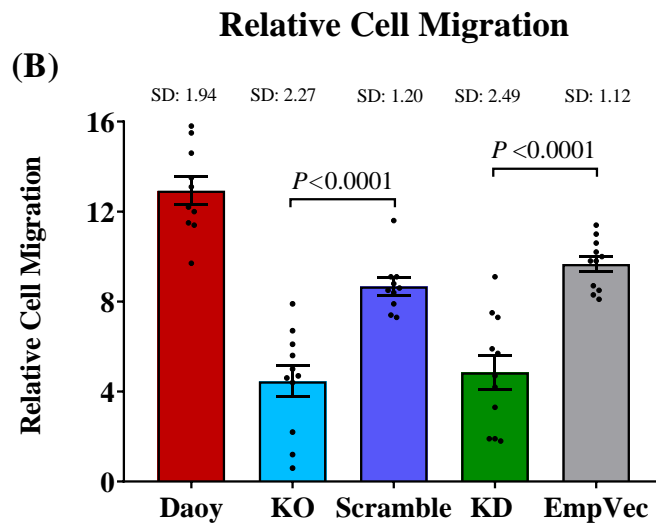
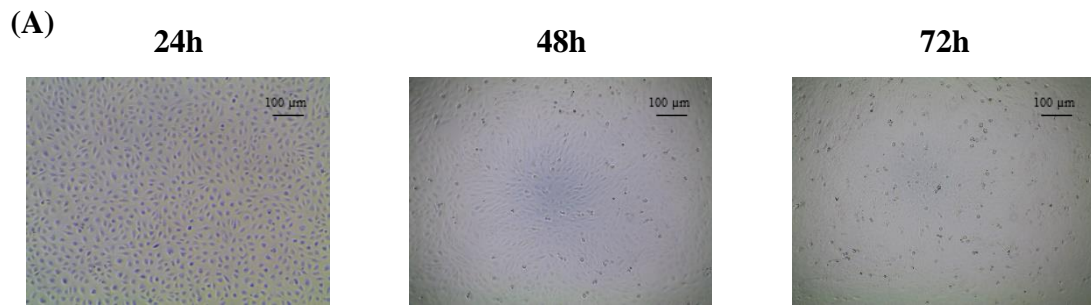


Figure 28: The effect of 1% FBS on the wound healing assay results

The relative cell migration in 1% FBS-containing media. The cells were cultured in 6-well plate and after 24 hours the cells were scratched by passing a sterile pipette tip throughout the middle of the well in a vertical and horizontal directions. Images were taken at the time of creating the scratch and after 24 hours and were analysed using TScratch software (CSElab, Zurich, Switzerland). The dots represent the values, the boxes represent the upper and lower quantiles, the middle line of the box represents the median, the (x) within the box represents the mean, the whiskers indicate the variability and the SD is the standard variation.



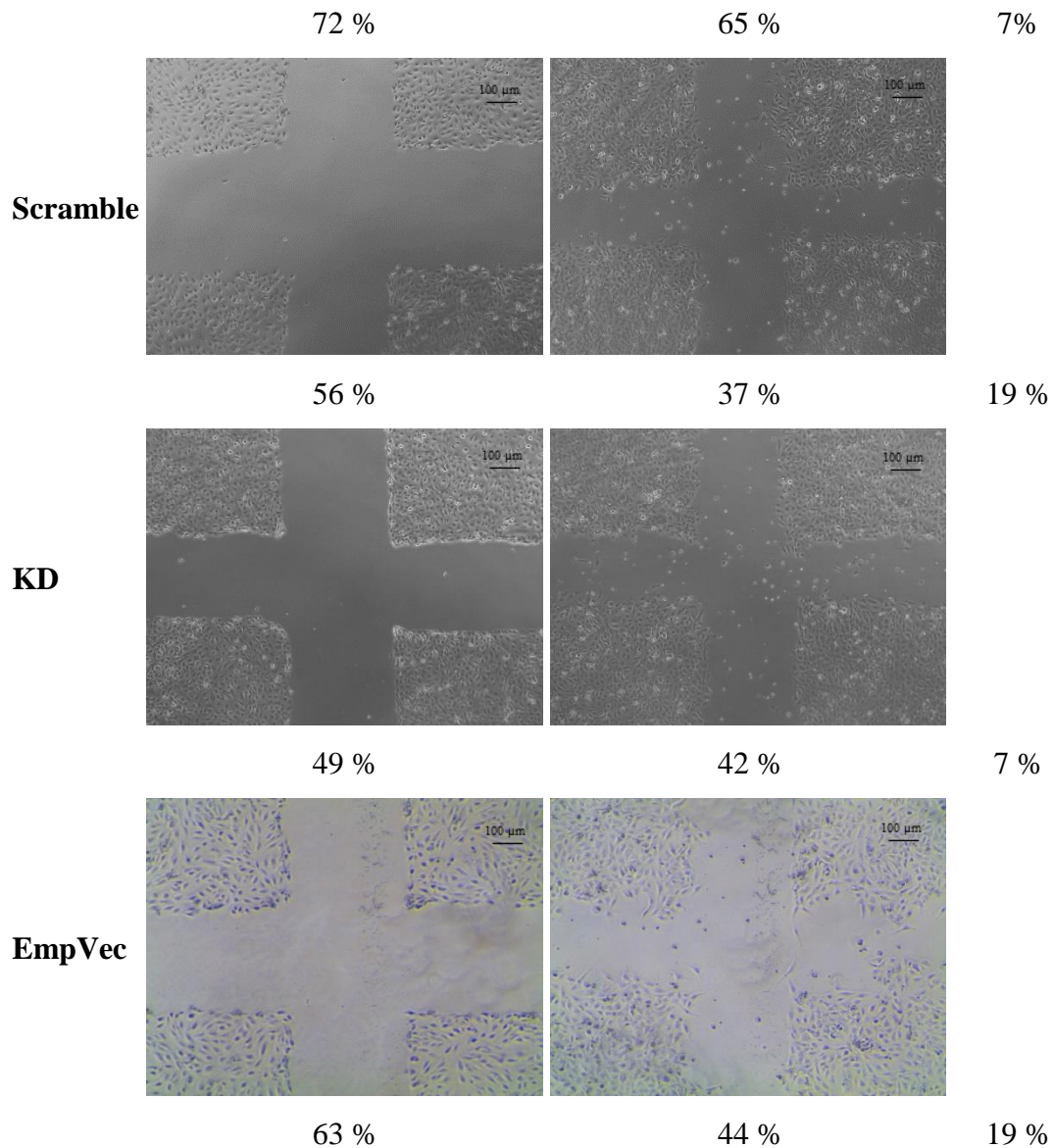


Figure 29: Modulating REST expression resulted in reducing the cells migration ability

The relative cell migration in FBS-free media. The images (A) are a representation of culturing the cell in FBS-free media for 3 days. (B) The bar chart is the average of three biological replicates, the dots represent the values, the P-values were calculated by the two tailed Student's t-test, and the error bars are SEM. The images (C) are a representation of the in vitro wound healing assay (a single biological repeat). See (Appendix 8) for the 'Tscratch' analysis images.

3.2.5.4 Disrupting REST Expression did Not Reduce the Sensitivity of the Cells to HDACis

The mechanism of action of HDACis is not completely well known though, they may depend on the HDACs complexes and/or the non-histone proteins to induce their lethal effect^{80, 166, 167}. REST repression complexes recruit several of HDAC enzymes which deacetylate histone and assist REST in repressing genes expression¹⁶⁸. Tumours with elevated REST expression such as medulloblastoma are often highly sensitive to HDACis which may suggest that these agents may induce their action through the HDACs in REST repression complexes.

In order to examine this assumption, the KO and the KD cells were treated with a single dose of the HDACis and the sensitivity of the cells was measured over a period of 72 hours using the MTT assay. The results showed that the rate of the cell death in the KO and KD cells was equivalent to the control cells (Figure 30). This finding may suggest that REST repression complexes are not the primary element for HDACis to induce their action and indicates that they may act through other HDAC complexes.

Collectively, the results of this part of the research showed that the absence of REST expression alone is not the main factor of reducing cellular multiplication or inducing differentiation. In addition, despite the elevated expression of REST in Daoy though, its repression complexes are not the main component for HDACis to induce their action and they may induce their action through other histone or non-histone proteins.

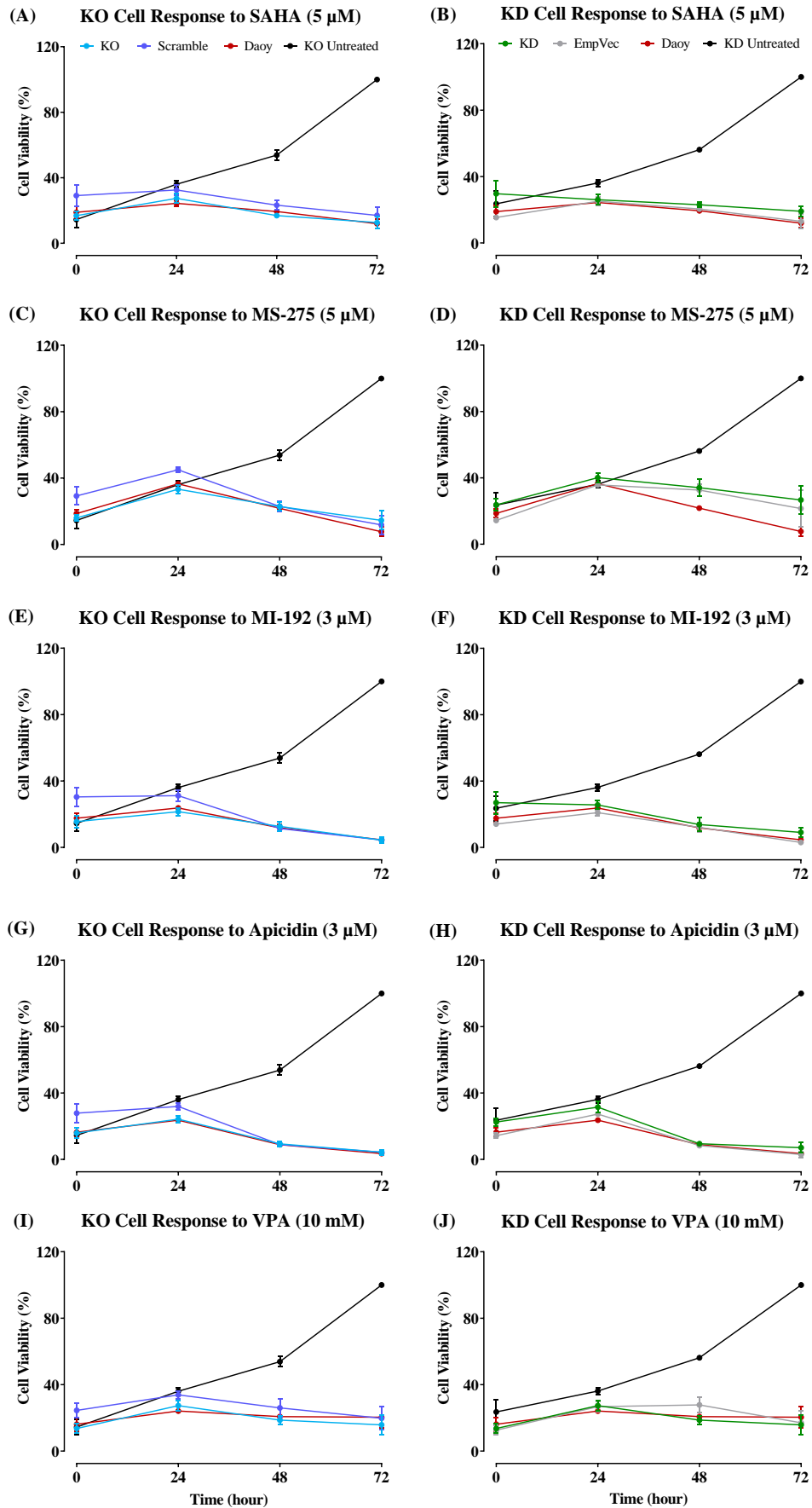


Figure 30: Disrupting REST expression did not affect response of the Daoy cells to HDACis

The sensitivity of the KO and KD cells to HDACis. The cells were seeded at a concentration of 3.5×10^4 cell/mL and the MTT absorbance was measured after 24 hours from the seeding. The cells were then treated with a single dose of the inhibitors (SAHA [5 μ M] (A & B), MS-275 [5 μ M] (C & D), MI-192 [3 μ M] (E & F), Apicidin [3 μ M] and VPA [10mM] (G & H) and the absorbance of the MTT was measured every 24 hours from the treatment for 3 consecutive days. The percentage was calculated by assuming the 72-hour untreated control value (the highest reading) as 100% and the other readings were proportioned to it. The results are the average of five experiments and the samples in each experiment were tested in triplicate and the error bars are SEM.

3.2.6 The Daoy Cells Express REST4 Isoform

REST4 isoform is an alternative splice form of REST full-length protein with a poor transcriptional repression role as it only retains five of the eight zinc fingers of REST and does not have the CTD. Hence, when REST4 binds to an RE1 site it does not efficiently recruit the repression complexes which causes an increase in the expression of REST target genes in neuronal cells ⁷. Accordingly, REST4 has been suggested to regulate the transcriptional repression by opposing REST function. In cancer, high expression of REST4 has been associated with several of non-neuronal tumours such as neuroblastoma, breast, and small cell lung cancers however, its expression in brain cancer is not well known ⁷. Also, the molecular regulation of REST4 expression is not fully understood. However, it has been reported that several of the RE1-containing genes such as SRRM4, ChAT, and VACHT may regulate REST4 expression which suggest REST regulation of REST4 ^{18, 169}. In this work, it was suggested that the Daoy cells may lack the expression of REST4 due to the domination of REST full length repression which may downregulate REST4 expression.

To investigate the expression of REST4 in the Daoy cells, the mRNA was amplified using REST4 exon-specific primers. The reaction included an mRNA sample of SH-SY5Y neuroblastoma cell line as a positive control as this cell line has been reported to express REST4 ¹⁷⁰. The results of the PCR amplification showed bands of 88 bp with the Daoy, the KO, the KD, and the SH-SY5Y cell (Figure 31). This finding demonstrates the expression of REST4 in the Daoy in the existence of REST full length.

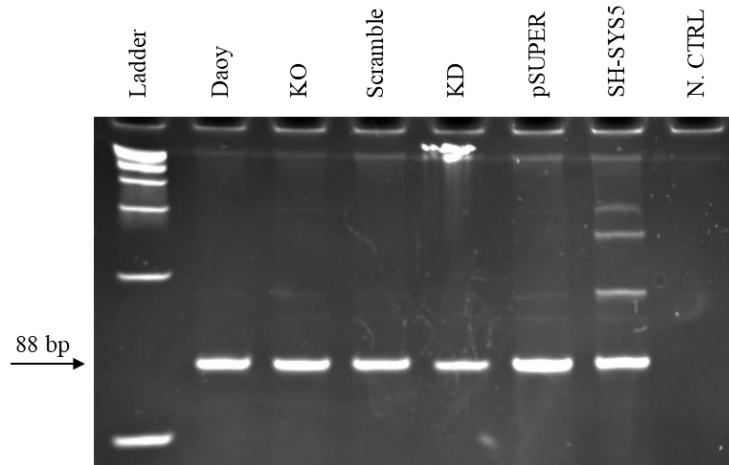


Figure 31: Daoy medulloblastoma cells expresses REST4

Gel electrophoresis of the RT-PCR products of REST4. Total RNA was reverse-transcribed and amplified using REST4 exon-specific primes. The reaction included a reaction for SH-SY5Y cell line as a positive control for REST4 amplification. The PCR products of REST4 (88 bp) were electrophoresed on 2% agarose gel alongside with a DNA ladder and visualized using ethidium bromide. The negative control is N.CTRL.

3.2.7 HDAC Inhibitors Decrease Cell Viability Independent of DNA Fragmentation

The results of this study have demonstrated the ability of the used HDACis to decrease the Daoy medulloblastoma cells viability which is possibly through the activation of the intrinsic apoptotic pathway. One of the key features of apoptosis is the activation of the endogenous endonucleases which fragment the DNA into small oligonucleosomal fragments and irreversibly drive the cell death. The fragmentation of the DNA forms laddering when electrophoresed on an agarose gel however, not all cancer cells show the DNA ladder when treated with anticancer drugs. In here, the study examined if the DNA fragmentation is the end products of the HDACis-induced cell death.

The analysis was performed by treating the cells with a single dose of the HDACis for 48 hours and the DNA was extracted from both of the attached and floated cells in order to capture the DNA fragmentation. To retain the small molecular weight fragments of the DNA, the extraction was performed by releasing the nuclear DNA without performing the

salt precipitation step. The HeLa cell was included as a positive control as it has been reported to form DNA ladder when treated with HDACis¹⁷¹. The electrophoresis results of this work showed a smeary band with the HeLa treated cells whereas, the Daoy did not show the laddering feature (Figure 32). This finding may suggest the presence of a different molecular regulation that regulates the Daoy cell death.

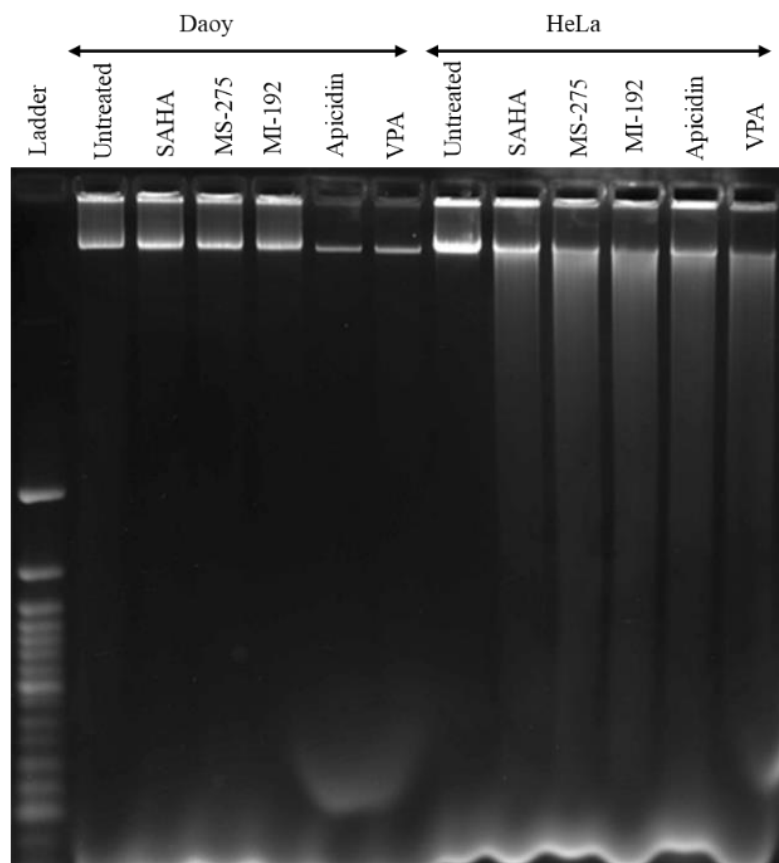


Figure 32: HDACis induced Daoy cell death independent of DNA fragmentation

DNA gel electrophoresis of the HDACis treated cells. The Daoy and HeLa cells were treated with a single dose of the HDACis (SAHA [5 μ M], MS-275 [5 μ M], MI-192 [3 μ M], Apicidin [3 μ M] and VPA [10mM]) for 48 hour and the DNA was extracted from both the attached and floated cells without performing the salt precipitation step. The DNA was electrophoresed on 2% agarose gel alongside with a DNA ladder and visualized using ethidium bromide.

3.3 Discussion

Medulloblastoma is a group of cerebellum tumours branded by elevation of REST expression in most of its subgroups. In literature, there has been some disagreement about REST contribution in cancer. For example, the *in vitro* analysis has shown that knocking down REST in human medulloblastoma cell lines such as Daoy and D283 resulted in repealing the tumorigenic potential of the cells, upregulating the expression of neuronal genes, and ultimately triggering the apoptosis regulation^{11, 14, 50}. Whereas, exogenous induction of REST into normal neuronal progenitors cells claimed to stimulate tumour formation and maintain the self-renewal potential of the tumour stem cells⁵³.

In contrast, several of gene expression profiling studies were performed using primary human medulloblastoma specimens to study the whole image of the genetic involvement^{39, 41, 44, 103}. However, none of these studies have proposed REST involvement, or at least, the exclusive repression of the RE1-containing genes. Despite the considerable research work that associated REST expression with medulloblastoma however, the medulloblastoma sequencing studies have not identified any direct or indirect link between the identified mutations which could contribute in increasing REST expression^{42, 104}. This was further supported by a recent study which revealed that knocking down REST expression resulted in inhibiting the glioblastoma cells migration yet, it did not stimulate cell death¹².

The main aim of this study was to identify the contribution of REST in medulloblastoma. In this research, I used GEO-NCBI gene profiling database to identify the difference in REST expression between the tumour and normal brain cerebellum and between the medulloblastoma subgroups and subtypes. I modulated REST expression in the Daoy medulloblastoma cells using the CRISPR/Cas9 and the shRNA approaches. Then I examined the effect of REST modulation on; the expression of the REST-regulated genes, the cell proliferation, the cell cycle, and the migration ability of the cells. Also, I examined the sensitivity of the REST-negative and REST expressing cells to HDACis.

The results of the GEO data analysis have revealed the elevated REST expression in the medulloblastoma subgroups compared to normal cerebellum. Whereas, the evidences from the research work of this study showed that blocking REST expression resulted in slightly reduction in the cell growth rate, increased the cell accumulation in G1 phase and

decreased the cells migration ability. However, it did not stimulate apoptosis. The results also demonstrated the high sensitivity of the Daoy medulloblastoma cells to the used HDACis yet, the HDAC enzymes in REST repression complexes were not the primary elements for the inhibitors to induce their action.

The following sections, will discuss the findings of the study, compare them to what it has been known and draw a final conclusion based on the evidences I have.

The Discussions main points

- WNT Medulloblastoma Subtype Exhibits the Highest REST Expression
- REST Repression of RE1 Genes is not Equivalent between the Subtypes
- Medulloblastoma Daoy Cell Showed High Sensitivity to HDACis
 - MI-192 Induced a Significant Cell Death within 12H of the Treatment
 - Apicidin Induced a Progressive Cell Death
 - MS-275 Showed a Significant Delay in Inducing Cell Death
 - SAHA Did not Completely Eradicate the Cell
 - Daoy Cell Showed Concentration-Dependent Sensitivity to VPA
- HDACis Induced a Prolonged Cell Cycle Delay and not a Complete Arrest
- Blocking REST Expression in Medulloblastoma did not Stimulate Apoptosis Mechanism
- Modulating REST Expression Slightly Reduced Cell Proliferation and Increased the Accumulation of the Cell in G1 Phase
- Modulation of REST Expression Significantly Reduced Cell Migration
- HDACs Recruited in REST Repression Complexes are not the Primary Element for HDACis to Induce Their Action
- Daoy Medulloblastoma REST4 Expression

3.3.1 WNT Medulloblastoma Subtype Exhibits the Highest REST Expression

Medulloblastoma is a cohort of heterogenous tumours which depends on specific cellular mechanisms to maintain its proliferation and tumorigenesis. Based on the genetics profiling, four distinct subgroups of medulloblastoma have been identified and each subgroup characterized by a domination of a specific cellular mechanism³⁹. Due to the high heterogeneity within each subgroup, twelve subtypes have been recently characterized based on the methylation and expression signatures⁴¹. In this study, I aimed to identify the subgroup and subtype that exhibit the highest expression of REST, which possibly helps in identifying the most possible pathway that mediates REST upregulation.

The findings of this study revealed the high expression of REST in medulloblastoma tumour compared to the normal brain tissue. Also, it showed that the medulloblastoma tumours enriched with WNT and SHH pathways displayed the highest expression of REST. The highest expression of REST was in the WNT β and WNT α subtypes whereas, the SHH subtypes showed variation in REST expression between moderate in the SHH β and SHH α subtypes to low in SHH γ and δ . The lowest expression of REST was identified in Group 4 α and β . Moreover, the expression of some of the RE1-containing genes was inversely correlated with the level of REST expression however, not all RE1-containing genes were equally repressed.

High expression of REST has been reported in most brain tumours including glioblastoma and medulloblastoma^{4, 13, 14}. However, the molecular mechanisms that control and maintain REST expression in cancers has not yet been known. In this study, the observed association of high REST expression with WNT and SHH pathways may reveal part of the regulations that maintain high REST expression. As REST is elevated in WNT and SHH, I will focus on these two mechanisms in attempt to identify the mechanism that enhances REST expression.

The WNT pathway is a signalling cascade, consists of a family of nineteen secreted glycoproteins that play a major role in regulating cell proliferation, migration, survival, and the self-renewal in stem cells¹⁷². Any perturbation in the WNT pathway level during neuronal stem cell proliferation can result in embryonic defect and may affect defining midbrain/hindbrain boundary, from which the cerebellum is developed¹⁷².

Overexpression of the WNT genes, in particular WNT1 and WNT3, causes acceleration in neural progenitor growth. WNT medulloblastoma subgroup was proposed to arise from a group of embryonic stem cells located below the cerebellum. The majority of this subgroup tumours have been found to harbour CTNNB1, TP53, and DDX3X mutations, and loss of chromosome 6³⁹.

One of the WNT pathway functions is to stabilize β -catenin (CTNNB1) protein and activate CTNNB1-dependent transcription¹⁷². β -catenin is transcriptional coactivator and central component of the WNT pathway and its expression is elevated during neuronal differentiation. The expression of WNT stabilizes β -catenin, also it assists in translocating β -catenin/TCF complex into the nucleus where it activates the transcription of its target genes. In medulloblastoma and several of other cancers, the regulation of β -catenin expression fails when CTNNB1 gene contains mutations that prevents proteasomal degradation of β -catenin¹⁷³. In addition, APC (adenomatous polyposis coli, a human tumour suppressor factor) which downregulates β -catenin, has been frequently found mutated in cancers¹⁷².

Two proposed mechanisms have been reported for the β -catenin/TCF complex which contribution in cancer. The first, the β -catenin/TCF complex has been found to activate Cyclin D1 (CCND1), which requires for neuronal stem cells progression through G1 phase to S phase¹⁷³. The second mechanism is that the Exon1a of REST contains a DNA conserved sequence that works as a putative binding site for β -catenin/TCF. Binding of the β -catenin/TCF complex to this site enhances REST transcription¹⁷⁴. Therefore, it could be concluded that the high REST expression in the WNT pathway could be due to the activation of REST transcription by β -catenin/TCF complex dependent mechanism and this warrant further investigation.

In contrast, the mechanism that upregulate REST expression in SHH is not fully identified. The SHH pathway plays a fundamental role in the carcinogenesis of the SHH enriched medulloblastoma subgroup. It consists of several Hedgehog (Hh) proteins that regulate embryonic cell proliferation and differentiation, and they orchestrate the development of the granular neuronal precursors in the cerebellum. During normal embryogenesis, Hh expression is upregulated, and when the cells reach their early postnatal stage the Hh expression is downregulated¹⁷⁵. However, in some tumours the expression of SHH enhances the stem cell self-renewal in the presence of other tumour pathways, which has

been suggested to give rise to medulloblastoma ¹⁷⁵. One of the common features of the SHH medulloblastoma is the PTCH1 gene mutation in addition to several of other mutations in Smo, SuFu, Gli and N-myc. PTCH1 gene encodes a transmembrane protein (PTCH1) that works as a receptor for the SHH pathway. Binding of an activated Hh protein to PTCH1 results in releasing a proliferation cell signal protein, known as smoothened (Smo). Hence, mutated PTCH1 protein cannot block Smo proliferation signal leading to activation of Gli1 (glioma-associated oncogene) and Gli2 transcription factors and increases the expression of cell proliferation genes such as cyclin D, cyclin E, and MYCN (a proto-oncogene protein) ¹⁷⁶. The interplay between SHH and REST is unclear however, many of the Gli1/2 target genes overlap with the β -catenin target genes, which may lead to elevate REST expression. Recently, it has been proposed that WNT/ β -catenin and SHH may collectively regulate the expression of mSin3 REST corepressor ¹⁷⁷.

The expression of REST in Group3 and 4 was relatively lower than the WNT and the SHH subgroups, conversely, the expression of some RE1-containing genes was moderately higher than the WNT and the SHH subgroups. Several pathways have been reported in Group3 tumours such as photoreceptor, protein translation, and telomere maintenance pathways ⁴⁴. Whereas, Group 4 has been reported to be enriched for MAP Kinase (a signal-regulated kinases), fibroblast growth factor receptor 1, and cell migration pathways ⁴¹. However, it is not completely known what factors maintains the proliferation of Group 3 and 4.

3.3.2 REST Repression of the RE1-containing Genes is not Equivalent between the Subtypes

REST is a transcriptional repressor recruits several chromatin and histone modifiers at the RE1 sites, leading to chromatin condensation and transcriptional repression. Elevated REST expression is predicted to cause an extensive repression of the RE1-containing genes. However, the expression analysis of the used microarray data showed that REST repression of RE1-containing genes was not even across the selected genes. For example, despite the elevated REST expression in the SHH subtypes yet, some subtypes such as SHH γ showed wide variations in the RE1-containing genes expression between the subtypes and among the RE1-containing genes as well. These variations could be referred to the heterogeneity of REST repression function. It has been reported that more than half

of REST binding sites showed low recruitment of REST corepressors which results in insufficient transcriptional repression¹⁷⁸. While, some RE1 sites showed more efficient binding and contain varying number of corepressors¹⁷⁸. Also, it has been proposed that some of the RE1 genes, which have a postsynaptic role in synaptic plasticity such as GluR2, are highly depending on the SHH regulation rather than the repression of REST^{179,180}. This may suggest that the regulation of the RE1-containing genes is not limited to REST repression machinery and possibly there are several of other pathways that have more superior control on their expression.

3.3.3 Medulloblastoma Daoy Cell Showed High Sensitivity to HDACis

Many tumours showed high sensitivity to HDACis however, the sensitivity is often different from one inhibitor to another and between the different types of the same cancer. The results of this study demonstrated the ability of the HDACis to induce a progressive reduction in the Daoy cell number in a time-dependent manner though, the anticancer activity was slightly different between the drugs. In this research, I used at least a drug from each chemical group of the HDACis. Some of these drugs are pan-inhibitors and the other are more selective. All the sensitivity analyses were performed within 72 hours as it has been reported that continuous treatment with HDACis for more than 72 hours could lead to a dramatic effect on cells viability due to the cytotoxicity rather than the acetylation status⁹¹.

The most noticeable difference between the inhibitors was the exposure time needed for an inhibitor to induce its anticancer effect. Based on the time-course analysis, MI-192 showed a significant cell death after 12 hours from the treatment. SAHA, Apicidin and VPA showed a significant anticancer effect after 24 hours from the treatment. Whereas, MS-275 showed some delay in its anticancer activity.

3.3.3.1 MI-192 Induced a Significant Cell Death within 12 Hours from the Treatment

MI-192 is a member of benzamide class of HDACis with a high selectivity to HDAC3 and HDAC2 and it showed more than 60% higher selectivity to HDAC3 than MS-275⁹⁵. In this study, MI-192 showed a rapid, progressive, and significant cell death which started after 12 hours from the treatment. MI-192 is one of the promising anticancer drugs

regrettably, no pharmacokinetic data were reported on this unique compound and its anticancer regulation is not well addressed ⁹⁵. A single study that was performed on cholangiocarcinoma (bile duct cancer) cell line reported that MI-192 significantly inhibited the activity of HDAC3, also it caused an elevation in the p53 expression which could promote apoptosis through the expression of BAX gene ¹⁴⁷.

HDAC3 has been found to take part in regulating the cell proliferation in a large number of cancers and its elevated expression been correlated with poor overall survival in breast, colon, lung, cervical, prostate and several of other cancers ⁹⁶. In medulloblastoma, the expression of HDAC3 has been reported to show a relatively similar level between normal cerebellum and the four medulloblastoma subgroups ⁵⁴. The elevated expression of HDAC3 has been reported to enhance the stability of β -catenin (a downstream element in WNT signalling pathway) which could maintain the growth of cancer stem cell in several tumours ⁹⁶. Knocking down the HDAC3 expression has been found to suppress the expression of the PI3K/Akt-mediated signalling pathways (promotes survival and growth in response to extracellular signals) and increase the caspases activity through downregulating the anti-apoptotic genes and upregulating the pro-apoptotic genes ¹⁸¹. In clinical trials, selective inhibition of HDAC3 in solid tumours was more effective and helped in reducing the toxicity produced by inhibiting several HDAC enzymes ⁸⁰. HDACs containing benzamide moiety such as MI-192 have been found to possess higher affinity to HDAC3 than other compounds ⁹⁶. The advantages of MI-192 in inducing a rapid and progressive cell death over the other used inhibitors may suggest the importance of using selective inhibitors in cancer therapy. Also, suggest the significance of exploring the pharmacokinetic of this inhibitor, which require further investigation.

3.3.3.2 Apicidin Induced a Progressive Cell Death

Apicidin is a selective inhibitor with a higher affinity to HDAC3 and HDAC2 ⁹³. The finding of this study showed that treating with Apicidin for 24-hours resulted in reducing the cell viability by around 20%, and it induced a progressive anticancer activity which reached to more than 50% at the 36-hours measurement.

The anti-proliferative activity of Apicidin has been reported in many cancers. In cervical and ovarian cancer cells, Apicidin has been reported to induce HeLa and SK-OV-3 (cervical and ovarian cancer cell line, respectively) cells death through altering the

expression of p21^{WAF1}, cyclin A and E-cadherin^{182, 183}. It also showed an apoptotic activity in the human promyelocytic leukaemia cell line (HL60) through activation of the mitochondria-dependent caspase pathway¹⁵⁰. In this study, the concentration used to treat the cell was the same between Apicidin and MI-192 (3 μ M), both inhibitors show progressive cell death however, the difference was in the high kinetic binding of the MI-192. Though, Apicidin has higher inhibition for HDAC3 and HDAC2 than MI-192¹⁸⁴. Collectively, the dynamic anticancer activity of MI-192 and Apicidin and their selectivity to HDAC3 may suggest HDAC3 as a potential therapeutic target in this tumour.

3.3.3.3 MS-275 Showed a Delay in Inducing Cell Death

MS-275 is a selective inhibitor and it showed a high selectivity to HDAC1 and to lesser extent, HDAC2 and HDAC3⁵⁵. Compared to the other inhibitors MS-275 showed a delay in its anticancer activity as it did not induce any significant reduction in the cell number after 24-hours from treatment. Though, at 36-hours it showed rapid and progressive cell death by more than 30%. This delay in stimulating the cell death has been referred to the slow binding and dissociation kinetic of MS-275⁹¹. The chemical structure of MS-275 contains a lipophilic aromatic ring which necessitates the disruption of most hydrogen bonds that connect a HDAC protein structure in order to accommodate this inhibitor, and when it binds it showed a long residence time⁹¹. However, the observed progressive cell death after the 36-hours may suggest that MS-275 has induced its action through stimulating specific cellular pathway that induced the rapid cell death.

The efficiency of MS-275 to block medulloblastoma cells growth has been reported in the *in vitro* and the *in vivo* analysis hence, it becomes one of the current potential treatment for medulloblastoma tumour⁸¹. In previous studies, the effect of MS-275 was evaluated on several paediatric solid tumours and has been found to increase histone acetylation and p21^{WAF} mRNA level however, it showed diverse effect on cell cycle. For example, in some cells MS-275 led to increase the accumulation in the G1 and the G2 cell cycle as it is the case with the Daoy cells whereas, in some other cell lines it stimulated apoptosis⁸¹. It is not completely known how MS-275 stimulate apoptosis however, the upregulation in the death receptor (Fas) expression has been suggested as a possible factor¹⁸⁵.

Fas is a cell membrane surface receptor that stimulates apoptosis when binds to a transmembrane protein known as Fas ligand (FasL) and activates apoptosis through

caspace-8 activation. Downregulation of Fas receptor expression by HDAC1 and HDAC3 has been reported in several cancers¹⁸⁵. Similarly, the low expression of CASP-8 has also been reported in more than 70% of medulloblastoma tumour samples, and it has been associated with unfavourable survival outcome in childhood medulloblastoma¹⁸⁶. Furthermore, the expression of cellular FLICE-inhibitory protein (c-FLIP) Fas inhibitor protein is upregulated in most cancers¹⁸⁵. All of these factors could lead to increase the resistance of cancer cells to death-receptor mediated apoptosis pathway¹⁸⁷. Nevertheless, treatment with MS-275 disrupts the former cancer strategies by selectively inhibiting HDAC1 and HDAC3 leading to increase the expression of Fas receptor on cell surface and upregulate the expression of CASP-8 gene¹⁸⁶. Also, MS-275 downregulates the expression of c-FLIP which results in redistributing the Fas receptors on cell surface and sensitizing the cells to FasL¹⁸⁵. These changes, in turn, elevate Caspase-8 activity, stimulate Bax release, and initiate apoptosis downstream signalling pathway^{34, 81}.

Another possible explanation of the high sensitivity of medulloblastoma cell to MS-275 is through increasing the acetylation of H3 and H4 at the DR4 (also known as TRAIL receptor 1 (TRAILR1)) promoter which results in increasing the expression of the DR4 receptor and stimulating apoptosis. Interestingly, in many medulloblastoma tissue samples and in the Daoy cell-line the expression of DR4 has been reported to be consistently downregulated compared to normal cerebellum³⁴. Collectively, this may explain the high sensitivity of the Daoy cells to MS-275.

The high sensitivity of the Daoy cells to MS-275 does not necessarily suggest the sensitivity of other medulloblastoma cell lines to this drug. In a previous study, the D283 medulloblastoma cell line was included in the analysis and it showed a minor sensitivity to this drug³⁴. This may suggest the contribution of the tumour cell regulation in defining the sensitivity to the HDACis treatment. Also, it is not well known why the medulloblastoma cells exhibit different sensitivity to the HDACis in general and to MS-275 in particular. However, the low sensitivity of some cancer cells to MS-275 has been referred to the overexpression of an endoplasmic reticulum (ER) stress regulator, known as glucose-regulated protein 78 (GRP78). GRP78 is an antiapoptotic factor with ability to chaperon newly-synthesized proteins across the ER membrane¹⁸⁸. Downregulation of GPR78 expression by HDAC1 has been reported in many cancers. It has been suggested that MS-275 inhibiting of HDAC1 may result in increasing the expression of GPR78 which

relieves the ER stress and blocks apoptosis. As a result, this mechanism could be a potential machinery for HDACis resistance¹⁸⁹.

3.3.3.4 SAHA Did not Completely Eradicate the Daoy Cells

SAHA at 5 μ M has induced a significant anticancer effect at the 24-hours of treatment which increased to more than 50% at the 48-hours measurement. However, SAHA did not completely eradicate the Daoy cells at the 72-hours even with 10 μ M concentration, which was used to establish the dose response curve.

SAHA is class I and class IIb pan-inhibitor with a high kinetic binding which can be observed by its relatively rapid induction of cell death. A prior study has shown more than 50% cell death when a similar concentration of SAHA was used to treat the D283 and the D341 medulloblastoma cell lines¹⁹⁰. The ability of SAHA to induce cells death among different medulloblastoma cell lines could be due to the efficiency of SAHA to inhibit a wider range of HDACs. Also, the antiproliferation effect of SAHA has been related to the post-transcriptional effect of SAHA on decreasing the REST protein level, which it could be through the proteasomal beta subunit (protein degradation)¹⁴.

SAHA has been found to activate both the extrinsic and the intrinsic apoptotic pathways. Activation of the extrinsic pathway was suggested to be through increasing the expression of Fas receptor on cell surface, which results in sensitizing the cell to FasL and initiating caspases downstream apoptosis pathway. Whereas, the activation of the intrinsic pathway is initiated by cleaving some of the anti-apoptotic factors such as Bcl-2, IKK α , IKK β , IKK γ and NF κ B proteins, which increase the acetylation of H3 and H4. Consequently, this results in upregulating the expression of p21^{WAF1}, releasing the cytochrome *c*, and ultimately inducing the cell death mechanisms^{82, 191}. Also, SAHA is believed to increase the intracellular level of ROS which causes an excessive oxidative stress and stimulates the cellular death regulations¹⁹².

It is not completely well known why SAHA does not stimulate complete cell death however, it has been proposed that treatment with SAHA leads to increase the expression of the caspase inhibitors which pauses the death receptor apoptotic pathway and interrupting the SAHA-induced apoptosis. However, this suggestion has been found to be a tumour cell-type dependent⁸². Also, it has been reported that treating cell lines with an

increasing concentration of SAHA yield to a non-reversible resistant in a subset of cells independent of the increase in HDAC1 or HDAC3. Though, it is also tumour cell-type dependent¹⁹³. Most SAHA-resistant cancer cells have been reported to highly express proliferation proteins such as cyclin A, surviving, ki-67, p21^{WAF1}, and p53 which may hinder the anti-tumour effect of SAHA¹⁹⁴. Collectively, this may explain why SAHA does not stimulate complete cell death.

3.3.3.5 The Daoy Cells Showed Concentration-Dependent Sensitivity to VPA

VPA is a pan HDAC inhibitor that showed an inhibitory effect on class I and class II α HDAC. In this study, VPA showed a significant anticancer effect after 24-hours from the treatment. Also, it showed a concentration-dependent effect. At low concentrations, the cell continued to grow and did not show any significant cell death. Yet, with the high concentrations, it induced a sharp decreased in cell growth by approximately 50% and the cells death became more noticeable. It is not completely understood how VPA induces cellular death however, the increase in caspase 3 has been reported in some cell lines after 72-hours from the treatment. However, the cleavage of caspase 8 and caspase 9 was not detected in the analysed cell lines¹⁹⁵. This may suggest that the VPA-induced apoptosis could be partially through a caspase-dependent pathway though, the activation of the caspases might not be through the classic apoptotic pathway¹⁹⁵.

VPA has been reported to inhibit the growth of the tumour cell through increasing the acetylation of H3 and H4, decreasing the expression of GSK3 β (neuronal cell development factor), and suppressing TP53, CDK4, and c-Myc which are important for the cell cycle progression. Also, VPA has been found to increase the expression of p21^{WAF1} pathway, and activates β -catenin, which works as a blocker for cell division¹⁹⁶. Likewise, it has been proposed that VPA induce degradation of RET-kinase (a proto-oncogene signalling molecules) resulting in inhibition of the RET downstream signalling pathway and interrupting the proliferation of cancer cells¹⁹⁷.

It has been observed that VPA can induce a rapid histone acetylation in cell culture though, the process that regulate the chromatin condensation may require more than 48 hours to be completed¹⁹⁸. Also, it has been claimed that treating with VPA often causes unexpected increase in REST gene expression, which could be due to the increase in the histone acetylation and the chromatin remodelling at *REST* promoter¹⁴. In this context, treating

cancer cells with low concentration of VPA may not inhibit the tumour cells growth due to the increase in REST expression which been proposed to drive cells proliferation¹⁴. Therefore, it has been suggested that a higher concentration or a longer VPA exposure is needed to inhibit the tumour cell growth¹⁴. In normal cells, it has been reported that the effect of the VPA-induced apoptosis is mitigated by increasing the phosphorylation of extracellular signal-regulated kinases (ERK1/2), a regulator of cell cycle and angiogenesis) which could lead to increase the expression of BCL-2 antiapoptotic protein and inhibit the release of cytochrome *c* from mitochondria¹⁹⁹.

Taken together, not all the medulloblastoma cells are highly sensitive to HDACis treatment, which may further prove the involvement of different molecular regulations in sustaining the tumour growth. Hence, the efficiency of a specific HDAC inhibitor is largely depending on identifying these molecular markers and employing them to evaluate the efficiency of the treatment. Also, it is observed that some HDACis that show a high selectivity for HDACs were more efficient in inducing cell death than the pan-HDACis. This could be due to the ability of the selective inhibitors to target the molecular regulations that specifically initiate the cellular death mechanisms. Whereas, the pan-inhibitors may drive the re-expression of the apoptosis initiating and inhibiting genes, which diminishes their anti-cancer effect. Moreover, it has been reported that the high selectivity of a HDAC inhibitor is considerably important to reduce the inhibition of inappropriate HDACs and to induce more anticancer action⁹¹.

Also, it has been reported that the activation or the repression of some genes are largely depending on the kinetic binding of HDACis. Therefore, HDACis with low binding kinetics such as MS-275 may induce longer effect on genes that control cell proliferation and apoptosis compare to the HDAC inhibitor with fast dissociation kinetics such as SAHA. This may suggest that the effect of HDACis on the cell viability may depend on the inhibitor-selectivity and the exposure length⁹¹.

3.3.4 HDACis Induced a Prolonged Cell Cycle Delay and not a Complete Arrest

Active progression in cell cycle is one of the cancer hallmarks and it is mediated by families of regulatory proteins including cyclin-dependent kinases (CDK), p21^{WAF1}, p27^{KIP1}, and p57^{KIP2}, CDK inhibitors as well as other regulatory mechanisms known as

checkpoints proteins²⁰⁰. The HDAC enzymes are known to deacetylate a wide range of histone and non-histone proteins including those control the cell cycle. In several studies, HDACis have been claimed to cause cell cycle arrest at G2 phase^{151, 152, 153, 154}. In contrast, the research work that used the time-course analysis approach reported the ability of HDACis to delay the transition between the cell cycle phases and they do not induce cell cycle arrest^{201, 202, 203}.

In this study, the effect of HDACis on the Daoy cell cycle was investigated using a time-course analysis. This approach helped in showing the dynamic and duration of each phase and aided in revealing if HDACis arrest the cell cycle. The results of this study showed a wide variation between the inhibitors in their effect on the cell cycle progression. Though, the general theme was that the transition between the phases was less active in the HDACis treated cells compared to the untreated cell with transient cell accumulation between the phases. Also, there was no significant similarity between the pan-inhibitors (SAHA & VPA) and between the selective-inhibitors (MS-275, MI-192 and Apicidin) though, SAHA and Apicidin showed relatively similar cell cycle accumulation. This may suggest that each inhibitor may induce different molecular regulations that affect the cell transition in cell cycle.

In most cancers, deacetylation of cell cycle genes is one of the factors in tumour cell proliferation. The role of HDAC enzymes in this regulation is mainly involved in regulating the expression of some CDK and CDK inhibitors. For example, HDAC1 and HDAC2 have been found to deacetylate p21^{WAF1}, p27^{KIP1}, and p57^{KIP2} genes promoters and negatively regulate their expression²⁰⁰. In variety of tumour cell lines loss of HDAC1 and HDAC2 resulted in interrupting the cell proliferation potential and drives cell death in medulloblastoma, glioblastoma, and colon cancer^{71, 204, 205}. HDAC3 is also important factor for the cyclin A stability which has a crucial role in S phase progression. It has been suggested that during mitosis the HDAC3 complexes deacetylate histone 3 and condensate the chromatin through A-kinase anchor proteins (AKAP8 & AKAP8L). This may serve as an indicator for mitotic checkpoint to regulate proper cell division²⁰⁶. Knocking down HDAC3 in HeLa cell reported to increase the accumulation in S and G2 phases²⁰⁷. HDAC10 is also regulates cell cycle progression via cyclin A and knocking down HDAC10 in non-small cell lung cancer resulted in cell accumulation in G2 phase²⁰⁰.

Comparing the findings of the cell cycle to the cell proliferation results of this study showed some correlation between the results. For example, MI-192 showed the fastest cell death and it also showed a significant decline in G1 phase and increase in S and G2 phases at the 6-hours measurement. Likewise, MS-275, which showed the slowest anticancer effect (36 hours), its effect on cell cycle was after 24 hours. SAHA, Apicidin and VPA also showed a synchronous effect on the cell cycle and cell viability. This correlation may suggest that the effect of HDACis is started by interrupting the cell cycle proliferation genes and simultaneously activating the cell death mechanism.

Taken together, the results suggest that the cell death induced by HDACis is not due to arresting the cell division at specific cell cycle phase, and it could be due to the initiation of cell death mechanism.

In this study, the cell cycle flow cytometry analysis can be improved by synchronizing the cell population using an agent such as vinblastine or colcemide or by serum starvation. These agents have the ability to arrest the cell cycle progression at a specific phase. This method could ensure that the cells begin cycling from the same phase which may help in improving the results of the time-course analysis¹⁵⁷. However, the synchronization may interfere with normal cycling, growth of cells, gene expression, and can result in significant cell death.

Additionally, the cell cycle effects of HDACis and REST can be further investigated using bromodeoxyuridine (BrdU). BrdU staining of DNA takes advantage of the incorporation of BrdU into newly synthesized DNA during the S phase. When the cells divide the fluorescence intensity of the BrdU is halved as a result of the decrease in the amount of BrdU per cell. The reappearance of the BrdU fluorescence signal in S-phase is an indicative of a complete cell cycle and the time taken can be used to estimate the cell cycle kinetics²⁰⁸. The advantage of this method is that it allows to determine the duration of a cell cycle phase without the need to induce potentially toxic synchronization agents²⁰⁸.

3.3.5 Blocking REST Expression in Medulloblastoma did not Stimulate Apoptosis Mechanism

In some studies, REST has been described as an oncogene in particular, in medulloblastoma and glioblastoma^{4, 9, 11, 12, 13}. The claim behind the oncogenic property of REST originated from the ability of REST to repress the expression of neuronal differentiation genes which blocks the cell differentiation and maintains the self-renewal potential of cancer cells. Therefore, modulating REST expression has been proposed as potential approach to treat cancer^{4, 9, 11, 12, 13}. This conclusion was built based on using the knockdown tools to reduce REST expression in xenograft animal models. Though, the partial expression of REST in the knockdown approaches may maintain some repression in different sets of neuronal genes which could affect the results interpretation.

In this study, the knockout approach was used to study the effect of REST modulation on the Daoy medulloblastoma cells. To the best of my knowledge, this is the first study that used CRISPR/Cas9 to knockout REST expression in a medulloblastoma cell line. In addition, this study used the shRNA knockdown approach to approve the knockout results.

However, the effect of REST modification was not limited to REST expression, and the impact was extended to a myriad number of REST-regulated genes. Comparing the REST-negative cells to the wildtype cell showed an increase in the expression of some RE1-containing genes by more than 5-fold change however, it did not result in differentiating the tumour stem cell or interrupting the oncogenic regulation. Noteworthy, the number of REST regulated genes has been estimated to exceed 2000 genes³. Despite these enormous changes though, the cells maintained their proliferative potential and did not show any morphological changes or cell death. In a similar context, the absence of REST expression in embryonic stem (ES) cells has been reported to cause inappropriate upregulation of a cohort of genes that are important for neuronal cell differentiation and function⁹. Despite, the expression of brain-specific genes including Secretogranin III (SCG3), Complexin 1 (Cplx1) and Stathmin 3 (Stmn3) however, it did not lead to the differentiation of the ES cells or affect their multipotent potential⁹.

Collectively, these findings may demonstrate the low importance of REST in regulating tumour cell proliferation and differentiation and could suggest the existence of other oncogenic regulations that maintain the self-renewal potential of the tumour cell. Also,

the results may suggest the lack of the tumour cell the primary components that are required for employing the differentiation factors. In addition, it may demonstrate the ability of the tumour regulation to avoid the progression in the maturation stages.

3.3.6 Modulating REST Expression Slightly Reduced Cell Proliferation and Increased the Accumulation of the Cells in G1 Phase

Cancers, in general, sustain their growth through mutations that affect one or several cells pathways and the growth continues unless a main factor in proliferation pathway was targeted. In this study, blocking REST expression resulted in reducing the growth of REST negative cells by approximately 20%, it also caused a slight accumulation in G1 cell cycle phase concomitant with a decrease in S phase.

These findings are in agreement with a previous study that used shRNA to knockdown REST expression in the Daoy cells⁵². In the study, they found that loss of REST resulted in increasing the accumulation in G1 phase with a concomitant decrease in the S phase however, it did not lead to cellular apoptosis. Also, they reported that loss of REST led to a decrease in the expression of MYCN (a proliferative marker) and an increase in the expression of certain antiproliferation makers such as p27 and UPS37⁵². This could suggest that REST may control the cellular proliferation through a p27-dependent mechanism⁵². Similarly, several of gene expression analysis studies were performed using primary human medulloblastoma however, the elevated REST expression was not proposed as a factor in sustaining the cell growth^{38, 39, 44, 41}.

In contrast, a number of other studies, have claimed that knocking down REST expression resulted in reducing the tumour cell growth and stimulated apoptosis^{11, 50, 115, 209}. For example, some studies used REST-VP16 vector to knockdown REST expression in medulloblastoma cell lines. According to Lawinger et al. REST-VP16 is a transcriptional activator form of REST that has the ability to compete with REST and upregulate the expression of the RE1-containing genes¹¹⁵. Also, it was used in some studies to differentiate the NSC and the myoblast C2C12 cell into neuronal cells²¹⁰. REST-VP16 was constructed by replacing both repressor domains of REST with herpes simplex virus activation domain (VP16)¹¹⁵. Lawinger et al. study has claimed that modulating REST expression in the Daoy, D341 and D283 medulloblastoma cell lines using REST-VP16 resulted in a massive cell death within 96 hours, however, the results of the *in vitro*

apoptosis were not presented in the publication ¹¹⁵. It has also been reported that transfecting a subcutaneously injected Daoy cells with REST-VP16 resulted in inhibiting the tumour growth, and the direct injecting of REST-VP16 into subcutaneously Daoy-formed tumours resulted in about 50% reduction in the tumour growth ¹¹⁵. In 2005, Fuller et al. have reproduced the former experiment on an intracranial Daoy-induced tumour, and they claimed the ability of REST-VP16 in blocking the tumour growth and stimulating apoptosis however, the study did not mention if the cellular death was observed in the *in vitro* analysis ¹¹.

In contrast, in three separate studies the expression of REST was knocked down in different glioblastoma cell lines using the shRNA system. The studies reported the effect of REST knockdown in reducing the tumour cell proliferation rate and migration ability ^{4, 12, 13}. Despite the similarity between the used cell lines, in particular, between Kamal et al. and Zhang et al. studies however, the apoptosis was only reported in the Kamal et al. and the Conti et al. studies ^{4, 13}. The Zhang et al. study concluded that the apoptosis was not stimulated by REST knockdown ¹². It is not clear why the knockdown of REST in the former studies led to different outcomes. However, the variation between the studies could be due the limitation in the techniques that were used to detect the cellular apoptosis. For example, the TUNEL assay requires careful analysis of the stained cells, as the duration of the proteinase K in the pre-treatment step may generate false-negative or false-positive results due to the enzymatic under-digestion or over-digestion, respectively. The published images of the TUNEL assay in Kamal et al. 2012 study did not clearly show the apoptotic cells and some of the green signals in the images may not related to apoptotic cells (Appendix 9). In contrast, the FACS analysis in the Zhang et al. study did not identify any significant apoptosis events both at early and late stages of cells growth ¹².

Taken together, REST is not a primary factor for the Daoy cell growth and the cell may sustain its growth through other cellular mechanisms. Blocking REST expression in this cell led to increase the expression of the neuronal genes and slight decline the cell growth however, it did not result in inducing the differentiation or cause cell death.

3.3.7 Modulation of REST Expression Significantly Reduced Cell Migration

Migration is a critical factor in early progression of the tumour cell to metastasis, and it has been linked, in part, to elevated REST expression ²¹¹. All medulloblastoma subgroups

have been reported to disseminate along the cerebrospinal fluid pathway with higher frequency in the Group 3 and 4 medulloblastomas ⁴¹. To gain more insight into the implication of REST knockout on the Daoy cell migration, I used wound healing assay to evaluate if the absence of REST results in decrease the migration.

The data showed that, knockout REST expression resulted in decreasing the migration ability of the Daoy cell. This finding is further supported by a previous study that showed knocking down REST expression using shRNA led to inhibit glioblastoma cells migration ¹². The migration inhibition has been referred to the upregulation of genes that are involved in migration and cytoskeleton (stopping cell growth) and some of these genes are regulated by REST such as BBC3 and DAXX ¹². This finding is in consistence with the concept of the neuronal stem cell development regulation. During neurogenesis REST expression is upregulated in NSCs which may contribute in their migration. Whereas, the mature neurons, which display low REST level, show very limited ability to migrate.

3.3.8 HDACs Recruited in REST Repression Complexes are not the Primary Element for HDACis to Induce Their Action

Medulloblastoma has been classified into four main subgroups most of them showed elevated REST expression. Interestingly, the tumours with elevated REST expression showed high sensitivity to HDACis. In this study, we hypothesised that HDACis induce their effect through the REST repression complexes which recruits several of HDACs. We found that disrupting REST activity alone did not affect the sensitivity of the cell to the HDACis. This may indicate that these inhibitors do not mainly depend on the REST recruited HDACs and they possibly arrest cancer growth through other HDACs complexes and/or non-histone protein yet, this requires further investigation. A previous study has suggested REST overexpression as a marker for HDACis treatment, although the findings of this study do not fully support this suggestion ¹⁴.

HDACis are multitarget anticancer drugs, and they can act through acetylating histone and non-histone proteins. In human cell, the acetylation sites are countless therefore, the cellular response to an inhibitor is very complex and most likely includes transcriptional and non-transcriptional regulations.

3.3.9 Daoy Medulloblastoma REST4 Expression

Comparing the expression of the RE1-containing genes between REST expressing and the REST modulated cells demonstrated the functional effect of REST on these genes. The exact mechanism of REST upregulation in cancer is not yet known however, the extensive repression of neuronal genes may suggest the exclusive expression of REST full-length protein isoform in the absence of REST4 isoform. REST4 is a transcriptional activator and it competes with REST full-length in binding to RE1 sites, resulting in upregulation of REST target genes in neuronal cells ⁷. Remarkably, REST4 expression has been found upregulated in post-mitotic neurons and in non-neuronal cancers that express neuronal phenotype such as breast and small cell lung cancers ^{7, 18}. In contrast, in normal non-neuronal cells the expression of REST4 has been reported to be downregulated as a result of downregulation of protein kinase A by CREB (cAMP response element-binding protein) pathway ³⁰. In this study, I proposed that the upregulation of REST expression in medulloblastoma could be due to the absence of REST4 expression in the Daoy cells.

The result of PCR amplification of REST4 mRNA show the amplification product of REST4, which may propose that there is no direct association between the expression of REST and REST4. This primary assumption is further supported by a recent glioma study which concluded that the expression of REST4 has no direct relation to REST expression and did not recommend the expression of REST4 as a prognostic biomarker due to its low expression ²¹². Regulation of REST4 transcription is not entirely clear though, it has been suggested that the expression of REST4 in neuronal cells is directly promoted by a neuronal-specific splicing regulator, known as SRRM4 (Serine/Arginine Repetitive Matrix 4, also known as nSR100), which activates the inclusion of the exon N ¹⁷. Remarkably, SRRM4 gene has been reported to include an RE1 site in its promoter which may suggest the involvement of REST in regulating its expression ¹⁷. Also, it has been reported that the expression of REST4 is increase when the expression of choline acetyltransferase (ChAT), and vesicular acetylcholine transporter (VACHT) genes is increased. Both genes contain an RE1 site in their promoters and they are regulated by Protein kinase A, which increases the expression of REST4 isoform ¹⁶⁹. However, the regulation of REST4 expression is complicated and not completely clear and needs further investigation.

3.4 Conclusion

The analysis revealed the elevated expression of REST in most the medulloblastoma subgroups and the highest expression of REST was identified in WNT subgroup. Whereas, the Group 4 α and β subtypes exhibited the lowest expression among all subtypes. This study concluded that blocking REST expression in medulloblastoma Daoy cells has led to; increase the expression of some RE1-containing genes, increase the cells accumulation in G1 phase, slightly reduced the cell proliferation rate, and decrease cells migration ability. However, it did not stimulate apoptosis. The results also showed the high sensitivity of the Daoy medulloblastoma cells to the used HDACis yet, the HDACs recruited in REST repression complexes are not the primary elements for the inhibitors to induce their action.

This is the first study to undertake CRISPR/Cas9 knockout approach to study the contribution of REST in medulloblastoma cell growth. This work has contributed in improving our understanding about REST involvement in cancer and it offers some important insights about REST contribution in cancer.

Chapter 4

4 Results II

4.1 Introduction

This study aimed to investigate the anticancer mechanism of HDACis in the Daoy medulloblastoma cells and explore their effect on normal neurons. The analysis was performed at the transcriptome level using the single cell next generation sequencing (scNGS) as the gene expression is affected by the phase of the cell cycle in the Daoy cells and by the cell heterogeneity in the normal neurons.

The objectives of this work

- ❖ investigate the SAHA and MS-275 anticancer regulation in the Daoy medulloblastoma cells
- ❖ identify the difference between SAHA (pan-HDACi) and MS-275 (selective inhibitor)
- ❖ investigate the effect of SAHA and MS-275 on the normal human neurons

The Roadmap

In this analysis, the Daoy medulloblastoma cells and the normal human neurons were treated with SAHA and MS-275 at 5 μ M concentrations. The untreated and treated cells were harvested into a single suspension and partitioned into nanolitre-scale reaction vesicles (GEMs) using the 10x Chromium 3” technology. After reverse-transcribing the RNA, the cDNA libraries were sequenced and the scNGS data were used to study the gene expression differences between the untreated and the treated cells.

In this study, I set off by establishing an appropriate HDACis treatment length to isolate the cells for the scNGS analysis. I took into account the Daoy cell viability and cell cycle analysis results that were reported in the Results I. I used the apoptosis Annexin V and PI assay to measure the proportion of the viable cells in each cell cycle phase. I determined the treatment duration on the Daoy cells. As the neurons were postmitotic and limited in number, I used the Daoy treatment regime with them. This chapter starts by showing the

results of the HDACis treatment length and then moves to present the scNGS analysis and findings.

4.2 The Results

4.2.1 Assessing the Apoptosis Level in SAHA and MS-275 Treated Daoy Cells

During apoptosis, cells pass through several stages of biochemical and gene expression changes which could result in externalization of the inward-facing phosphatidylserine (PS) on the surface of the cell ²¹³. The expression of PS is a hallmark during early and late stages of apoptosis and can be detected using Annexin V protein labelled with fluorescein isothiocyanate (FITC). Annexin V is an anticoagulant protein with a high affinity to PS and has been used to study apoptosis ²¹⁴. Similarly, PI has been used to stain the DNA in late stages of apoptosis as the cell membrane permeability increases before cell death. Whereas, double staining with Annexin V-FITC and PI can be used to distinguish early apoptotic cells from late apoptotic cells using FACS analysis. In early apoptotic cells, the externalization of the PS results in Annexin V-FITC (Annexin V+/PI-) binding which causes an increase in the 'forward' light scatter signal. In late apoptosis, the PI passes the cell membrane and intercalates with DNA which results in increasing the PI 'side' scatter light signal (Annexin V+/PI+).

To study the apoptotic effect of SAHA and MS-275, the Daoy cells were treated with 5 μ M of the drugs, harvested at 30, 36 and 42 hours from the treatment and analysed by FACS. The result of the untreated control (42 hours) showed that the majority of cells (87%) were viable with around 6% of cells being in the late stage of apoptosis as indicated by Annexin V and PI signals. The treated cells showed a gradual reduction in the percentage of the viable cells associated with an increase in the ratio of the early and late apoptotic cells. The treatment for 30-hours resulted in reducing the percentage of the viable (Annexin V-/PI-) cells to around 75% (Figure 33 A and B). With the progression in the treatment, the percentage of the cells in late apoptosis stage (Annexin V+/PI+) showed a significant increase ($P \leq 0.05$) to ~25% and ~35% at the 36 and the 42-hours, respectively. Collectively, this analysis showed the presence of more than 65% viable cells at the time between the 36 and the 42-hours (Figure 33 A and B).

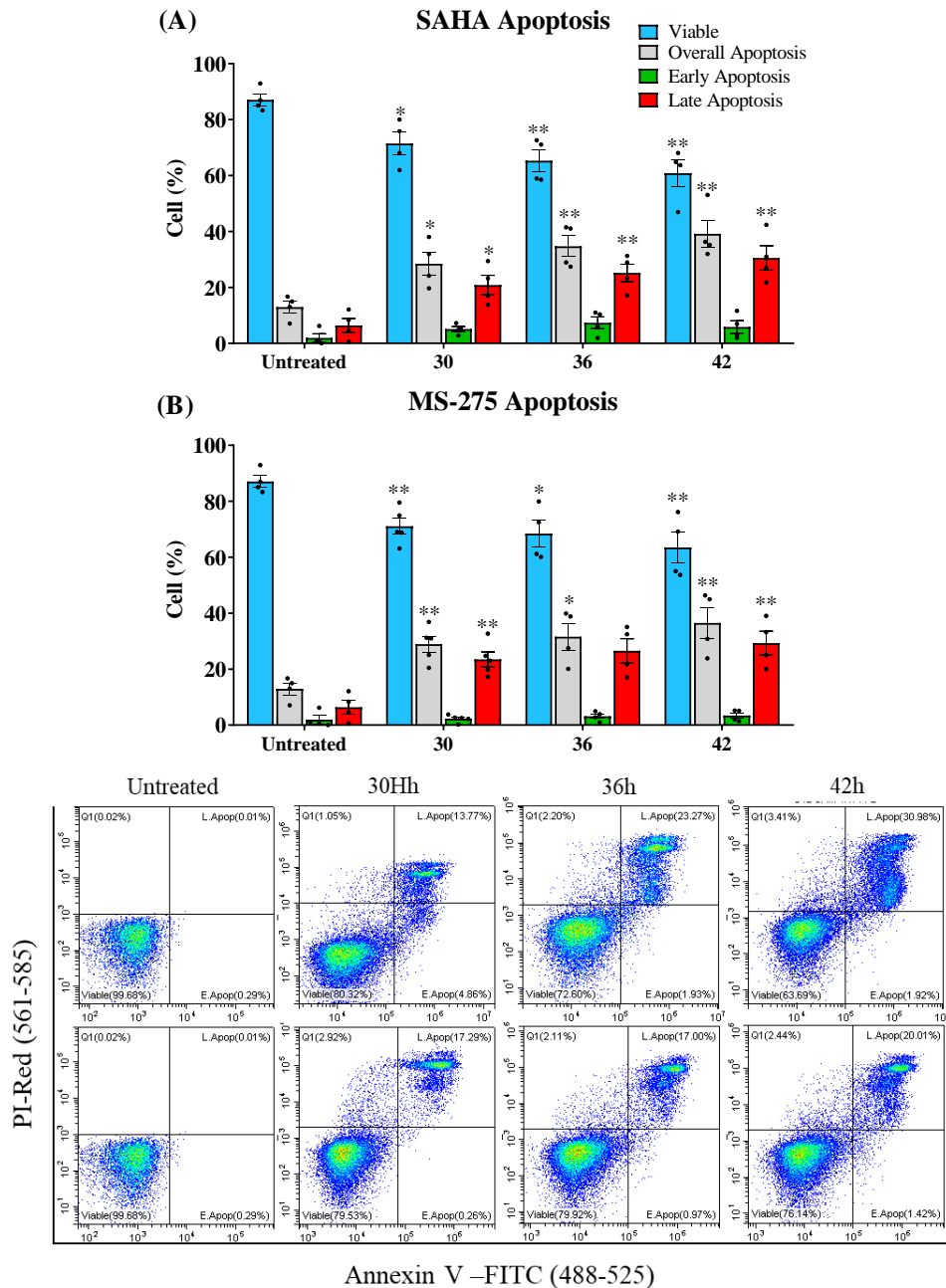


Figure 33: Evaluating the apoptosis level in SAHA and MS-275 treated cells

The bar charts show the percentage of viable and apoptotic cells at 30, 36 and 42 hours of the Daoy SAHA (A) and MS-275 (B) treated cells (5 μ M concentration). The cells were stained with Annexin V and PI and the results are the average of 4 biological replicates. The dots represent the values, the P-value was calculated using the two tailed Student's t-test (* $P \leq 0.05$, ** $P \leq 0.01$) by comparing the values of a time point to the untreated control, and the error bars are SEM. The two-dimensional dots plots (C) are a representation of 30.000 events that were measured on FACS. The viable cells are

(Annexin V-/PI-), early apoptotic cells are (Annexin V-/PI+), and late apoptotic cells are (Annexin V+/PI+).

4.2.2 Estimating the Treatment Length Based on the MTT and FACS Analysis

The results of the cell viability reported in the Results I (section 0) showed that the minimum treatment time required for SAHA and MS-275 to reduce the cell viability is between the 24 to the 36 hours (Figure 34 A). At this time frame the percentage of the viable cells was ~70%. Similarly, the apoptosis analysis results showed the presence of more than 65% viable cells and around 30% dead cells at the treatment time between the 32 to 42 hours (Figure 34 C). The results of the cell cycle analysis at this time frame (Results I section 3.2.2.4) suggested the presence of approximately 30% of the cells in G1, more than 15% in S, and around 40% in G2 phase in the cells treated with SAHA. Whereas, the MS-275 results showed the presence of more than 60% in G1 and around 15% in each of S and G2 phases (Figure 34 B).

Based on these results, the scNGS analysis was performed by treating the cells for the 36 hours. At this time point; there are more than 60% viable cells, there are enough cells to present each phase of cell cycle, and the anticancer effect of HDACis was observed in the apoptosis analysis (Figure 34).

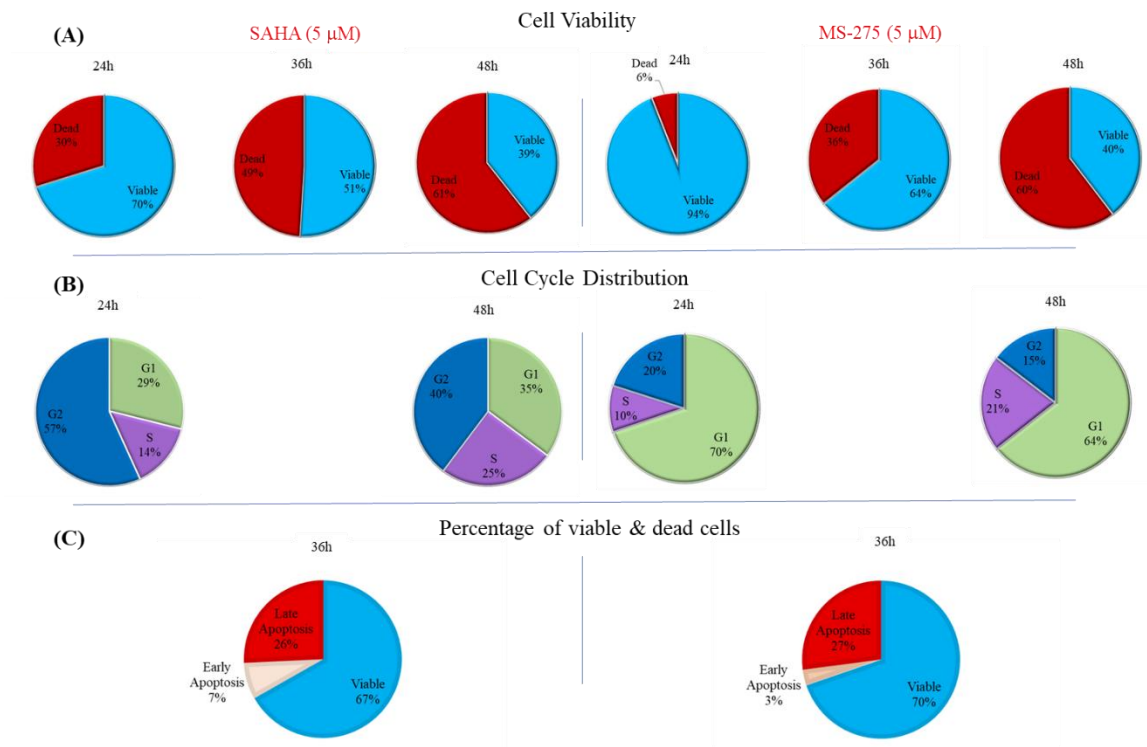


Figure 34: Estimating the scNGS treatment duration length using the MTT and FACS results

The pie charts present a summary of the MTT assay, the cell cycle, and the apoptosis results of the Daoy SAHA- and MS-275-treated cells (5 μ M). The MTT assay (A) shows the percentage of viable vs. dead cell at the 24, 36 and 48 time points. The cell cycle charts (B) (PI flowcytometry analysis) show the cells distribution in the cell cycle phases at 24 and 48 hours. The apoptosis (C) (Annexin V/PI flowcytometry) charts display the percentage of viable to early and late apoptotic cells at 36 hours.

4.2.3 The scNGS Samples Preparation

The scNGS analysis was performed by treating passage (1) Daoy cells and human neurons with SAHA and MS-275 for 36 hours. In this study, six treatment conditions were analysed using the 10x Chromium single cell kit and the RNA libraries were sequenced on Illumina 500 (Table 5).

Table 5: Single cell samples identification Acronym

Sample Number	Condition	Hereinafter referred to as
1	Daoy Untreated	D.Vehicle
2	Daoy - SAHA	D.SAHA
3	Daoy -MS-275	D.MS-275
4	Neurons Untreated	N.Vehicle
5	Neurons-SAHA	N.SAHA
6	Neurons-MS-275	N.MS-275

As standard practice, all the cells were examined microscopically before and after the 36-hours of the treatment. The microscopic examination after the 36-hours showed a minor fraction of floating cells in the untreated Daoy and neurons cultures (estimated to be <3% of the total cell count). Whereas, the treated Daoy cells showed a noticeable increase in the detached cells which estimated to be between 10% to 15%. The neuron culture showed many small floated spherical cells compared to the untreated neurons yet, they can only be seen under microscope (Figure 35).

At the time of the 10x Chromium preparation, the cells were stained with DAPI and the viable cells were collected by a FACS sorter after gating for the debris, dead, and doublet cells (Appendix 10). This approach yielded approximately 5000 cells per each Daoy sample. The counts of the sorted neurons were 2000 cells for the untreated, 5000 cells for SAHA, and 1200 cells for the MS-275 treated neurons. The cells were then loaded into a 10x chip and sequenced on an Illumina 500 platform. See (Figure 36) for more information about the scNGS workflow.

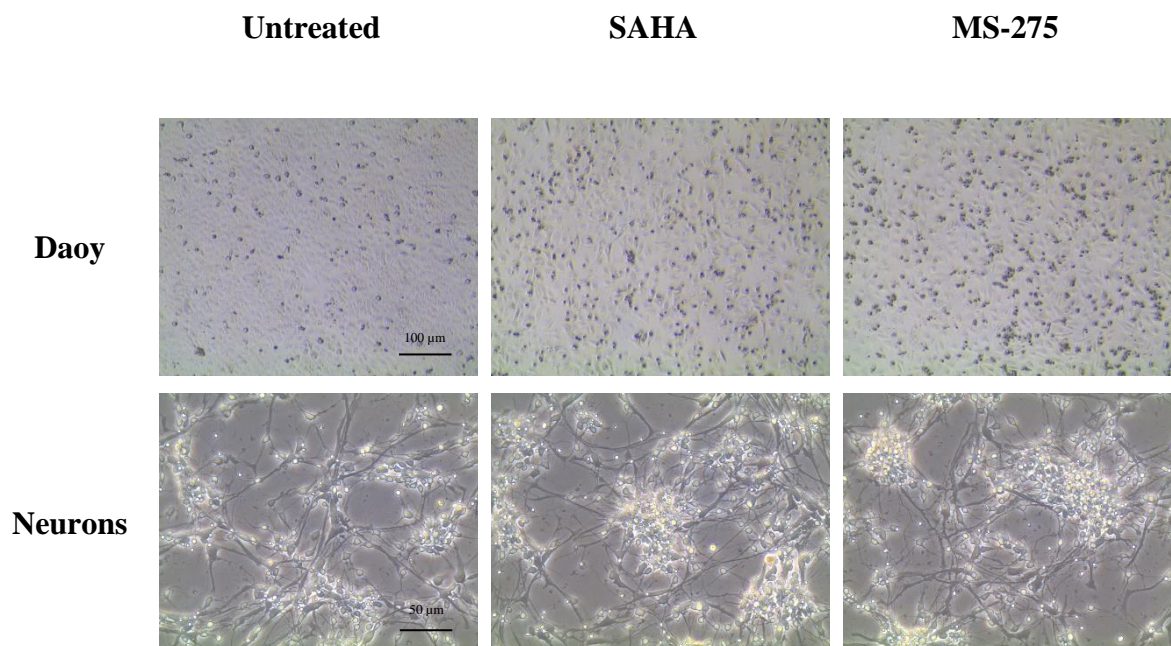


Figure 35: Microscopic images for SAHA and MS-275 (-/+ Daoy and neurons at 36 hours

The Daoy cells and the normal human neurons were treated with 5 μ M concentration of SAHA and MS-275 for 36 hours. The images were taken after 36-hours using inverted microscope.

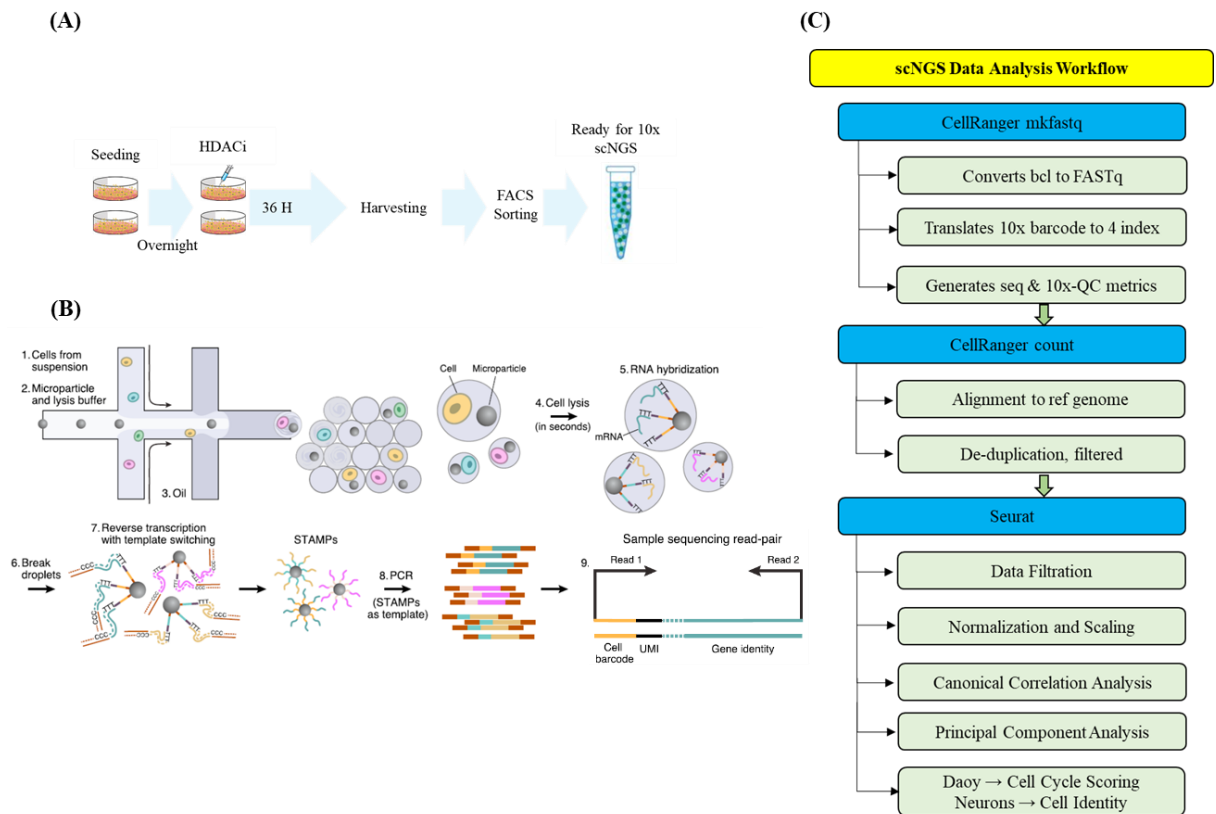


Figure 36: Schematic representation of the scNGS analysis workflow

The scNGS analyses were carried out by treating the cells with SAHA and MS-275 for 36 hours. After harvesting the cells, they were sorted on a FACS sorter (A). The cells were loaded into a 10x Chromium chip to generate GEMs (Gel Bead in Emulsions) and the RNA was reverse-transcribed, amplified, and used to generate the cDNA libraries (B). The libraries were sequenced on an Illumina 500, and the data were demultiplexed using the CellRanger pipelines. Next, the data were analysed using the Seurat R package (C). The data were passed through several stages of data filtration, normalization, and scaling, and the quality improved data were used in the subsequent analysis. (STAMPs is single-cell transcriptomes attached to microparticles). The caption was adapted from (Macosko et al., 2015)²¹⁵.

4.2.4 scNGS data Demultiplexing

The generated 10x scNGS data (Illumina raw base call (bcl) files format) were demultiplexed to FASTq (text files containing sequence data with a quality score for each base) files format using the 10x CellRanger mkfastq pipeline. The CellRanger pipelines were used to demultiplex the Chromium scNGS data, align the reads to the reference

genome, generate barcode matrices, identify the gene count, and perform gene expression analysis. Upon the data demultiplexing, several single-cell specific quality control measures were examined including the number of the targeted cells, the mean sequencing reads per cell, the mean genes per cells, the sequencing depth, and the Q30 of the bases.

The output of this analysis showed that the number of the analysed Daoy cells was greater than 1700 in the D.Vehicle and in D.SAHA samples, and it reached to more than 2700 cells with the D.MS-275 cells. Whereas, the count of the untreated and treated neurons was between 1100 to 1300 cells (Figure 37 A). The low count of the neurons is possibly due to the inaccurate counting of the neurons which resulted in loading fewer cells into the 10x chip.

With the sequencing depth, the recommended depth for the 10x scNGS analysis is > 95% saturation. Yet, despite the several attempts of resequencing to a higher depth the sequence saturation of all the samples did not reach to the recommended level. The sequencing depth of the D.MS-275 cells was 34% and it was lower than 18% in the D.Vehicle and D.SAHA. Whereas, the sequencing depth of the neurons was between the 50% and 60% (Figure 37 B). As a consequence, the low sequencing saturation affected the mean reads per cell and the number of the detected genes. The number of the detected genes in the Daoy samples was between 3000 to 5000 genes, and the detected genes of the neuron samples were between 1000 to 1300 genes.

In addition, the quality of the sequencing data was evaluated using the Q30 values on the level of; the barcode, the RNA, the sample index, and the UMI. The Q30 value is defined as the probability of having an incorrect base call in 1000 bases (i.e. a Q30 of 99% means; every 1000 bp sequencing reads will likely containing an error). The Q30 results of all the samples were more than 85%, apart from the Illumine barcode reads of the N.Vehicle and the N.MS-275 which were 63% and 52%, respectively.

Collectively, these results showed that the sequencing depth was suboptimal in particular with the Daoy samples which could affect identifying some of the cellular regulations especially and the expression of the low abundant genes may be underrepresented in the data set. Nevertheless, the number of the targeted cells and the quality of sequencing data could be sufficient, at least, to address some of the research questions of this thesis.

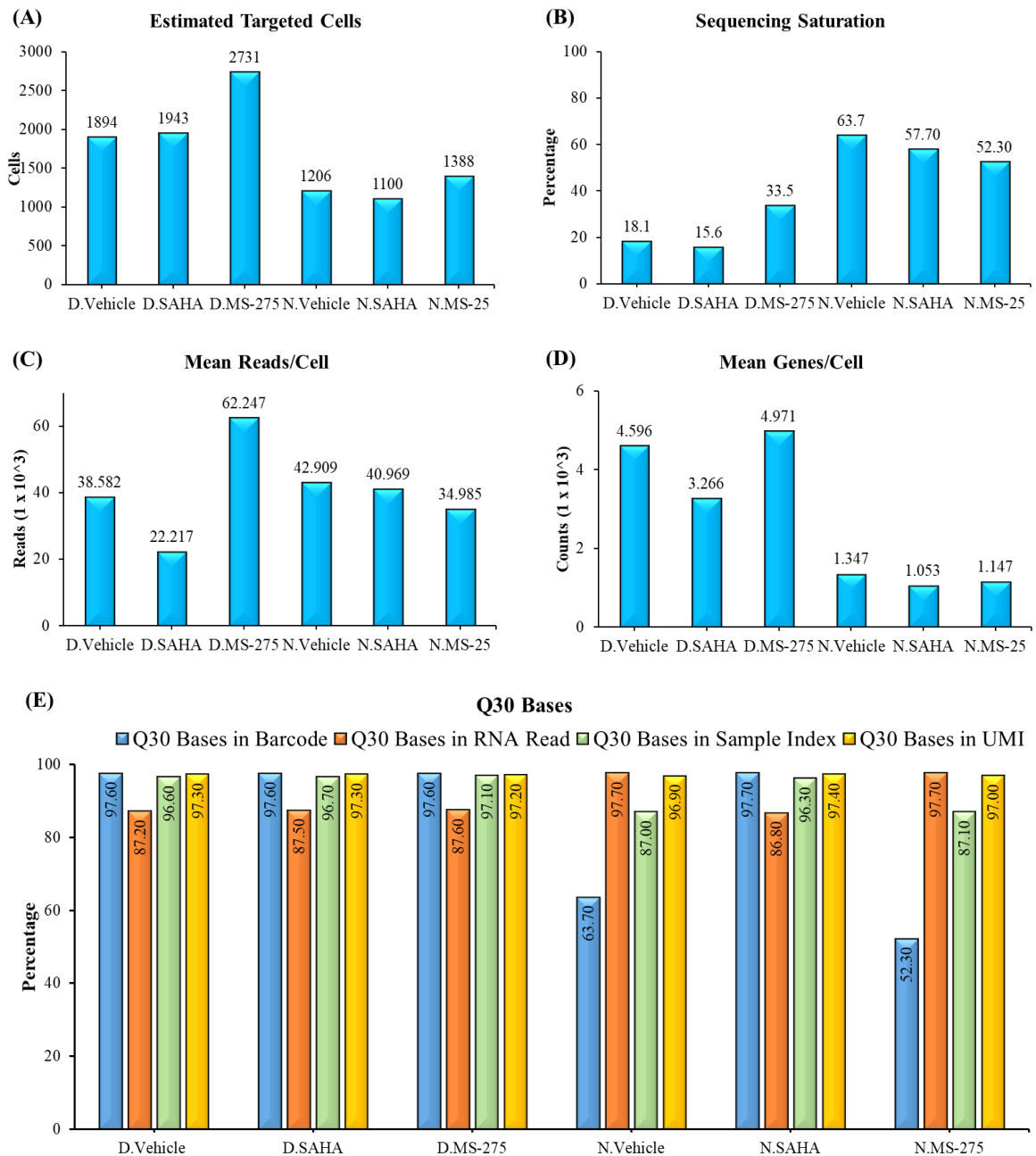


Figure 37: Statistical summary of the 10x scNGS data quality measures

The sequencing data were demultiplexed using the CellRanger mkfastq and count pipelines. The quality of the 10x libraries were evaluated on the level of; the number of the targeted cells (A), the sequence saturation (B), the mean read per cell (C), and the median genes per cell (D). The quality of the data was also evaluated using the Q30 bases of the barcode, the RNA reads, the sample index reads, and the UMI reads (E).

4.2.4.1 The Initial Visualization of the 10x scNGS Data

The generate data of all the samples were further passed by several steps of data analysis (Figure 38). First the data were processed through the CellRanger aggr which combined all the data and subjected them to dimensional reduction using t-Distributed Stochastic Neighbour Embedding (t-SNE) analysis. t-SNE is a nonlinear dimensionality reduction technique used to visualize high-dimensional data in a low-dimensional space of two or three dimensions ²¹⁶.

In this stage, the t-SNE plot was used to demonstrate the transcriptome landscape for a sum of 10.262 single cells (Figure 39). This primary analysis revealed a high-dimensional separation between the tumour and the normal cells and across the untreated and treated samples which may indicate the high transcriptome heterogeneity between the cells. However, it should be noted that the position of the cells and their clustering is significantly depending on the parameters that were applied in the dimensional reduction. The dimensional distribution of the cells is also different from one analysis tool to another.

In order to examine the heterogeneity, the fold change expression of the highly variable genes ($P < 0.001$) of each sample was extracted and visualized on a heatmap plot (Figure 39). The heatmap plot revealed a considerable heterogeneity in the gene expression patterns between the untreated and the treated cells and across the tumour and normal cells. For example, the HDACis treated tumour and normal cells showed a distinct expression patterns to the untreated cells. Also, there was a noticeable difference in the expression patterns between the tumour and normal cells. Comparing the expression patterns between the SAHA- and MS-275-treated cells showed some similarity in both cell types (Figure 39).

Further, the biological function of these genes was explored using GenCLiP 2.0 Gene Ontology (GO) mining server by annotating the genes of each condition. The GO terms of the untreated Daoy cells showed a wide range of cell regulations including proteolysis, cell cycle, response to stress, and negative regulation of cell death. The apoptotic regulation and cell death terms were more frequent with the HDACis treated Daoy cells. The untreated neurons showed a high enrichment in GO terms that encompass supporting normal cell growth, gene expression, and neuronal functions. In contrast, the treated

neurons showed GO terms such as extracellular organelle and vesical, cellular response to stress, macromolecule catabolic, and neuronal differentiation process.

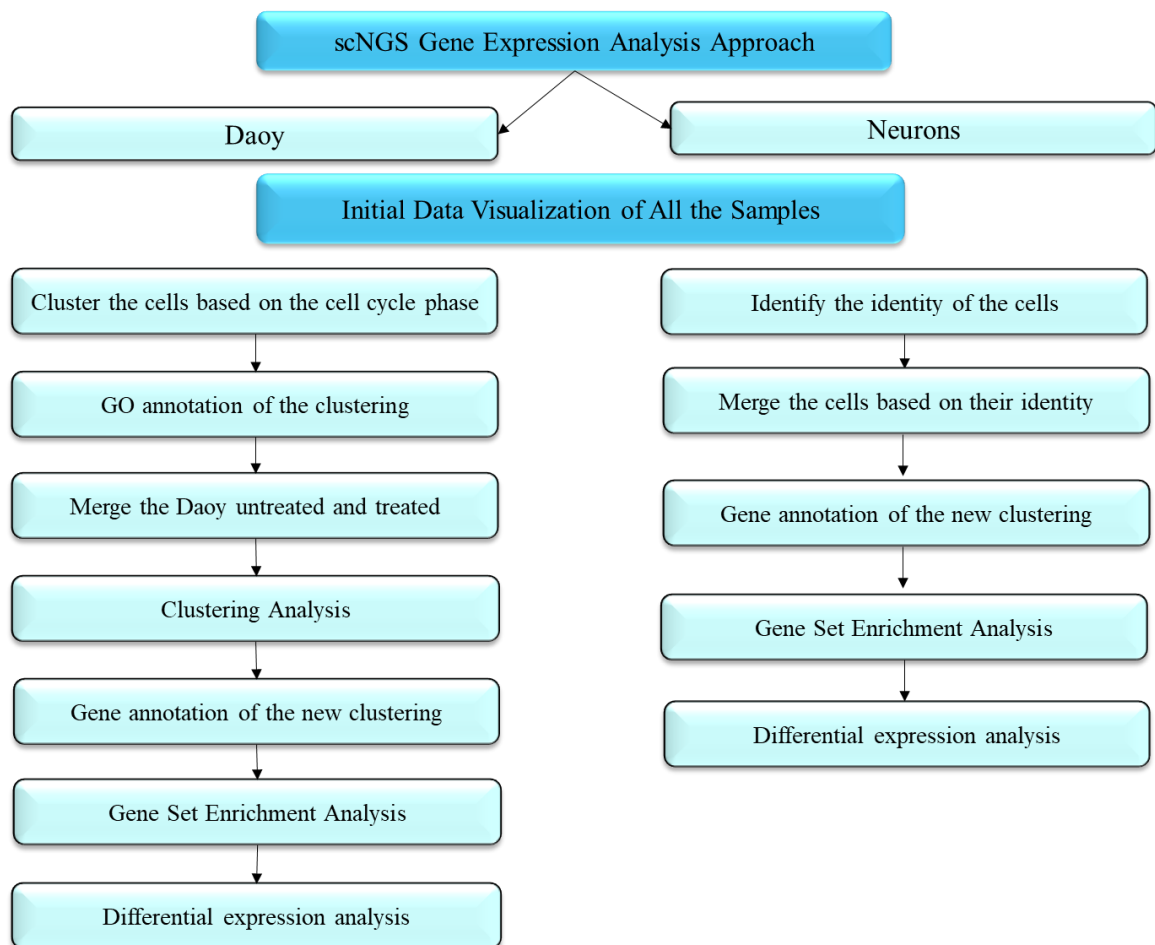


Figure 38: Schematic representation of the data analysis workflow

The quality improved data were processed through several steps of data analysis. First, the expression of all the samples was visualized on two-dimensional *t*-SNE projector and the gene expression was presented on a heatmap. Next, each of the Daoy and the neurons were processed independently. The Daoy cells were analysed by clustering the cells based on their cell cycle phase and the cells were then subjected to GO annotation analysis. As treating with HDACis affected the cells cycle clustering, all the treatment conditions were merged in one data set and the data were subjected to; clustering analysis, GO analysis, Gene Set Enrichment Analysis (GSEA), and differential expression analysis. The analysis of the neurons established by identifying the identity of the cells in each cluster and the clusters of the untreated and treated cells were merged based on the similarity in their identity. The data were then subjected GO analysis, GSEA, and differential expression analysis.

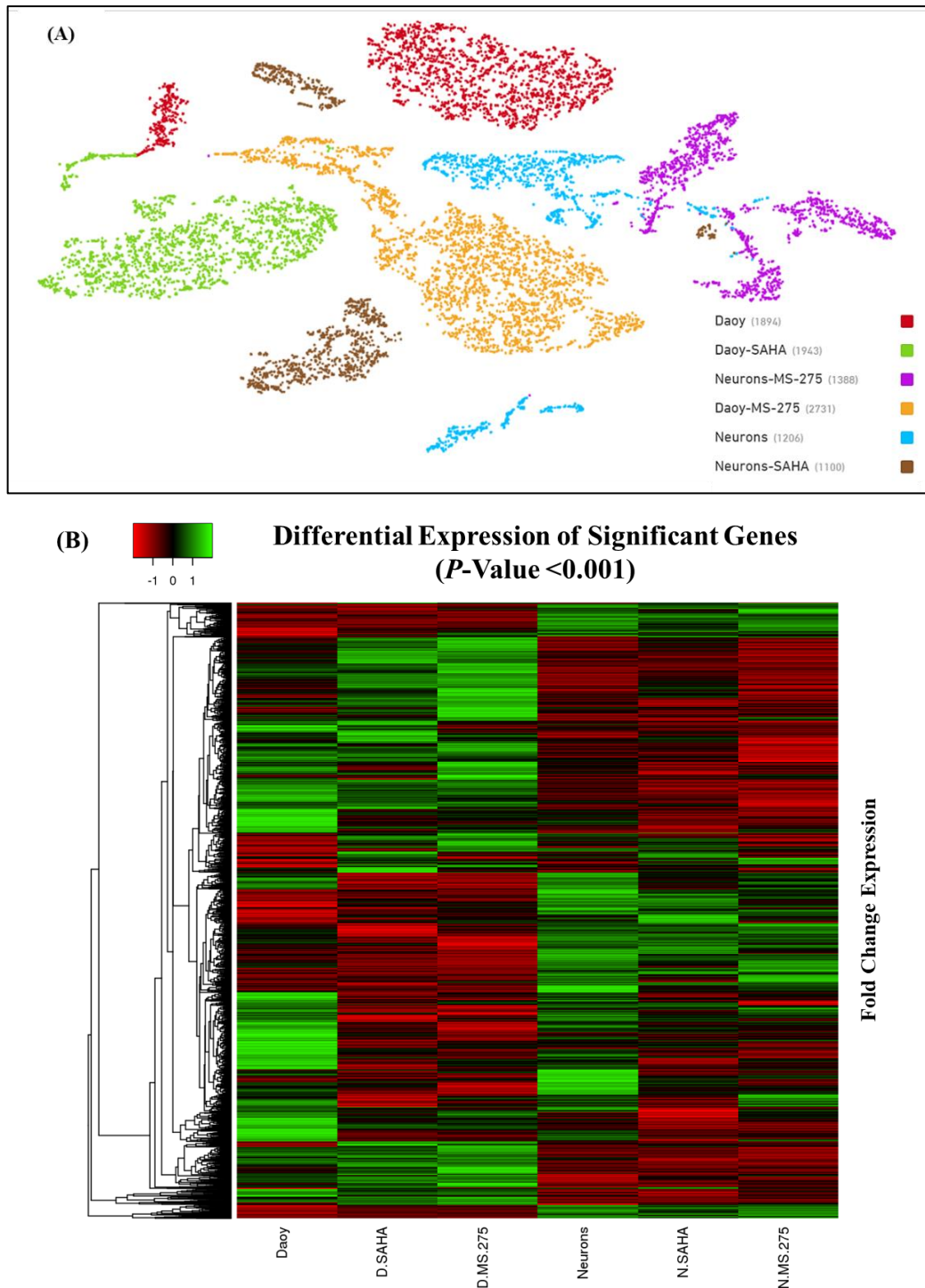


Figure 39: Visualization of the untreated and treated Daoy cell and neurons

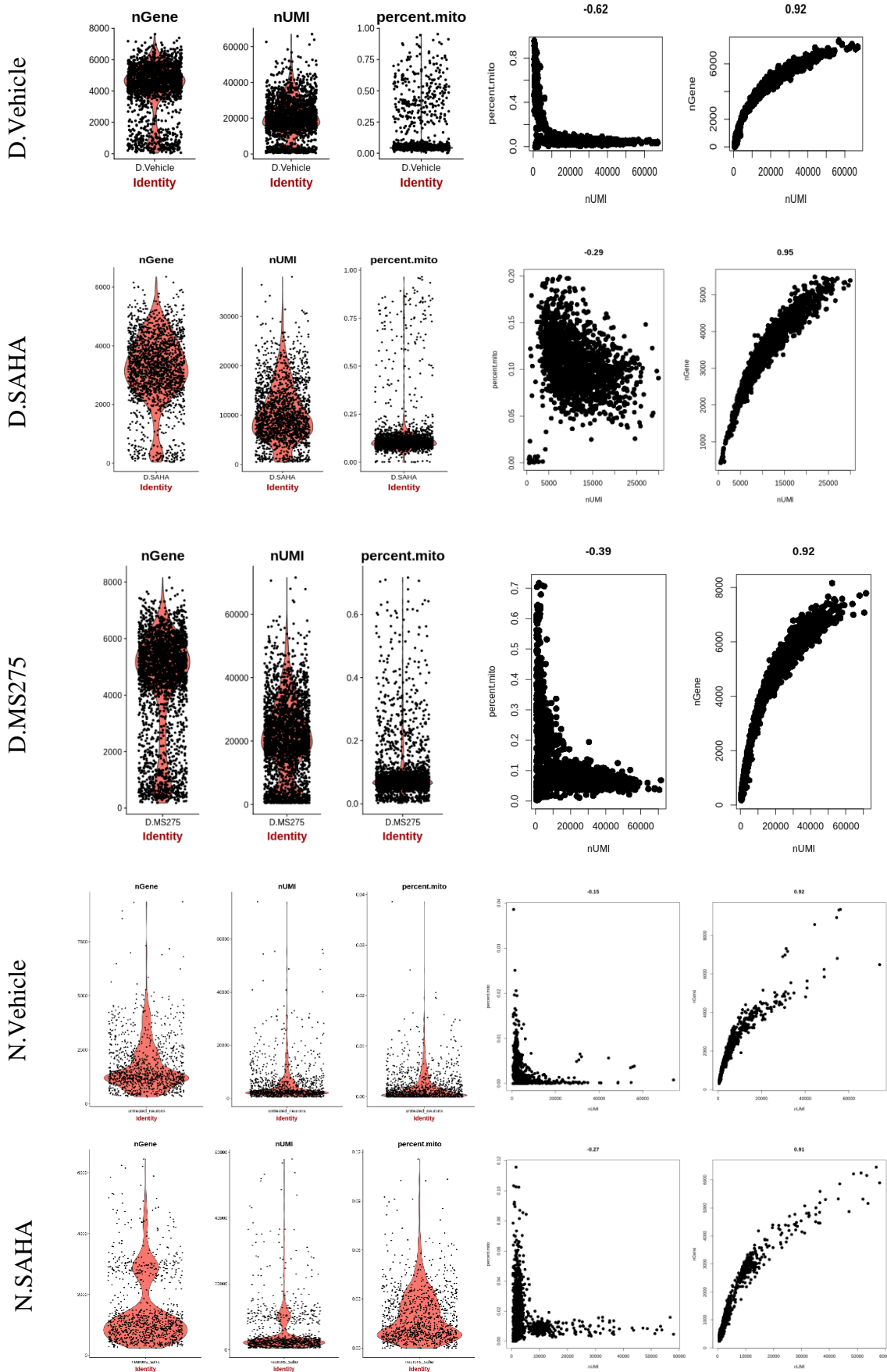
The *t*-SNE scatterplot (A) show the clustering of ~10,262 cells based on their gene expression. The data sets of the 6 samples were processed using the CellRanger aggr pipeline and the gene expression of each cell was subjected to PCA and presented on a *t*-SNE plot. Interestingly the scNGS data revealed two populations of Daoy and neuronal cells which requires further investigation. Each dot corresponds to one single cell and the cells were coloured according to the sample. The *t*-SNE plot was produced by CellRanger

Loupe. (B) The heatmap shows the differential expression of the highly variable genes ($P < 0.001$) of the untreated and treated Daoy and neurons. The rows represent the genes and the columns represent the samples. The colour and the intensity of the boxes are z-score values and were calculated by centring the fold change expression values to zero mean and all the data were scaled to 1 SD. The light green boxes indicate upregulated genes, the red indicate the lower expression and no differential expression is black. The hierarchical clustering (left) is the average linkage and was calculated based on the similarity of gene expression patterns. The heatmap was generated using the Heatmapper online tool ¹⁴⁴.

4.2.5 Improving the Quality of the 10x scNGS Generated Data

As the generated data from the CellRanger-pipelines contain high level of biological background signal (cell-free RNA noise) the data were subjected to several steps of filtration and quality improvement. These analyses were performed using the Seurat R package which was also used to merge the data sets and visualize the DGE between the untreated and treated cells. The first step in data quality improvement was to exclude the cells with fewer than 300 genes and the genes that were detected in less than 3 cells. Next, Seurat was used to calculate the total number of the UMI (nUMI) counts, the percentage of mitochondrial genes (percent.mito) and the number of the genes (nGene) for each cell and the values were presented using violin and scattered plots (Figure 40).

The number of the detected genes in the Daoy cells plots was between 3000 to 5000 genes however, there were some cells with more than 5000 genes. Also, the percentage of the mitochondrial genes were around 0.2% of the sum of the detected genes. With the neurons, the number of the detected genes in the majority of the cells was between 1000 to 1500 genes yet, few cells displayed more than 2000 genes. Whereas, the percentage of the mitochondrial genes was $\leq 0.05\%$. With all the samples, the small subsets of cells with a clear outlier number of genes and UMIs were assumed as potential multiplets. The elevated expression of the mitochondrial genes could be indicative of poorer cell quality and it may be a result of apoptosis and/or cell lysis.



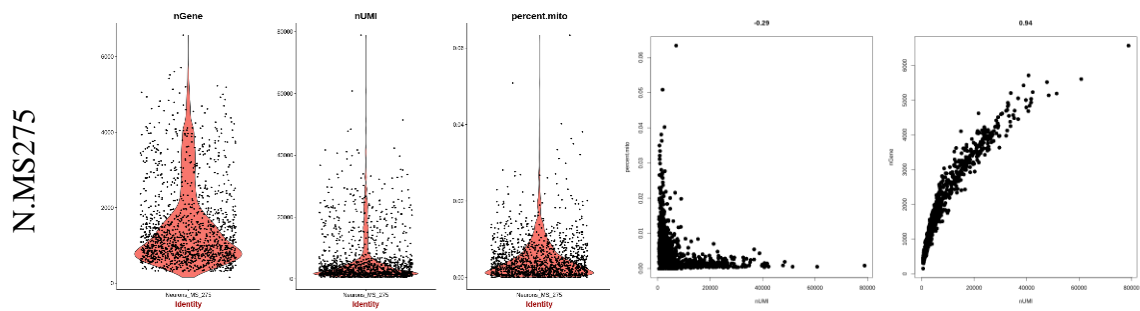


Figure 40: Exploring the scNGS Data to improve the quality

The number of the genes (*nGene*), UMI (*nUMI*) and the percentage of mitochondrial genes (*percent.mito*) were calculated for each sample using *Seurat (CreateSeuratObject)* function. The data were presented as violin and scatter plots to show the subset of cells that have clear outlier number of *nGene*, UMIs, and *percent.mito*. The violin plots show the calculated number of the gene (first column), UMI (second column), and *percent.mito* (third column) for each sample. The scatter plots present the expression of the UMIs vs. *percent.mito*, and the UMIs vs. *nGene*.

Hence, the cells with a clear outlier number of genes and the mitochondrial genes were filtered out. Also, the cells with low gene count were considered as dying/dead, empty droplets and were filtered out, as well. Next, the quality improved data of each sample was normalized, scaled, and subjected to clustering analysis. The outputs of these analysis were dimensionally reduced and displayed on t-SNE plots and the data were used in the subsequent analysis.

4.2.6 Daoy scNGS Data analysis

4.2.6.1 SAHA and MS-275 Affected the Expression of the Daoy Cell Cycle-Specific Markers

In this study, the scNGS data analysis was established by investigating each Daoy sample independently. The principal component analysis (PCA) revealed the presence of 4 distinct clusters in the D.Vehicle sample whereas, D.SAHA and D.MS-275 showed the presence of 5 and 6 clusters, respectively (Figure 41 A).

Initially, and as the phase of the cell cycle is possibly the main source of the transcriptome heterogeneity within each sample also, it could be the driver of the cells clustering, the analysis was carried out by characterizing the cell cycle phase of each cell using *Seurat*

(CellCycleScoring) function. The analysis was performed by calculating the S and G2/M phase scores for each cell using a pre-set of 97 genes that have a significant cell cycle–dependent expression¹²⁸. The scoring of each cell was based on the genes anticorrelated expression thus, the cells expressing these markers should be not be in G1 or quiescent (G0) phases (Figure 41 B).

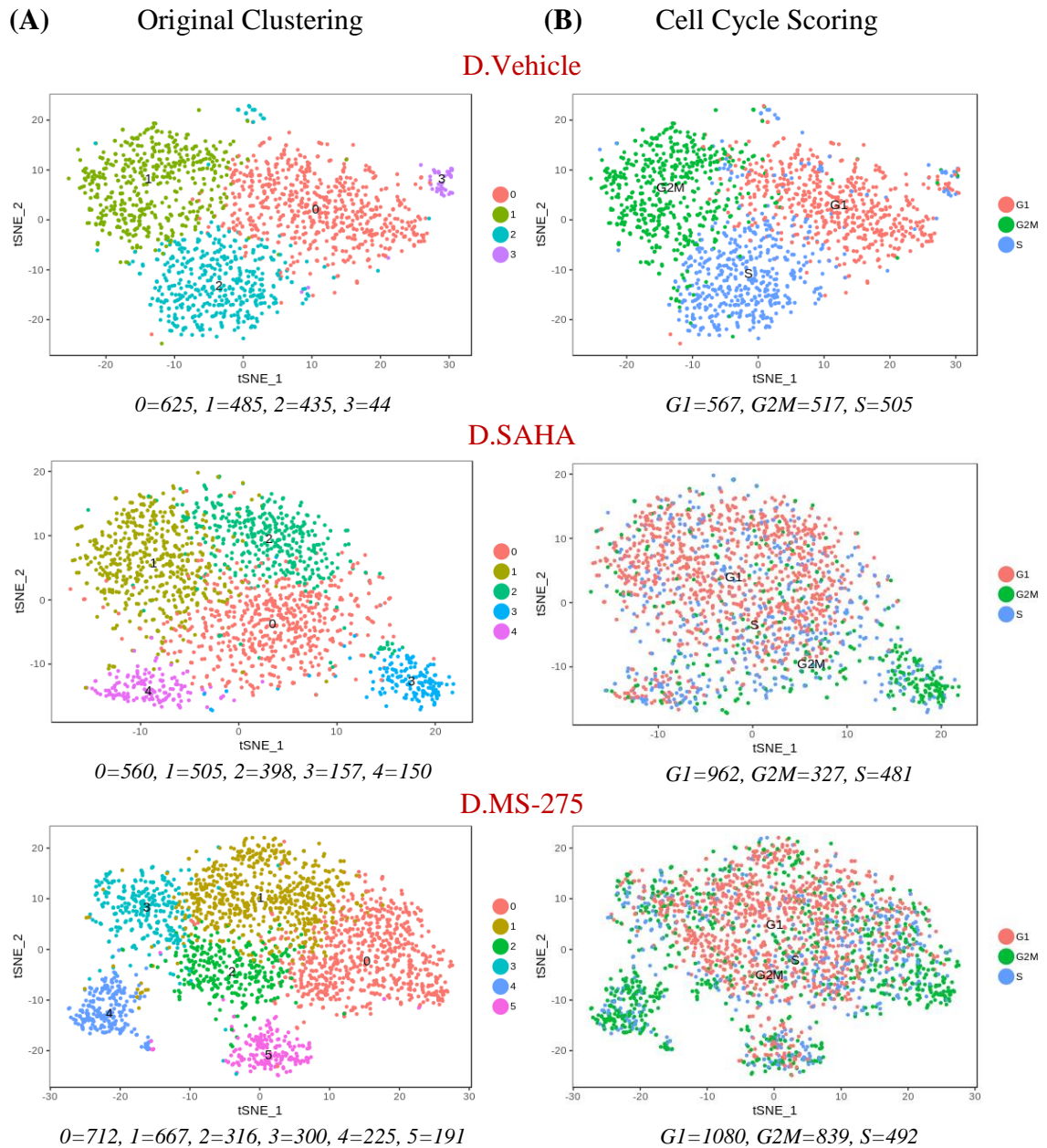


Figure 41: The clustering of the Daoy treated cells was independent of the cell cycle phase

The *t*-SNE plots in column (A) show the original clustering-analysis results of D.Vehicle, D.SAHA, and D.MS-275. The *t*-SNE plots in column (B) show the cell cycle scoring analysis results generated by the Seurat (*CellCycleScoring*) Function. The numbers below each projector are the cell count of each cluster.

The outcome of this analysis showed that the clustering of the D.Vehicle was mainly driven by the expression of cell cycle genes, apart from cluster 3 which showed a distinct cluster located outside the three main clusters (Figure 41 B). In contrast, the cell cycle scoring of the D.SAHA and D.MS-275 cells showed extensive overlap between the different phases of the cells which may indicate the effect of SAHA and MS-275 on the cell cycle gene expression (Figure 41 B).

Further, and in order to demonstrate the effect of HDACis on the expression of the cell cycle markers, the expression of the S and G2M specific genes of each cell was visualized using heatmaps. The heatmaps of the D.Vehicle showed high, specific, and more frequent expression patterns of the S and G2M markers in the cells that were classified as either S or G2M phase, respectively (Figure 42 A and B). Whereas, the expression patterns were different with D.SAHA and D.MS-275. For instance, the expression of the S phase markers was not limited to the cells that were classified as S phase, and many of the G1 and G2M classified cells showed the expression of these markers. Similarly, the G2M markers were expressed in cells that were classified as S and G1 (Figure 42 A and B).

To explore the variations between the clusters, I used the functional annotation analysis to annotate the upregulated and downregulated genes of each cluster. The annotation results of the D.Vehicle showed some variations in GO categories between the four clusters. For example, the upregulated genes in cluster (1, 2 and 3) showed wide range of GO terms including cell cycle transition, mitotic nuclear division, and G2/M transition of mitotic cell cycle. Similarly, the downregulated genes showed a broad range of GO annotations such as cell differentiation, regulation of cell differentiation, and cell death. Noticeably, cluster (3) which consists of 44 cells showed upregulation of more than 50 genes that were annotated as caspase-independent apoptosis (Table 6).

With D.SAHA, there was wide variations in the GO terms between the clusters. For example, the downregulated genes in cluster 1 and 2 showed an enrichment by GO terms such as regulation of (non-apoptotic) programmed cell death. In contrast, cluster 4 showed upregulation of genes that were annotated as cell cycle phase transition, apoptosis inhibitors, and caspase-independent cell death (Table 6).

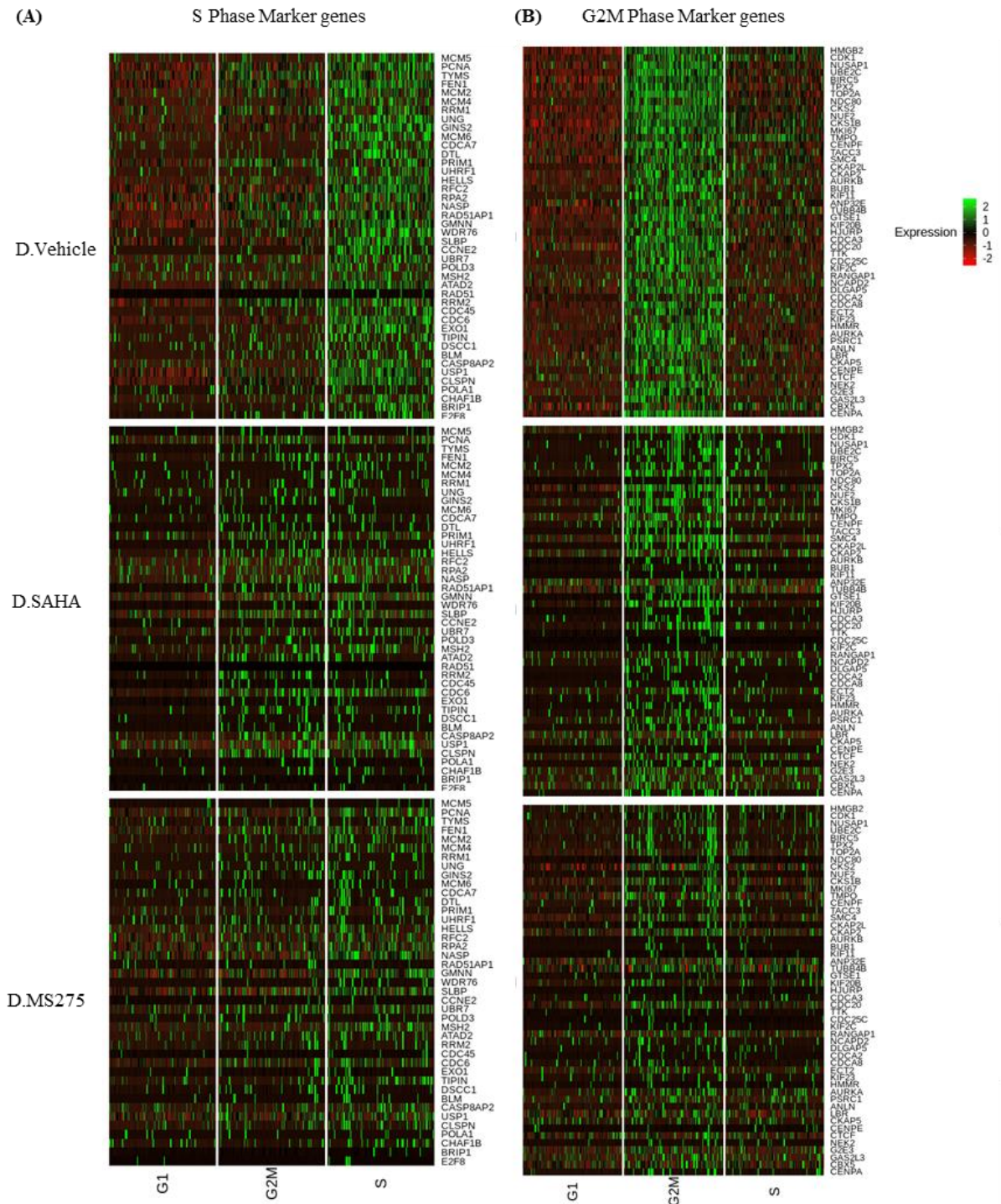


Figure 42: Visualization of the cell cycle markers in D.Vehicle, D.SAHA, and D.MS-275

The heatmaps visualize the expression of 97 cell cycle markers (43 genes for S phase (A), and 54 genes for G2M phase (B)) across the untreated and treated Daoy cells. The rows represent the genes, the columns represent the cell cycle phase, and each column within a row represents a cell. The green boxes indicate upregulated genes, the red indicate the lower expression and the no differential expression is black.

Likewise, the cluster (0) of D.SAHA showed an enrichment in GO categories that are highly relevant to cell death. Cluster (3) showed an enrichment in categories of mitotic cell cycle, chromosome condensation, and DNA replication and downregulation of genes that were annotated as regulators of the extracellular exosome (Table 6).

Also, D.MS-275 showed wide variations in GO terms between the 6 clusters. For example, cluster (0) and (3) showed upregulation in the genes that are involved in RNA transcription and downregulation in cell proliferation genes. Cluster (1) and (4) showed downregulation of genes that are involved in cell cycle transition and also, in the genes that function as negative regulators of apoptosis. Cluster (2) and (5) showed downregulation of genes that regulate cell differentiation and upregulation in genes that were annotated as negative regulators of cell death (Table 6).

Collectively, the GO results of the D.Vehicle suggest the expression of cell cycle genes whereas, some of the D.SAHA and D.MS-275 clusters showed GO terms related to the regulation of caspase-independent cell death. Treating with SAHA and MS-275 resulted in affecting the expression of the cell cycle regulating genes which consequently affected the accuracy of the cell cycle sorting analysis. Based on this analysis, comparing the DGE between the untreated and treated cell of the same cell cycle phase is not possible under the current situation.

Table 6: Summary of the GO terms that were more frequent for each cluster

D.Vehicle		
Cluster	GO Annotation (Upregulated Genes)	GO Annotation (Downregulated Genes)
0	negative regulation of cell cycle	mitotic cell cycle cycle transition from G1 to S phase
1	mitotic cell cycle checkpoint negative regulation of cell cycle	regulation of cell proliferation cell differentiation regulation of cell death
2	Progression in mitotic cell cycle DNA metabolic process	negative regulation of cell cycle
3	programmed cell death positive regulation of apoptotic process	mitotic cell cycle regulation of mitotic cell cycle
D.SAHA		
0	apoptotic process cell differentiation	extracellular region
1	homeostatic process regulation of biological characteristic	cell cycle regulation of (non-apoptotic) programmed cell death
2	membrane organization	regulation of proteolysis activation of apoptosis regulation of (non-apoptotic) programmed cell death
3	mitotic cell cycle condensed chromosome DNA replication mitotic cell cycle phase transition	extracellular exosome negative regulation of biological process (i.e. gene expression, protein modification)
4	apoptosis inhibitor activity caspase-independent cell death cell cycle phase transition	mRNA metabolic process membrane organization intracellular transport protein synthesis elongation
D.MS-275		
0	regulation of transcription from RNA polymerase II promoter	cell proliferation
1		negative regulation of cell death (caspase-independent cell death) apoptotic process cell cycle phase transition
2	regulation of cell migration regulation of apoptotic process	cell differentiation nervous system development
3	extracellular organelle	growth
4	mitotic cell cycle regulation of mitotic cell cycle phase transition	negative regulation of cell death cell differentiation
5	negative regulation of programmed cell death apoptotic process	extracellular organelle

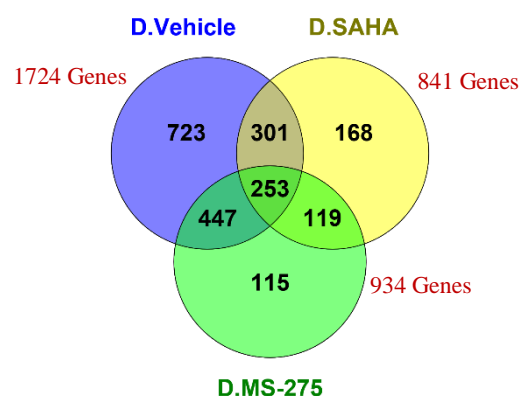
4.2.6.2 Merging the D.Vehicle, D.SAHA, and D.MS-275 Data Sets

In order to study the anticancer effect of SAHA and MS-275, the three Daoy-cell conditions were merged in one Seurat object and the data were normalized, dimensionally reduced, and visualized on t-SNE plots (Figure 44 A). The new dimensional scale of the merged data set displayed the D.Vehicle with high similarity to its original unmerged scale. Though, the dimensions of the D.SAHA and D.MS-275 cells showed some differences compared to their unmerged condition. The plots did not show overlap between the three conditions and each sample maintained its own clustering identity with very few cells of the D.SAHA sample were overlapping with the other two conditions (Figure 44 A). Comparing the detected genes between the three conditions showed a considerable reduction in the number of the genes in the HDACis treated cells. For example, 1724 genes were detected in the D.Vehicle cells and the number reduced to 841 and 934 genes in D.SAHA and D.MS-275, respectively (Figure 43).

Next, the merged data set was subjected to the clustering analysis based on the new PCA values. The new clustering of the D.Vehicle did not result in a considerable difference when compared to the unmerged clustering yet, the number of the cells within each cluster was different when compared to the unmerged (original) clustering (Figure 44 B). Whereas, the number of the clusters of the D.SAHA and D.MS-275 was less than the unmerged condition. For example, D.SAHA, was clustered into two clusters with 1563 cells in the main cluster. Also, the number of the D.MS-275 clusters was reduced to 4 clusters with 1404 cells in the main cluster (Figure 44 B).

Figure 43: Illustration of the number of detected D.Vehicle, D.SAHA, and D.MS-275 genes

The Venn diagram shows the number of the detected genes in D.Vehicle, D.SAHA and D.MS-275 that showed a significant differential expression.



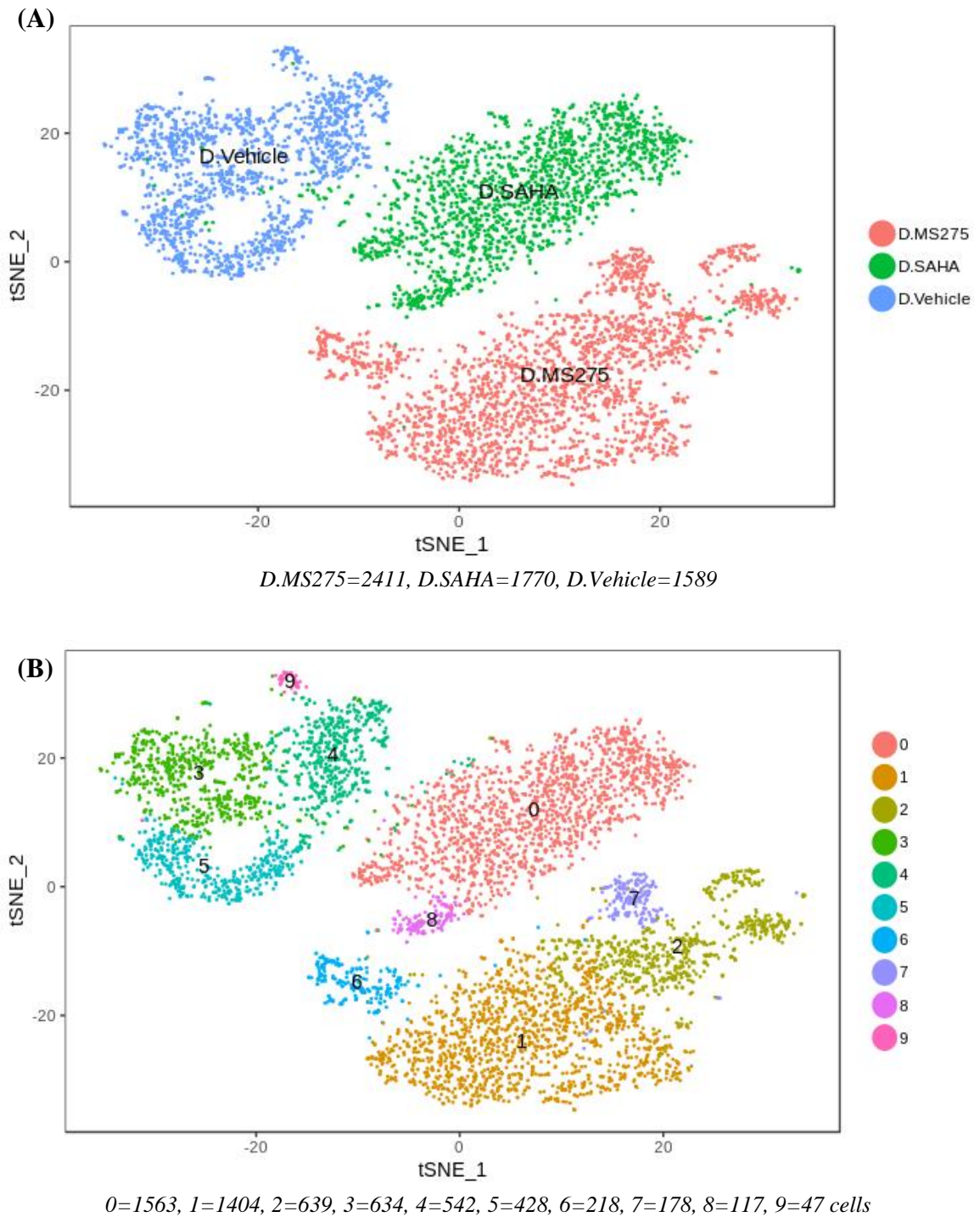


Figure 44: Merging the three conditions into one Seurat object to study the DGE

The data sets of the D.Vehicle, D.SAHA, and D.MS-275 samples were merged, normalized, dimensionally scaled, and displayed on t-SNE plot (A). Next, the merged data (A) were subjected to clustering analysis based on the new PCA of the three samples, and the new clustering was displayed on t-SNE plot (B).

To calculate the differential gene expression (DGE) between the untreated and the treated cells, the merged data set was subjected to Seurat (FindAllMarkers) function which calculates the log fold-change and the P -value for each differentially expressed gene. The outcome of this analysis showed a significant ($P > 0.001$) upregulation and downregulation of more than 2600 genes across the three conditions.

Further, the expression values of the genes that showed shared differential expression across the three conditions were used to explore the effect of SAHA and MS-275 on the Daoy cells. The analysis identified 253 shared genes which were functionally annotated, and their expression was presented on a heatmap plot (Figure 45).

The heatmap showed a considerable difference between the untreated and treated cells and across the treated cells, as well. Treating with SAHA and MS-275 resulted in a significant ($P > 0.001$) downregulation of several genes families that were annotated as cell cycle regulators, cell cycle checkpoint, and positive regulators of cellular process (Figure 45). Also, the MS-275 treated cells showed the expression of more than 23 genes that were annotated as regulators for cell death (Figure 45).

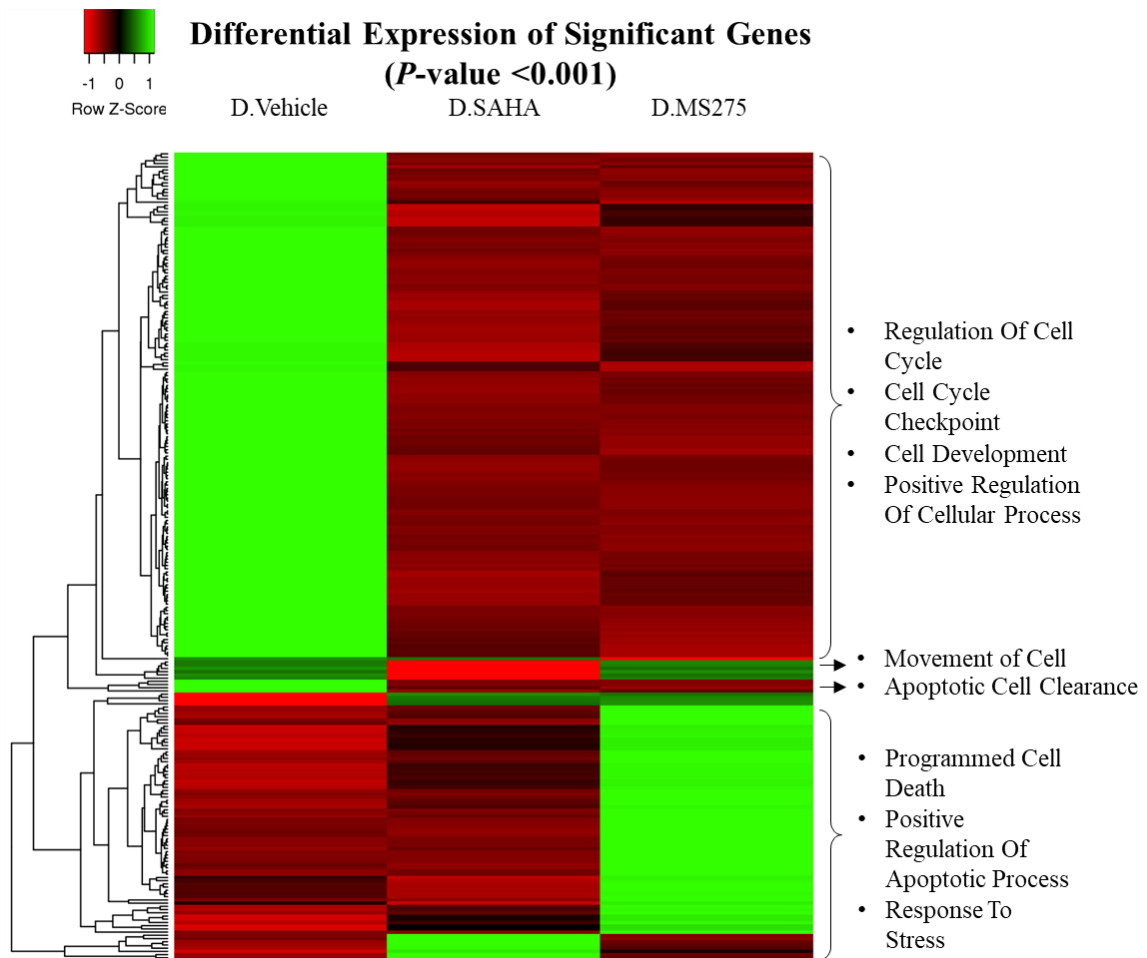


Figure 45: The differential expression of the highly variable genes across the Daoy untreated and treated cells

The heatmap shows the differential expression of 253 highly variable genes ($P < 0.001$) shared between the untreated and treated Daoy cells. The rows represent the genes, the columns represent the treatment-condition, and the terms on the right are the GO annotations terms. The colour and the intensity of the boxes are z-score values and were calculated by centring the fold change expression values to zero mean and the data were scaled to 1 SD. The light green boxes indicate upregulated genes, the red indicate the lower expression and the no differential expression is black. The hierarchical clustering is the average linkage and was calculated based on the similarity in the gene expression patterns.

Further, the merged data set was used to study the anticancer regulation of SAHA and MS-275 in the subsequent analysis. However, as the clustering of the merged set was not similar to the clustering of the single sample, also as not all the clusters of the single sample analysis showed the anticancer effect of the drugs in the earlier analysis, the main cluster of D.SAHA (0) and D.MS-275 (1) were further subjected to the functional annotation analysis to determine if they include the clusters that displayed the cell death regulations.

The results of D.SAHA cluster (0) upregulated genes showed several GO terms with > 4.13 GenClip Enrichment Score ((GES), significant > 1)¹³⁰. The terms were included the negative regulation of cell cycle and positive regulation of programmed cell death. The downregulated genes showed high enrichment in GO terms of cell cycle transition, negative regulation of cell death, and cell differentiation (GES: > 20).

Likewise, the upregulated genes of the D.MS-275 cluster (1) showed a significant enrichment in GO categories associated with cell death, response to stress, and cellular response to chemical stimulus (GES: >6). Whereas, the downregulated genes revealed a significant enrichment in GO categories that were highly relevant to mitotic cell cycle process (GES: 14.89), negative regulation of apoptotic process (GES: 5.43), and programmed cell death (GES: 4.75). Despite, the functional differences between all the previous GO terms yet, there was high similarity in the genes across the GO terms.

Collectively, these findings suggest the anticancer effect of SAHA and MS-275 in cluster 0 and 1 therefore, they were used in the subsequent analysis to study the anticancer molecular regulation. Hereinafter the cluster (0) referred to as D.SAHA, and the cluster (1) referred to as D.MS-275.

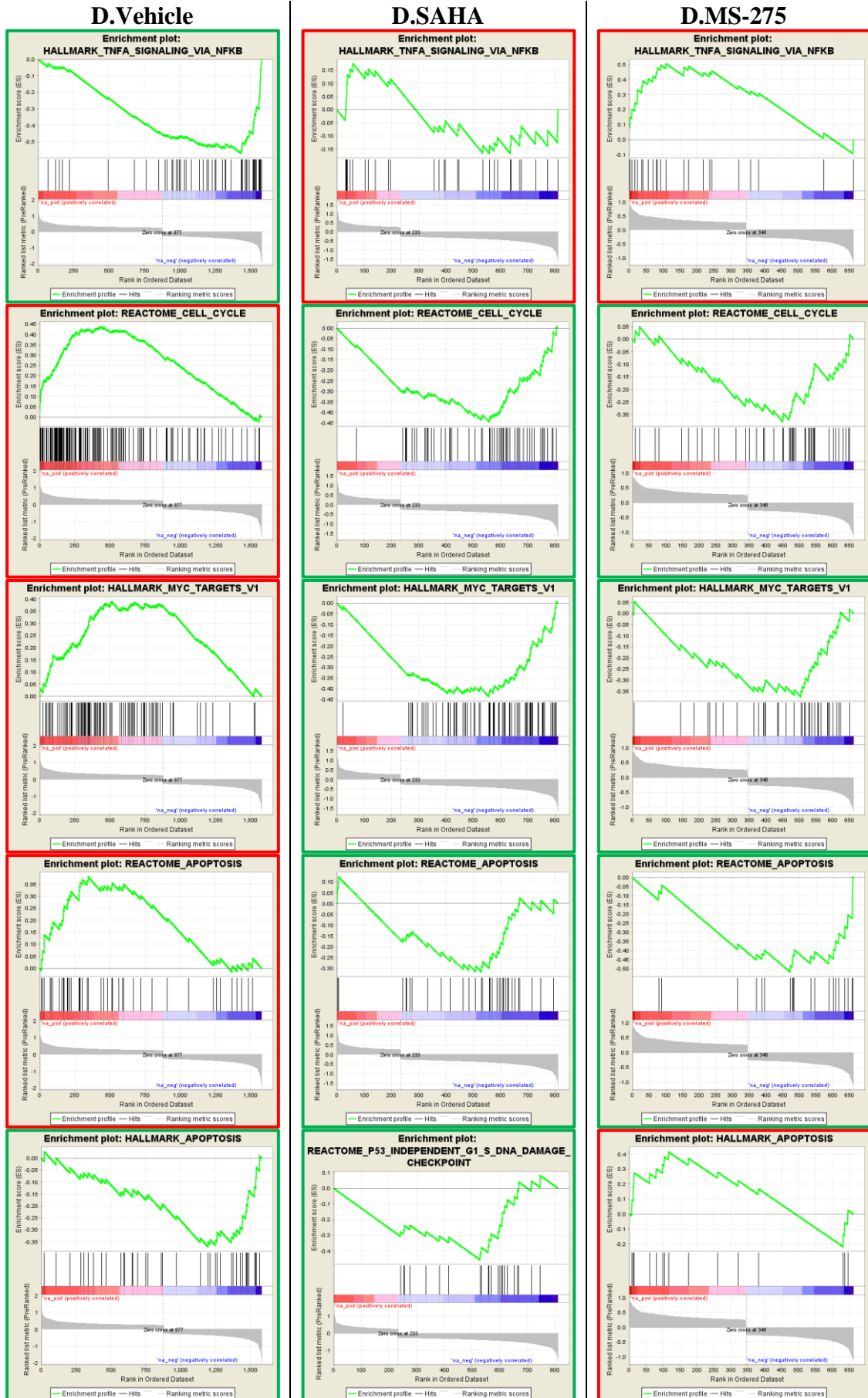
4.2.6.3 Dissecting the Molecular Regulation of the Daoy Untreated and Treated Cells

In order to study the anticancer regulation of the HDACis, the study started by exploring the molecular regulations of the D.Vehicle, D.SAHA, and D.MS-275 samples. The analysis was carried out by examining the gene enrichment for each sample using the Gene Set Enrichment Analysis (GSEA) at Broad Institute¹³¹. The analysis was performed by ranking the upregulated and downregulated genes as per the decrease in their fold change values and the ranked lists were used to run the GSEA. The GSEA define the genes at the

top of the ranked list as ‘positive phenotype’ and gives them a positive enrichment score (the majority of the genes are upregulated) whereas, it defines the genes at the bottom of the list as ‘negative phenotype’ and scores them with negative ES (majority of the genes are downregulated).

The GSEA results of the D.Vehicle cells showed several cellular pathways with statistically significant ES [false discovery rate q -value (FDR q) <0.25, and nominal P -value <0.01] (Table 7). The majority of these pathways were largely related to the cell growth mechanisms. For instance, the results of the positive phenotype displayed high enrichment in cell cycle, DNA replication, Myc and E2F targets pathways (Figure 46). Whereas, the negative phenotype showed high enrichment in TNF α signalling via NF κ B, hypoxia, p53 pathway, MAPK and KRAS pathways which have significant role in regulating the cell growth, as well (Figure 46). Interestingly, the analysis also revealed the presence of two different subsets of genes that showed negative phenotype and enriched with genes that were identified as regulators for apoptosis (Table 7).

The results of the D.SAHA and D.MS-275 showed an inverse phenotype to the molecular regulations of the D.Vehicle sample (i.e. the positive phenotype in the D.Vehicle becomes negative in the D.SAHA and D.MS-275) (Figure 46). For example, the results of D.SAHA and D.MS-275 negative phenotype showed a significant (FDR q <0.25, nominal P <0.01) enrichment with terms such as Myc (Targets V1), cell cycle, and p53 pathways. Whereas, the positive phenotype results showed high enrichment with TNF α signalling via NF κ B, p53 and, MAPK signalling pathways (Table 7).



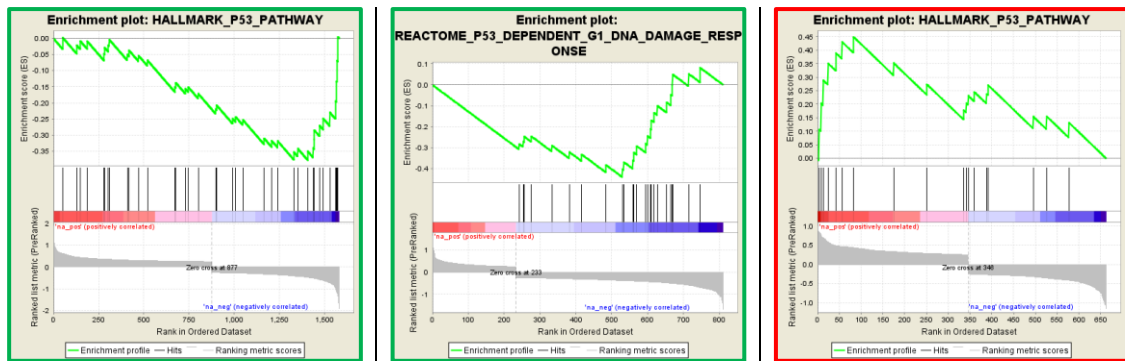


Figure 46: GSEA enrichment plots of the highly enriched molecular regulations

The GSEA was carried out by ranking the upregulated and downregulated genes based on the decrease in their fold change and the ES was calculated by walking down the ranked list. In the above charts, the horizontal middle line in red and blue colours is the rank ordered list of the upregulated and downregulated genes, respectively, and the decrease in the intensity of the bar colour represents the decrease in the fold change. The vertical black bars represent the gene hits, the vertical grey bars represent the ranking metric scores of the genes, the positive values indicate correlation with the phenotype profile and the negative values indicate the inverse correlation, and the green fluctuating curve shows the enrichment score. The red framed-charts show the gene set enrichment at the top of the ranked list (Positive ES) and the green framed-charts display gene set enrichment at the bottom of the list (Negative ES).

Table 7: GSEA results of the highly enriched gene sets of the Daoy cells

(Pathways)	Size ¹	ES ²	NES ³	NOM p-val ⁴	FDR q-val ⁵
D.Vehicle					
Reactome_Cell_Cycle	141	0.437	3.585	0	0
Hallmark_Myc_Targets_V1	108	0.390	3.020	0	0
Hallmark_E2F_Targets	102	0.497	3.754	0	0
Reactome_DNA_Replication	79	0.515	3.620	0	0
Reactome_Apoptosis	44	0.379	2.250	0	0.0011
Hallmark_TNFA_Signaling_Via_NFKB	54	-0.570	-3.222	0	0
Hallmark_Hypoxia	41	-0.568	-2.958	0	0
Hallmark_Apoptosis	41	-0.370	-1.952	0.001	0.042
Hallmark_P53_Pathway	38	-0.376	-1.923	0.005	0.039
Kegg_MAPK_Signaling_Pathway	27	-0.557	-2.533	0	3.70E-04
Hallmark_KRAS_Signaling_Up	27	-0.542	-2.492	0	4.23E-04
D.SAHA					
Hallmark TNFA Signalling Via NFKB	29	0.174	0.99	0.438	0.932
Hallmark Myc Targets V1	73	-0.437	-2.36	0.000	0.001
Reactome Cell Cycle	59	-0.445	-2.17	0.000	0.001
Reactome Apoptosis	33	-0.317	-1.39	0.117	0.146
Reactome P53 Dependent G1 DNA Damage Response	25	-0.441	-1.81	0.015	0.019
D.MS-275					
Hallmark_TNFA_Signaling_Via_NFKB	25	0.505	2.477	0	0.002
Hallmark_MTORC1_Signaling	22	0.380	1.793	0.018	0.060
Hallmark_P53_Pathway	18	0.448	1.985	0.002	0.019
Kegg_MAPK_Signaling_Pathway	17	0.484	2.015	0.002	0.020
Hallmark_Apoptosis	15	0.415	1.680	0.021	0.094
Reactome_Cell_Cycle	44	-0.328	-1.938	0.005	0.016
Hallmark_Myc_Targets_V1	36	-0.374	-2.018	0.003	0.010
Reactome_Apoptosis	20	-0.516	-2.287	0	0.003

The light red shaded rows show the positive phenotype and the light green display the negative phenotype. The statistically insignificant pathways are in dark red font colour.

¹ The number of the detected genes.

² Enrichment Scores.

³ Normalized Enrichment Score (used to compare analysis results across gene sets).

⁴ Nominal P-value (statistical significance of the enrichment score).

⁵ False discovery rate (the probability that the NES represents a false positive finding).

4.2.6.4 Study the Differential Expression between the HDACis Untreated and Treated Daoy Cells

The results of the GSEA revealed a significant change in several cellular pathways between the untreated and treated cells. The changes in the HDACis treated cells involved the downregulation of genes that regulate the cell proliferation and upregulation of genes that are part of cellular pathways such as TNF α Signalling via NF κ B, and Myc Pathways. Also, the results showed a significant expression difference between subsets of genes that possibly have some contribution in regulating the apoptosis regulations. In order to identify the most potential driver genes across the different pathways, the genes of each pathway were compared to the other pathways. The investigation showed that each pathway has a conserved set of genes however, some of the genes were more frequent, in particular, across the cell cycle, Myc and the apoptosis pathways (Figure 47). Also, 9 genes were shared between the TNF α Signalling via NF κ B and the apoptosis pathways (Figure 47).

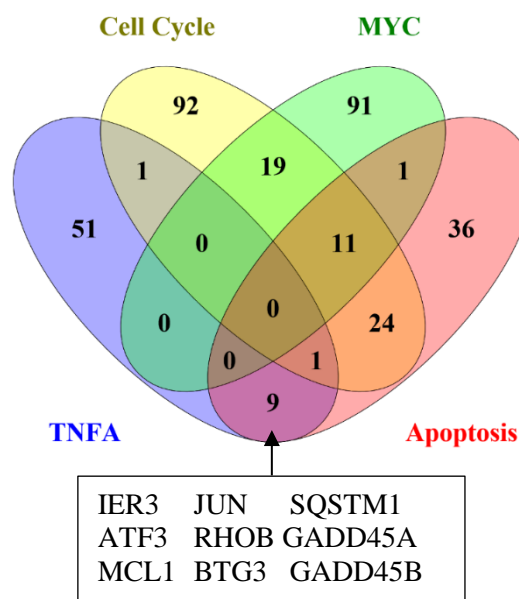


Figure 47: Representation of the genes that showed high enrichment scores across the identified pathways

The genes that showed high ES in the TNF α Signalling via NF κ B, cell cycle, Myc, and apoptosis pathways were compared to identify the shared genes between them. The diagram was prepared by combining the genes that present each pathway in the untreated and treated cells.

4.2.6.4.1 TNF α Signalling via NF κ B Molecular Pathways

Further, to present the gene expression difference between the D.Vehicle, D.SAHA, and D.MS-275 cells, the fold change expression was extracted from the merged data set and presented on bar charts. With the TNF α Signalling via NF κ B pathway, the number of the detected differentially expressed genes across the three conditions was 62 genes, with 9 genes showed shared differential expression (PHLDA2, ATP2B1, AREG, TUBB2A, CDKN1A, CCL2, FOSL1, CEBPD, and PLAUR) (Figure 48). D.SAHA, showed the expression of 7 exclusive genes (EIF1, CD44, SAT1, SOD2, CXCL1, CCND1, and BIRC3) whereas, the expression of TRIB1 (reported to help in sensitizing cells to TRAIL-induced apoptosis)²¹⁷ was only detected in the D.MS-275 cells. The highest fold change between the SAHA and MS-275 treated to the untreated cells was in the upregulation of AREG (inhibits the growth of certain cancer cells)²¹⁸ and downregulation of CCL2 (support primary cell tumour growth and metastasis)²¹⁹ (Figure 49).

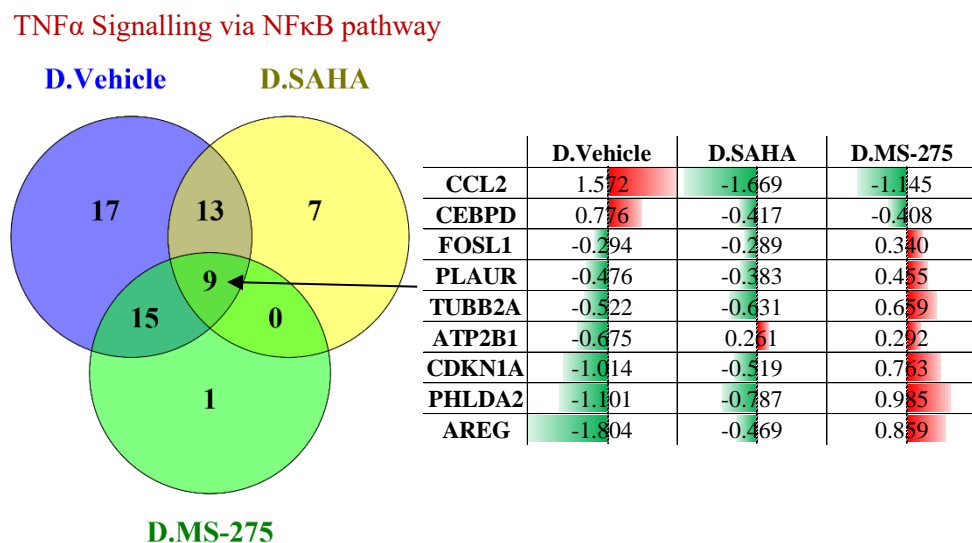


Figure 48: Illustration of the DGE with high enrichment scores in TNF α Signalling via NF κ B pathway

The genes with high ES in the TNF α Signalling via NF κ B pathway were compared in order to identify the shared genes between the HDACis untreated and treated cells. The table shows the fold change expression of the shared genes across the three conditions, upregulated expression in red and downregulated expression in green.

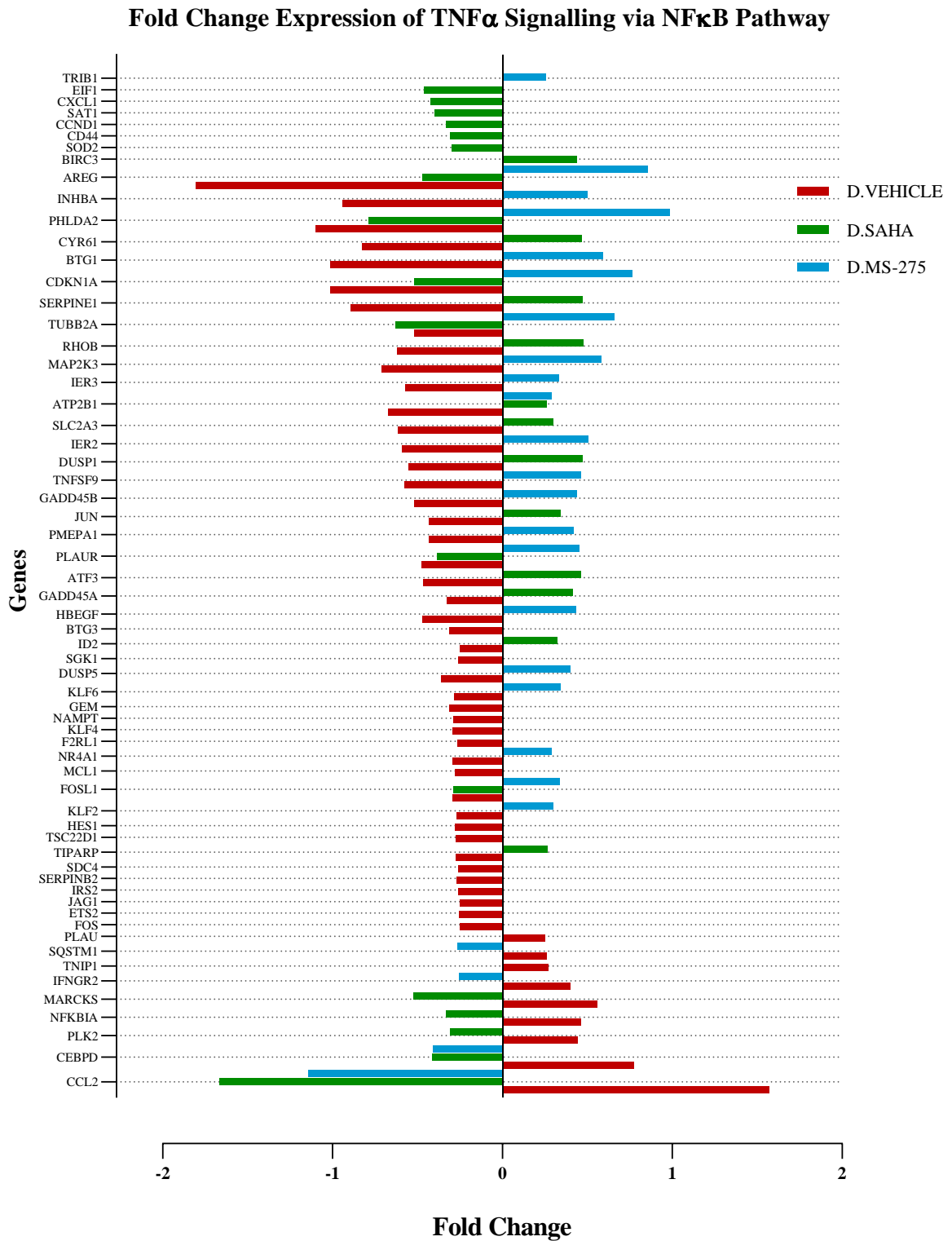


Figure 49: Fold change expression of the TNF α Signalling via NF κ B pathway

The bar chart displays the fold change expression of 62 genes that showed high enrichment score in TNF α Signalling via NF κ B pathway. The red bars are the D.Vehicle, the green are the D.SAHA, and the blue are the MS-275.

4.2.6.4.2 Treating with SAHA and MS-275 Deactivated Myc Signalling Pathway

The gene set analysis identified 122 genes as components of Myc (HALLMARK MYC TARGETS V1) (NOM $P < 0.0001$) pathway however, only 24 genes showed shared differential expression between the three conditions (Figure 50). Comparing the expression showed that the majority of these genes were upregulated in the untreated cell whereas, treating with HDACis resulted in downregulating 113 genes in HDACis treated cells (Figure 51).

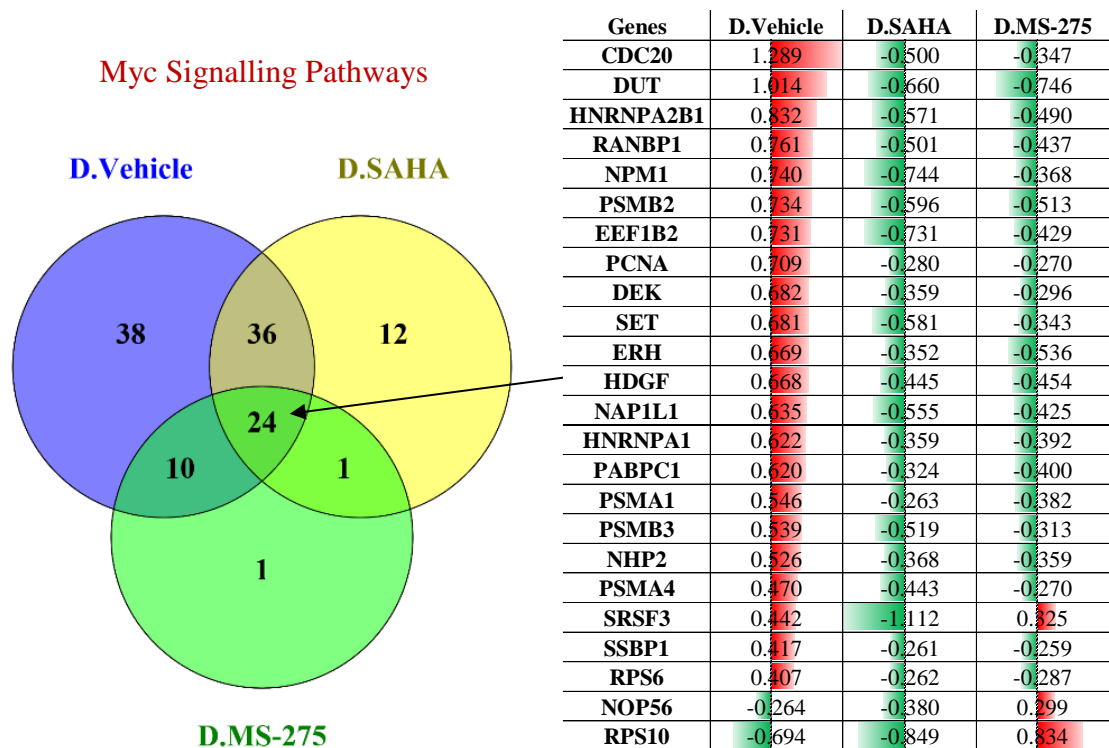


Figure 50: Illustration of the DGE with high enrichment scores in Myc Signalling pathway

The genes that showed high ES in the Myc pathway were compared in order to identify the shared genes between the HDACis treated and untreated cells. The table shows the fold change expression of the shared genes across the three conditions, upregulated expression in red and downregulated expression in green.

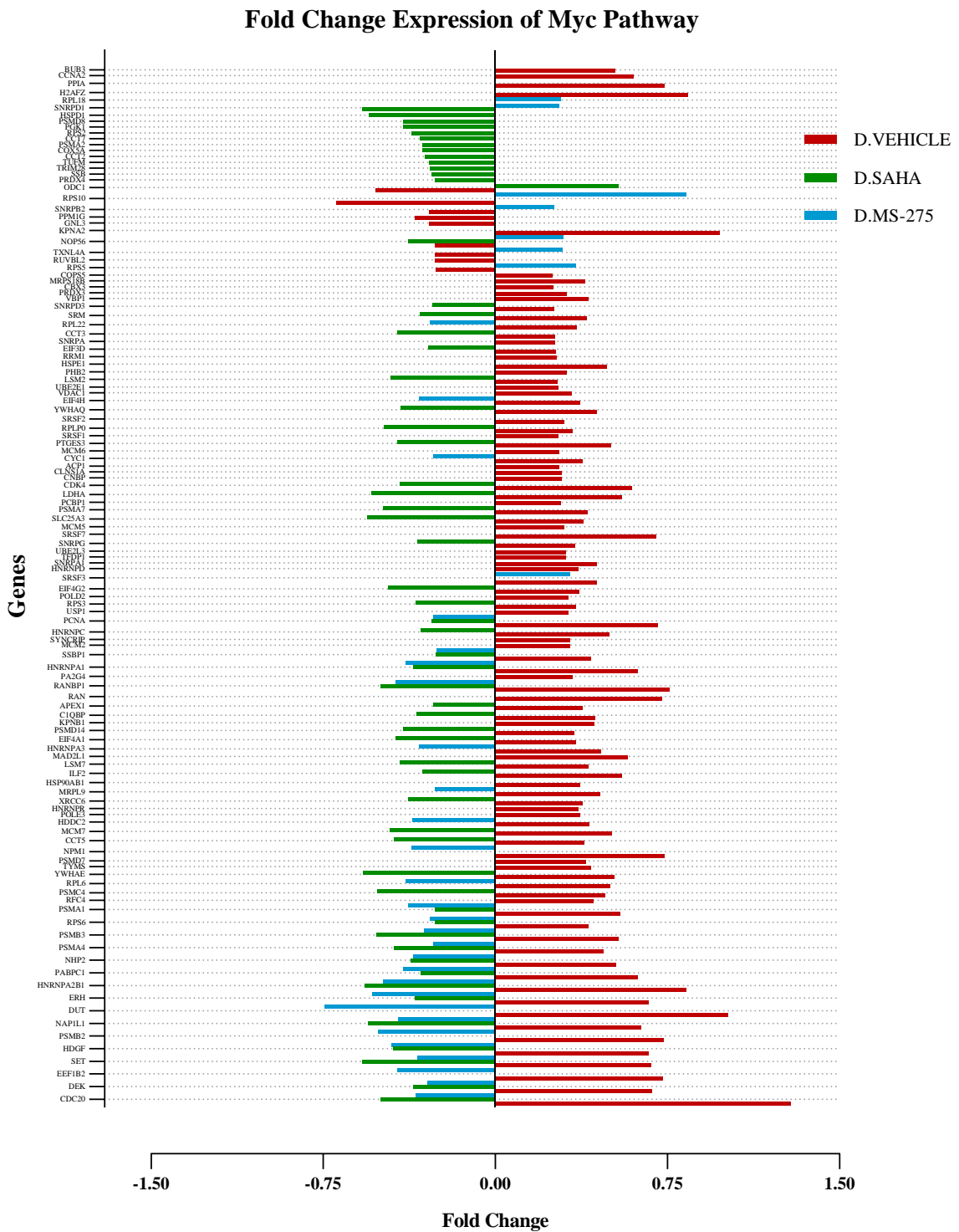


Figure 51: Fold change expression of the Myc signalling pathway

The bar chart displays the fold change expression of 122 genes that showed high enrichment score in Myc signalling pathway. The red bars are the D.Vehicle, the green are the D.SAHA, and the blue are the MS-275.

4.2.6.5 Treating with SAHA and MS-275 Decreased the Expression of Cell Cycle Specific Genes

The gene set enrichment analysis showed high enrichment of 148 genes in the cell cycle pathway (NOM $P \leq 0.005$). Several of these genes showed more than one-fold significant differential expression with 32 genes were shared across the three conditions (Figure 52). Treating with HDACis results in reducing the expression of large number of these genes. (Figure 53).

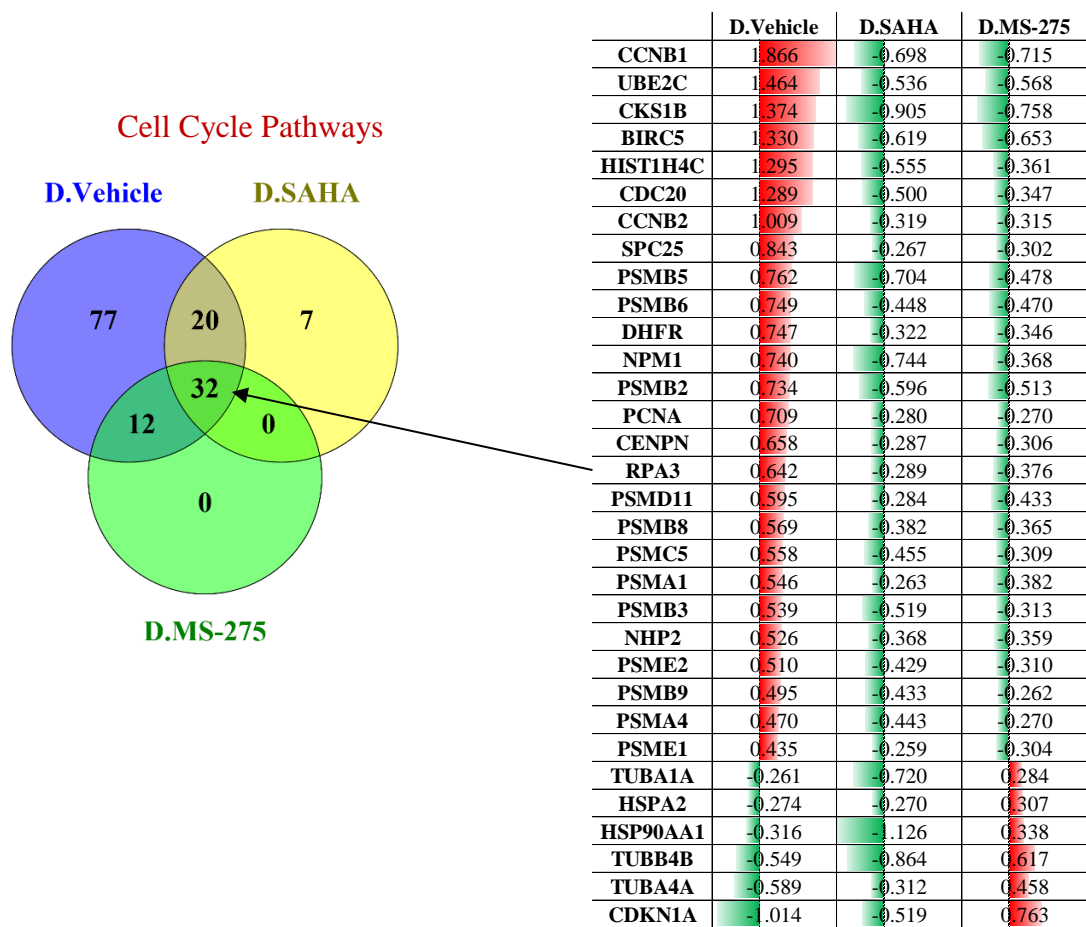


Figure 52: Illustration of the DGE with high enrichment scores in cell cycle signalling pathway

The genes that showed high ES in the cell cycle pathway were compared to identify the shared genes between the HDACis treated and untreated cells. The table shows the fold change expression of the shared genes across the three conditions, upregulated expression in red and downregulated expression in green.

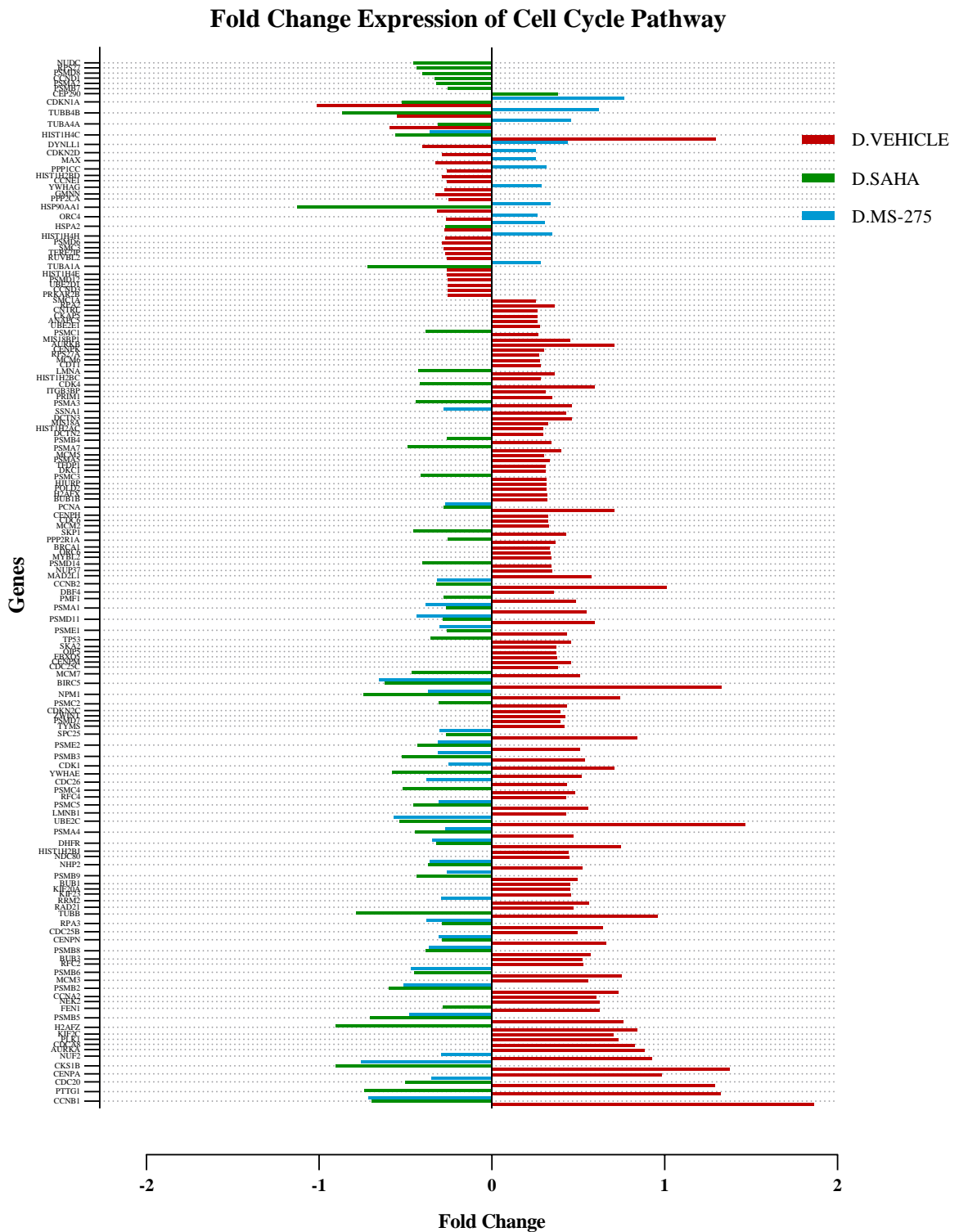


Figure 53: Fold change expression of the cell cycle regulating genes

The bar chart displays the fold change expression of 148 genes that showed high enrichment score in cell cycle pathway of the GSEA analysis. The red bars are the D.Vehicle, the green are the D.SAHA, and the blue are the MS-275.

4.2.6.6 The expression of the Apoptosis Genes

The GSEA analysis identified several subsets of genes that were identified as regulators for apoptosis in each condition. With the untreated Daoy cells, two subsets of genes were associated with the positive and the negative phenotypes with 7 genes were shared between the two phenotypes (HMGB2, BID, TNFSF10, LMNA, PMAIP1, DFFA, and H1F0) (Figure 54 and Figure 55). Across the three conditions, D.SAHA and D.MS-275 showed differential expression of 33 and 20 genes respectively, with 17 shared genes (Figure 56)

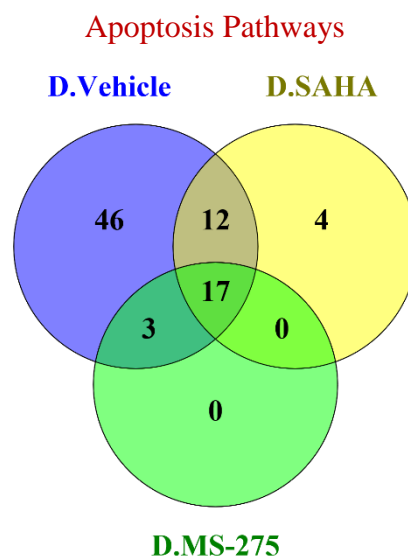


Figure 54: Illustration of the DGE with high enrichment scores in cell apoptosis signalling pathway

The genes that showed high ES in the apoptosis pathway were compared in order to identify the shared genes between the HDACis treated and untreated cells.

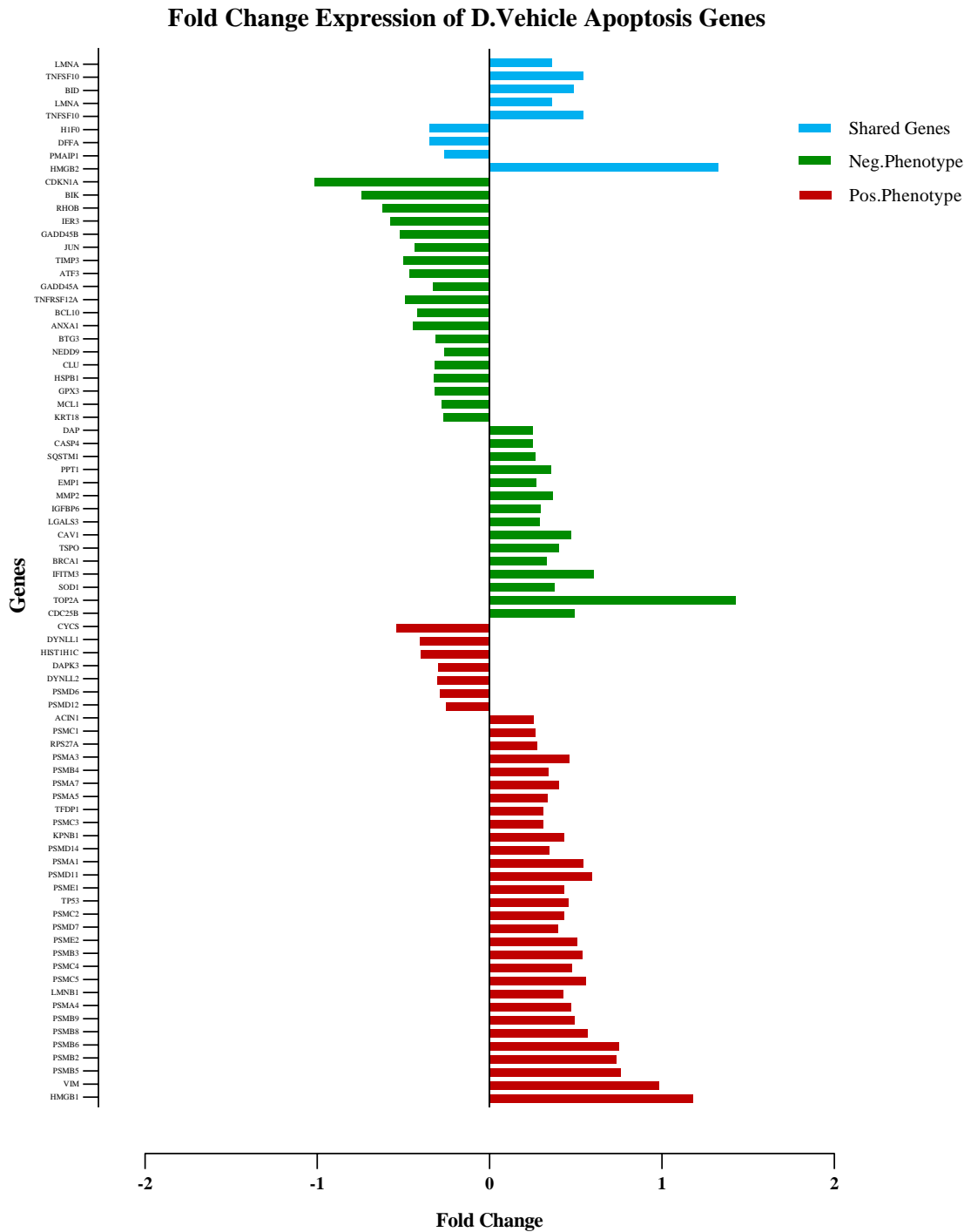


Figure 55: Fold change expression of the D.Vehicle positive and negative phenotype apoptotic genes

The bar chart displays the fold change expression of 80 genes that showed high enrichment score in the positive and negative phenotype of the apoptosis regulation. The blue bars present the shared genes between the positive and negative phenotypes, the green bars represent the negative phenotype and the red bars show the positive phenotype.

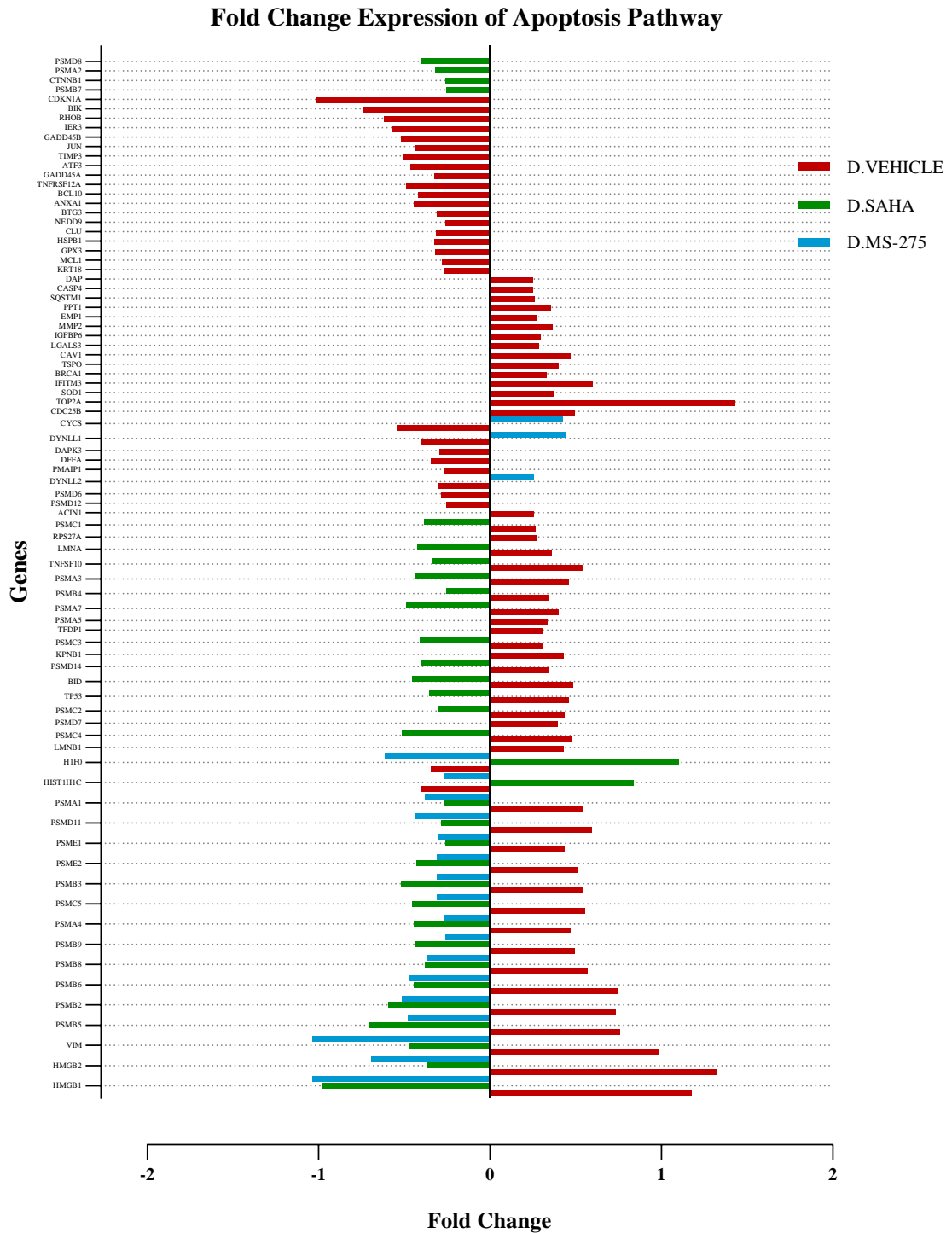


Figure 56: Fold change expression of the apoptotic genes

The bar chart displays the fold change expression of 82 genes that showed high enrichment score in apoptosis regulation of the GSEA analysis. The red bars are the D.Vehicle, the green are the D.SAHA, and the blue are the MS-275.

4.2.7 Normal Human Neurons scNGS Data Analysis

As the cell-type is possibly the main element of the transcriptional heterogeneity between the neurons, the analysis was established by identifying the cells identity of each cluster using the Cell-type Specific Expression Analysis (CSEA) server ¹²⁹. The analysis was carried out using the maker genes that characterized each cluster and the identity of the cells was assigned based on the significance of the *P*-value (Appendix 11).

The analysis predicted the identity of the neurons as cortex, striatum, and amygdala neurons (Figure 57). The t-SNE plot displayed the cortex neurons as two distinct clusters (hereinafter referred to as Cortex.1 and Cortex.2) with more than 150 cells in each cluster. Similarly, the striatum neurons formed two distinct clusters, the first (hereinafter referred to as Striatum.1) has more cells and was captured in the three conditions were the neurons of the second Striatum cluster were not among the N.SAHA neurons. Due to the predominance of Cortex.1, Cortex.2 and Striatum.1 across the three conditions, the subsequent analysis was performed using these cells (Figure 57).

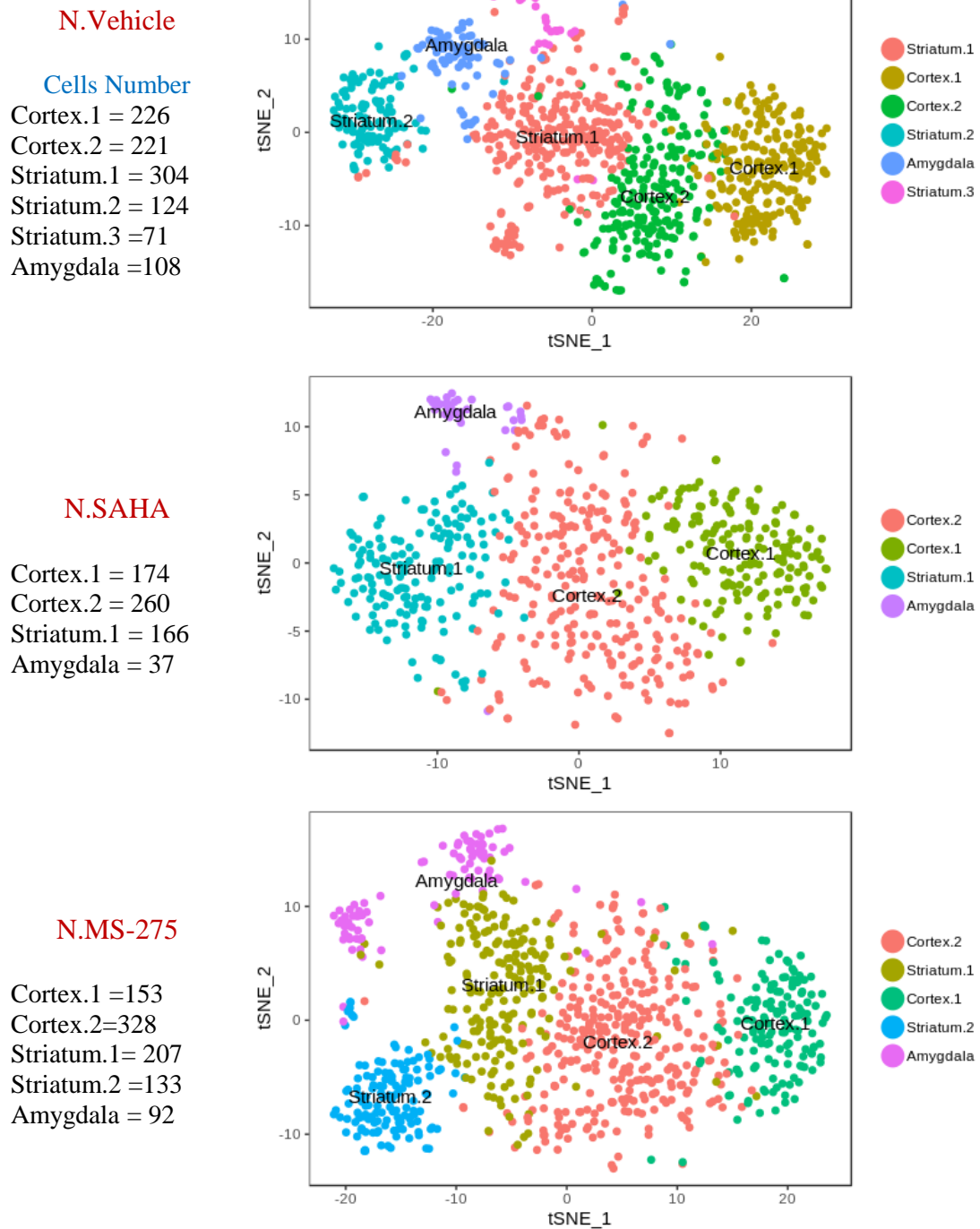


Figure 57: t-SNE plots of the untreated and treated neurons

The t-SNE plots display the dimensional reduction of the untreated; N.Vehicle (A) and treated neurons N.SAHA (B), and N.MS-275 (C). The dimensional scaling was performed using the quality improved data and the analysis was carried out using the Seurat R package. The cells identity of each cluster was characterized based on the expressed genes of each cluster using the CSEA server analysis.

4.2.7.1 Clustering the Neurons Based on their Type

In order to study the effect of SAHA and MS-275 on the normal neurons, the analysis was carried out by extracting the cluster data set of each cell type (i.e. Cortex.1, Cortex.2, and Striatum.1) and the clusters with the same identity (i.e. Cortex.1 of N.Vehicle, N.SAHA, and N.MS-275) were merged in a single Seurat object. The data were then normalized, dimensionally reduced, and displayed on t-SNE plots (Figure 58). In this analysis, the merge function was implemented as the Seurat (Combined) function, which combined the whole three conditions in one Seurat object, did not allowed comparing the expression across the clusters of the same identity and it only allowed comparing the differential expression across the three conditions as whole.

The t-SNE space plots of the merged clusters revealed a significant transcriptional heterogeneity across the conditions. For example, the clustering of SAHA was located in a close proximity to the N.Vehicle with some overlap between the cells. Whereas, the MS-275 clusters showed a considerable distance to the other two conditions in the three cell types (i.e. Cortex.1, Cortex.2, and Striatum.1) which may indicate the significant effect of MS-275 on the normal cell gene expression (Figure 58).

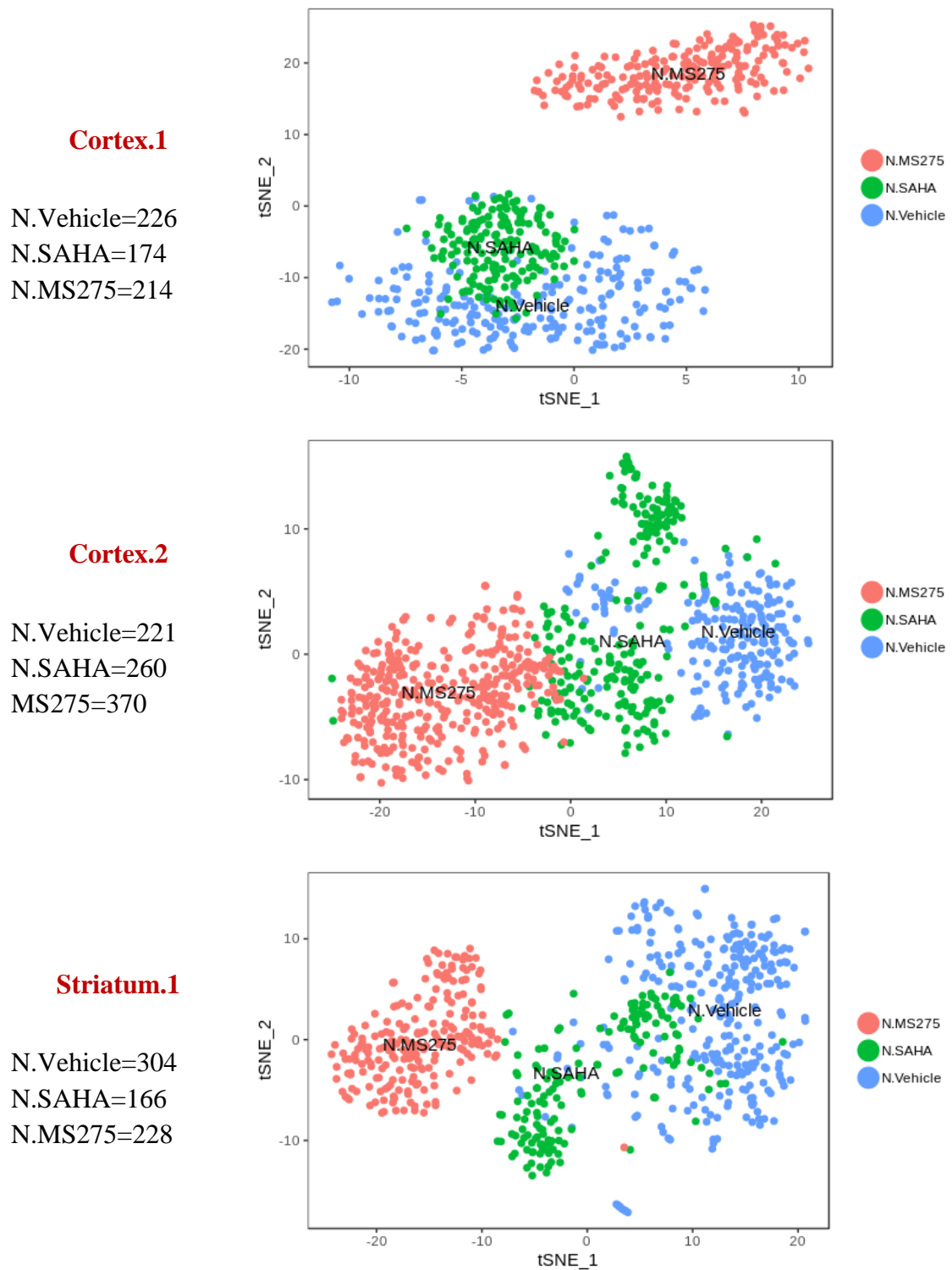


Figure 58: t-SNE plots of the merged Cortex.1, Cortex.2, and Striatum.1 data set

The data sets of Cortex.1, Cortex.2 and Striatum.1 of each condition were extracted and the clusters with the same cell identity across the three conditions were merged in one object using the Seurat R package. The numbers on the left are the cell count of each condition.

In order to show the transcriptional heterogeneity across the different cell types, the fold change expression of the above t-SNE clusters were presented on heatmap plot (Figure 59 A). The heatmap showed considerable differences between the three treatment conditions and across the different cell types. For instance, the expression patterns showed extensive difference between the untreated and treated neurons also, there was slight difference between the SAHA and MS-275 treated cells. Similarly, there was some differences between the different cell types in particular between the cortex and the striatum neurons (Figure 59 A).

Additionally, the major differences in the expression patterns across the three treatment conditions on the heatmap were classified into five sections (A, B, C, D, and E) and the genes in each section were functionally annotated. The annotation analysis showed the downregulation of several cellular regulations in the HDACis treated cells including the cell cycle, the translation, and the ATPase activity genes. In addition, the analysis showed downregulation of a subset of genes annotated as negative regulators for cell death (Figure 59 B).

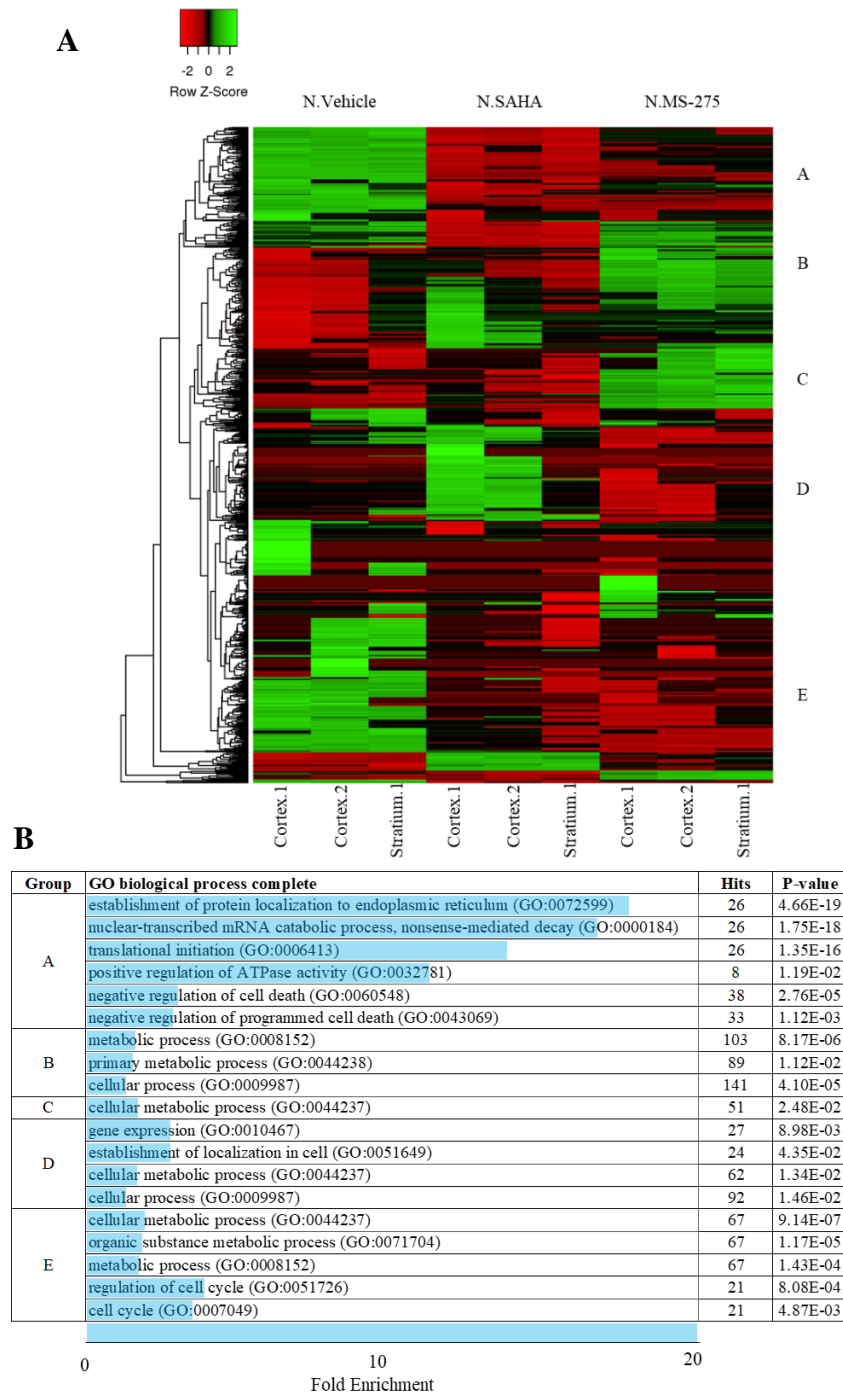


Figure 59 : The expression differences between the three neurons samples and across the different cell types

The expression of the highly variable genes (fold change ≥ 1) of each cell type and for each treatment condition was filtered out and the mean values were z-score to zero and scaled to 1 SD and presented on a heatmap plot (A). The genes that formed distinct differential expression patterns (A, B, C, D and E) across the clusters were subjected to functional annotation using GenClip annotation tool and the pathways that characterized each group

was presented in table (B). The blue bars are represent the fold enrichment score of each Go term.

4.2.7.2 Exploring the Effect of HDACis on the Normal Neurons

In order to investigate the effect of HDACis on normal cells, the genes of each cell cluster (Figure 58) were subjected to GSEA. The results of GSEA revealed several cellular regulations both in the untreated and treated neurons however, the majority of these pathways were statistically insignificant (Table 8). Several of these regulations showed an inverse phenotype between the untreated and treated neurons including Myc and cell cycle pathways (Figure 60). Noticeably, Myc pathway showed an inverse correlation between the cortex and the striatum neurons (the HDACis treated cortex neurons showed the positive phenotype whereas, the striatum neurons displayed the negative phenotype) (Figure 60). Also, the MTORC1 pathway was one of the pathways that showed gene set enrichment however, it did not show any significant enrichment in the N.SAHA Cortex.1 and Cortex.2, N.Vehicle Cortex.2, and N.MS-275 Striatum.1 (Table 8).

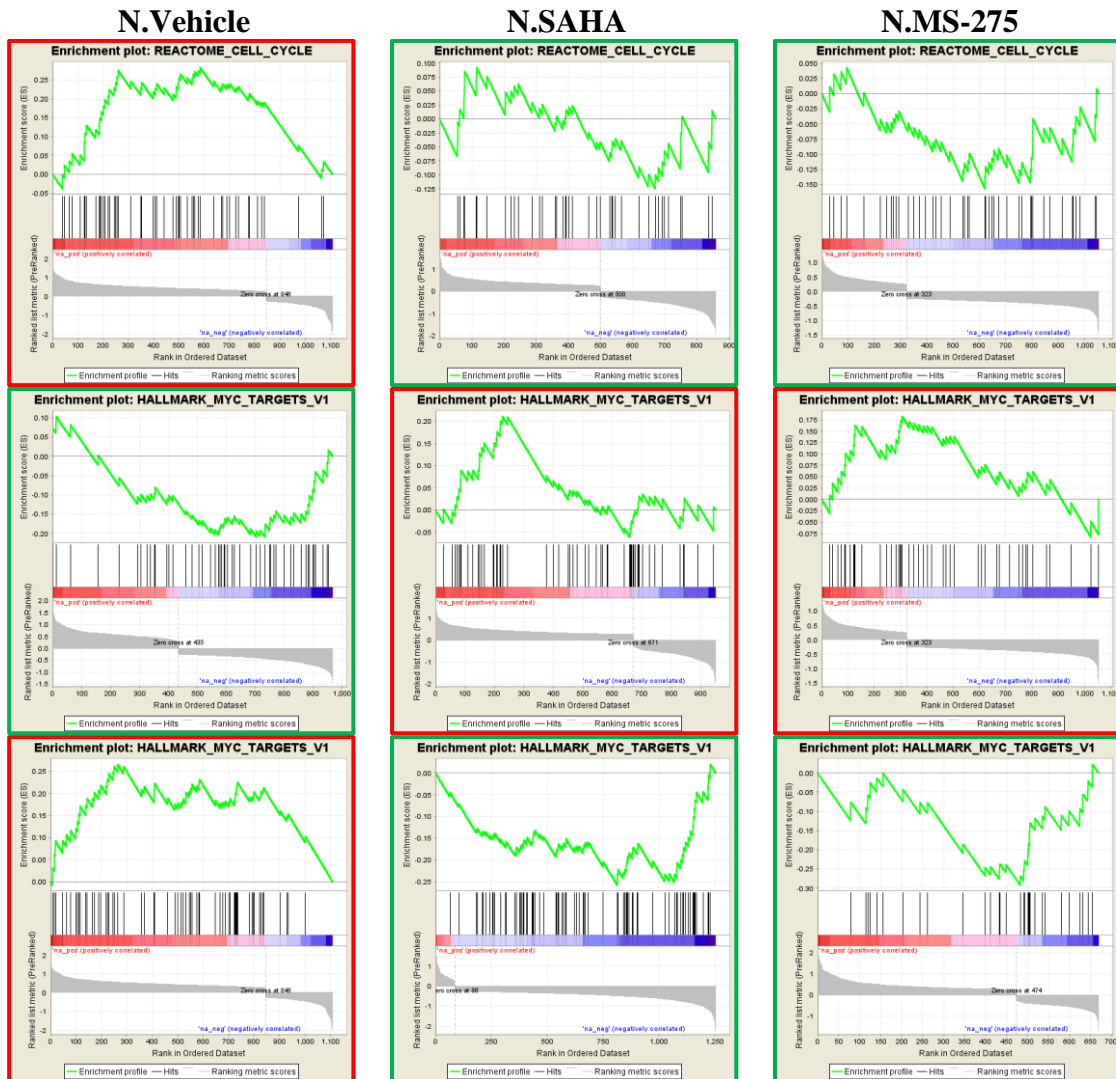


Figure 60: GSEA enrichment plots of the highly enriched gene sets of the neurons

The GSEA was carried out by ranking the upregulated and downregulated genes based on the decrease in their fold change, and the ES was calculated by walking down the ranked list. In the above charts, the horizontal middle line in red and blue colours is the rank ordered list of the upregulated and downregulated genes, respectively, and the decrease in the intensity of the bar colour represents the decrease in the fold change. The vertical black bars represent the gene hits, the vertical grey bars represent the ranking metric scores of the genes, the positive values indicate the correlation with the phenotype profile, the negative values indicate the inverse correlation, and the green fluctuating curve shows the enrichment score. The red framed-charts show the gene set enrichment at the top of the ranked list (Positive ES) and the green framed-charts display gene set enrichment at the bottom of the list (Negative ES).

Table 8: GSEA results for some of the highly enriched gene sets of the neurons

Name	Size ¹	ES ²	NES ³	NOM p-val ⁴	FDR q-val ⁵
N.Vehicle Cortex.1					
REACTOME_DEVELOPMENTAL_BIOLOGY	30	0.381	1.745	0.015	0.061
HALLMARK_MTORC1_SIGNALING	30	0.216	0.978	0.485	1
REACTOME_CELL_CYCLE_MITOTIC	33	0.083	0.390	0.997	0.998
REACTOME_METABOLISM_OF_RNA	105	-0.663	-4.965	0.000	0
REACTOME_METABOLISM_OF_PROTEINS	114	-0.655	-4.957	0.000	0
HALLMARK_MYC_TARGETS_V1	51	-0.209	-1.292	0.124	0.145
REACTOME_CELL_CYCLE	38	-0.108	-0.609	0.944	0.951
N.SAHA Cortex.1					
REACTOME_TRANSLATION	71	0.486	3.083	0.000	0
REACTOME_METABOLISM_OF_PROTEINS	98	0.403	2.672	0.000	0
REACTOME_CELL_CYCLE	47	0.249	1.436	0.052	0.351
HALLMARK_MYC_TARGETS_V1	56	0.211	1.243	0.171	0.724
N.MS-275 Cortex.1					
REACTOME_TRANSLATION	54	0.556	3.521	0.000	0
REACTOME_METABOLISM_OF_PROTEINS	78	0.458	3.255	0.000	0
REACTOME_METABOLISM_OF_MRNA	60	0.447	2.888	0.000	0
HALLMARK_MYC_TARGETS_V1	48	0.182	1.095	0.357	0.365
HALLMARK_MTORC1_SIGNALING	35	-0.234	-1.244	0.199	1.000
REACTOME_CELL_CYCLE	46	-0.156	-0.911	0.599	1.00
HALLMARK_E2F_TARGETS	32	-0.107	-0.556	0.951	1.000
N.Vehicle Cortex.2					
HALLMARK_MYC_TARGETS_V1	43	0.123	0.625	0.912	1.000
REACTOME_METABOLISM_OF_RNA	94	-0.703	-5.127	0.000	0.000
REACTOME_TRANSLATION	88	-0.728	-5.123	0.000	0.000
N.SAHA Cortex.2					
REACTOME_METABOLISM_OF_RNA	59	0.097	0.599	0.960	0.947
REACTOME_METABOLISM_OF_PROTEINS	74	-0.177	-0.965	0.520	0.890
REACTOME_METABOLISM_OF_MRNA	54	-0.132	-0.669	0.875	1.000
HALLMARK_MYC_TARGETS_V1	46	-0.126	-0.610	0.925	0.995
REACTOME_CELL_CYCLE	44	-0.124	-0.605	0.939	0.928
N.MS-275 Cortex.2					
REACTOME_TRANSLATION	77	0.585	3.753	0.000	0.000
REACTOME_ACTIVATION_OF_THE_MRNA	31	0.590	2.846	0.000	0.000

HALLMARK_MTORC1_SIGNALING	36	-0.218	-1.187	0.250	0.872
REACTOME_CELL_CYCLE	32	-0.219	-1.134	0.307	0.921
HALLMARK_MYC_TARGETS_V1	44	-0.105	-0.602	0.942	1.000
N.Vehicle Striatum.1					
REACTOME_CELL_CYCLE	55	0.282	1.477	0.070	0.150
HALLMARK_MYC_TARGETS_V1	66	0.266	1.471	0.063	0.135
HALLMARK_E2F_TARGETS	37	0.245	1.158	0.282	0.415
HALLMARK_MTORC1_SIGNALING	36	-0.209	-1.249	0.158	0.299
REACTOME_METABOLISM_OF_PROTEINS	50	-0.144	-0.908	0.614	0.602
N.SAHA Striatum.1					
REACTOME_CELL_CYCLE	51	-0.331	-1.464	0.058	0.046
HALLMARK_MYC_TARGETS_V1	81	-0.257	-1.228	0.185	0.508
HALLMARK_MTORC1_SIGNALING	30	-0.165	-0.655	0.872	0.885
N.MS-275 Striatum.1					
REACTOME_TRANSLATION	54	0.337	1.659	0.019	0.029
REACTOME_METABOLISM_OF_PROTEINS	64	0.311	1.589	0.024	0.038
HALLMARK_MYC_TARGETS_V1	31	-0.292	-1.510	0.066	0.044

The light red shaded rows show the positive phenotype and the light green display the negative phenotype. The statistically insignificant pathways are in dark red font colour.

¹ The number of the detected genes.

² Enrichment Scores.

³ Normalized Enrichment Score (used to compare analysis results across gene sets).

⁴ Nominal P-value (statistical significance of the enrichment score).

⁵ False discovery rate (the probability that the NES represents a false positive finding).

4.2.7.2.1 The Effect of HDACis on Myc Signalling Pathways

Further, the gene differential expression of Myc signalling pathway of each cell type was used in order to compare the variation in the response to HDACis between the cells. The expression results showed the upregulation of most genes in the untreated striatum and the downregulation of the majority of genes in the treated cells (Figure 61). In contrast, the expression of the Myc genes in the untreated cells showed a combination of upregulation and downregulation with more than 70% of the genes were downregulated in Cortex.1. Yet, the cortex neurons treating with HDACis showed upregulation of Myc pathway-genes (Figure 61). It should be noted that the ES of Myc pathway was statistically insignificant.

Fold Change Expression of Myc Pathway

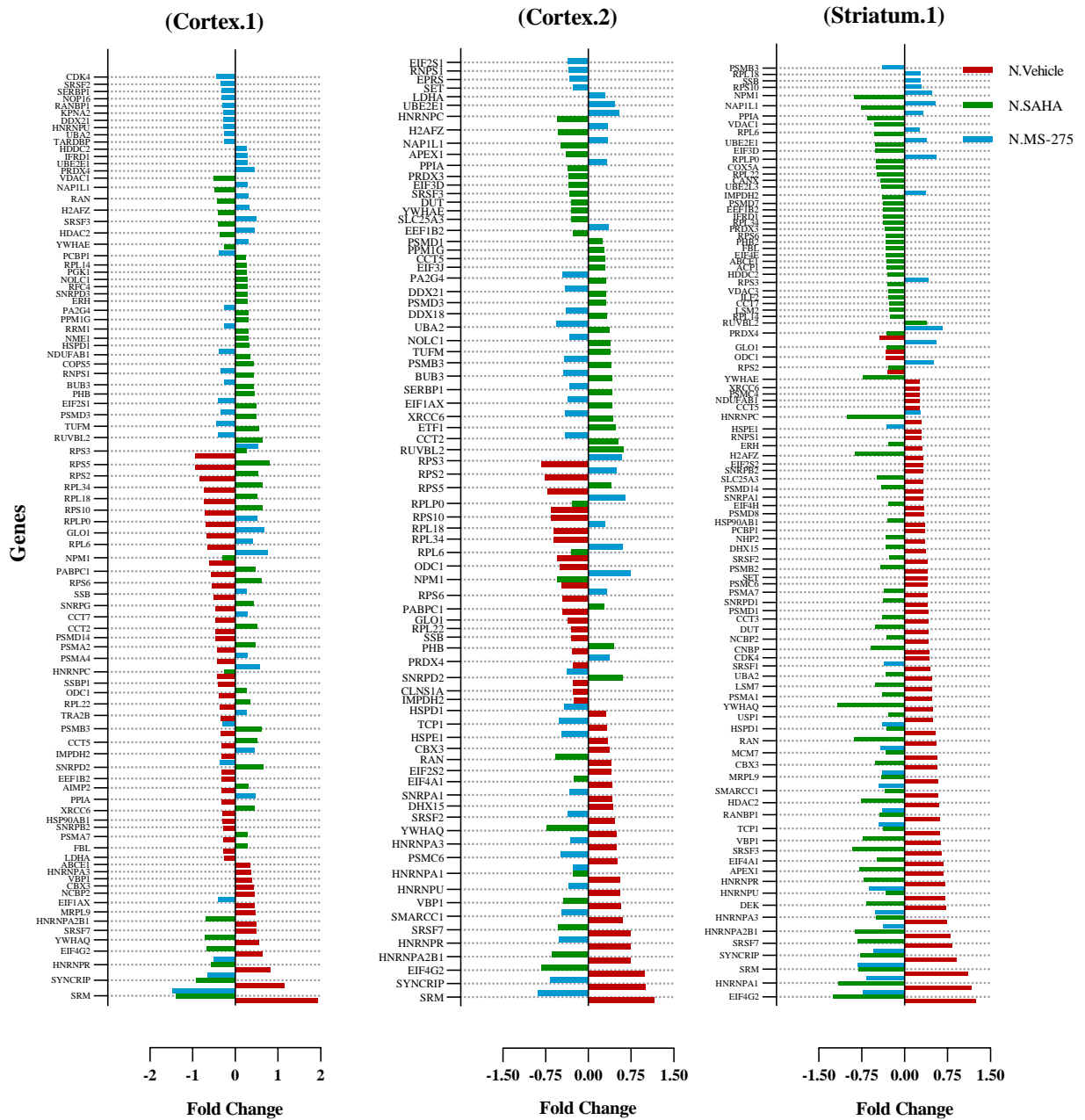


Figure 61: Fold change expression of Myc Pathway across the different neuron cells

The charts display the fold change expression of Myc pathway in Cortex.1, Cortex.2, and Striatum.1. The red bars are the N.Vehicle, the green are the N.SAHA, and the blue are the N.MS-275.

4.2.7.2.2 The Effect of HDACis on Cell Cycle Pathway

The GSEA results of the cell cycle pathway were insignificant both the untreated and treated neurons. The N.Vehicle (Cortex.1) and N.MS-275 (Striatum.1) also did not show any gene set enrichment for cell cycle genes. In order to explore the effect of the SAHA and MS-275 on the neurons, the expression of the genes that were identified as component of the cell cycle pathway was presented on charts. The general theme across the different types of the neurons is the inverse expression in the HDACis treated to the untreated neurons (Figure 62). The annotation analysis of these genes showed several GO terms that were associated with cell cycle, nuclear division, and regulation of transcription. The genes that were annotated as a cell cycle arrest were further compared across the different conditions however, the expression of these genes was not detected in the majority of the cells (Table 9). The expression of few genes was more informative such as NPM1 which showed upregulation in MS-275-treated neurons and the expression of CCND2 which showed downregulation in most HDACis treated neurons. It should be noted that the ES of Myc pathway was statistically insignificant.

Table 9: The DGE of the genes that were annotated as cell cycle arrest

Genes	Cortex.1			Cortex.2			Striatum.1		
	N.Vehicle	N.SAHA	N.MS-275	N.Vehicle	N.SAHA	N.MS-275	N.Vehicle	N.SAHA	N.MS-275
CDKN1A	0	0	0	0	0	0.421	-0.731	0	1.087
CDKN2A	0	0	0	0	0	0	-0.404	0	0.524
NPM1	-0.607	-0.304	0.758	-0.464	-0.546	0.736	0	-0.885	0.477
RAD9A	0	0.467	0	0	0.629	0	0	0.915	0
CDKN1B	0	0	0	0	0	0	0.501	0	0
CDK4	0	0	-0.444	0	0	0	0.432	0	0
PSMC6	0	0	0	0.509	0	-0.486	0.406	0	0
RAD1	0	0	0	0	0.513	0	0	0	0
CDKN2D	0	0	-0.261	0	0.307	0	0	0	0
GMNN	-0.495	0.583	0	0	0.289	0	0	0	0
RFC4	0	0.273	0	0	0	0	0	0	0
CCNH	-0.267	0	0	0	0	0	0	0	0
HDAC1	-0.325	0	0	0	0	0	0	0	0
CCND3	0	0	-0.265	0	0	0	0	0	0
SKP1	0	0	0	0	0	-0.298	0	0	0
HSP90AA1	-0.346	0.601	-0.274	0	0.575	-0.400	0	0	0
BUB3	0	0.437	-0.257	0	0.415	-0.445	0	0	0
RPA2	0	0	0	0	0	0	0.359	-0.262	0
CEP57	0.483	0	-0.515	0.495	0	-0.457	0.478	-0.359	0
PTTG1	0	0.341	0	0	0	0	0.500	-0.361	0
RAD21	0	0	-0.313	0.536	0	0	0.569	-0.508	0
PPP2CA	0	0	0	0	0	0	0.460	-0.578	0
CCND2	0.740	-0.630	-0.337	0.844	-0.497	0	0.806	-0.850	0
MAX	0	0.315	-0.406	0	0	0	0.306	0	-0.342
MCM7	0	0	0	0	0	0	0.563	-0.336	-0.416
TERF1	0	0.391	-0.433	0	0.320	-0.586	0.374	0	-0.503

Fold Change Expression of Cell Cycle Pathway

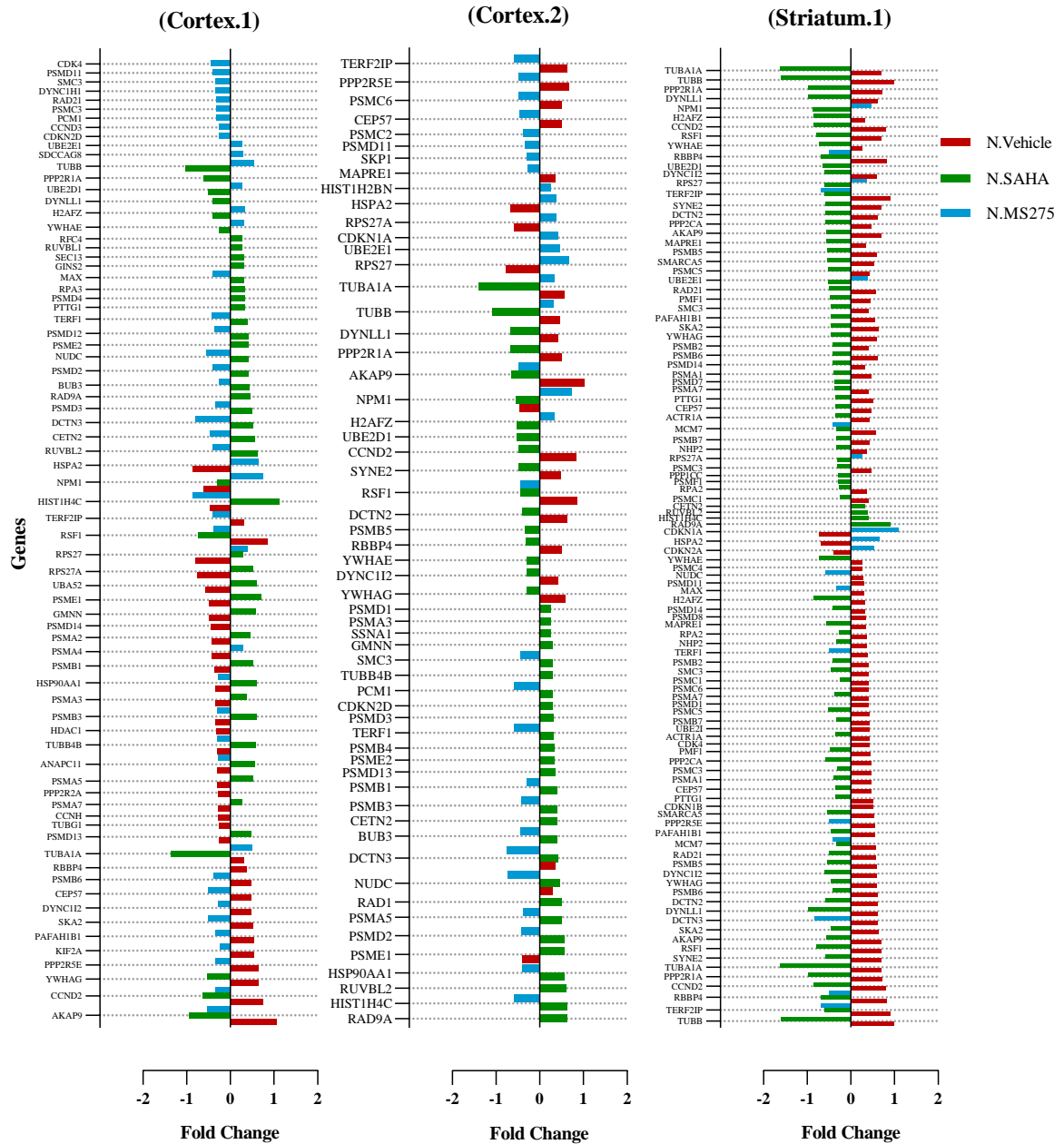


Figure 62: Fold change expression of the cell cycle component genes across the different neuron cells

The charts display the fold change expression of the genes that were identified as components for cell cycle pathway in Cortex.1, Cortex.2, and Striatum.1. The red bars are the N.Vehicle, the green are the N.SAHA, and the blue are the N.MS-275.

4.2.8 The Expression of HDAC and HAT Genes

In cancer, aberrant expression of acetylation and deacetylation regulating genes has been frequently observed in a broad range of tumours and they contribute to the overall concept of cancer epigenetic therapy ⁶. However, it is not known whether the changes in the acetylation condition are due to the alterations in HDACs and HATs genes expression. In this study, the expression of HDACs and HATs in the untreated and treated Daoy cells and neurons was extracted from the scNGS data in order to explore their expression in tumour and normal cells.

The results revealed the elevated expression of HDAC1 and HDAC2 in D.Vehicle, D.SAHA, and D.MS275. Also, SAHA-treated cells showed a statistically significant ($P>0.0001$) increase in HDAC3 by 0.3-fold change compared to the D.Vehicle and D.MS-275. The results also showed an increase in the SIRT7 in SAHA- and MS-265-treated cells (Figure 63).

The neurons result of the HDACs and HATs expression showed an upregulation in HDAC2 in the untreated and treated neurons and it reached to 0.4-fold change ($P>0.0001$) higher in the MS-275-treated Cortex.1. The results showed a significant ($P>0.05$) decrease in the ATAT1 expression level in the MS-275-treated Cortex.2 and Striatum.1 neurons by 0.3- and 0.7-fold change, respectively (Figure 65 and Figure 66). The results also showed a slight increase in HDAC and HAT enzymes in small subsets of cells however, the expression was statistically insignificant due to the small size of these populations when compared to the overall population of a sample (

, Figure 64, Figure 65, Figure 66).

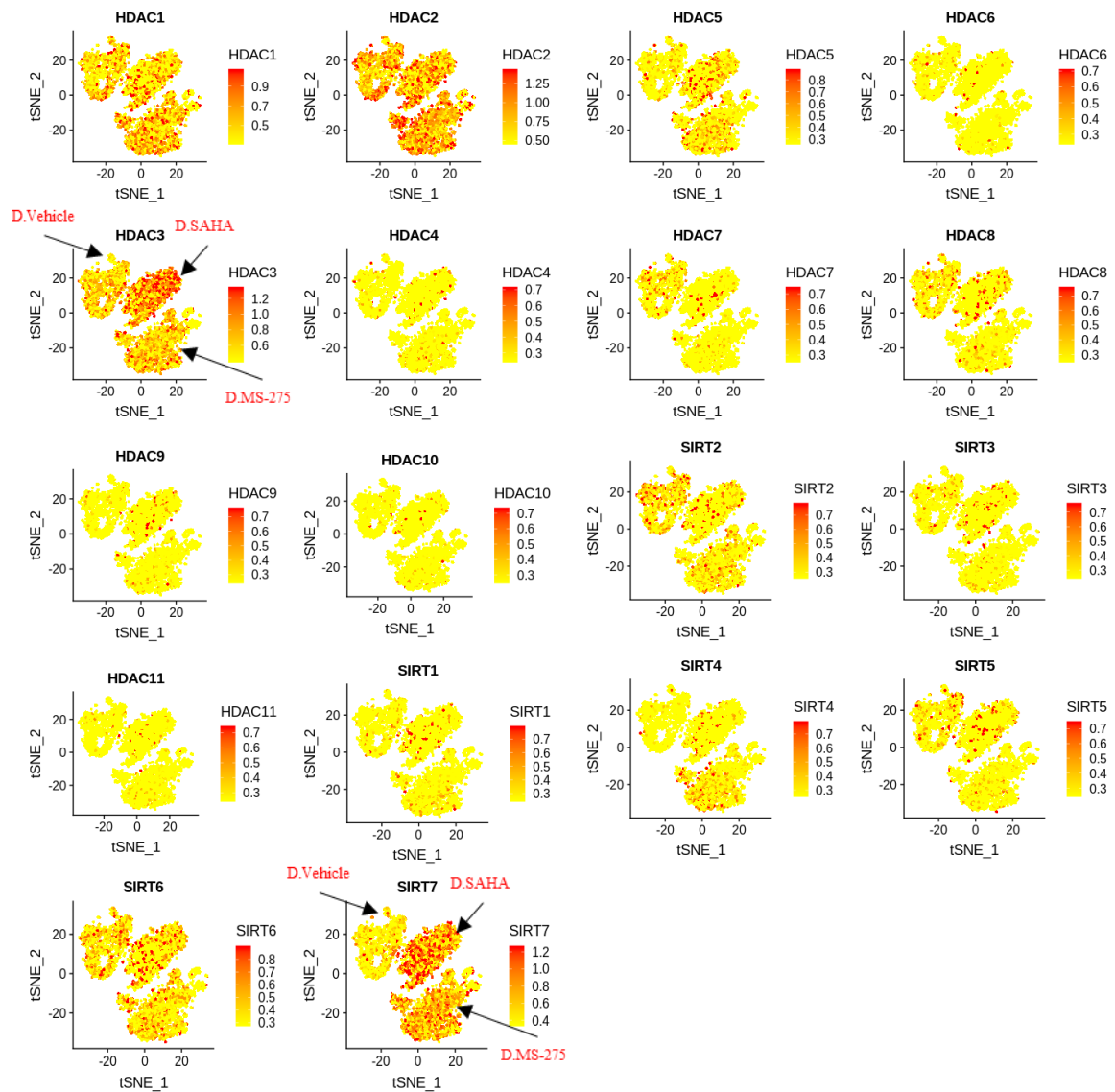


Figure 63: t-SNE plots of the HDAC genes in the Daoy untreated and treated cells

The t-SNE plots show the average fold change expression of HDAC genes in the Daoy untreated and treated cells. Each dot represents a cell and the level of the expression is represented by a gradient increase in colour from yellow to red as it appears in the legend of each plot. The plots were produced by the Seurat R package and each plot has a different expression scale (the package is less flexible). The clusters identity is presented in the HDAC2 and SIRT7 plots.

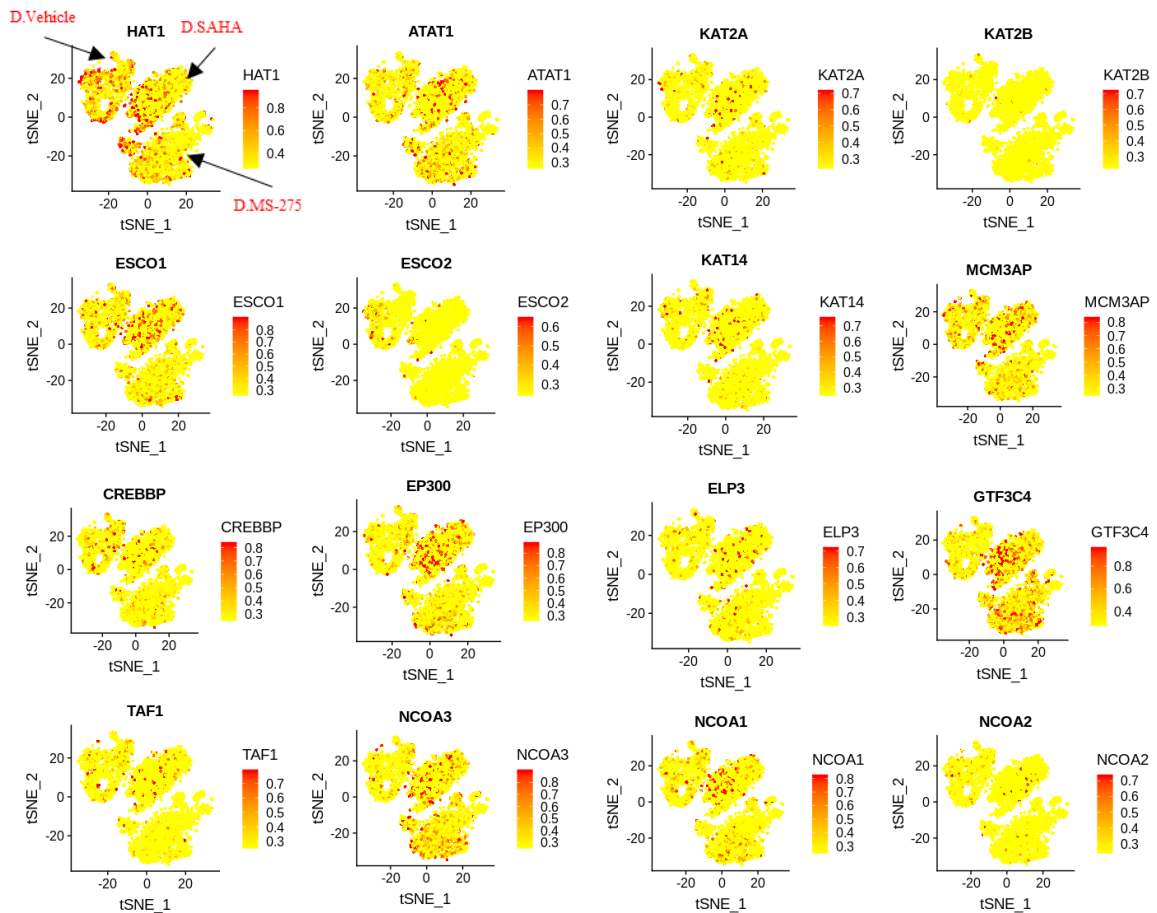


Figure 64: t-SNE plots of HATs genes in the Daoy untreated and treated cells

The t-SNE plots show the fold differential expression of HATs genes in the Daoy untreated and treated cells. Each dot represents a cell and the level of the expression is represented by a gradient increase in colour from yellow to red as it appears in the legend of each plot. The plots were produced by the Seurat R package and each plot has a different expression scale (the package is less flexible). The clusters identity is presented in the HAT1 plot.

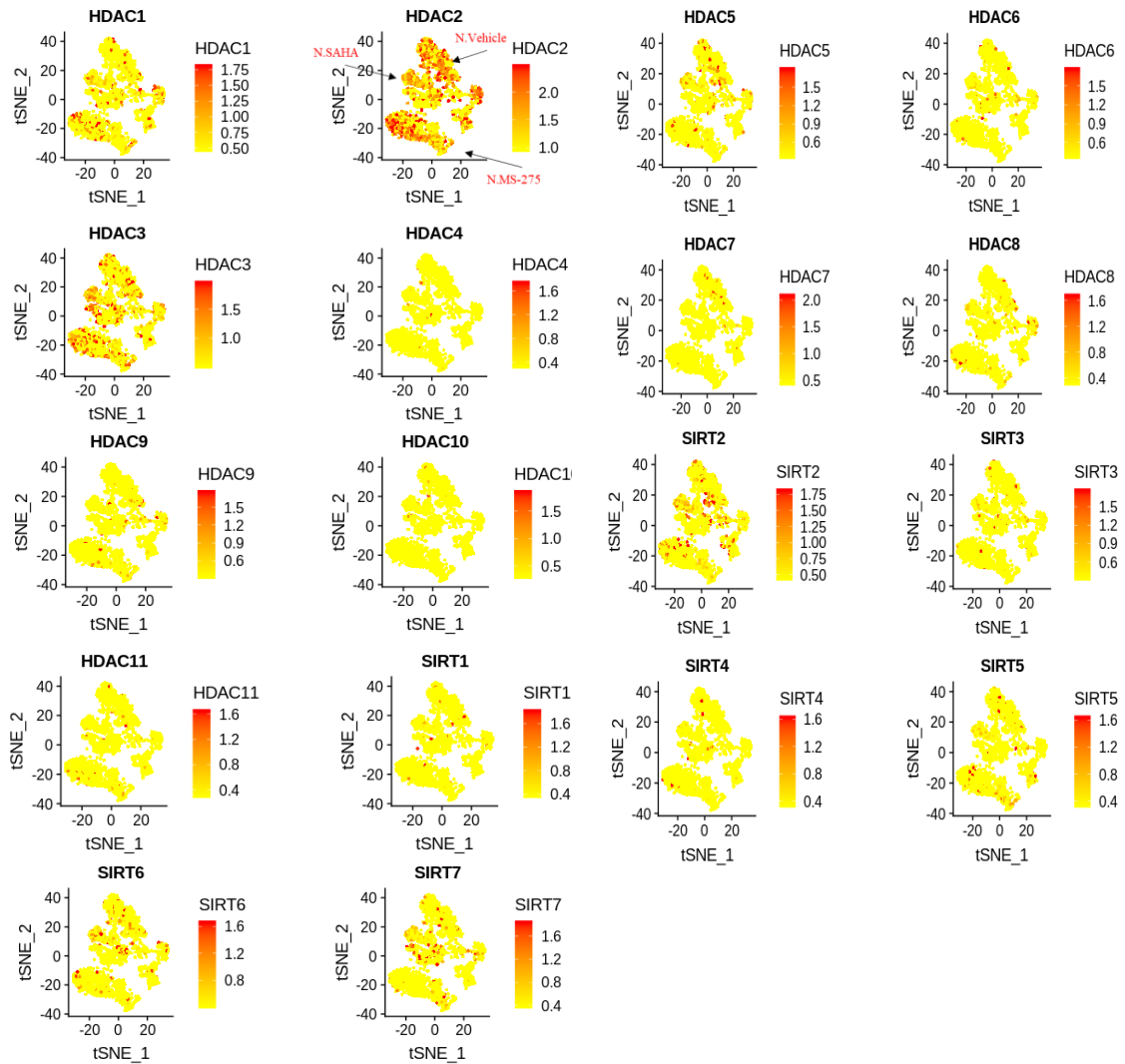


Figure 65: t-SNE plots of HDAC genes in the untreated and treated human neurons

The t-SNE plots show the fold differential expression of HDAC genes in the untreated and treated neurons. Each dot represents a cell and the level of the expression is represented by a gradient increase in colour from yellow to red as it appears in the legend of each plot. The plots were produced by the Seurat R package and each plot has a different expression scale (the package is less flexible). The clusters identity is presented in the HDCA2 plot.

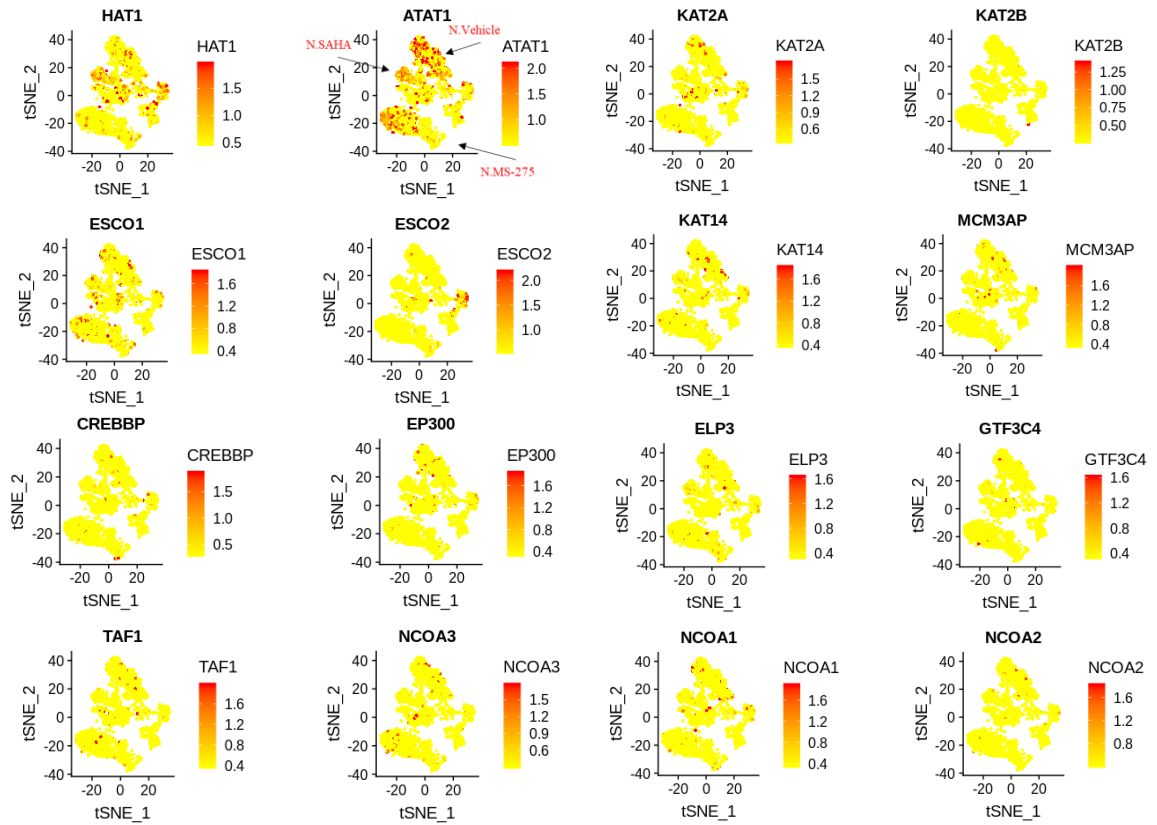


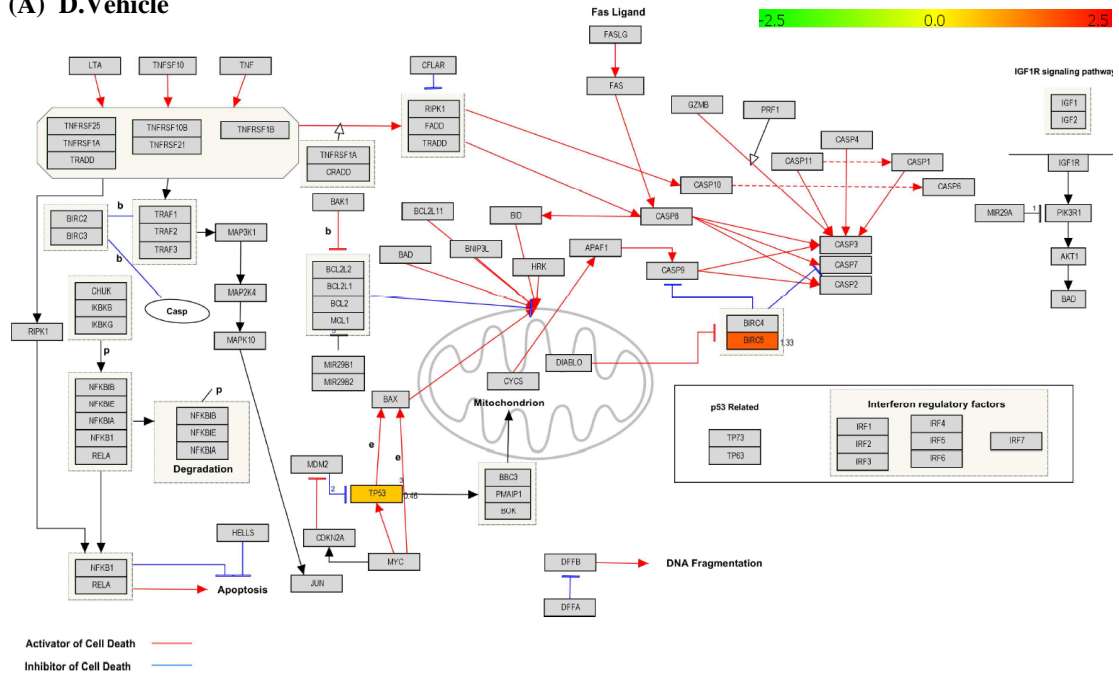
Figure 66: t-SNE plots of HATs genes in the untreated and treated neurons

The t-SNE plots show the fold differential expression of HATs genes in the untreated and treated neurons. Each dot represents a cell and the level of the expression is represented by a gradient increase in colour from yellow to red as it appears in the legend of each plot. The plots were produced by the Seurat R package and each plot has a different expression scale (the package is less flexible). The clusters identity is presented in the ATAT1 plot.

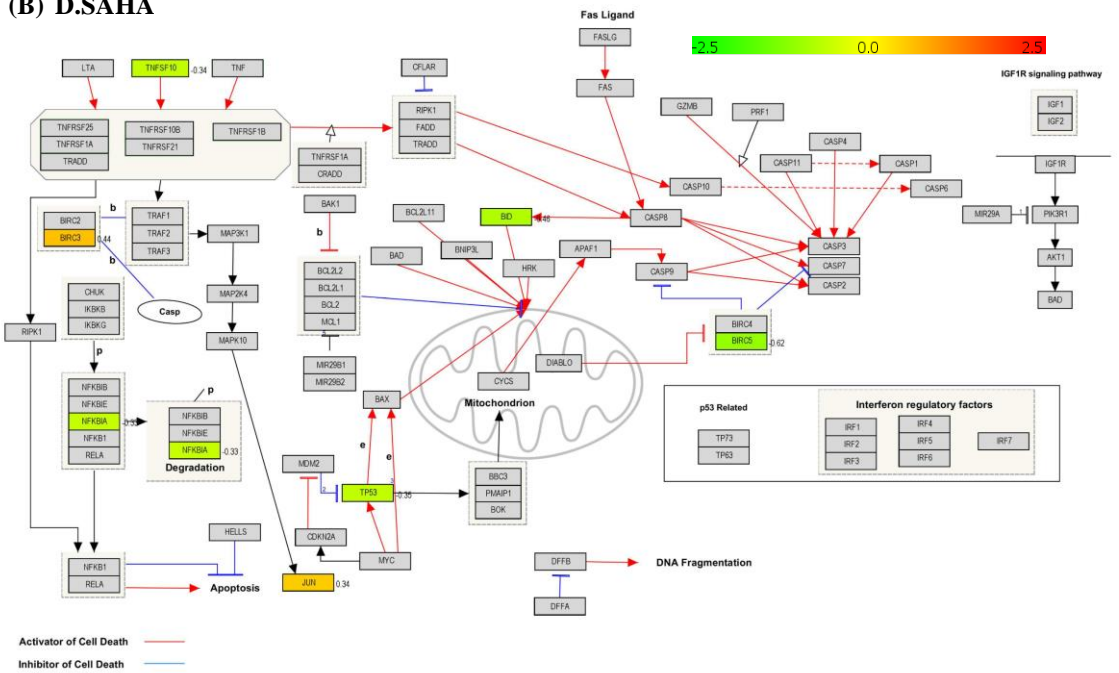
4.2.9 Pathway Analysis of the Untreated and Treated Samples

Further, the gene expression values of the differentially expressed genes of each sample were uploaded into the PathVisio pathway visualization software. The pathway analysis identified several pathways with high representation including TNF α and apoptosis pathways. The pathway analysis did not show high representation of the differentially expressed genes in all the examined pathways and limited number of the genes were represented in the pathways. For example, D.SAHA showed downregulation of genes that regulate apoptosis such as BID, BRIC5, TNFSF10 and TB53. With the D.MS-275 BIRCS and CYCS were only represented in the apoptosis pathway in addition to interferon IRF3 and IRF7. The N.SAHA showed two genes BNP3L and DFFA where the N.MS-25 presented JUN only (Figure 67).

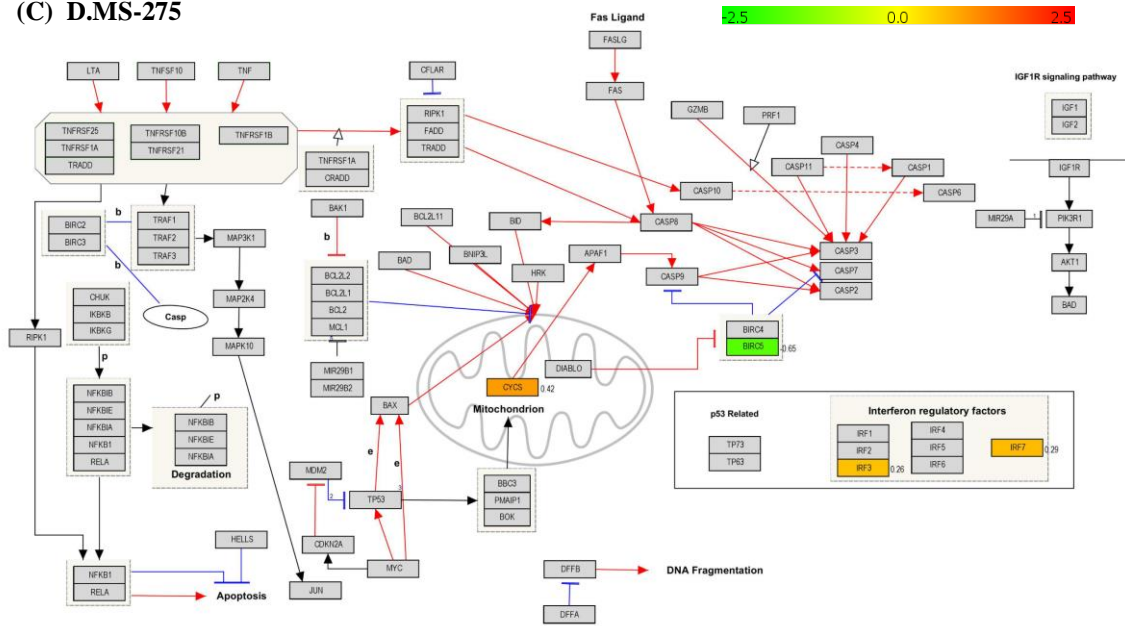
(A) D.Vehicle



(B) D.SAHA

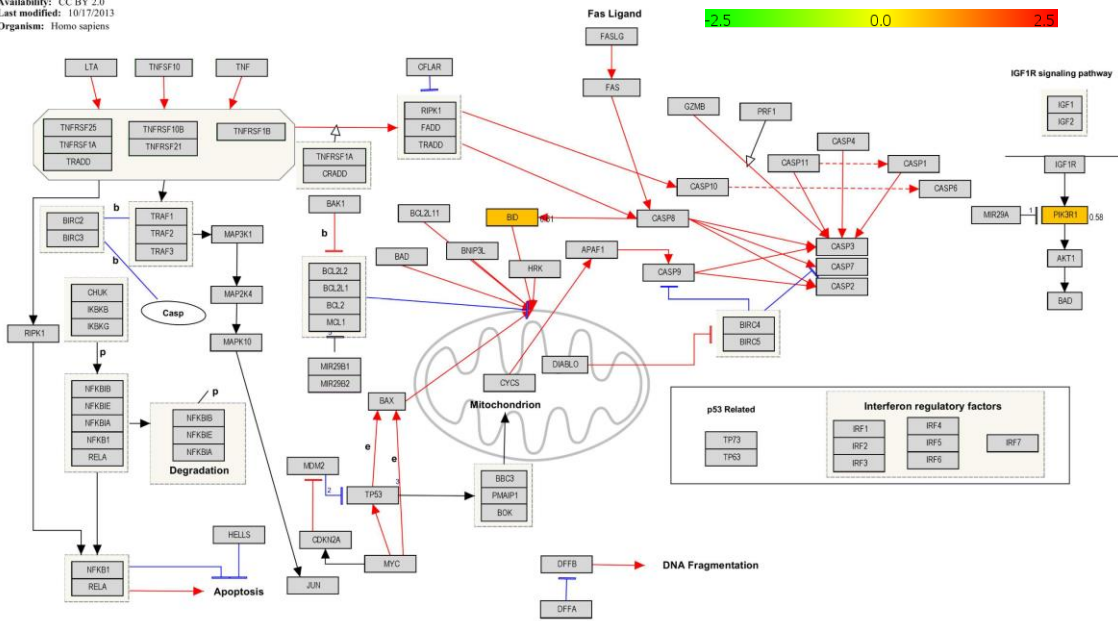


(C) D.MS-275



(D) N.Vehicle

Title: Apoptosis
 Availability: CC BY 2.0
 Last modified: 10/17/2013
 Organism: Homo sapiens



Activator of Cell Death — red line
 Inhibitor of Cell Death — blue line

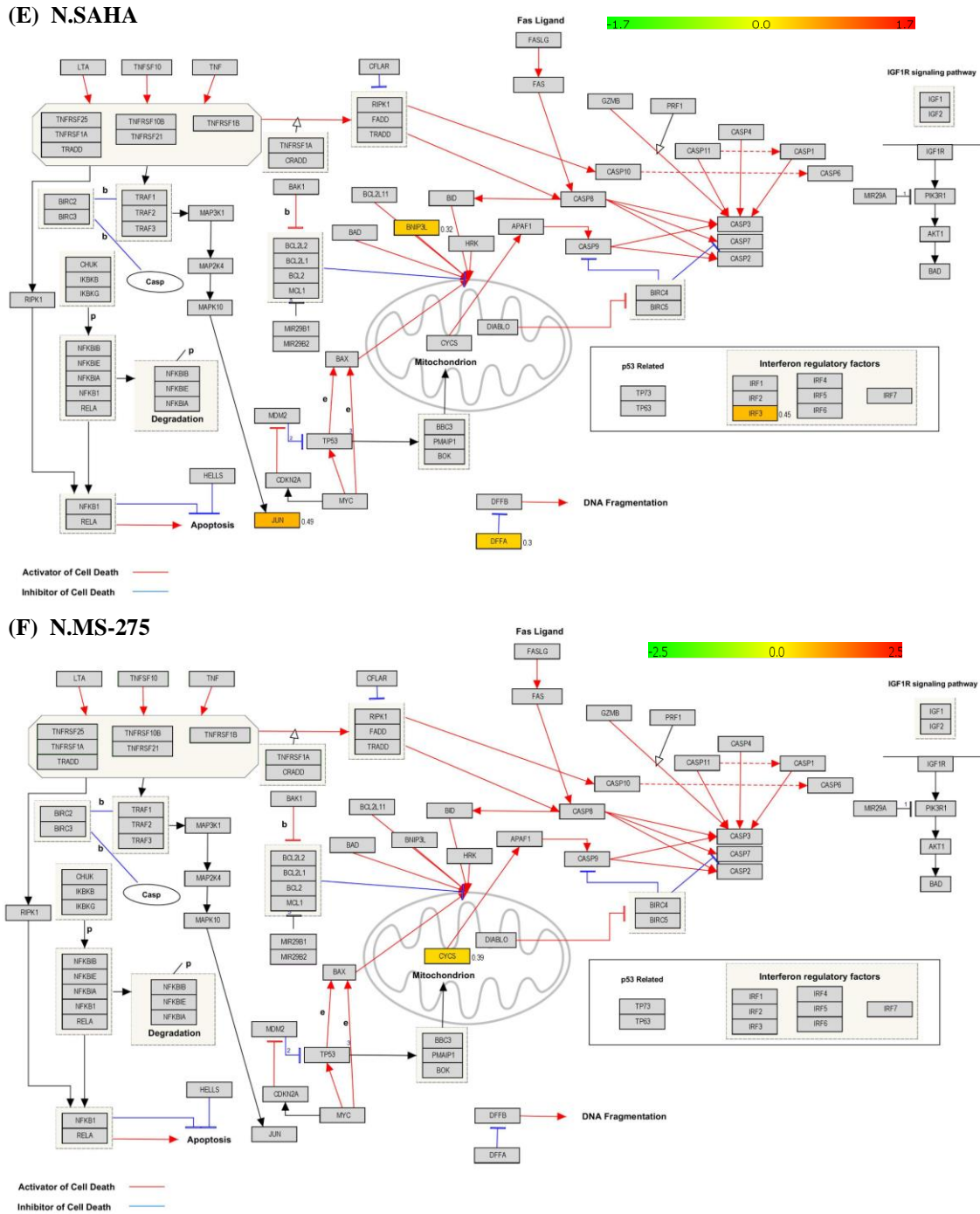


Figure 67: Pathway analysis of the differentially expressed genes

The differentially expressed genes of each sample were visualised using the PathVisio software and the analysis was performed by including the genes ID and expression values of all the genes. (A) D.Vehicle, (B) D.SAHA, (C) D.MS-275, (D) N.Vehicle, (E) N.SAHA, (F) N.MS-275. The expression level of a gene is represented by the change in the colour from green to red and the expression value is shown next to the box. The gradient bar represent the expression values, green as downregulated and red as upregulated.

4.3 Discussion

HDAC enzymes are a group of epigenetic molecular switches that regulate genes expression, cellular proliferation, survival and apoptosis. Thus, they have been attractive targets for cancer therapy. The aim of targeting HDACs is to reverse the effect of the epigenetic abnormalities that support the cancer cell proliferation. In contrast, the HDAC inhibitors are a group of molecular compounds that block the HDAC binding site and they have attracted a substantial *in vitro* and *in vivo* research interest. The results of the *in vitro* analysis have revealed the potency of certain HDACis in inducing anticancer effect through several downstream mechanisms including cell-cycle arrest, blocking angiogenesis, inhibition of metastasis, inducing autophagy, and stimulate apoptosis^{73, 220}. Whereas, the findings of the *in vivo* analysis exhibited the high selectivity of HDACis to target tumour cells with minimal effect on normal cells⁶⁰.

However, even though several studies have proposed some possible HDACis anticancer mechanisms, there have been several research questions remained unexplored. Accordingly, in this study, I set out to obtain a more in-depth knowledge of HDAC-dependent cancer regulation in tumour and normal cells using large-scale droplet-based single-cell transcriptome profiling. This approach was used to explore the transcriptome variability between cells and to avoid the effect of the transcriptome heterogeneity between the cells. Unravelling tumour heterogeneity may help in; unveiling the molecular regulation that sustains cancer cell progression, the molecular action of anticancer drugs, and identifying the subclone resistance to therapy. In this study, I tried to; identify the molecular regulation of HDACs in sustaining the medulloblastoma cell growth, investigate the molecular mechanisms of how HDACis initiate the cell death mechanism, and explore the effect of the HDACis on the molecular regulations of normal cells.

In order to address these questions, I profiled the gene expression of the Daoy medulloblastoma cells and non-cancerous human neurons pre- and post-treating them with SAHA (a pan-Inhibitor) and MS-275 selective inhibitor (HDAC1 and to lesser extent, HDAC2 and HDAC3). As the scNGS gene expression data often contain technical and biological noises, I subjected the data to stringent quality improvement measures and I used the quality improved data in the analysis. I studied the most dominating pathways

using the gene set enrichment analyses, and I used the differential expression analysis to explore the differences in the molecular regulations between the cells.

The evidence of this study may suggest the ability of HDACis to disturb the cancer regulation through disrupting the pathways that support the cell cycle such as Myc and TNF α via NF κ B pathways. The results showed the considerable effect of HDACis on gene transcription of the normal cells in particular on genes that drive the cellular differentiation. The following sections, will discuss the findings of the study, compare them to what it has been known and draw a conclusion based on the evidences.

4.3.1 Assessing the Quality of the scNGS

Several studies have tried to decipher the therapeutic mechanisms of HDACis using the microarray and the NGS bulk analysis. The findings of these studies have suggested several cellular factors that collectively result in stimulating cell death mechanisms^{83, 153, 221, 222, 223}. Yet, the HDACis anticancer regulations are often intricate and embedded in a network of molecular interactions that occur simultaneously which make the bulk analysis of heterogenous cells less likely to reveal the molecular regulations behind these networks.

As any analytical approach, the scNGS analysis has several technical and biological factors that may limit the ability of the generated data in addressing some important regulations. The quality of the scNGS data depends significantly on the number of the targeted cells and the sequencing depth, and it also highly affected by the technical and biological noises. Thus, in order to generate meaningful results, the data were subjected to several levels of quality controls assessment to filter out poor data before investigating the gene expression.

4.3.1.1 Assessing the Quality Based on the Number of the Analysed Cells

The number of the individual cells is an important factor for generating a statistically significant result. In this study, I aimed to target at least 2000 cells for each condition. The data of the tumour cells showed the presence of more than 1800 cells in the D.Vehicle and D.SAHA samples and it reached to more than 2700 with the MS-275-treated cells. Whereas, the number of the analysed neurons was less than 1400 cells. The main factor of not achieving the aimed number was due to the inaccurate count of the neurons. As per the 10x Genomics recommendations, the number of the loaded cells should be accurately measured with considering the multiplets rate and the percentage of the dead cells.

In the subsequent data improvement analysis, the number of the cells was further reduced after filtering out the poor-quality cells. The count of the Daoy samples was more than 1700 cells where, the count of the neurons reduced to around 1000 cells in the untreated and MS-275-treated cells, and it was less than 700 cells in the SAHA-treated neurons. Calculating the gene differential expression between the different conditions of the same cell identity showed statistically significant results ($P < 0.0001$) which may suggest the suitability of the data to identify the difference in gene expression across the samples.

4.3.1.2 Assessing the Quality Based on the Sequencing Saturation and Depth

The sequencing saturation is the average number of reads (mRNA, cell-barcode, and UMI) that confidently mapped to known reference bases, and it is used to estimate the number of additional reads to detect a new transcript. Whereas, the sequencing depth is the number of the transcripts that were detected for each cell²²⁴. The values of these measures are important to ensure; obtaining the most transcriptome of a single cell, accurate identification of gene expression, detecting genes with low abundance, and reducing the technical noise. The recommended sequencing saturation for the scNGS is $>85\%$ and the recommended depth is $>50,000$ reads for the RNA-rich cells such as cell lines.

In this study, the sequencing saturation of the Daoy samples was less than 33% and it resulted in reducing the sequencing depth to a suboptimal level. The sequencing saturation of the neurons was between 52 to 63% where the sequencing depth was between the 35 and 43 thousand read per cell. Despite several attempts to improve the magnitude of the sequencing depth though, the number of reads did not show any significant improvement. This could be due to a technical problem and it may result from an inaccurate normalization of the cDNA libraries between the samples. The low sequencing depth often affect the reliability of gene detection in particular genes with low transcriptome abundance. Accordingly, the low sequencing depth of the Daoy untreated- and SAHA-treated cells could have an impact on the interpretation of the findings¹²¹.

Despite the higher sequencing depth of the neurons in comparison to the Daoy cells however, the number of the detected genes in the Daoy samples was higher (between 3000 to 5000 genes) than the neurons (1000 to 1300 genes). This could be due to the nature of cancer cells which require more functional genes for the cell proliferation, metabolism,

DNA repair, chromosome stability, cell matrix interactions, cell communication, tumour invasion, angiogenesis, and inhibiting apoptosis ²²⁵.

4.3.1.3 Assessing the Quality Based on the Q30 and the Background Noise

The Q30 score is another important factor as the scNGS data often contain technical and biological noise. The average Q30 of the data (the Barcode, the RNA, the sample index, and UMI) in all the samples exceeded the 80% which considered an average score with Illumina sequencing and it may indicate the optimal quality of the reads.

The data showed that the majority of the cells in each treatment condition have a relatively equivalent number of genes however, there were cells with a higher number of genes when compared to the whole population. The analysis also exposed cells with low number of genes which could result from having a free-RNA. Additionally, the analysis displayed a subset of the Daoy cells with a higher mitochondrial gene count compared to the majority of the cells which often results from have broken cells where the mRNA is lost and the RNAs enclosed in mitochondria is retained ²²⁶. Therefore, the data were subjected to multiple levels of quality improvement analysis using the CellRanger and the Seurat analysis tools and the effect of the multiplets, free-RNA background, and the mitochondrial genes were removed. The cell-specific bias such as the dropout (is a true zero value in gene expression matrix could result from absence of gene expression) and the batch effect were also removed by data normalization ²²⁷.

4.3.1.4 The Analytical Approach used to Process the Data

As the phase of the cell cycle is the main driver of the transcriptome heterogeneity in the Daoy cells, each cell was scored according to the expression of a pre-set of the cell cycle genes ¹²⁸. This analysis was carried out to allow the comparison between the data set of the untreated and the treated cells based on the cell cycle phase (i.e. G1 phase of untreated compared to G1 of treated). The result of the untreated Daoy cells showed that the clustering of the cells was mainly driven by the cell cycle phase. This finding demonstrated the active proliferation of the tumour cells and it also displayed the transcriptional heterogeneity across cells of the same genetic identity.

In contrast, the cell cycle scoring of the SAHA- and MS-275-treated cells showed an extensive overlap between the cells and the expression of the cell cycle genes was

considerably different when compared to the untreated cells. These results clearly demonstrated the effect of HDACis on the cell cycle genes which makes the comparison of the gene expression based on the cell cycle phase is inapplicable.

The alternative approach was to merge the three Daoy samples into one data set. The data were then subjected for clustering analysis which resulted in clustering the cells according to the transcriptome similarity between the three samples. The outcome of this approach showed that each sample maintained a clear distance from the other samples and the untreated cells maintained their original (unmerged) clustering (Figure 44). Whereas, the treated cells showed a new clustering with a smaller number of clusters and very minimal overlap between the SAHA- and MS-275-treated cells. Interestingly, the cluster of the MS-275-treated cells showed a considerable distance to the untreated cell whereas, the SAHA-treated cells were positioned near to the untreated cells. This outcome is further demonstrated the considerable effect of HDACis on gene transcription, and it also suggests that the ability of MS-275 to induce more transcriptional variations compared to SAHA.

The clusters were then subject to GO annotation analysis to identify the clusters that exhibit the HDACis effect. The GO annotation analysis showed the enrichment of the main clusters, which have the majority of the cells, of SAHA- and MS-275-treated cells with GO terms of apoptosis and cell cycle regulations. Hence, these clusters were used to study the anticancer regulation. Further, the differential expression of the upregulated and downregulated genes of each cluster was used to run a preranked GSEA analysis in order to identify the gene set enriched-pathways of each cluster. This analysis mainly depends on grouping the genes that share common biological function, chromosomal location, or regulation according to priori defined sets of genes. The results of the GSEA was evaluated based on; the ES (reflects the overrepresentation of a genes set), the statistical significance of the ES (account for the size of the set and presented by the normalized ES), and proportion of false positives (FDR)¹³¹. Typically, this analysis is significantly affected by the number of the expressed and detected genes²²⁸. The results of the Daoy samples showed several gene set-enriched pathways with a statistically significant ES. However, the GSEA results of the neuron clusters did not reach the statistical significance in the majority of the identified pathways despite the presences of more 30 genes in each pathway. The main factor that affected the neurons GSEA results could be the low number of the genes that play a significant role in a particular pathway. This could be due to; the

biological regulation that determine the response to the HDACis, or a technical matter as for example the suboptimal sequencing depth.

4.3.2 HDACis Affected the Expression of Several Cellular Pathways

HDACis are known by their ability to induce extensive transcriptome changes in tumour and normal cells. These changes were suggested to contribute, at least, in part in the HDACis anticancer effect and cell proliferation. Using SAHA and MS-275, I showed that these inhibitors induced a transcriptional activation of several cellular pathways in the Daoy cells including TNF α -Signalling-via-NF κ B, p53, and apoptosis pathways. They also induced transcriptional repression of cell cycle and Myc pathways. The most noticeable theme between the two inhibitors was their ability to induce a transcriptional pausing of the cell cycle regulating genes in both the transformed and normal cells. The two drugs showed some slight differences in the number of the differentially expressed genes and also in the gene set enrichment analysis. On the cell type level, the response to the two drugs showed also some differences between the different neurons. Interestingly, the effect of the HDACis was not limited on upregulating the transcription of genes but it also contributed in transcription downregulation. Likewise, previous HDACis transcriptome analysis showed considerable upregulation and downregulation of a large number of genes ^{105, 153, 229, 230}.

The transcriptional repression function of HDACis is not completely understood. The Genome-wide analysis that were applied to identify the localization of HDAC suggested that the function of HDACis is often associated with activating gene transcription ²³¹. The downregulation activity of HDACis could be a result of deacetylating non-histone proteins which function as transcription factors ²³². This assumption is further supported by a recent study which suggested the ability of HDACis to target the transcription elongation complex (bromodomain-containing protein 4 (BRD4)) and inhibit its activity ²³³.

The patterns of changes in genes expression -apart from the apoptotic regulation- are relatively similar for different inhibitors yet, they are highly variable between transformed cells ^{105, 234, 235, 236, 237}. Some changes in gene transcription are possibly due to the direct effect of HDACis on gene promoter where other could be secondary and downstream effects. Also, the changes that occur at the start of the acetylation may not reflect the anticancer effect in tumour cell, or the tolerance regulation in the normal cell ²³⁶. In

addition, the anticancer mechanism may occur at any time from the exposure to prior the cell death. Also, the cell apoptosis regulations in a response to an inhibitor are different between various cells and with different inhibitors¹⁴⁶.

4.3.2.1 HDACis Disrupted the Expression of Cell Cycle-Specific Genes

The active progression in cell cycle is the main factor of tumour cell growth and it is one of the treatment targets. Cancer cells sustain their growth through activating the cell cycle pathway whereas, the ability of the anticancer agents to disrupt the cell cycle regulation is a central factor in inhibiting tumour cell growth and it may leads to cell death²³⁸.

In this study, the GSEA results of the untreated Daoy cells a showed a positive phenotype of several pathways including the cell cycle, Myc, E2F and DNA replication pathways. These pathways are often amplified among many different human cancers and they have pivotal role in cell growth, proliferation, and tumorigenesis^{84, 239, 240, 241}. The cell cycle pathway of the untreated Daoy cells showed a significant enrichment of 141 genes that were annotation as regulator for cell cycle, DNA replication, mitosis, nuclear division, and active transition in cell cycle. Some of these genes have also a direct role in cell cycle transition including the cyclin-dependent kinase (CDK) genes such as CCNB1, CDC20, CDKN2D. The CDKs are a family of proteins that regulate the transcription of cell cycle regulating genes and they play an essential function in regulating normal cell division²⁴². Overexpression of cyclins is frequently observed in human malignancies and their expression has been associated with aggressive cancer and poor prognosis^{80, 243}. The GSEA results also showed the downregulation of genes that have a direct effect on inhibiting the progression in cell cycle and the DNA repair mechanisms such as CDKN1A, BIRC5, PCNA, HSPA2, and HSP90AA1.

In contrast, the GSEA results of the HDACis treated cells showed a negative phenotype of the cell cycle pathway. The most significant differential expression was in CDK genes such as CCNB1, CDC20, CKS1B, and CCNB2. The finding also showed the downregulation of genes that are components in G1 and S phase checkpoint signalling such as CDK1 and CDK4. The transcriptional inhibition of CDK1 and CDK4 has been suggested to arrest the cell cycle and allow DNA repair to occur, which may trigger apoptosis when cellular damage cannot be properly repaired in transformed cells⁸⁰.

The results also showed a robust increase in CDKN1A (also known as p21^{CIP1}, hereinafter referred to as p21^{WAF1}) expression, which was more noticeable in the MS-275-treated cells compared to the SAHA. p21^{WAF1} is a CDK inhibitor with a high potential to arrest cell cycle progression at G1 phase by inhibiting the activity of the CDKs. It is also involved in regulating transcription, apoptosis, DNA repair, and cell motility²³⁸. In several tumours, the downregulation of p21^{WAF1} was connected with tumour cell growth where its upregulated expression was associated with anticancer regulation²³⁸. It has been reported that p21^{WAF1} inhibits the DNA replication by binding to the proliferating cell nuclear antigen (PCNA) which inhibits the cell cycle and allow the DNA repair²⁴⁴. The increase in the p21^{WAF1} expression has been reported to inhibit caspase-induced apoptosis by binding to caspase-2 and caspase-3 in the cytoplasm and block their activity^{220, 238}. However, it has been suggested that p21^{WAF1}-arrested cells may undergo apoptosis following the activation of proapoptotic genes in a p53-dependent or -independent manner²⁴⁴.

The exact regulation of p21^{WAF1} induction is not well known however, it has been suggested to occur though the p53 depletion in wild-type expressing tumour cells⁸³. Despite the expression of a non-functional form of p53 protein in the Daoy cells, the treatment with HDACis in this study resulted in upregulated p21^{WAF1} expression which may indicate the existence of an alternative regulation and it warrant further investigation^{83, 113}.

Treating the normal human neurons with HDACis also caused a considerable effect on genes transcription resulted in up or downregulation of several subsets of genes however, many of the identified pathways were statistically insignificant. The effect of SAHA and MS-275 on the neurons cell cycle genes was slightly different and the MS-275-exposed cells showed more gene downregulation compared to SAHA. The GSEA results of the treated normal human neurons showed a negative phenotype of several cellular pathways compared to the untreated neurons. For instance, the negative phenotype of the cell cycle and Myc pathways was common in all treated neurons whereas the mTORC1 positive phenotype was only observed in the untreated cortex.1 neurons. The most noticeable difference in the cell cycle-regulating genes between the Daoy and the neurons was the absence of the CDK genes expression in the neurons. Where the expression of p21^{WAF1} was only detected in the Corext.2 neurons treated with MS-275. The transcriptional

changes induced by the inhibitors suggest their effect in modulating gene transcription in normal cells which may impair the cells ability to maintain their biological function and consequently could lead several of downstream implications.

Comparing the cell cycle genes between the Daoy and the neurons identified 19 shared genes however, the annotation analysis of these genes showed that these genes were involved in general biological functions including histone and tubulin regulation with eleven genes annotated as ribosomal genes.

Collectively, the cell cycle gene expression results showed the ability of the HDACis to downregulate the CDK genes and upregulate the p21^{WAF1} gene expression which could support the stimulation of the apoptosis pathway. In contrast, the expression of the CDK genes was not detected in the untreated and treated neurons. This may suggest that the anticancer effect of HDACis could depend on CDK and p21^{WAF1} in tumour cells. Whereas, the regulation of the cell cycle in normal cells is less dynamic hence the effect of HDACis on the transcripts did not lead to the activation of death mechanisms. Collectively, these findings may demonstrate how tumour cells sustain their growth and suggest CDKs and p21^{WAF1} as therapeutic targets.

4.3.2.2 HDACis Disrupted the Expression of Myc Pathway

Further the results of the untreated Daoy cells showed a statistically significant up or downregulation of a large number of genes that were associated with Myc pathway. Myc expression has been reported in many cancers and in medulloblastoma. However, the expression of Myc genes is significantly variable across the medulloblastoma subgroups²³⁹. Treating with SAHA and MS-275 resulted in a significant disruption in the expression of a subset of genes that were identified as Myc components pathway. Myc regulation has critical part in several aspects of cancer biology, including proliferation, migration and treatment response where, treating with HDACis has been suggested to suppress Myc-oncogenic function. Myc has been suggested to induce the proliferation activity through interacting with a number of HDACs including HDAC1, HDAC2 and HDAC3⁸³. Accordingly, the expression of HDACs in tumour cells has been reported to contribute in Myc-driven proliferation. Tumours with elevated expression of Myc and HDAC2 have been reported to show higher sensitivity to class I HDACis⁵⁴. Inhibition of HDAC2 in medulloblastoma Group3 has been reported to reduce the stabilization of Myc protein and

induce cell death⁵⁴. Myc-induced apoptosis has been reported to occur through indirect downregulating the antiapoptotic proteins such as Bcl-2 and Bcl-xL, and through p53 - dependent and independent manners²⁴⁵.

In this study, exposing the neurons to SAHA and MS-275 HDACis resulted in varying response across the different neuron types. The GSEA results showed a negative phenotype of Myc in all the different types of the neurons apart from the MS-275-treated Cortex.1 which displayed a positive phenotype. However, the Myc pathway was statistically insignificant in all treatment conditions.

The expression of Myc in normal cells has been suggested as the developmental signals as Myc works as a factor to integrate the growth signals to support cell growth²⁴⁰. Where, the expression of Myc in postmitotic neurons has been suggested to drive cell cycle re-entry and emerged as a potential pathogenic factor which could lead to neuronal degeneration and death²⁴⁶. The results of this study may indicate the deactivation of Myc pathway however, the conclusion cannot build on the current results.

4.3.2.3 HDACi Disrupted the Expression of TNF α signalling via NF κ B Pathway

In this study, the GSEA results of the untreated Daoy cells showed a statistically significant negative phenotype of TNF α signalling via NF κ B pathway. Tumour necrosis factor (TNF) is a cytokine that binds to TNF cell surface receptors receptor (TNFR) 1 and TNFR2 and upon its ligation it activates either of three pathways; the Nuclear Factor kappa-light-chain-Enhancer of Activated B Cells (NF κ B) pathway, MAPK pathways, or cell death pathway²⁴⁷. TNF has a complicated role in cancer as it stimulates proliferation, migration, and angiogenesis in cancers that are resistant to TNF-induced cytotoxicity²⁴⁷. TNF has also been suggested to induce cell death through the TNFR1 which is universally expressed on most cell types and has a direct role in NF- κ B activation. The ligation of TNF with TNFR1 results in recruitment of TNFR1-associated death domain protein (TRADD) which works on promoting apoptosis when binds to caspase-8 in presence of Fas Associated Via Death Domain (FADD)²⁴⁷. It could also promote survival through TNF Receptor Associated Factor 2 (TRAF2) via JNK-dependent kinase cascade²⁴⁸.

The expression results of the Daoy untreated cells showed the downregulation of CCL2, CEBPD (stimulates the cancer cell proliferation through E2F1), NF κ B Inhibitor Alpha

(NFKBIA) which collectively promote; the cell growth, reduce the inflammatory processes, and inhibit apoptosis^{249, 250, 251}. The results also showed the downregulation of INHBA, CDKN1A, and PHLDA2 which were suggested to work as tumour suppressor genes²⁵².

The GSEA results of SAHA- and MS-275-treated Daoy cells showed the positive phenotype of TNF α signalling via NF κ B pathway (SAHA FDR q-val=0.932, and MS-275 FDR q-val=0.002). The gene expression results showed the inverse expression of CCL2, CEBPD, NFKBIA, INHBA, CDKN1A, and PHLDA2 and several of other cytokine genes that are components of TNF α signalling via NF κ B pathway such as TNFSF9, IER2 and MAP2K3. It is unclear whether HDACis have a direct effect on cytokine gene regulation or the change is caused due to a secondary effect of HDACis. Similarly, it is not known if the expression of NF- κ B is directly regulated by acetylation²⁵³. Additionally, it is not well known how TNF stimulates apoptosis especially and it activates NF- κ B which has a significant contribution in supporting the cell proliferation, cell differentiation, and cell death as well. However, it has been suggested that TNF may induce cell death through activating Caspase 3²⁴⁷. In several studies, combining HDACis treatment with NF κ B with proteasome inhibitors enhanced the tumour cell death of Hodgkin lymphoma cells and glioblastomas and has been suggested to limit the toxicity associated with using either drugs²⁵⁴.

4.3.3 The Expression of HDAC and HAT Genes

It has been commonly assumed that the imbalance in the HDACs and HATs expression is the causative of increasing the deacetylation level in various cancers. Whereas, treating with HDACis has been suggested to reverse the epigenetic states which suppresses the cell growth and stimulates apoptosis²⁵⁵. In this study, the scNGS data were used to explore the expression of HDAC and HAT enzymes before and after the HDACis treatment. The results of the Daoy cells showed an increase in the HDAC1 and HDAC2 level in the untreated and treated cells. Where treating with SAHA resulted in a significant increase in HDAC3.

The upregulated HDACs expression has been reported in various types of neuronal and non-neuronal cancers however, the expression is vary greatly between tumours¹⁴⁶. The expression is also inversely correlated with the overall survival rate and significantly

associated with active tumour progression and poor prognosis^{146, 256, 257}. In brain tumours, HDACs have been found to play a key role in sustaining cell growth. For example, in glioblastoma the expression of HDAC1, HDAC3 and HDAC6 has been reported to be significantly higher than non-plastic brain tissue, where the expression of HDAC9 is frequently reported with prognostically poor glioblastoma multiforme patients²⁵⁷. Elevated HDAC2 has been reported in medulloblastoma SHH, Group 3 and Group 4 subgroups and it was also connected with poor prognosis⁵⁴. The expression of HDAC5, HDAC9, and SIRT1 was also associated with the increasing in medulloblastoma tumour progression and was suggested as drug targets⁴⁵. Blocking the expression of HDAC2 or HDAC3 has been found to inhibit the tumour growth and induce apoptosis which may suggest their oncogenic properties^{147, 193}. Several studies have reported the decrease in HDAC3 expression when treating with HDACis however, in this study treating the Daoy cells with SAHA resulted in upregulating the expression of HDAC3^{147, 193}. It is not known why SAHA increased HDAC3 expression however, it has been reported that treating with SAHA often results in reducing the expression of the HDAC enzymes at the protein level where the mRNA level remained unchanged¹⁴⁷. Similarly, a previous clinical trial reported that the expression of HDACs remained unchanged in pre- and post-treatment with SAHA²⁵⁸. This may suggest the ability of HDACis to induce their effect on the protein level only where they do not affect the active transcription of the HDAC enzyme.

The results also showed an upregulation in HDAC2 expression in a small subset of the untreated and treated neurons with a noticeable increase in the MS-275-treated cortex neurons. The elevated expression of HDAC2 in neurons has been reported to have a critical role in regulating neuronal cell differentiation, and its expression has been reported in mature neurons¹⁰². The current evidence of this study cannot completely explain the effects of HDACis on neurons and if it will lead to a cytotoxic effect. The role of HDACs in regulating neuronal survival or death is intricate and involved several regulations. For example, the activity of HDAC1, HDAC4, HDAC5 or HDAC6 has been reported to contribute in inducing neurons death^{259, 260}. Whereas, the expression of HDAC2, HDAC3, HDAC7 or SIRT1 has been suggested to promote neuronal survival^{260, 261}.

The expression results of this study also showed an increase in SIRT7 expression in the SAHA- and MS-275-treated Daoy cells. SIRT7 is a deacetylase enzyme that has a high involvement in various cellular processes in normal cells. In cancer cells, SIRT7 has been

reported to have an oncogenic property ²⁶². Overexpression of SIRT7 has been found to protect tumour cell against DNA damage and support the tumour cell survival ²⁶². It is not clear why treating with HDACi resulted in upregulating SIRT7 expression. However, it has been reported that treating with HDACis, in particular SAHA, does not significantly inhibit SIRT7 enzymatic activity even at high concentration of SAHA ²⁶³. This is consistent with the ability of SAHA to inhibit Class I and II HDACs enzymatic activity and not class III HDACs.

The results also showed a slight decrease in the α -tubulin acetyltransferase 1 (ATAT1) expression in the MS-275-treated Cortex.2 and Striatum neurons. ATAT1 is microtubule acetyltransferase and play a major part in destabilizing the microtubules and accelerating their dynamic ²⁶⁴. The relation between the HDACis treatment and ATAT1 expression has not been studied previously, and the decrease of ATAT1 in the MS-275-treated Cortex.2 and Striatum could result in decreasing the microtubule dynamics and conformation ²⁶⁵. Several of previous studies have examined the roles of HAT members in controlling neuron fate and they concluded that the increase in HAT activity is often associated with apoptosis ^{265, 266}. For example, enhancing EP300 or CREBBP HAT activity has been reported to promote the apoptosis of dopaminergic neurons and cerebellar granule neurons, respectively ^{265, 266}.

Collectively, the results of HDACs and HATs expression showed the upregulated expression of HDAC1 and HDAC2 in the Daoy medulloblastoma cells which may suggest their direct role in increasing the deacetylation level and proposed them as a potential treatment target. The results also showed an increase in HDAC3 mRNA expression in the SAHA-treated cells which may suggest the ability of HDACis to induce their effect on the HDAC protein but not the transcriptional levels. Hence, the efficiency of HDACis treatment should be monitored on the HDAC protein level. Incomplete HDACis treatment may result in restoring the deacetylation back to its upregulated level. However, the critical effect of HDACis on neuronal cell survival needs further exploration.

4.3.4 The limitation of the scNGS

In this study, the scNGS analysis showed great advantages as it allowed me to; measure the transcriptome at single cell level, study cell-to-cell heterogeneity, assign cells into their cell cycle phases, and identify the highly variable genes that drive the variability across a

population of cells. However, there were some technical and biological factors that may impacted the quality of the data and the finding interpretations. In addition to the suboptimal sequencing saturation and sequencing depth that were addressed previously, the used 10x Chromium kit (V2) is another factor that could have an effect in reducing the sequencing depth. The efficiency of this version in capturing and reverse-transcribing mRNA to cDNA is not significantly high and it displayed a high frequency of not detection transcripts with low abundance¹²¹. Recently, the 10x Genomics has released a new version (Chromium V3') which showed a significant increase in the detection level and more transcripts per cell.

In the biological side, the scNGS analysis showed several limitations. For example, it does not measure the expression of non-coding RNA such as microRNA and Long non-coding RNA . Thus, the number of the expressed genes are lower compared to RNA-seq bulk analysis. The analysis is also subject to cell-size variation, cell cycle phase, transcriptional bursting and temporal fluctuations¹²¹. The transcriptional bursting is a state where the transcription from DNA to RNA occur in random fluctuating bursts or pulses followed by variable periods of inactivity. The transcriptional burst often affects the total transcript number which it could impact the number of detected genes per cell^{121, 267}.

The ability of scNGS to identify most of the potential therapeutic targets is also limited by abundance of transcripts. The abundance of transcripts is controlled by the functional category to the gene and the quantity that is needed for producing certain proteins. For example, the expression of genes with high abundance such as collagens and matrix metalloproteinases are more redundant in scNGS, where not all low-abundance genes such as cytokines are detectable. Also, some proteins work in small intracellular compartment therefore, their transcriptome often less than the genes that are involved in major cellular regulations. This often leads to increase the frequency of dropout events (i.e. none of gene-transcripts are captured)²²⁷. At the statistical level, the heterogeneity of the analysed cells is often result in a negative binomial or multimodal distribution (data are not normally distributed) and this may affect the statistical tests that assume the normal distribution of the data²⁶⁸. Hence, the findings of the scNGS should be interpreted with caution.

Finally, pathway or network analyses were performed to gain biological insight into the underlying molecular regulation as it could reduce the complexity and help in explain the findings however, the results of this analysis did not show high representation of the genes

in the identified pathways. The main limitation in this analysis was due to the suboptimal sequencing depth of the current transcriptomic data which impacted the detection of genes and affected the subsequent bioinformatic analysis. The findings representation could be improved by using commercial systems such as Ingenuity Pathway Analysis and iPathwayGuide software.

5 General Discussion

5.1 Summary of the Research Aims and Methodology

In this thesis, I have investigated the contribution of REST, HDACs, and HDACis in medulloblastoma tumorigenesis and treatment response. To study the contribution of REST, I used CRISPR/Cas9 system to knockout REST expression in the Daoy medulloblastoma cells, one of the most frequently used cell lines in medulloblastoma studies⁴³. In addition, and as CRISPR/Cas9 has not been used previously to modulate REST expression, I used the shRNA knockdown system to confirm the knockout findings. I examined the effect of blocking REST expression on the cell growth, cell-cycle, and cell migration ability, and I explored if the HDACis induce their action through the HDACs recruited in REST repression complexes.

Further, I investigated the anticancer molecular regulation of SAHA and MS-275 using the Daoy medulloblastoma cells, and I explored their effect on normal human neurons. I carried out the analysis at the transcriptome level using the single cell next generation sequencing analysis and I applied the PCA to compare the gene expression of the untreated- and treated-Daoy and neurons cells in order to explore the molecular regulation of HDACis.

5.2 Knockout REST did not Induce Medulloblastoma Cell Death

This study has found that the expression of REST is elevated in the medulloblastoma subgroups compared to normal cerebellum and its expression has important role in regulating the transcription of some RE1-containing genes. Blocking REST expression resulted in increasing the cell accumulation in G1 phase and decreasing the cells migration ability however, it did not reduce the Daoy cells proliferation or stimulate apoptosis. The results also displayed the high sensitivity of the Daoy cells to the used HDACis yet, the HDAC enzymes in REST repression complexes were not the primary elements for the inhibitors to induce their action.

Collectively, these data suggest that REST is not a main regulator of the Daoy cell growth, and the tumour may depend on other factors to sustain its self-renewal potential. Also, the induction of the Daoy medulloblastoma cell death by HDAC inhibitors is not dependent

on, or affected by, REST expression status rather, they may work through other HDAC complexes.

This conclusion does not support what it has been proposed previously to use REST expression as a clinical marker for HDACis treatment efficiency in medulloblastoma ¹⁴. These findings could suggest the lack of the tumour cell the primary components required for employing the differentiation factors. In addition, it demonstrated the ability of the tumour regulation to avoid progression in the maturation stages despite the expression of the neuronal genes.

These conclusions are in congruent with some of the latest research findings. For example, Das et al., (2013) used shRNA to knockdown REST expression in the Daoy cells and they found that loss of REST resulted in increasing the accumulation in G1 phase with a concomitant decrease in the S phase however, it did not lead to cellular apoptosis. Also, they reported that loss of REST expression led to; a decrease in the expression of MYCN (a proliferative marker), and an increase in the expression of certain antiproliferation markers such as p27 and UPS37 ⁵². Similarly, Zhang et al., (2016) modulated REST expression in glioblastoma U-87 and U-251 cell lines using the shRNA knockdown system and they found that knocking down REST expression resulted in inhibiting the glioblastoma cells migration yet, it did not stimulate cell death or reduce tumour size ¹². In addition, several of gene expression analysis studies were performed using primary human medulloblastoma however, the elevated REST expression was not proposed as a factor in sustaining the cell growth ^{38, 39, 41, 44}.

One important part of my work was using both of the knockout and knockdown approaches in order to examine the contribution of REST and to validate the findings. The knockout approach resulted in completely blockage of REST expression hence, it limited the effect of the partial expression of REST in the shRNA knockdown approach which can induce a repression on different subsets of genes and affect with results interpretation. This aspect could clearly indicate the importance of using a correct experimental tool to reach more evident conclusion.

5.3 HDACis Effected the Cell Cycle Regulation in Tumour and Normal Cells

The findings of this study showed that treating the tumour cells with HDACis resulted in a considerable decrease in the number of the expressed genes compared to the untreated cells. The treatment also resulted in activating the TNF α signalling via NF κ B pathway and deactivating the cell cycle and Myc pathways.

The expression of several genes that are known by their significant function in cells faith such as CDKN1A, CCNB1, CDC20, CCNB2, CCL2, CXCL1, NPM1, CCND1, AREG, TOP2A and BIRC3 was also affected by the treatment (Table 10). The dynamic changes in gene expression pattern in a response to HDACis may provide important insight into the cellular response.

The significant effect of SAHA and MS-275 on the cell cycle genes was clearly demonstrated on reducing the expression of most cell cycle regulations which resulted in delaying the progression in the cell cycle and increasing the accumulation in cell cycle phases, as it was demonstrated in the cell cycle analysis. These data therefore strongly suggest the ability of HDACis to exert an inhibitory effect on the cell cycle in cancer cells which could be one of the anticancer regulations.

Exposing the normal cell to HDACis also caused considerable changes on the transcriptome level. These changes were diverse between the untreated and treated neurons and across the different neuron types. For example, HDACis resulted in downregulating the expression of the genes that were annotated as regulator for; cell cycle, translation, ATPase activity, and the nonsense-mediated decay of mRNAs. The data also show a considerable cell-to-cell variation in total transcript level. The difference in the cell response to SAHA and MS-275 was observed in ability of each inhibitor to regulate different sets of genes that are components in the metabolic activity, cellular process, and cell-cell communication mechanisms. These changes are potentially harmful on normal cell and may lead to impair their normal biological function.

Table 10: Gene information

Gene	Abbreviation	Function
Cyclin-Dependent Kinase Inhibitor 1A	CDKN1A	Inhibits cellular proliferation in response to DNA damage ²⁶⁹
Cyclin B1	CCNB1	Essential for controlling the cell cycle at the G2/M (mitosis) transition ²⁷⁰
Cell division cycle 20	CDC20	Interacts with several proteins at multiple points in the cell cycle ²⁷¹
Cyclin B2	CCNB2	Essential for controlling the cell cycle at the G2/M (mitosis) transition ²⁷²
C-C motif chemokine ligand 2	CCL2	A chemokine and it stimulates host anti-tumour activities ²⁷²
C-X-C motif chemokine ligand 1	CXCL1	Aberrant expression of this protein is associated with the growth and progression of certain tumours ²⁷³
Cyclin D1	CCND1	Regulator of progression through G1 phase during the cell cycle ²⁷⁴
Amphiregulin	AREG	Inhibits the growth of various types of cancers ²⁷⁵
Topoisomerase (DNA) II Alpha	TOP2A	Encodes a DNA topoisomerase which controls the topologic states of DNA during transcription ²⁷⁶
Baculoviral IAP Repeat Containing	BIRC3	Inhibits apoptosis by binding to tumour necrosis factor receptor-associated factors TRAF1 and TRAF2 ²⁷⁷
Nucleophosmin	NPM1	In complex with MYC, NPM1 enhances the transcription of MYC target genes and tumour suppressors p53/TP53 ²⁷⁸

Four studies in the literature (Chiba et al., 2004, bolden et al., 2013, Halsall et al., 2015, Markozashvili et al., 2016) have compared the effect of HDACis on normal and tumour cells in order to understand why tumour cells are more sensitive and how normal cells tolerate the hyperacetylation effect ^{279, 105, 280, 281}. The studies profiled the gene expression using microarray analysis after treating the normal and their tumour counterpart cells with HDACis. The drug concentrations, exposure time and the cell lines were different between the studies (Table 11). The rationale behind choosing the used concentrations and time was not built on an experimental approach, apart from Bolden et al., study which used the CDKN1A (cell cycle progression) gene expression to select for the treatment duration

length¹⁰⁵. The findings of the microarray gene expression profiling were different between the studies and revealed different cellular mechanisms (Table 11).

Only Halsall et al., study has claimed that the molecular regulations which protect normal cells from the hyperacetylation effect is through down-regulation of the expression of HAT enzymes which in minimized protein hyperacetylation, slowed the growth and re-balanced the gene expression²⁸⁰. However, in this study there were several sources of uncertainty. For example, the immunoblotting analysis of global histone showed an increase in the acetylation level in the treated cells during the first 120 minutes and this contradicts what they claimed about the HAT downregulation.

Typically, HDACis induce an increase in the acetylation level until the drug loses its pharmacokinetic activity or is washed out. The study by Bolden et al., showed a sustained increase throughout the treatment with SAHA (25 μ M) for 32 hours. Similarly, the increase in the acetylation was reported in several of other studies that used non-disease cell lines^{106, 107, 108}. The study by Halsall et al. did not take into account comparing the decrease of HAT genes in the normal cells to the transformed cells as the expression of HAT components could decrease in transformed cells, as well²⁸⁰.

Another limitation in the Halsall et al., study is that the fold-change of the HAT genes was small and only measured by microarray methodology. Inspecting the HAT expression results at GEO (GSE65297) showed that the changes in the HAT gene expression also varies between the biological replicates and some values could be considered as outliers when compared to the other replicates. It is well known that the sensitivity of microarrays is affected by several factors including the amount of the mRNA and the hybridization. Yet, these limitations are irrelevant if the microarray was used for screening first and then the expression results should be verified independently. Real-time PCR is the method of choice for most researchers especially when the fold change in gene expression is low. However, the study did not verify the expression of the KAT component genes despite it was the main question of the study. The Halsall et al., study also included clustering of the genes according to their expression changes over time. However, the criteria of selection was very limiting as they used an algorithm that allowed selection of very few groups with a very small number of genes²⁸⁰. This approach may have an advantage of showing very limited subgroup of genes however, it eliminates large groups of genes that may have similar cellular mechanisms.

HDAC inhibitor/s	Cell line	Treatment Time	Gene profiling	Findings	Limitations
Identification of genes up-regulated by histone deacetylase inhibition with cDNA microarray and exploration of epigenetic alterations on hepatoma cells (Chiba et al., 2004) ²⁶¹					
TSA (0.67µM)	Hepatoma cell lines / primary hepatocytes	24 H	Microarray analysis & Chromatin immunoprecipitation	Treated normal hepatocyte showed no significant increase in gene expression (> 5-fold changes). Only one gene, PRDX1 (cell cycle), was detected as a common upregulated gene between hepatoma cells and normal hepatocytes. In hepatoma cell the expression of p27 (apoptosis), cysteine-rich 61 (CYR61), and connective tissue growth factor (CTGF) (proliferation), NIPSNAP1 (neurotransmitter binding) were increased by more than 5-fold in multiple cell lines. ChIP assay demonstrated a good correlation between mRNA expression of the four gene and their histone acetylation.	The results did not reveal the molecular regulation effect that protect normal cell from the hyperacetylation
HDAC inhibitors induce tumor-cell-selective pro-apoptotic transcriptional responses (bolden et al., 2013) ⁹³					
Vorinostat (2.5, 5, 10, 25, and 50µM) Romidepsin (2.5, 5, 10, 25, and 50nM)	Normal and transformed foreskin fibroblasts cells	4 and 12 H	Microarray analysis	The selective induction of apoptosis in transformed cell is due to alterations in the expression of pro-survival and pro-apoptotic BCL2 family in a direction that favours cell death. Though, in normal cells, the expression is also observable though the balance is relatively neutral.	Both cell types are rapidly proliferating
Cells adapt to the epigenomic disruption caused by histone deacetylase inhibitors through a coordinated, chromatin-mediated transcriptional response (Halsall et al., 2015) ²⁶²					
Vorinostat (0.5, 2.5, and 12.5µM) & VPA (0.2, 1, and 5mM)	Human lymphoblastoid cells	30, 60, 120 min	Microarray analysis	Down-regulation of (KAT) Minimising protein hyperacetylation, slowing growth and re-balancing patterns of gene expression	<ol style="list-style-type: none"> 1. The acetylation level continued to increase 2. The expression of KAT components could also decrease in transformed and cancer cells, 3. The fold change of KAT components genes was small. And the results of microarray were not conformed by qPCR 4. The clustering algorithm for gene expression analysis was very narrowing which could exclude a lot of molecular mechanisms
Histone deacetylase inhibitor abexinostat affects chromatin organization and gene transcription in normal B cells and in mantle cell lymphoma (Markozashvili et al., 2016) ²⁶³					
Abexinostat (100nM)	Human mantle cell lymphoma cell lines & Lymphoblastoid cell line	1 and 24 H	ChIP-on-chip data analysis	Different subsets of genes changed their expression at 24 h in abexinostat-treated cells: CD6, CTSE, GSTP1 and CCND1 were overexpressed in the control cells while CD6, CD5, CTSE and GSTP1 were overexpressed in MCL	The results did not explain the involvement of the gene in normal cell respond

Table 11: Summary of the four studies

Collectively, the four studies were designed to understand the molecular regulation of HDACis in tumour and normal cells yet, each study came to different conclusions which may reflect the variation between the cell models used and the experimental approaches. The findings of these studies have been inadequate to demonstrate the cellular mechanism that reduce the hyperacetylation effect of HDACis. There are several factors that possibly contributed in limiting the research outcomes of these studies. For example, the cultured cells are often in different phases of the cell cycle and each phase has different gene expression. Hence, the bulk analysis results often present the average of the variations in gene expression of all the phases which could hide many cellular mechanisms and show some variations between biological replicates.

One of the objectives of this study was addressing the controversy about which HDACis treatment regime is better: treating with a selective HDACis (e.g. MS-275 (Entinostat)) or a pan-HDACis (e.g. SAHA (Vorinostat)). The data of this study did not allow to further explore this debate due to the low sequencing depth of the Daoy cells which may underrepresent some important regulations. No convincing experimental or clinical evidence is currently available to support using either type of HDACis. However, evidence from some clinical trials suggests that monotherapy of selective blocking of a HDAC or several HDACs might not be sufficient in achieving complete cell death^{254, 282, 283}.

Despite the promising results in some of the pre-clinical studies, most HDACis used in clinical trials failed to achieve the treatment goals as single agents²⁵⁴. Monotherapy treatment using HDACis have shown varying antitumor activity however, with some solid tumours they did not show a favourable outcome. In recent years, it has become abundantly obvious that HDACis are unlikely to make a substantial effect when used alone hence, a rational combination of therapy is largely important to induce more effective treatment. In clinical trials, many of the combination therapies that were performed using cytotoxic chemotherapy and hypomethylating drugs have not met the regulatory approval yet or been adopted in clinical use⁸⁰.

Combination treatment with DNA damaging agents or ionizing radiation has been reported to increase the DNA double-strand breaks and delay the tumour growth^{79, 100}. SAHA combination with DNA damaging agent has been reported to enhance the treatment through upregulating the expression of Bax (a proapoptotic gene) and downregulating RD51, RD55, Ku70, and ku86 expression which results in suppression of the DNA repair

mediated by homologous recombination^{79, 284}. Also, in a number of *in vitro* studies SAHA combination treatment with ionizing radiation and chemotherapy have been found to enhance the radio-sensitivity and promote apoptosis⁷⁹. Combination therapy with agent that interfere with cell cycle checkpoints, mitosis, antiapoptotic proteins, or proteasome activity has also shown an encouraging preclinical effectiveness^{79, 100}. Hopefully, the theoretical bases of HDACis in combination treatment will successfully be translated into more effective therapies to treat cancers in the near future. This will offer an advantage over the current conventional treatment which exhibit adverse side effect on normal cells.

The findings of this study have contributed in improving our understanding about the REST involvement in cancer regulation and suggested new conclusions about the contribution of REST expression in brain tumours. Also, it showed that the cancer cell growth does not mainly depend on REST expression otherwise, the treatment of cancer would become more approachable with modulating a single factor. Investigating the HDACis anticancer regulation in this study has provided a deeper understanding about the ability of HDACis to induce their effects across multiple pathways including the cell cycle, TNF α signalling via NF κ B pathway, Myc pathways, and inhibiting cell migration. Despite the relatively high tolerance of normal cell to HDACis however, this study demonstrated the ability of HDACis to cause considerable changes on the transcriptome level in normal cells. This study provides additional evidence with respect to the effect of HDACis on gene regulation in health and disease.

5.4 Future Work

The work presented in this thesis has potential to lead to deeper investigations of several molecular regulations however, they have been left for the future due to lack of time. There are number of research ideas that should be considered for future works:

The off-target effect of CRISPR/Cas9 in the KO cell clone was not examined in this study due to the high cost of the NGS analysis. It is highly recommended to sequence the KO cell clone genome.

The KO and KD cell clones showed a significant increase in the expression of the measured RE1 genes however, it has not been confirmed if the increase is caused as a results of direct REST modulation or due to a downstream effect. In future work, it is highly recommended to re-induce the expression of REST in order to approve the direct REST effect.

The Daoy cell line contains a subpopulation of CD133⁺ and CD133⁻ cells. In this study, the KO and KD cell clones were established from a single cell growth yet, it is not known if the cells expressing the CD133 marker. It is highly recommended to screen the cell marker of the KO and KD cells using the FACS analysis.

The findings of this study suggested that the expression of REST in the Daoy medulloblastoma cell line does not have a significant effect on cell growth and the cell continued to grow even in the absence of REST expression. However, this conclusion was built on one experimental cell model which represents the SHH medulloblastoma subtype. It is not completely known if the other cell models would show the same cell response to REST modulation. Also, it is not known if other cell lines are sensitivity to HDACis.

The findings of this study also showed that the HDACis induced Daoy cell death independent of DNA fragmentation. However, it is not known if this event was due to the dysregulation of the DNA fragmentation machinery in the Daoy cell or it was due to the ability of HDACis to induce a caspase-independent cell death.

Due to the low sequencing depth of the scNGS data, the results did not help in exploring the molecular regulation of the HDACis in tumour and normal cells. Future analysis should consider using high depth scNGS data in order to avoid the underrepresentation of genes. In additional to the gene expression analysis, the proteomic analysis using mass

spectrometry analysis can be used to characterize the affinity and selectivity of HDACis toward HDACs multiprotein complexes. Incorporating the proteomic and the genomic analysis can help in systematically and confidently determine the HDACis to HDACs interaction specificity.

As the effect of HDACis on gene expression could be a direct effect of increasing the promoter acetylation, or it could be due to a downstream effect, the chromatin immunoprecipitation followed by high-throughput DNA sequencing can be used in future analysis to determine the entire subset of genes targeted by HDACis which could help in clarifying their mechanism of action and assess in predicting inhibitor efficacy.

The results of treating the tumour cells with HDACis suggested the activation of TNF α signalling via NF κ B pathway. Whereas this signalling pathway is well investigated however, its contribution in HDACis anticancer effect remain a topic of investigation.

In literature, the regulation and function of HDACis in nonhistone protein compared with HDACs are still understudied, and the involvement of nonhistone in the HDACis anticancer regulation has not been well investigated. In order to gain more comprehensive understanding about the HDACis anticancer effect, the involvement of nonhistone proteins should be consider in future work.

The question of which treatment regime is better: the selective HDACis or the pan-HDACis remained unaddressed. Profiling the effect of HDACis at the transcriptome and proteome level may help in addressing this question.

Although the acetylation of histone tails has an effect on the stability of an individual nucleosome and the chromatin fibre however, it is not known if the cell death is due to the ability of HDACis to impair the DNA packaging regulation during mitosis.

5.5 Final Conclusion

In this thesis, I explored the contribution of REST, HDAC, and HDACis in medulloblastoma using CRISPR/Cas9 system and scNGS analysis. The experimental evidence of this thesis suggests the low importance of REST expression in regulating tumour cell growth or inducing cell death. It revealed also the ability of HDACis to induce their anticancer effect independent of HDACs recruited in REST repression. The data presented in this research demonstrated the ability of HDACis to alter gene expression and induce a considerable effect on the cell cycle, Myc and TNF α via NF κ B pathways. The central theme underlying the synergism between these pathways is their ability to inhibit the cell cycle regulation in tumour cells. Whatever the mechanisms involved, the data of my research suggest that the use of HDACis should carefully be revised even with their minimal side-effect in clinical trials.

Identifying the regulatory network is not the final outcome of a study rather, it is an intermediate stage connecting the genotype and the epigenotype to the global cell behaviours. Better understanding of the molecular networks of HDACs and the underlying anticancer mechanisms of HDACis and their off-target effects will certainly help in developing more rational HDACis treatment strategies. The research of HDACis has revealed several of significant findings that collectively have improved our understanding in cancer tumorigenesis and will have major contribution in clinical treatment.

6 Bibliography

1. Chong, J. A. *et al.* REST: a mammalian silencer protein that restricts sodium channel gene expression to neurons. *Cell* **80**, 949–957 (1995).
2. Wood, I. C. *et al.* Interaction of the repressor element 1-silencing transcription factor (REST) with target genes. *Journal of molecular biology* **334**, 863–874 (2003).
3. Otto, S. J. *et al.* A new binding motif for the transcriptional repressor REST uncovers large gene networks devoted to neuronal functions. *The Journal of neuroscience* **27**, 6729–6739 (2007).
4. Conti, L. *et al.* REST controls self-renewal and tumorigenic competence of human glioblastoma cells. *PloS one* **7**, e38486 (2012).
5. Johnson, R. *et al.* REST regulates distinct transcriptional networks in embryonic and neural stem cells. *PLoS biology* **6**, e256 (2008).
6. Ma, X., Ezzeldin, H. & Diasio, R. Histone deacetylase inhibitors: current status and overview of recent clinical trials.(vol 69, pg 1911, 2009). *DRUGS* **69**, 2102–2102 (2009).
7. Wagoner, M. P. *et al.* The transcription factor REST is lost in aggressive breast cancer. *PLoS genetics* **6**, e1000979 (2010).
8. Westbrook, T. F. *et al.* A genetic screen for candidate tumor suppressors identifies REST. *Cell* **121**, 837–848 (2005).
9. Jørgensen, H. F. *et al.* REST selectively represses a subset of RE1-containing neuronal genes in mouse embryonic stem cells. *Development* **136**, 715–721 (2009).
10. Majumader, S. REST in good times and bad: roles in tumor suppressor and oncogenic activities. *Cell Cycle* **5**, 1929–1935 (2006).
11. Fuller, G. N. *et al.* Many human medulloblastoma tumors overexpress repressor element-1 silencing transcription (REST)/neuron-restrictive silencer factor, which can be functionally countered by REST-VP16. *Molecular cancer therapeutics* **4**, 343–349 (2005).
12. Zhang, D. *et al.* Inhibition of REST Suppresses Proliferation and Migration in Glioblastoma Cells. *International journal of molecular sciences* **17**, 664 (2016).
13. Kamal, M. M. *et al.* REST regulates oncogenic properties of glioblastoma stem cells. *Stem Cells* **30**, 405–414 (2012).
14. Taylor, P. *et al.* REST is a novel prognostic factor and therapeutic target for medulloblastoma. *Molecular cancer therapeutics* **11**, 1713–1723 (2012).

15. Da Silva, P. B. G. *et al.* Establishment of a novel human medulloblastoma cell line characterized by highly aggressive stem-like cells. *Cytotechnology* **68**, 1545–1560 (2016).
16. Faronato, M. & Coulson, J. M. REST (RE1-silencing transcription factor). <http://AtlasGeneticsOncology.org> 208 (2011).
17. Raj, B. *et al.* Cross-regulation between an alternative splicing activator and a transcription repressor controls neurogenesis. *Molecular cell* **43**, 843–850 (2011).
18. Chen, G.-L. & Miller, G. M. Extensive alternative splicing of the repressor element silencing transcription factor linked to cancer. *PLoS One* **8**, e62217 (2013).
19. Huang, Z. & Bao, S. Ubiquitination and deubiquitination of REST and its roles in cancers. *FEBS letters* **586**, 1602–1605 (2012).
20. Johnson, R. *et al.* Identification of the REST regulon reveals extensive transposable element-mediated binding site duplication. *Nucleic acids research* **34**, 3862–3877 (2006).
21. Mortazavi, A., Thompson, E. C. L., Garcia, S. T., Myers, R. M. & Wold, B. Comparative genomics modeling of the NRSF/REST repressor network: from single conserved sites to genome-wide repertoire. *Genome research* **16**, 1208–1221 (2006).
22. Bruce, A. W. *et al.* The transcriptional repressor REST is a critical regulator of the neurosecretory phenotype. *Journal of neurochemistry* **98**, 1828–1840 (2006).
23. Gao, Z. *et al.* The master negative regulator REST/NRSF controls adult neurogenesis by restraining the neurogenic program in quiescent stem cells. *The Journal of Neuroscience* **31**, 9772–9786 (2011).
24. Calderone, A. *et al.* Ischemic insults derepress the gene silencer REST in neurons destined to die. *The Journal of neuroscience* **23**, 2112–2121 (2003).
25. Ooi, L. & Wood, I. C. Chromatin crosstalk in development and disease: lessons from REST. *Nat. Rev. Genet.* **8**, 544–54 (2007).
26. Li, K. K. W. *et al.* miR-124 is frequently down-regulated in medulloblastoma and is a negative regulator of SLC16A1. *Hum. Pathol.* **40**, 1234–43 (2009).
27. Nesti, E., Corson, G. M., McCleskey, M., Oyer, J. A. & Mandel, G. C-terminal domain small phosphatase 1 and MAP kinase reciprocally control REST stability and neuronal differentiation. *Proceedings of the National Academy of Sciences* **111**, E3929–E3936 (2014).
28. Wan, M. *et al.* SCF beta-TrCP1 controls Smad4 protein stability in pancreatic cancer cells. *The American journal of pathology* **166**, 1379–1392 (2005).

29. Willis, N. A. *et al.* BRCA1 controls homologous recombination at Tus/Ter-stalled mammalian replication forks. *Nature* (2014). doi:10.1038/nature13295
30. Satoh, J., Kawana, N. & Yamamoto, Y. ChiP-seq data mining: remarkable differences in nr5f/rEst target genes between human Esc and Esc-derived neurons. *Bioinformatics and Biology insights* **7**, 357 (2013).
31. Ooi, L., Belyaev, N. D., Miyake, K., Wood, I. C. & Buckley, N. J. BRG1 chromatin remodeling activity is required for efficient chromatin binding by repressor element 1-silencing transcription factor (REST) and facilitates REST-mediated repression. *Journal of Biological Chemistry* **281**, 38974–38980 (2006).
32. Inui, K. *et al.* Stepwise assembly of functional C-terminal REST/NRSF transcriptional repressor complexes as a drug target. *Protein Science* **26**, 997–1011 (2017).
33. Ballas, N., Grunseich, C., Lu, D. D., Speh, J. C. & Mandel, G. REST and its corepressors mediate plasticity of neuronal gene chromatin throughout neurogenesis. *Cell* **121**, 645–657 (2005).
34. Aguilera, D. G. *et al.* Reactivation of death receptor 4 (DR4) expression sensitizes medulloblastoma cell lines to TRAIL. *Journal of neuro-oncology* **93**, 303–318 (2009).
35. Gong, C. *et al.* Stimulation of medulloblastoma stem cells differentiation by a peptidomimetic targeting neuropilin-1. *Oncotarget* **9**, 15312 (2018).
36. Huang, G.-H. *et al.* Medulloblastoma stem cells: Promising targets in medulloblastoma therapy. *Cancer science* **107**, 583–589 (2016).
37. Wu, X. *et al.* Clonal selection drives genetic divergence of metastatic medulloblastoma. *Nature* **482**, 529–533 (2012).
38. Thompson, M. C. *et al.* Genomics identifies medulloblastoma subgroups that are enriched for specific genetic alterations. *Journal of Clinical Oncology* **24**, 1924–1931 (2006).
39. Jones, D. T. *et al.* ICGC PedBrain: dissecting the genomic complexity underlying medulloblastoma. *Nature* **488**, 100 (2012).
40. Phoenix, T. N. *et al.* Medulloblastoma genotype dictates blood brain barrier phenotype. *Cancer cell* **29**, 508–522 (2016).
41. Cavalli, F. M. *et al.* Intertumoral Heterogeneity within Medulloblastoma Subgroups. *Cancer Cell* **31**, 737–754 (2017).
42. Pugh, T. J. *et al.* Medulloblastoma exome sequencing uncovers subtype-specific somatic mutations. *Nature* **488**, 106–110 (2012).

43. Ivanov, D. P., Coyle, B., Walker, D. A. & Grabowska, A. M. In vitro models of medulloblastoma: Choosing the right tool for the job. *Journal of Biotechnology* **236**, 10–25 (2016).
44. Hooper, C. M., Hawes, S. M., Kees, U. R., Gottardo, N. G. & Dallas, P. B. Gene Expression Analyses of the Spatio-Temporal Relationships of Human Medulloblastoma Subgroups during Early Human Neurogenesis. *PLoS one* **9**, e112909 (2014).
45. Roussel, M. F. & Stripay, J. L. Epigenetic drivers in pediatric medulloblastoma. *The Cerebellum* 1–9 (2017).
46. Ellison, D. W. *et al.* Definition of disease-risk stratification groups in childhood medulloblastoma using combined clinical, pathologic, and molecular variables. *Journal of Clinical Oncology* JCO–2010 (2010).
47. Lou, E. *et al.* Complete and sustained response of adult medulloblastoma to first-line sonic hedgehog inhibition with vismodegib. *Cancer biology & therapy* **17**, 1010–1016 (2016).
48. Packer, R. J., Zhou, T., Holmes, E., Vezina, G. & Gajjar, A. Survival and secondary tumors in children with medulloblastoma receiving radiotherapy and adjuvant chemotherapy: results of Children’s Oncology Group trial A9961. *Neuro-oncology* **15**, 97–103 (2012).
49. Fossati, P., Ricardi, U. & Orecchia, R. Pediatric medulloblastoma: toxicity of current treatment and potential role of protontherapy. *Cancer treatment reviews* **35**, 79–96 (2009).
50. Su, X., Kameoka, S., Lentz, S. & Majumder, S. Activation of REST/NRSF Target Genes in Neural Stem Cells Is Sufficient To Cause Neuronal Differentiation. *Mol. Cell. Biol.* **24**, 8018–8025 (2004).
51. Gopalakrishnan, V. REST and the RESTless: in stem cells and beyond. (2009).
52. Das, C. M. *et al.* The deubiquitylase USP37 links REST to the control of p27 stability and cell proliferation. *Oncogene* **32**, 1691–1701 (2013).
53. Su, X. *et al.* Abnormal expression of REST/NRSF and Myc in neural stem/progenitor cells causes cerebellar tumors by blocking neuronal differentiation. *Molecular and cellular biology* **26**, 1666–1678 (2006).
54. Ecker, J. *et al.* Targeting class I histone deacetylase 2 in MYC amplified group 3 medulloblastoma. *Acta neuropathologica communications* **3**, 1 (2015).
55. Micelli, C. & Rastelli, G. Histone deacetylases: structural determinants of inhibitor selectivity. *Drug discovery today* (2015).

56. Jones, D. T., Northcott, P. A., Kool, M. & Pfister, S. M. The role of chromatin remodeling in medulloblastoma. *Brain Pathology* **23**, 193–199 (2013).
57. Ogiwara, H. *et al.* Targeting p300 addiction in CBP-deficient cancers causes synthetic lethality by apoptotic cell death due to abrogation of MYC expression. *Cancer discovery* **6**, 430–445 (2016).
58. Haberland, M., Montgomery, R. L. & Olson, E. N. The many roles of histone deacetylases in development and physiology: implications for disease and therapy. *Nature Reviews Genetics* **10**, 32–42 (2009).
59. Gil, J., Ramirez-Torres, A. & Encarnación-Guevara, S. Lysine acetylation and cancer: A proteomics perspective. *Journal of Proteomics* **150**, 297–309 (2017).
60. Ververis, K., Hiong, A., Karagiannis, T. C. & Licciardi, P. V. Histone deacetylase inhibitors (HDACs): multitargeted anticancer agents. *Biologics: targets & therapy* **7**, 47 (2013).
61. Chen, H. P., Zhao, Y. T. & Zhao, T. C. Histone deacetylases and mechanisms of regulation of gene expression. *Critical ReviewsTM in Oncogenesis* **20**, (2015).
62. Wagner, J. M., Hackanson, B., Lübbert, M. & Jung, M. Histone deacetylase (HDAC) inhibitors in recent clinical trials for cancer therapy. *Clinical epigenetics* **1**, 117 (2010).
63. Miller, K. M. *et al.* Human HDAC1 and HDAC2 function in the DNA-damage response to promote DNA nonhomologous end-joining. *Nature structural & molecular biology* **17**, 1144–1151 (2010).
64. Bhaskara, S. *et al.* Deletion of histone deacetylase 3 reveals critical roles in S phase progression and DNA damage control. *Molecular cell* **30**, 61–72 (2008).
65. Yan, W. *et al.* Histone deacetylase inhibitors suppress mutant p53 transcription via histone deacetylase 8. *Oncogene* **32**, 599–609 (2013).
66. Martin, M., Kettmann, R. & Dequiedt, F. Class IIa histone deacetylases: regulating the regulators. *Oncogene* **26**, 5450–5467 (2007).
67. Özdag, H. *et al.* Differential expression of selected histone modifier genes in human solid cancers. *BMC genomics* **7**, 90 (2006).
68. Milde, T. *et al.* HDAC5 and HDAC9 in medulloblastoma: novel markers for risk stratification and role in tumor cell growth. *Clinical Cancer Research* **16**, 3240–3252 (2010).
69. Wang, Z. *et al.* HDAC6 promotes cell proliferation and confers resistance to temozolomide in glioblastoma. *Cancer letters* **379**, 134–142 (2016).

70. Deubzer, H. E. *et al.* HDAC11 is a novel drug target in carcinomas. *International journal of cancer* **132**, 2200–2208 (2013).
71. Coni, S. *et al.* Selective targeting of HDAC1/2 elicits anticancer effects through Gli1 acetylation in preclinical models of SHH Medulloblastoma. *Scientific Reports* **7**, 44079 (2017).
72. Rettig, I. *et al.* Selective inhibition of HDAC8 decreases neuroblastoma growth in vitro and in vivo and enhances retinoic acid-mediated differentiation. *Cell death & disease* **6**, e1657 (2015).
73. Oehme, I. *et al.* Histone deacetylase 10 promotes autophagy-mediated cell survival. *Proceedings of the National Academy of Sciences* **110**, E2592–E2601 (2013).
74. Lee, S. J. *et al.* Sonic hedgehog-induced histone deacetylase activation is required for cerebellar granule precursor hyperplasia in medulloblastoma. *PloS one* **8**, e71455 (2013).
75. Li, Z. & Zhu, W.-G. Targeting histone deacetylases for cancer therapy: from molecular mechanisms to clinical implications. *International journal of biological sciences* **10**, 757 (2014).
76. Suresh, P., Devaraj, V., Srinivas, N. R. & Mullangi, R. Review of bioanalytical assays for the quantitation of various HDAC inhibitors such as vorinostat, belinostat, panobinostat, romidepsin and chidamine. *Biomedical Chromatography* **31**, e3807 (2017).
77. Sharma, S., Kelly, T. K. & Jones, P. A. Epigenetics in cancer. *Carcinogenesis* **31**, 27–36 (2010).
78. New, M., Olzscha, H. & La Thangue, N. B. HDAC inhibitor-based therapies: Can we interpret the code? *Molecular oncology* **6**, 637–656 (2012).
79. Wu, Z. *et al.* The effects of SAHA on radiosensitivity in pancreatic cancer cells by inducing apoptosis and targeting RAD51. *Biomedicine & Pharmacotherapy* **89**, 705–710 (2017).
80. Bose, P., Dai, Y. & Grant, S. Histone deacetylase inhibitor (HDACI) mechanisms of action: emerging insights. *Pharmacology & therapeutics* **143**, 323–336 (2014).
81. Häcker, S. *et al.* Histone deacetylase inhibitors prime medulloblastoma cells for chemotherapy-induced apoptosis by enhancing p53-dependent Bax activation. *Oncogene* **30**, 2275–2281 (2011).
82. Gillenwater, A. M., Zhong, M. & Lotan, R. Histone deacetylase inhibitor suberoylanilide hydroxamic acid induces apoptosis through both mitochondrial and Fas (Cd95) signaling in head and neck squamous carcinoma cells. *Molecular cancer therapeutics* **6**, 2967–2975 (2007).

83. Newbold, A., Falkenberg, K. J., Prince, H. M. & Johnstone, R. W. How do tumor cells respond to HDAC inhibition? *The FEBS journal* **283**, 4032–4046 (2016).
84. Kachhap, S. K. *et al.* Downregulation of homologous recombination DNA repair genes by HDAC inhibition in prostate cancer is mediated through the E2F1 transcription factor. *PloS one* **5**, e11208 (2010).
85. Hrgovic, I. *et al.* Histone deacetylase inhibitors interfere with angiogenesis by decreasing endothelial VEGFR-2 protein half-life in part via a VE-cadherin-dependent mechanism. *Experimental dermatology* **26**, 194–201 (2017).
86. Yamaguchi, T. *et al.* Histone deacetylases 1 and 2 act in concert to promote the G1-to-S progression. *Genes & development* **24**, 455–469 (2010).
87. Mottet, D. *et al.* HDAC4 represses p21WAF1/Cip1 expression in human cancer cells through a Sp1-dependent, p53-independent mechanism. *Oncogene* **28**, 243–256 (2009).
88. Kelly, W. K. & Marks, P. A. Drug insight: histone deacetylase inhibitors—development of the new targeted anticancer agent suberoylanilide hydroxamic acid. *Nature Reviews Clinical Oncology* **2**, 150 (2005).
89. Mann, B. S. *et al.* Vorinostat for treatment of cutaneous manifestations of advanced primary cutaneous T-cell lymphoma. *Clinical Cancer Research* **13**, 2318–2322 (2007).
90. Mahalingam, D. *et al.* Combined autophagy and HDAC inhibition: a phase I safety, tolerability, pharmacokinetic, and pharmacodynamic analysis of hydroxychloroquine in combination with the HDAC inhibitor vorinostat in patients with advanced solid tumors. *Autophagy* **10**, 1403–1414 (2014).
91. Lauffer, B. E. *et al.* Histone deacetylase (HDAC) inhibitor kinetic rate constants correlate with cellular histone acetylation but not transcription and cell viability. *Journal of Biological Chemistry* **288**, 26926–26943 (2013).
92. Connolly, R. M., Rudek, M. A. & Piekarz, R. Entinostat: a promising treatment option for patients with advanced breast cancer. *Future Oncology* **13**, 1137–1148 (2017).
93. Marinova, Z., Leng, Y., Leeds, P. & Chuang, D.-M. Histone deacetylase inhibition alters histone methylation associated with heat shock protein 70 promoter modifications in astrocytes and neurons. *Neuropharmacology* **60**, 1109–1115 (2011).
94. Rosato, R. R., Almenara, J. A. & Grant, S. The histone deacetylase inhibitor MS-275 promotes differentiation or apoptosis in human leukemia cells through a process regulated by generation of reactive oxygen species and induction of p21CIP1/WAF1 1. *Cancer research* **63**, 3637–3645 (2003).

95. Boissinot, M. *et al.* Induction of differentiation and apoptosis in leukaemic cell lines by the novel benzamide family histone deacetylase 2 and 3 inhibitor MI-192. *Leukemia research* **36**, 1304–1310 (2012).
96. Adhikari, N., Amin, S. A., Trivedi, P., Jha, T. & Ghosh, B. HDAC3 is a potential validated target for cancer: An overview on the benzamide-based selective HDAC3 inhibitors through comparative SAR/QSAR/QAAR approaches. *European journal of medicinal chemistry* (2018).
97. Choi, J. H. *et al.* Apicidin induces endoplasmic reticulum stress-and mitochondrial dysfunction-associated apoptosis via phospholipase C γ 1-and Ca²⁺-dependent pathway in mouse Neuro-2a neuroblastoma cells. *Apoptosis* **17**, 1340–1358 (2012).
98. Cheong, J.-W. *et al.* Induction of apoptosis by apicidin, a histone deacetylase inhibitor, via the activation of mitochondria-dependent caspase cascades in human Bcr-Abl-positive leukemia cells. *Clinical Cancer Research* **9**, 5018–5027 (2003).
99. Caponigro, F. *et al.* Phase II clinical study of valproic acid plus cisplatin and cetuximab in recurrent and/or metastatic squamous cell carcinoma of Head and Neck-V-CHANCE trial. *BMC cancer* **16**, 918 (2016).
100. Thotala, D. *et al.* Valproic acid enhances the efficacy of radiation therapy by protecting normal hippocampal neurons and sensitizing malignant glioblastoma cells. *Oncotarget* **6**, 35004 (2015).
101. Shi, P. *et al.* Synapse microarray identification of small molecules that enhance synaptogenesis. *Nature communications* **2**, 510 (2011).
102. Montgomery, R. L., Hsieh, J., Barbosa, A. C., Richardson, J. A. & Olson, E. N. Histone deacetylases 1 and 2 control the progression of neural precursors to neurons during brain development. *Proceedings of the National Academy of Sciences* **106**, 7876–7881 (2009).
103. Northcott, P. A. *et al.* Medulloblastoma comprises four distinct molecular variants. *Journal of Clinical Oncology* **29**, 1408–1414 (2011).
104. Parsons, D. W. *et al.* The genetic landscape of the childhood cancer medulloblastoma. *Science* **331**, 435–439 (2011).
105. Bolden, J. *et al.* HDAC inhibitors induce tumor-cell-selective pro-apoptotic transcriptional responses. *Cell death & disease* **4**, e519 (2013).
106. Franci, G. *et al.* The class I-specific HDAC inhibitor MS-275 modulates the differentiation potential of mouse embryonic stem cells. *Biology open* **BIO20135587** (2013).
107. Drogaris, P. *et al.* Histone deacetylase inhibitors globally enhance h3/h4 tail acetylation without affecting h3 lysine 56 acetylation. *Scientific reports* **2**, 220 (2012).

108. Sanders, Y. Y. *et al.* Histone deacetylase inhibition promotes fibroblast apoptosis and ameliorates pulmonary fibrosis in mice. *European Respiratory Journal* **erj00951–2013** (2014).
109. Namekawa, T., Ikeda, K., Horie-Inoue, K. & Inoue, S. Application of Prostate Cancer Models for Preclinical Study: Advantages and Limitations of Cell Lines, Patient-Derived Xenografts, and Three-Dimensional Culture of Patient-Derived Cells. *Cells* **8**, 74 (2019).
110. Kaur, G. & Dufour, J. M. Cell lines: Valuable tools or useless artifacts. (2012).
111. Jedrzejczak-Silicka, M. in *New Insights into Cell Culture Technology* (IntechOpen, 2017).
112. Jacobsen, P., Jenkyn, D. & Papadimitriou, J. Establishment of a human medulloblastoma cell line and its heterotransplantation into nude mice. *Journal of Neuropathology & Experimental Neurology* **44**, 472–485 (1985).
113. Wayne, S. *et al.* The p53 tumor suppressor protein protects against chemotherapeutic stress and apoptosis in human medulloblastoma cells. *Aging (Albany NY)* **7**, 854 (2015).
114. Srivastava, V. K. & Nalbantoglu, J. Flow cytometric characterization of the DAOY medulloblastoma cell line for the cancer stem-like phenotype. *Cytometry Part A* **73**, 940–948 (2008).
115. Lawinger, P. *et al.* The neuronal repressor REST/NRSF is an essential regulator in medulloblastoma cells. *Nature medicine* **6**, 826–831 (2000).
116. Huang, Z. *et al.* Deubiquitylase HAUSP stabilizes REST and promotes maintenance of neural progenitor cells. *Nature cell biology* **13**, 142–152 (2011).
117. Watanabe, Y. *et al.* Conversion of myoblasts to physiologically active neuronal phenotype. *Genes & development* **18**, 889–900 (2004).
118. Hsu, P. D., Lander, E. S. & Zhang, F. Development and applications of CRISPR-Cas9 for genome engineering. *Cell* **157**, 1262–1278 (2014).
119. Wilson, R. C. & Doudna, J. A. Molecular mechanisms of RNA interference. *Annual review of biophysics* **42**, 217–239 (2013).
120. Vara, J., Perez-Gonzalez, J. A. & Jimenez, A. Biosynthesis of puromycin by *Streptomyces alboniger*: characterization of puromycin N-acetyltransferase. *Biochemistry* **24**, 8074–8081 (1985).
121. Haque, A., Engel, J., Teichmann, S. A. & Lönnberg, T. A practical guide to single-cell RNA-sequencing for biomedical research and clinical applications. *Genome medicine* **9**, 75 (2017).

122. Cong, L. *et al.* Multiplex genome engineering using CRISPR/Cas systems. *Science* **339**, 819–23 (2013).
123. Gebäck, T., Schulz, M. M. P., Koumoutsakos, P. & Detmar, M. TScratch: a novel and simple software tool for automated analysis of monolayer wound healing assays: Short Technical Reports. *Biotechniques* **46**, 265–274 (2009).
124. Darzynkiewicz, Z. Critical aspects in analysis of cellular DNA content. *Current protocols in cytometry* 7–2 (2010).
125. Satija, R., Farrell, J. A., Gennert, D., Schier, A. F. & Regev, A. Spatial reconstruction of single-cell gene expression data. *Nature biotechnology* **33**, 495 (2015).
126. Lun, A. T., McCarthy, D. J. & Marioni, J. C. A step-by-step workflow for low-level analysis of single-cell RNA-seq data with Bioconductor. *F1000Research* **5**, (2016).
127. Chung, N. C. & Storey, J. D. Statistical significance of variables driving systematic variation in high-dimensional data. *Bioinformatics* **31**, 545–554 (2014).
128. Kowalczyk, M. S. *et al.* Single-cell RNA-seq reveals changes in cell cycle and differentiation programs upon aging of hematopoietic stem cells. *Genome research* (2015).
129. Xu, X., Wells, A. B., O'Brien, D. R., Nehorai, A. & Dougherty, J. D. Cell type-specific expression analysis to identify putative cellular mechanisms for neurogenetic disorders. *Journal of Neuroscience* **34**, 1420–1431 (2014).
130. Wang, J.-H. *et al.* GenCLiP 2.0: a web server for functional clustering of genes and construction of molecular networks based on free terms. *Bioinformatics* **30**, 2534–2536 (2014).
131. Subramanian, A. *et al.* Gene set enrichment analysis: a knowledge-based approach for interpreting genome-wide expression profiles. *Proceedings of the National Academy of Sciences* **102**, 15545–15550 (2005).
132. Kutmon, M. *et al.* PathVisio 3: an extendable pathway analysis toolbox. *PLoS computational biology* **11**, e1004085 (2015).
133. Slenter, D. N. *et al.* WikiPathways: a multifaceted pathway database bridging metabolomics to other omics research. *Nucleic acids research* **46**, D661–D667 (2017).
134. Rivero-Hinojosa, S. *et al.* Proteomic analysis of Medulloblastoma reveals functional biology with translational potential. *Acta neuropathologica communications* **6**, 48 (2018).
135. Chen-Plotkin, A. S. *et al.* Variations in the progranulin gene affect global gene expression in frontotemporal lobar degeneration. *Human molecular genetics* **17**,

- 1349–1362 (2008).
136. Henriquez, N. V. *et al.* Comparative expression analysis reveals lineage relationships between human and murine gliomas and a dominance of glial signatures during tumour propagation in vitro. *Cancer research* **canres–1299** (2013).
 137. Svoboda, L. K. *et al.* Overexpression of HOX genes is prevalent in Ewing sarcoma and is associated with altered epigenetic regulation of developmental transcription programs. *Epigenetics* **9**, 1613–1625 (2014).
 138. Amani, V. *et al.* Characterization of 2 Novel Ependymoma Cell Lines With Chromosome 1q Gain Derived From Posterior Fossa Tumors of Childhood. *Journal of Neuropathology & Experimental Neurology* **76**, 595–604 (2017).
 139. Ngo, T., Barisone, G. A., Lam, K. S. & D'acutet\iotaaz, E. MXD3 regulation of DAOY cell proliferation dictated by time course of activation. *BMC cell biology* **15**, 30 (2014).
 140. Vogel, C. *et al.* Sequence signatures and mRNA concentration can explain two-thirds of protein abundance variation in a human cell line. *Molecular systems biology* **6**, 400 (2010).
 141. Da Silva, P. B. G. *et al.* High OCT4A levels drive tumorigenicity and metastatic potential of medulloblastoma cells. *Oncotarget* **8**, 19192 (2017).
 142. Barrett, T. *et al.* NCBI GEO: archive for functional genomics data sets—update. *Nucleic acids research* **41**, D991–D995 (2012).
 143. Sharov, A. A., Schlessinger, D. & Ko, M. S. ExAtlas: An interactive online tool for meta-analysis of gene expression data. *Journal of bioinformatics and computational biology* **13**, 1550019 (2015).
 144. Babicki, S. *et al.* Heatmapper: web-enabled heat mapping for all. *Nucleic acids research* **44**, W147–W153 (2016).
 145. Bruce, A. W. *et al.* Genome-wide analysis of repressor element 1 silencing transcription factor/neuron-restrictive silencing factor (REST/NRSF) target genes. *Proc. Natl. Acad. Sci. U.S.A.* **101**, 10458–63 (2004).
 146. Eckschlager, T., Plch, J., Stiborova, M. & Hrabeta, J. Histone deacetylase inhibitors as anticancer drugs. *International journal of molecular sciences* **18**, 1414 (2017).
 147. Yin, Y. *et al.* Histone deacetylase 3 overexpression in human cholangiocarcinoma and promotion of cell growth via apoptosis inhibition. *Cell death & disease* **8**, e2856 (2017).
 148. Grabarska, A. *et al.* Histone Deacetylase Inhibitor SAHA as Potential Targeted Therapy Agent for Larynx Cancer Cells. *Journal of Cancer* **8**, 19 (2017).

149. Ungerstedt, J. *et al.* Role of thioredoxin in the response of normal and transformed cells to histone deacetylase inhibitors. *Proceedings of the National Academy of Sciences of the United States of America* **102**, 673–678 (2005).
150. Kwon, S. H. *et al.* Apicidin, a histone deacetylase inhibitor, induces apoptosis and Fas/Fas ligand expression in human acute promyelocytic leukemia cells. *Journal of Biological Chemistry* **277**, 2073–2080 (2002).
151. Lee, E. J. *et al.* Histone deacetylase inhibitor scriptaid induces cell cycle arrest and epigenetic change in colon cancer cells. *International journal of oncology* **33**, 767–776 (2008).
152. Finzer, P., Kuntzen, C., Soto, U., zur Hausen, H. & Rösl, F. Inhibitors of histone deacetylase arrest cell cycle and induce apoptosis in cervical carcinoma cells circumventing human papillomavirus oncogene expression. *Oncogene* **20**, 4768 (2001).
153. Dong, Z. *et al.* HDAC inhibitor PAC-320 induces G2/M cell cycle arrest and apoptosis in human prostate cancer. *Oncotarget* **9**, 512 (2018).
154. Bernhart, E. *et al.* Histone deacetylase inhibitors vorinostat and panobinostat induce G1 cell cycle arrest and apoptosis in multidrug resistant sarcoma cell lines. *Oncotarget* **8**, 77254–77267 (2017).
155. Vermes, I., Haanen, C. & Reutelingsperger, C. Flow cytometry of apoptotic cell death. *Journal of immunological methods* **243**, 167–190 (2000).
156. Darzynkiewicz, Z., Halicka, H. D. & Zhao, H. in *Polyploidization and Cancer* 137–147 (Springer, 2010).
157. Pozarowski, P. & Darzynkiewicz, Z. in *Checkpoint Controls and Cancer* 301–311 (Springer, 2004).
158. Debode, F., Marien, A., Janssen, É., Bragard, C. & Berben, G. Influence of the amplicon length on real-time PCR results. *Biotechnologie, Agronomie, Société et Environnement* **21**, 3–11 (2017).
159. Manterola, L. *et al.* A small noncoding RNA signature found in exosomes of GBM patient serum as a diagnostic tool. *Neuro-oncology* **16**, 520–527 (2014).
160. Ma, C. *et al.* A comprehensive meta-analysis of circulation miRNAs in glioma as potential diagnostic biomarker. *PloS one* **13**, e0189452 (2018).
161. Rice, J., Roberts, H., Rai, S. N. & Galandiuk, S. Housekeeping genes for studies of plasma microRNA: A need for more precise standardization. *Surgery* **158**, 1345–1351 (2015).
162. Chen, G.-L. & Miller, G. M. Alternative REST Splicing Underappreciated. *eNeuro* **5**, (2018).

163. Kool, M. *et al.* Molecular subgroups of medulloblastoma: an international meta-analysis of transcriptome, genetic aberrations, and clinical data of WNT, SHH, Group 3, and Group 4 medulloblastomas. *Acta neuropathologica* **123**, 473–484 (2012).
164. Schroeder, K. & Gururangan, S. Molecular variants and mutations in medulloblastoma. *Pharmacogenomics and personalized medicine* **7**, 43 (2014).
165. Nyegaard, S., Christensen, B. & Rasmussen, J. T. An optimized method for accurate quantification of cell migration using human small intestine cells. *Metabolic Engineering Communications* **3**, 76–83 (2016).
166. Chueh, A. C., Tse, J. W., Tögel, L. & Mariadason, J. M. Mechanisms of histone deacetylase inhibitor-regulated gene expression in cancer cells. *Antioxidants & redox signaling* **23**, 66–84 (2015).
167. Marks, P. & Xu, W.-S. Histone deacetylase inhibitors: Potential in cancer therapy. *Journal of cellular biochemistry* **107**, 600–608 (2009).
168. Watson, P. J. *et al.* Insights into the activation mechanism of class I HDAC complexes by inositol phosphates. *Nature communications* **7**, 11262 (2016).
169. Shimojo, M. & Hersh, L. B. Regulation of the cholinergic gene locus by the repressor element-1 silencing transcription factor/neuron restrictive silencer factor (REST/NRSF). *Life sciences* **74**, 2213–2225 (2004).
170. Yu, M. *et al.* Alteration of NRSF expression exacerbating 1-methyl-4-phenylpyridinium ion-induced cell death of SH-SY5Y cells. *Neuroscience research* **65**, 236–244 (2009).
171. Felisbino, M. B., Tamashiro, W. M. & Mello, M. L. S. Chromatin remodeling, cell proliferation and cell death in valproic acid-treated HeLa cells. *PLoS One* **6**, e29144 (2011).
172. Anastas, J. N. & Moon, R. T. WNT signalling pathways as therapeutic targets in cancer. *Nature reviews. Cancer* **13**, 11 (2013).
173. Lin, C.-M. *et al.* Apigenin-induced lysosomal degradation of beta-catenin in Wnt/beta-catenin signaling. *Scientific Reports* **7**, 372 (2017).
174. Nishihara, S., Tsuda, L. & Ogura, T. The canonical Wnt pathway directly regulates NRSF/REST expression in chick spinal cord. *Biochemical and biophysical research communications* **311**, 55–63 (2003).
175. Gupta, S., Takebe, N. & LoRusso, P. Targeting the Hedgehog pathway in cancer. *Therapeutic advances in medical oncology* **2**, 237–250 (2010).
176. Ruch, J. M. & Kim, E. J. Hedgehog signaling pathway and cancer therapeutics: progress to date. *Drugs* **73**, 613–623 (2013).

177. Halder, D. *et al.* Suppression of Sin3A activity promotes differentiation of pluripotent cells into functional neurons. *Scientific Reports* **7**, (2017).
178. Yu, H.-B., Johnson, R., Kunarso, G. & Stanton, L. W. Coassembly of REST and its cofactors at sites of gene repression in embryonic stem cells. *Genome research* **21**, 1284–1293 (2011).
179. Gulino, R. & Gulisano, M. Involvement of brain-derived neurotrophic factor and sonic hedgehog in the spinal cord plasticity after neurotoxic partial removal of lumbar motoneurons. *Neuroscience research* **73**, 238–247 (2012).
180. Gulino, R., Parenti, R. & Gulisano, M. Sonic Hedgehog and TDP-43 Participate in the Spontaneous Locomotor Recovery in a Mouse Model of Spinal Motoneuron Disease. *Journal of Functional Morphology and Kinesiology* **2**, 11 (2017).
181. Zhang, L. *et al.* Bakkenolide A inhibits leukemia by regulation of HDAC3 and PI3K/Akt-related signaling pathways. *Biomedicine & Pharmacotherapy* **83**, 958–966 (2016).
182. Ueda, T., Takai, N., Nishida, M., Nasu, K. & Narahara, H. Apicidin, a novel histone deacetylase inhibitor, has profound anti-growth activity in human endometrial and ovarian cancer cells. *International journal of molecular medicine* **19**, 301–308 (2007).
183. Han, J.-W. *et al.* Apicidin, a histone deacetylase inhibitor, inhibits proliferation of tumor cells via induction of p21WAF1/Cip1 and gelsolin. *Cancer research* **60**, 6068–6074 (2000).
184. Khan, N. *et al.* Determination of the class and isoform selectivity of small-molecule histone deacetylase inhibitors. *Biochemical Journal* **409**, 581–589 (2008).
185. Rao-Bindal, K., Zhou, Z. & Kleinerman, E. MS-275 sensitizes osteosarcoma cells to Fas ligand-induced cell death by increasing the localization of Fas in membrane lipid rafts. *Cell death & disease* **3**, e369 (2012).
186. Pingoud-Meier, C. *et al.* Loss of caspase-8 protein expression correlates with unfavorable survival outcome in childhood medulloblastoma. *Clinical Cancer Research* **9**, 6401–6409 (2003).
187. Wang, Q. *et al.* Down-regulation of cellular FLICE-inhibitory protein (Long Form) contributes to apoptosis induced by Hsp90 inhibition in human lung cancer cells. *Cancer cell international* **12**, 54 (2012).
188. Chen, Y., Tsai, Y.-H. & Tseng, S.-H. HDAC Inhibitors and RECK Modulate Endoplasmic Reticulum Stress in Tumor Cells. *International Journal of Molecular Sciences* **18**, 258 (2017).
189. Baumeister, P., Dong, D., Fu, Y. & Lee, A. S. Transcriptional induction of GRP78/BiP by histone deacetylase inhibitors and resistance to histone deacetylase

- inhibitor-induced apoptosis. *Molecular cancer therapeutics* **8**, 1086–1094 (2009).
190. Spiller, S. E., Ravanpay, A. C., Hahn, A. W. & Olson, J. M. Suberoylanilide hydroxamic acid is effective in preclinical studies of medulloblastoma. *Journal of neuro-oncology* **79**, 259–270 (2006).
 191. Lakshmikanthan, V., Kaddour-Djebbar, I., Lewis, R. W. & Kumar, M. V. SAHA-sensitized prostate cancer cells to TNF-alpha-related apoptosis-inducing ligand (TRAIL): Mechanisms leading to synergistic apoptosis. *International journal of cancer* **119**, 221–228 (2006).
 192. You, B. R. & Park, W. H. Suberoylanilide hydroxamic acid-induced HeLa cell death is closely correlated with oxidative stress and thioredoxin 1 levels. *International journal of oncology* **44**, 1745–1755 (2014).
 193. Fedier, A., Dedes, K. J., Imesch, P., Von Bueren, A. O. & Fink, D. The histone deacetylase inhibitors suberoylanilide hydroxamic (Vorinostat) and valproic acid induce irreversible and MDR1-independent resistance in human colon cancer cells. *International journal of oncology* **31**, 633–641 (2007).
 194. Sun, P.-C. *et al.* Suberoylanilide hydroxamic acid induces apoptosis and sub-G1 arrest of 320 HSR colon cancer cells. *Journal of biomedical science* **17**, 76 (2010).
 195. Schwartz, C. *et al.* Valproic acid induces non-apoptotic cell death mechanisms in multiple myeloma cell lines. *International journal of oncology* **30**, 573–582 (2007).
 196. Jung, G.-A. *et al.* Valproic acid induces differentiation and inhibition of proliferation in neural progenitor cells via the beta-catenin-Ras-ERK-p21Cip/WAF1 pathway. *BMC cell biology* **9**, 66 (2008).
 197. Xu, Y. *et al.* Induction of apoptosis and autophagy in metastatic thyroid cancer cells by valproic acid (VPA). *International journal of clinical and experimental pathology* **8**, 8291 (2015).
 198. Ageberg, M., Rydström, K., Relander, T. & Drott, K. The histone deacetylase inhibitor valproic acid sensitizes diffuse large B-cell lymphoma cell lines to CHOP-induced cell death. *American journal of translational research* **5**, 170 (2013).
 199. Michaelis, M. *et al.* Valproic acid induces extracellular signal-regulated kinase 1/2 activation and inhibits apoptosis in endothelial cells. *Cell death and differentiation* **13**, 446 (2006).
 200. Li, Y., Peng, L. & Seto, E. HDAC10 regulates cell cycle G2/M phase transition via a novel Let-7-HMGA2-Cyclin A2 pathway. *Molecular and cellular biology* MCB–00400 (2015).
 201. Dasgupta, T., Antony, J., Braithwaite, A. W. & Horsfield, J. A. HDAC8 inhibition blocks SMC3 deacetylation and delays cell cycle progression without affecting cohesin-dependent transcription in MCF7 cancer cells. *Journal of Biological*

- Chemistry jbc*–M115 (2016).
202. Alao, J. P., Olesch, J. & Sunnerhagen, P. Inhibition of type I histone deacetylase increases resistance of checkpoint-deficient cells to genotoxic agents through mitotic delay. *Molecular cancer therapeutics* 1535–7163 (2009).
 203. Vallo, S. *et al.* HDAC inhibition delays cell cycle progression of human bladder cancer cells in vitro. *Anti-cancer drugs* **22**, 1002–1009 (2011).
 204. Göder, A. *et al.* HDAC1 and HDAC2 integrate checkpoint kinase phosphorylation and cell fate through the phosphatase-2A subunit PR130. *Nature communications* **9**, 764 (2018).
 205. Wang, X.-Q. *et al.* Knockdown of HDAC1 expression suppresses invasion and induces apoptosis in glioma cells. *Oncotarget* **8**, 48027 (2017).
 206. Li, Y. *et al.* A novel histone deacetylase pathway regulates mitosis by modulating Aurora B kinase activity. *Genes & development* **20**, 2566–2579 (2006).
 207. Vidal-Laliena, M. *et al.* Histone deacetylase 3 regulates cyclin A stability. *Journal of Biological Chemistry jbc*–M113 (2013).
 208. Welschinger, R. & Bendall, L. J. Temporal tracking of cell cycle progression using flow cytometry without the need for synchronization. *JoVE (Journal of Visualized Experiments)* e52840 (2015).
 209. Immaneni, A. *et al.* REST-VP16 activates multiple neuronal differentiation genes in human NT2 cells. *Nucleic acids research* **28**, 3403–3410 (2000).
 210. Gopalakrishnan, V. *et al.* Myoblast-derived neuronal cells form glutamatergic neurons in the mouse cerebellum. *Stem Cells* **28**, 1839–1847 (2010).
 211. Mandel, G. *et al.* Repressor element 1 silencing transcription factor (REST) controls radial migration and temporal neuronal specification during neocortical development. *Proceedings of the National Academy of Sciences* 201113486 (2011).
 212. Li, C. *et al.* REST, not REST4, is a risk factor associated with radiotherapy plus chemotherapy efficacy in glioma. *Drug design, development and therapy* **12**, 1363 (2018).
 213. Elmore, S. Apoptosis: a review of programmed cell death. *Toxicol Pathol* **35**, 495–516 (2007).
 214. Van Engeland, M., Nieland, L. J., Ramaekers, F. C., Schutte, B. & Reutelingsperger, C. P. Annexin V-affinity assay: a review on an apoptosis detection system based on phosphatidylserine exposure. *Cytometry: The Journal of the International Society for Analytical Cytology* **31**, 1–9 (1998).

215. Macosko, E. Z. *et al.* Highly parallel genome-wide expression profiling of individual cells using nanoliter droplets. *Cell* **161**, 1202–1214 (2015).
216. Wattenberg, M., Viégas, F. & Johnson, I. How to use t-sne effectively. *Distill* **1**, e2 (2016).
217. Gendelman, R. *et al.* Bayesian network inference modeling identifies TRIB1 as a novel regulator of cell-cycle progression and survival in cancer cells. *Cancer research* **77**, 1575–1585 (2017).
218. Liu, J.-F., Tsao, Y.-T. & Hou, C.-H. Amphiregulin enhances intercellular adhesion molecule-1 expression and promotes tumor metastasis in human osteosarcoma. *Oncotarget* **6**, 40880 (2015).
219. Lim, S. Y., Yuzhalin, A. E., Gordon-Weeks, A. N. & Muschel, R. J. Targeting the CCL2-CCR2 signaling axis in cancer metastasis. *Oncotarget* **7**, 28697 (2016).
220. Li, Y. & Seto, E. HDACs and HDAC inhibitors in cancer development and therapy. *Cold Spring Harbor perspectives in medicine* **6**, a026831 (2016).
221. Mrakovcic, M., Bohner, L., Hanisch, M. & Fröhlich, L. F. Epigenetic Targeting of Autophagy via HDAC Inhibition in Tumor Cells: Role of p53. *International journal of molecular sciences* **19**, 3952 (2018).
222. Wu, L., Feng, H., Hu, J., Tian, X. & Zhang, C. Valproic acid (VPA) promotes the epithelial mesenchymal transition of hepatocarcinoma cells via transcriptional and post-transcriptional up regulation of Snail. *Biomedicine & Pharmacotherapy* **84**, 1029–1035 (2016).
223. Hutt, D. M., Roth, D. M., Vignaud, H., Cullin, C. & Bouche-careilh, M. The histone deacetylase inhibitor, Vorinostat, represses hypoxia inducible factor 1 alpha expression through translational inhibition. *PloS one* **9**, e106224 (2014).
224. Tarazona, S., Garcia-Alcalde, F., Dopazo, J., Ferrer, A. & Conesa, A. Differential expression in RNA-seq: a matter of depth. *Genome research* **21**, 2213–2223 (2011).
225. Sager, R. Expression genetics in cancer: shifting the focus from DNA to RNA. *Proceedings of the National Academy of Sciences* **94**, 952–955 (1997).
226. Jiang, X. *et al.* A small molecule that protects the integrity of the electron transfer chain blocks the mitochondrial apoptotic pathway. *Molecular cell* **63**, 229–239 (2016).
227. Gong, W., Kwak, I.-Y., Pota, P., Koyano-Nakagawa, N. & Garry, D. J. DrImpute: imputing dropout events in single cell RNA sequencing data. *BMC Bioinformatics* **19**, 220 (2018).
228. Tripathi, S., Glazko, G. V. & Emmert-Streib, F. Ensuring the statistical soundness of competitive gene set approaches: gene filtering and genome-scale coverage are

- essential. *Nucleic acids research* **41**, e82–e82 (2013).
229. Glaser, K. B. *et al.* Gene expression profiling of multiple histone deacetylase (HDAC) inhibitors: defining a common gene set produced by HDAC inhibition in T24 and MDA carcinoma cell lines. *Molecular cancer therapeutics* **2**, 151–163 (2003).
230. Kim, Y. J. *et al.* HDAC inhibitors induce transcriptional repression of high copy number genes in breast cancer through elongation blockade. *Oncogene* **32**, 2828 (2013).
231. Wang, Z. *et al.* Genome-wide mapping of HATs and HDACs reveals distinct functions in active and inactive genes. *Cell* **138**, 1019–1031 (2009).
232. Sanchez, G. J. *et al.* Genome-wide dose-dependent inhibition of histone deacetylases studies reveal their roles in enhancer remodeling and suppression of oncogenic super-enhancers. *Nucleic acids research* **46**, 1756–1776 (2017).
233. Greer, C. B. *et al.* Histone deacetylases positively regulate transcription through the elongation machinery. *Cell reports* **13**, 1444–1455 (2015).
234. White, C. H. *et al.* Mixed effects of suberoylanilide hydroxamic acid (SAHA) on the host transcriptome and proteome and their implications for HIV reactivation from latency. *Antiviral research* **123**, 78–85 (2015).
235. Chambers, A. *et al.* Histone acetylation-mediated regulation of genes in leukaemic cells. *European Journal of Cancer* **39**, 1165–1175 (2003).
236. Kang, M. R. *et al.* Gene expression profiling of KBH-A42, a novel histone deacetylase inhibitor, in human leukemia and bladder cancer cell lines. *Oncology letters* **3**, 113–118 (2012).
237. Majumdar, G., Adris, P., Bhargava, N., Chen, H. & Raghov, R. Pan-histone deacetylase inhibitors regulate signaling pathways involved in proliferative and pro-inflammatory mechanisms in H9c2 cells. *BMC genomics* **13**, 709 (2012).
238. El-Deiry, W. S. p21 (WAF1) mediates cell-cycle inhibition, relevant to cancer suppression and therapy. *Cancer research* **76**, 5189–5191 (2016).
239. Roussel, M. F. & Robinson, G. W. Role of MYC in Medulloblastoma. *Cold Spring Harbor Perspectives in Medicine* **3**, a014308 (2013).
240. Schaub, F. X. *et al.* Pan-cancer alterations of the MYC oncogene and its proximal network across the Cancer Genome Atlas. *Cell systems* **6**, 282–300 (2018).
241. Pfister, S. X. & Ashworth, A. Marked for death: targeting epigenetic changes in cancer. *Nature Reviews Drug Discovery* **16**, 241 (2017).
242. Zupkovitz, G. *et al.* The cyclin-dependent kinase inhibitor p21 is a crucial target for histone deacetylase 1 as a regulator of cellular proliferation. *Molecular and cellular*

- biology* **30**, 1171–1181 (2010).
243. Dolatabadi, S. *et al.* Cell cycle and cell size dependent gene expression reveals distinct subpopulations at single-cell level. *Frontiers in genetics* **8**, 1 (2017).
244. Abbas, T. & Dutta, A. p21 in cancer: intricate networks and multiple activities. *Nature Reviews Cancer* **9**, 400 (2009).
245. Adams, C. M., Hiebert, S. W. & Eischen, C. M. Myc induces miRNA-mediated apoptosis in response to HDAC inhibition in hematologic malignancies. *Cancer research* **76**, 736–748 (2016).
246. Lee, H. *et al.* The neuronal expression of MYC causes a neurodegenerative phenotype in a novel transgenic mouse. *Am. J. Pathol.* **174**, 891–7 (2009).
247. Wang, X. & Lin, Y. Tumor necrosis factor and cancer, buddies or foes? 1. *Acta Pharmacologica Sinica* **29**, 1275–1288 (2008).
248. Wu, Y. & Zhou, B. TNF-alpha/NF-kappaB Snail pathway in cancer cell migration and invasion. *British journal of cancer* **102**, 639 (2010).
249. Bredlau, A.-L. *et al.* Medu-15. Ccl2/ccr2/il-6 Loop: A Potential Therapeutic Target For Pediatric Medulloblastomas. *Neuro-oncology* **19**, iv40 (2017).
250. Wybranska, I. *et al.* Apoptosis-related gene expression in glioblastoma (LN-18) and medulloblastoma (Daoy) cell lines. *Hum. Cell* **26**, 137–48 (2013).
251. Pan, Y.-C. *et al.* CEBPD reverses RB/E2F1-mediated gene repression and participates in HMDB-induced apoptosis of cancer cells. *Clinical cancer research* **16**, 5770–5780 (2010).
252. Gottlieb, A. *et al.* RITA displays anti-tumor activity in medulloblastomas independent of TP53 status. *Oncotarget* **8**, 27882–27891 (2017).
253. Bolden, J. E., Peart, M. J. & Johnstone, R. W. Anticancer activities of histone deacetylase inhibitors. *Nature reviews Drug discovery* **5**, 769 (2006).
254. Suraweera, A., O’Byrne, K. J. & Richard, D. J. Combination Therapy With Histone Deacetylase Inhibitors (HDACi) for the Treatment of Cancer: Achieving the Full Therapeutic Potential of HDACi. *Frontiers in oncology* **8**, 92 (2018).
255. Chatterjee, A., Rodger, E. J. & Eccles, M. R. Epigenetic drivers of tumourigenesis and cancer metastasis. in *Seminars in cancer biology* **51**, 149–159 (2018).
256. Cao, L.-L. *et al.* The expression of histone deacetylase HDAC1 correlates with the progression and prognosis of gastrointestinal malignancy. *Oncotarget* **8**, 39241 (2017).

257. Lee, D. H., Ryu, H.-W., Won, H.-R. & Kwon, S. H. Advances in epigenetic glioblastoma therapy. *Oncotarget* **8**, 18577 (2017).
258. Munster, P. *et al.* Phase I trial of vorinostat and doxorubicin in solid tumours: histone deacetylase 2 expression as a predictive marker. *British journal of cancer* **101**, 1044 (2009).
259. Lebrun-Julien, F. & Suter, U. Combined HDAC1 and HDAC2 depletion promotes retinal ganglion cell survival after injury through reduction of p53 target gene expression. *ASN neuro* **7**, 1759091415593066 (2015).
260. Wu, Y. *et al.* Loss of GCN5 leads to increased neuronal apoptosis by upregulating E2F1-and Egr-1-dependent BH3-only protein Bim. *Cell death \& disease* **8**, e2570 (2017).
261. Ma, C. & D'Mello, S. R. Neuroprotection by histone deacetylase-7 (HDAC7) occurs by inhibition of c-jun expression through a deacetylase-independent mechanism. *J. Biol. Chem.* **286**, 4819–28 (2011).
262. Mei, Z. *et al.* Sirtuins in metabolism, DNA repair and cancer. *Journal of Experimental \& Clinical Cancer Research* **35**, 182 (2016).
263. Kim, J.-H. *et al.* Identification of a novel SIRT7 inhibitor as anticancer drug candidate. *Biochemical and biophysical research communications* **508**, 451–457 (2019).
264. Nakakura, T. *et al.* Intracellular localization of α -tubulin acetyltransferase ATAT1 in rat ciliated cells. *Med Mol Morphol* **49**, 133–43 (2016).
265. Jin, H. *et al.* alpha-Synuclein negatively regulates protein kinase C δ expression to suppress apoptosis in dopaminergic neurons by reducing p300 histone acetyltransferase activity. *Journal of Neuroscience* **31**, 2035–2051 (2011).
266. Rouaux, C. *et al.* Critical loss of CBP/p300 histone acetylase activity by caspase-6 during neurodegeneration. *The EMBO journal* **22**, 6537–6549 (2003).
267. Kar, G. *et al.* Flipping between Polycomb repressed and active transcriptional states introduces noise in gene expression. *Nature communications* **8**, 36 (2017).
268. Bacher, R. & Kendzierski, C. Design and computational analysis of single-cell RNA-sequencing experiments. *Genome biology* **17**, 63 (2016).
269. Cazzalini, O., Scovassi, A. I., Savio, M., Stivala, L. A. & Prosperi, E. Multiple roles of the cell cycle inhibitor p21CDKN1A in the DNA damage response. *Mutation Research/Reviews in Mutation Research* **704**, 12–20 (2010).
270. Zhao, P. *et al.* Upregulation of cyclin B1 plays potential roles in the invasiveness of pituitary adenomas. *Journal of Clinical Neuroscience* **43**, 267–273 (2017).

271. Chang, D. Z. *et al.* Increased CDC20 expression is associated with pancreatic ductal adenocarcinoma differentiation and progression. *Journal of hematology & oncology* **5**, 15 (2012).
272. Wu, T., Zhang, X., Huang, X., Yang, Y. & Hua, X. Regulation of cyclin B2 expression and cell cycle G2/m transition by menin. *Journal of Biological Chemistry* **285**, 18291–18300 (2010).
273. Wang, N. *et al.* CXCL1 derived from tumor-associated macrophages promotes breast cancer metastasis via activating NF-kappaB/SOX4 signaling. *Cell death & disease* **9**, 880 (2018).
274. Jensen, L. B. *et al.* Frequent amplifications and deletions of G 1/S-phase transition genes, CCND1 and MYC in early breast cancers: a potential role in G 1/S escape. *Cancer Biomarkers* **5**, 41–49 (2009).
275. Stoll, S. W. *et al.* Membrane-Tethered Intracellular Domain of Amphiregulin Promotes Keratinocyte Proliferation. *Journal of Investigative Dermatology* **136**, 444–452 (2016).
276. An, X. *et al.* The prognostic significance of topoisomerase II alpha protein in early stage luminal breast cancer. *BMC Cancer* **18**, 331 (2018).
277. Wang, D. *et al.* BIRC3 is a novel driver of therapeutic resistance in Glioblastoma. *Sci Rep* **6**, 21710 (2016).
278. Di Matteo, A. *et al.* Structural investigation of nucleophosmin interaction with the tumor suppressor Fbw7 γ . *Oncogenesis* **6**, e379 (2017).
279. Chiba, T. *et al.* Identification of genes up-regulated by histone deacetylase inhibition with cDNA microarray and exploration of epigenetic alterations on hepatoma cells. *Journal of hepatology* **41**, 436–445 (2004).
280. Halsall, J. A., Turan, N., Wiersma, M. & Turner, B. M. Cells adapt to the epigenomic disruption caused by histone deacetylase inhibitors through a coordinated, chromatin-mediated transcriptional response. *Epigenetics & chromatin* **8**, 29 (2015).
281. Markozashvili, D. *et al.* Histone deacetylase inhibitor abexinostat affects chromatin organization and gene transcription in normal B cells and in mantle cell lymphoma. *Gene* **580**, 134–143 (2016).
282. Lin, K.-T. *et al.* HDAC inhibitors augmented cell migration and metastasis through induction of PKCs leading to identification of low toxicity modalities for combination cancer therapy. *Clinical Cancer Research* (2012).
283. Marsh, A. M. *et al.* Histone deacetylase inhibitors: recent outcomes from clinical trials and the implications for oncology treatment approaches. *Clinical Investigation* **3**, 571–594 (2013).

284. Xing, J. *et al.* Sensitization of suberoylanilide hydroxamic acid (SAHA) on chemoradiation for human cervical cancer cells and its mechanism. *European journal of gynaecological oncology* **36**, 117–122 (2014).
285. Darzynkiewicz, Z., Halicka, H. D., Zhao, H. & Podhorecka, M. in *Cell Cycle Synchronization* 85–96 (Springer, 2011).
286. Sharpe, J. J. & Cooper, T. A. Unexpected consequences: exon skipping caused by CRISPR-generated mutations. *Genome biology* **18**, 109 (2017).
287. Sionov, R. V., Vlahopoulos, S. A. & Granot, Z. Regulation of Bim in health and disease. *Oncotarget* **6**, 23058 (2015).
288. Huang, K. *et al.* Cleavage by Caspase 8 and mitochondrial membrane association activate the BH3-only protein bid during TRAIL-induced apoptosis. *Journal of Biological Chemistry* **291**, 11843–11851 (2016).
289. Zhang, H. *et al.* Onco-miR-24 regulates cell growth and apoptosis by targeting BCL2L11 in gastric cancer. *Protein & cell* **7**, 141–151 (2016).

7 Appendices

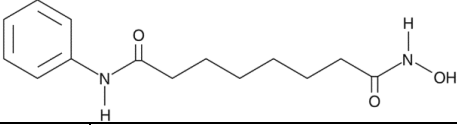
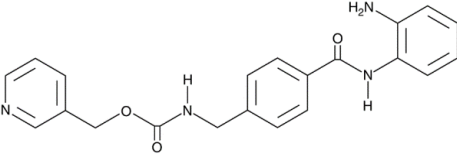
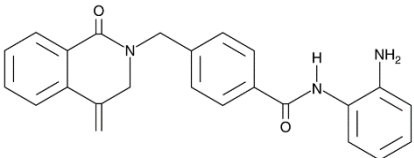
Appendix 1: Partial list of non-histone protein substrates of HDACs

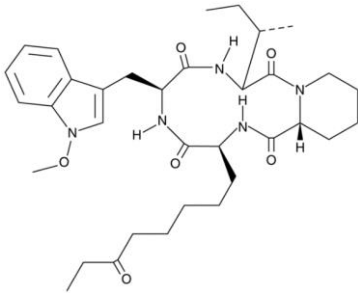
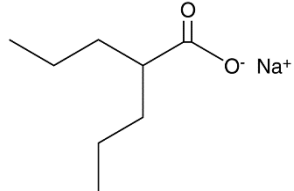
This table was adapted from⁶⁰.

Effect of acetylation	Protein	Intracellular function	HDAC implicated
Increased DNA-binding affinity	p53	Tumour suppressor	
	SRY sex-determining region Y	Transcription factor	HDAC3
	STAT3 signal transducer and activator of transcription	Signalling mediator	HDAC1, 2, 3
	GATA1	Transcription factor	HDAC3, 4, 5
	GATA2	Transcription factor	HDAC3, 5
	E2F1	Transcription factor	HDAC1
	MyoD	Transcription factor	HDAC1
Decreased DNA-binding affinity	YY1 transcriptional repressor protein	Transcription factor	HDAC1, 2, 3
	HMG-A1 High Mobility Group	Nuclear factor	
	HMG-N2	Nuclear factor	
	p65	Transcription factor	
Increased transcriptional activation	p53	Tumour suppressor	
	HMG-A1	Nuclear factor	
	STAT3	Signalling mediator	HDAC1, 2, 3
	AR	Nuclear receptor	HDAC1
	ER α (basal)	Steroid hormone receptors	HDAC1
	GATA1 GATA-binding factor	Transcription factor	HDAC3, 4, 5
	GATA2	Transcription factor	HDAC3, 5

	GATA3	Transcription factor	
	EKLF	Transcription factor	HDAC1
	MyoD myogenic differentiation	Transcription factor	HDAC1
	E2F1	Transcription factor	HDAC1
	RUNX3 Runt-related transcription factor	Tumour suppressor	HDAC1, 5
Decreased transcriptional activation	ER α (ligand-dependent)	Steroid hormone receptors	HDAC1
	HIF1 α Hypoxia-inducible factor	Transcription factor	
Increased protein stability	p53	Tumour suppressor	HDAC1
	c-MYC	Oncoprotein	
	AR	Nuclear receptor	HDAC1
	ER α Estrogen receptor	Steroid hormone receptors	HDAC1
	E2F1 E2F transcription factor	Transcription factor	HDAC1
	Smad7	Signalling mediator	HDAC1, 3
	RUNX3	Tumour suppressor	HDAC1, 5
Decreased protein stability	HIF1 α	Transcription factor	
Promotes protein–protein interaction	STAT3	Signalling mediator	HDAC1, 2, 3
	AR androgen receptor	Nuclear receptor	HDAC1
	EKLF Erythroid Kruppel-like factor	Transcription factor	HDAC1
	Importin α	Nuclear import factors	
Disrupts protein–protein interaction	NF- κ B nuclear factor kappa-B	Transcription factor	
	Ku70 ATP-dependent DNA helicase	DNA-repair protein	
	Hsp90 heat-shock protein	Chaperone	HDAC6

Appendix 2: The chemical information about the used HDACis

SAHA	
	
Formal Name	N1-hydroxy-N8-phenyl-octanediamide
Synonyms	Suberoylanilide Hydroxamic Acid (Vorinostat)
Molecular Formula	C ₁₄ H ₂₀ N ₂ O ₃
Formula Weight	264.3
MS-275	
	
Formal Name	N-[[4-[[[(2-aminophenyl) amino]carbonyl]phenyl] methyl]-3-pyridinylmethyl ester, carbamic acid
Synonyms	Entinostat, SNDX 275
Molecular Formula	C ₂₁ H ₂₀ N ₄ O ₃
Formula Weight	376.4
MI-192	
	
Formal Name	N-(2-aminophenyl)-4-[(3,4-dihydro-4-methylene-1-oxo-2(1H)-isoquinolinyl) methyl]-benzamide
Synonyms	Has no other names
Molecular Formula	C ₂₄ H ₂₁ N ₃ O ₂
Formula Weight	383.4

122 Apicidin 	
Formal Name	cyclo[(2S)-2-amino-8-oxodecanoyl-1-methoxy-L-tryptophyl-L-isoleucyl-(2R)-2-piperidinecarbonyl]
Synonyms	OSI 2040
Molecular Formula	C ₃₄ H ₄₉ N ₅ O ₆
Formula Weight	623.8
Valproic Acid (sodium salt) 	
Formal Name	2-propyl-pentanoic acid, monosodium salt
Synonyms	2-Propylvaleric Acid Sodium Valproate
Molecular Formula	C ₈ H ₁₅ O ₂ • Na
Formula Weight	166.2

Appendix 3: The proposed plan for gene expression analysis using bulk NGS

RNA-seq approach four time-points were suggested to generate snapshots of the treatment response (1st Untreated, 2nd At the start of expression of cell apoptosis, 3rd A middle point: the start of the apoptosis & apoptosis, 4th When cell death >40%).

With the second time point, I suggested to use an apoptotic marker that could indicate the initiation of the apoptosis mechanism. After a thorough search for an appropriate marker for apoptosis initiation I found that BIM gene expression could be the most potential marker. Bim is essential protein for initiating intrinsic apoptosis pathway due its ability in activating most anti-apoptotic proteins and involvement in recognising a large number of apoptosis stimuli under many normal and disease conditions. Bim expression has been detected in a wide variety of tissues including brain, liver, heart, lung, kidney in additional to hematopoietic cells and several of other tissues ²⁸⁷. Normally, Bim expression level is low and increases with the stimulation of cell death. Increase Bim expression has been reported to deactivate most anti-apoptotic proteins of BCL2 superfamily and activate Bax and Bak pro-apoptotic factors leading to increase the permeability of mitochondrial outer membranes ²⁸⁸. Where, knocking-out Bim expression results in decrease apoptosis though, it does not induce a major effect on cell survival ²⁸⁹. In addition, it has been reported that blocking Bim expression resulted in stopping Bax activation ²²⁶. Uncontrolled expression of Bim is typically associated with increase in cell damage and it has been connected with neurodegenerative diseases, diabetes, and liver damage. Bim expression is tightly regulated at transcriptional, translational and post-translational levels, which may ensure a sensible activation of Bim when required ²⁸⁷.

It should be noticed that using the increase in the acetylation level to identify a time-point is also not indicative as it causes wide variations in gene expression that are not necessarily represent the cell response or the anticancer mechanism of the inhibitors.

Appendix 4: NGS Experimental Considerations

In optimal condition of cell culture, there are several biological variations that present on many levels and could limit the ability of the bulk cell analysis to uncover the molecular regulations. One of the factors is the cell cycle effect which results in heterogeneity within an identical cell population. The cell cycle has a strong and timely association with gene expression and showed a considerable variation in total transcript number between the phases ²⁴³. For example, G1 subpopulation of cells is often characterized by low total transcript level with a downregulation in most of the proliferation associated genes ²⁴³. The variation in transcript numbers often results in altering the response to the internal and external signals and could lead to change the path of cell proliferation or differentiation ²⁴³. RNA-seq analysis of pooled cells typically generate average gene expression of different subpopulations especially and the tumour cells are in a continuous transition throughout the cell cycle phases. Cell synchronization (bringing the cell to the same phase of cell cycle) could be suggested as a possible solution to overcome the cell cycle effect though, the cells are often lose the synchrony when progressing through the G1 phase and thereby they become less synchronous in other phases ²⁸⁵.

Another possible biological factor with tumour cell lines is that with each cell division there could be additional mutations that were not present in the precursor cell. With continuous growth of a cell line there inevitably an accumulation of additional mutations within a single cell that could advantage the growth of a particular cell, promote heterogeneity, and ultimately could change the treatment response.

Up to date, most of our knowledge in understanding the anticancer effect of HDACis came from studies that averaged data from mixed populations of cells. Such data are largely affected by the proportion of the cells at different stages of cell growth which may affect detecting some important molecular regulation.

Appendix 5: The Suggested Time-points for the Bulk NGS analysis and how they could be used to address the molecular mechanisms

With such approach a time-course treatment should be done in order to give snapshots for the molecular changes that happen during the treatment. Though, the selection for these time-points should be grounded on specific cellular response or markers as the arbitrary selection may not show the initiation or downregulation of certain cellular mechanisms. Several of previous works were performed using random time-points of treatment yet, the findings did not help in addressing the mechanism of action of HDACis.

- **Fist time point Untreated** (2 samples, DAOY, Control)

This will represent the default genes expression for each cell line.

➤ **Including these samples will help in**

❖ **Comparing the results of treated cell to untreated cell of the same cell line will be used to study:**

- the variation in genes expression before and after treatment.
- the acetylation difference between different inhibitors
- understand why some inhibitors are more efficient in blocking tumorigenesis than other
- identifying the cellular mechanisms that prompt the cell death for these inhibitors

❖ **The cross- analysis between the DAOY and the control will help:**

- validate and support the results of DAOY cell data analysis
- understand the mechanism that trigger apoptosis in DAOY
- understand how cancer cells sustain their proliferation
- how cancer cell and normal cell responses to HDACis
- understand if deacetylation is one of the cancer growth mechanism and how cancer cell induces deacetylation mechanism

❖ **Control cancer vs. control normal**

- illustrates the effect of HDACis on normal cell
- describes how can normal cell resist the effect of hyperacetylation (Hyperacetylation Rescue Mechanism)
- suggests the possible side effect of HDACis treatment

- **Second time point: At the start of expression of cell apoptosis genes** (8 samples: 3 DAOY+ 3Control + untreated DAOY and Con)

There will be large changes in genes expression though, I need to focus on how the HDACis stimulate the apoptosis. So, I need to focus on the genes that have high DGE though they are more related to apoptosis regulation. This time point could show initial signal that stimulate the apoptosis. Though it is very difficult to know what is it.

Comparing the expression between the control and the tumour will help in identifying this time point.

- ❖ DAOY: shows the apoptotic pathway that is involved in cell death, also it will help in identifying the difference in hyperacetylation effect between the inhibitors
- ❖ Control: shows the effect of HDACis on genes expression in normal cells
- ❖ Untreated cells: as all the cells are actively dividing cell, the genes expression levels will be different during their proliferation. Therefore, this control may help in understand the expression profile of the treated cells

- **Third time point: A middle point between the start of the apoptosis and apoptosis** (8 Samples: 3 DAOY+ 3 Control + untreated DAOY and Con)

- ❖ DAOY: the regulation that initiates the apoptosis
- ❖ Control: the regulation that rescue the against the hyperacetylation, if there is any, or there is not regulation and differentiation of the cell protect it from cell death. Check the expression of DNA repair and other genes families.

- **Fourth time point: At the initiation of caspases (point of no return)** (8 Samples: 3 DAOY+ 3 Control + untreated DAOY and Con)

- ❖ DAOY: the regulation of apoptosis mechanism
- ❖ Control: understand the rescue mechanism or the faith of normal cell

Stage 5: NGS Results validation

Western blot and qPCR will be used in order to validate the finding of NGS analysis.

The limitation of Bulk NGS analysis

- HDACis may induce their action through non-histone proteins

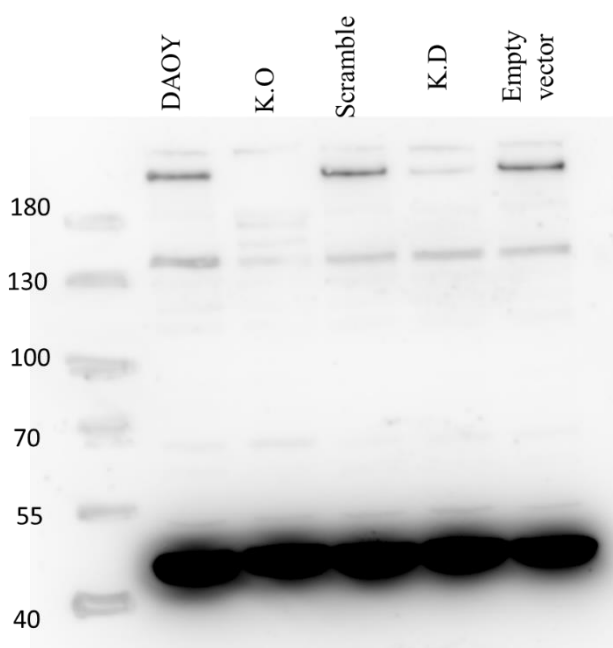
- In culture plate each cell has a different stage of cell cycle, therefore, they will show different genes expression between replicates.

It could be reduced by synchronize them. For example, using colcemid to as arrest them in metaphase stage and then release them however, the cells may lose their synchronisation after a few hours.

- The differential gene expression of HDACis may represent the acetylation effect and not the cell response to maintain the balance between the acetylation and deacetylation, or to stimulate apoptosis.
- Identifying the treatment time is very critical though, it is difficult to identify exactly when the cells start to response to the effect of HDACis (Hyper-acetylation).
- As cancer cells are polyploidy and they have large number of mutations, it not easy to map all the results of the NGS to the Ref-seq.
- During the data analysis: there will be a large number of genes that show high differential gene expression though, they are not related to the cell response to HDACis which may make identifying the regulation that control normal cell response very difficult.
- Points to consider:
 - **Acetylated gene expression response:** very changeable, the high or the low gene expression variation represent the acetylation effect and not the cell response to maintain the balance between the acetylation and deacetylation.
 - **When the cell started to response to correct the hyper-acetylation effect:** could be early or late, and to identify the time I may measure the expression of the genes that regulate the HDAC and HAT genes expression.
 - **Identify the hyper-acetylation rescue mechanism:** is time dependent, and can be identified by genes expression.
 - As measuring acetylation alone will show the effect of the inhibitors and histone modification, and does not represent if the cells started to correct the hyper-acetylation.

Genes expression could be the alternative to identify the cell correction response. However, not all expression variation is indicator for the rescue mechanism. Some genes are very sensitive to acetylation and their expression is increased or decrease by more than 8 folds though, I cannot use them as the change in their expression is not a correction mechanism.

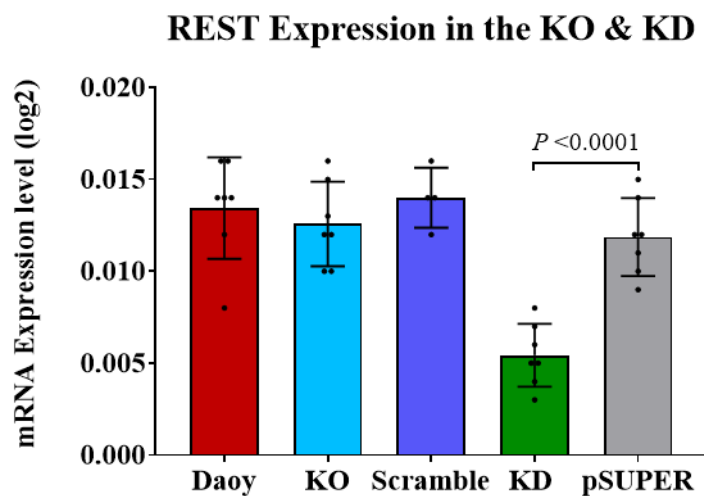
Appendix 6: Western blot of REST protein (Complete image)



The blot shows the complete image of the anti-REST antibody western blot analysis. According to the manufacturer's information, the anti-REST antibody (OriGene, TA330562) is a synthetic peptide towards the middle region of human REST. Previously, I have tried to identify the immunoreactive bands with the help of one of my co-supervisors however, we could not identify which isoform an immunoreactive band is related to. Similarly, Chen et al., 2018¹⁶² have concluded the following:

“Unfortunately, despite the mRNA evidence, not all REST protein isoforms have been experimentally verified and they are usually observed as unexpected sizes due to post-translational modifications, making it challenging to determine whether an unknown immunoreactive band is non-specific or a REST isoform. For example, REST4 and RESTC (a new REST isoform that is not much known about it) are predicted as 37 and 86 kDa yet, they were observed as 53 and 130 kDa, respectively, while the full-length REST has been reported as variable sizes ranging from 120 to 200 kDa. So, even if detectable by WB, specific REST isoforms might be simply considered as non-specific and excluded from being presented in publication, such may explain why RESTC was not reported until recently”¹⁶².

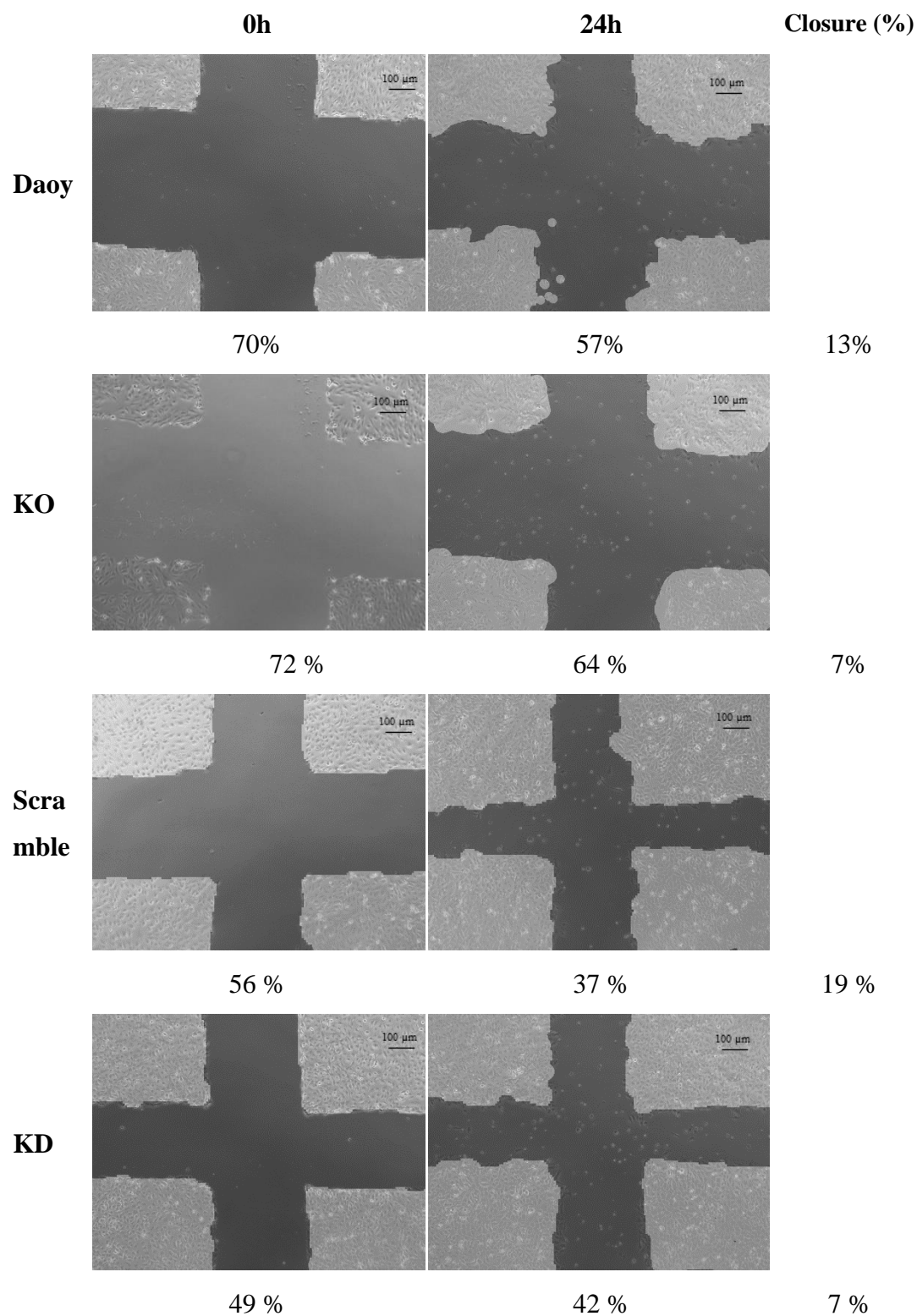
Appendix 7: REST mRNA expression in the KO cell clone

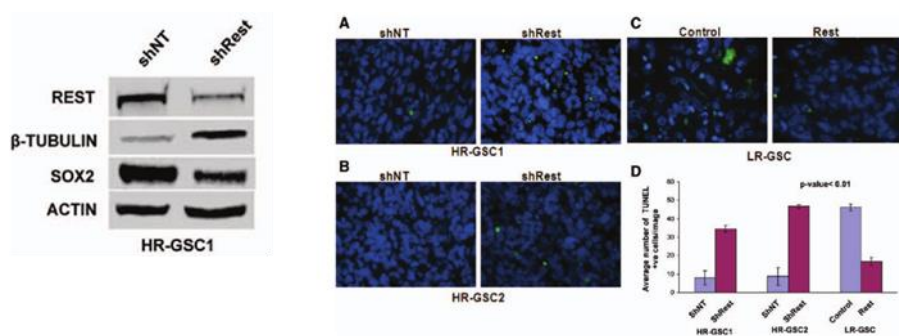
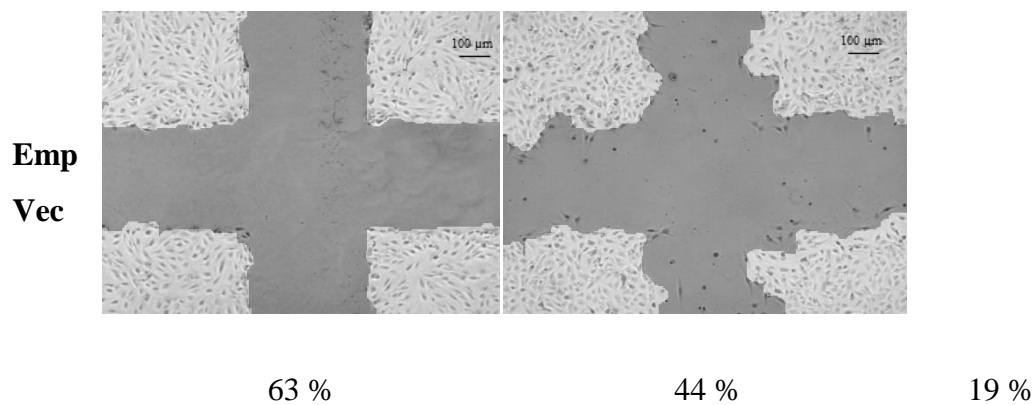


Interestingly, the KO mRNA was included in this reaction and it did not show any significant reduction in the transcriptional level (

Figure 23). The expression of REST mRNA in the KO reaction could be due to the presence of a truncated form of REST mRNA which it possibly generated by splicing out or deletion of the edited exon 2 during the transcription. This truncated mRNA can be degraded by nonsense-mediated decay or by blocking the access of the ribosomes during the translation²⁸⁶. However, the Thus, the qPCR analysis may not accurately represent the functional effect of CRISPR/Cas9 modulation in the KO cell.

Appendix 8: Cell migration assay analysis images

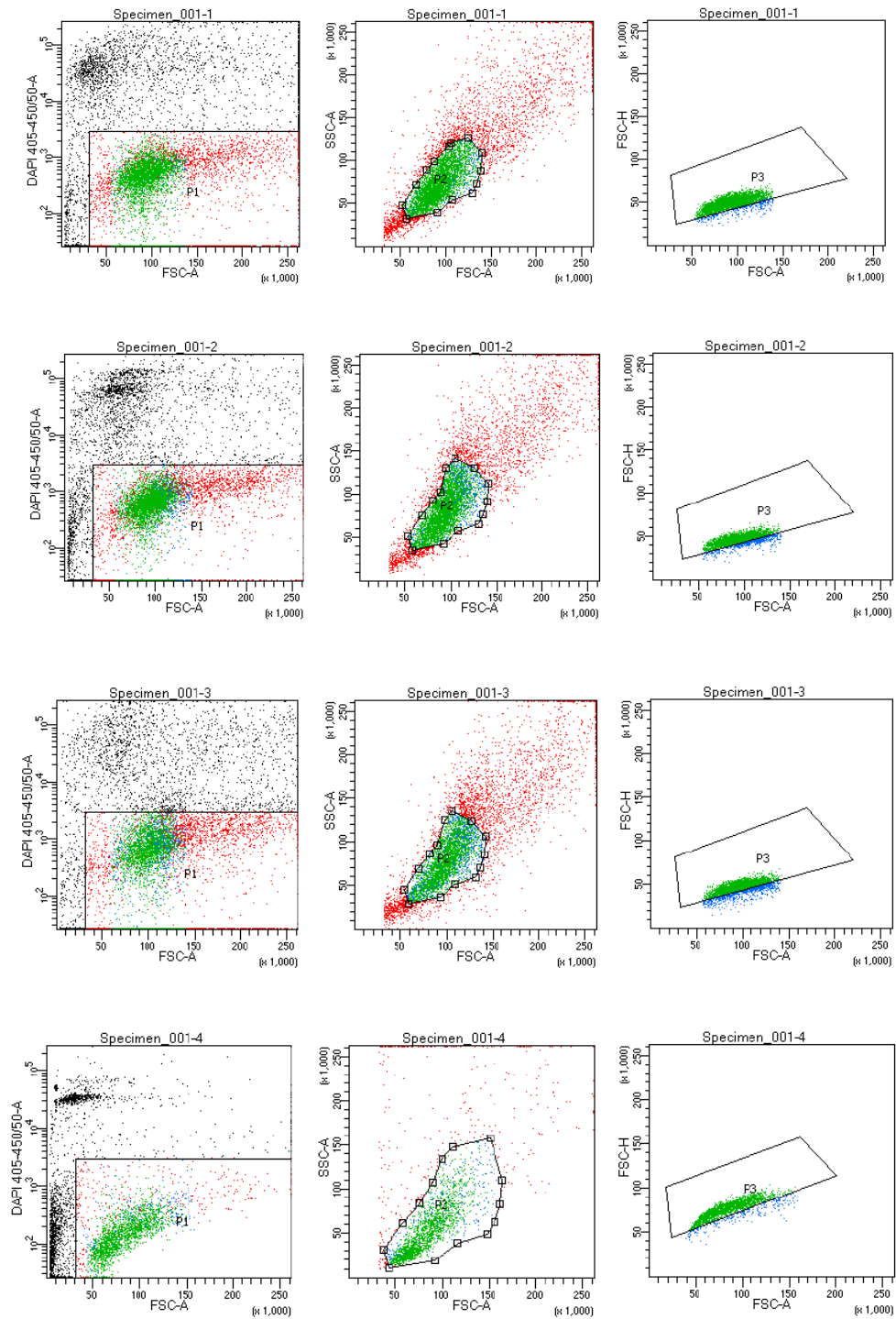


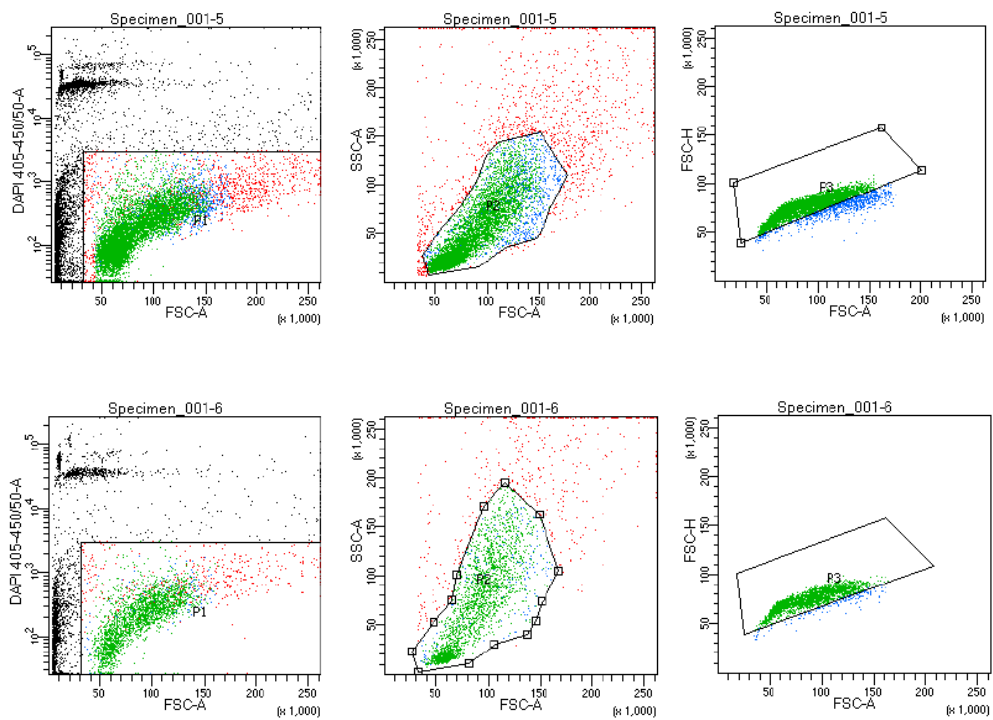


Appendix 9: shRNA and TUNEL Assay Images of Kamal et al, 2012 Study

The above images were taken from Kamal et al, 2012 study to demonstrate the level of shRNA knockdown and the apoptosis identified. These images were used here as a reference for the reader only.

Appendix 10: scNGS Cell Sorting (BD FACSDiva)





Appendix 11: The neurons gene list that were used to identify the cells identity

N.Vehicle			
0	Striatum.Late.Infancy	2.70E-31	Striatum.Late.Infancy : BLOC1S1, RPS29, NDUFA4, UQCRB, RPL7, FAU, RPS12, RPS20, RPL35A, C12ORF57, RPL37, RPS18, RPL32, RPS27A, RPS5, RPL34, RPL30, RPL38, RPS10, RPL23, RPL28, RPL27A, RPL18, PFDN5, RPL31, RPL12, RPL23A, RPL9, RPS7, RPL24, RPS14, RPS28, SSR4, RPS24, RPLP1, RPL39, RPL27, RPS23, RPL11, RPS15A, RPL26, RPS27, RPS9, RPL36, RPS8
1	Cortex.Early.Mid.Fetal	3.55E-34	Cortex.Early.Mid.Fetal : CTTNBP2, BCL7A, HMGCR, SIAH1, NELL2, FAMI10B, DAB1, SATB2, CDK5R1, CD24, YTHDF2, DOK5, GNAI1, DAAMI, WASF1, MARCKSL1, KLF6, WDR47, FRMD4B, TNPO1, PTP4A1, CHL1, SLA, RNF219, MEF2C, SCN3A, SLC38A1, TNIK, CXADR, KIDINS220, CRMP1, FAMI13A, REEP1, BRD3, NEUROD6, ITSN1, STMN2, CSRP2, KLF7, RUNX1T1, NEUROD2, ZNF195, RNF182, SLC37A3, BHLHE22, NCAM1, NHSL1, SRGAP1, PDIK1L, PAK2, EPM2AIP1, GNG2, MAPK8, BCL11A, MAPT, BZW2, MLLT3, FNBP1L, FSD1L, VCAN, CCDC112, MAP1B, KBTBD6, SOX11, ZNF300
2	Cortex.Early.Mid.Fetal	1.03E-09	Cortex.Early.Mid.Fetal : TCF4, CTTNBP2, SLA, CXADR, KIDINS220, MLLT3, NFIB, LBH, MEIS2, DCX, SEMA3C, MAPT, FAMI13A, NEUROD2, SOX4, AUTS2, SOX11
3	Striatum.Early.Fetal	2.45E-166	Striatum.Early.Fetal : SMC1A, H2AFX, BUB3, LMNB2, G3BP1, TOX3, CEP57, TMX1, ANP32E, NCAPG, IPO5, ECT2, NRM, CKAP2, RNASEH2B, PLK1, DBF4, UHRF1, TCF12, HAUS8, ER12, UBE2C, PAICS, DTMYK, RNF138, KIFC1, OIP5, BUB1B, HAT1, HNRNPK, CTNNAL1, SNRNP, CBX5, FAM83D, RAD21, KIF14, AURKA, CENPN, NKAIN3, PRR11, CDK2, MCM3, UBE2T, CDH2, ASF1B, ARRD3, FSTL1, MPHOSPH9, DLGAP5, CDK5RAP2, ARHGAP11A, TKI, HMGNB, RAD51AP1, PSMC3IP, TMEM97, ZFP36L2, PHF19, TMEM123, ACTL6A, FAMI111A, BRCA2, CKS1B, CCDC18, PMAIP1, CEP135, PPP1CC, MPPED2, RFC3, TUBB6, ZNF273, MCM5, CYR61, LBR, BRCA1, ASPM, KIF2C, CDK4, TROAP, H2AFX, SYNE2, HJURP, POLD3, BTG3, CNTLN, RAD18, CENPE, SMC3, SASS6, BLM, PSRC1, RFC5, CENPV, DNAJC9, SSRP1, BARD1, NAP1L1, RRM1, MCM7, UBA2, SMCHD1, PRKDC, BRIP1, HNRNPF, KIF22, HMGNI, E2F1, ELAVL1, NASP, DEPDC1, FANCI, ATAD2, ER11, FBXO5, PHIP, C4ORF46, GTSE1, MELK, CHD1, KIF23, NUSAP1, CLIC1, CHAF1A, PPAT, RCC1, PCNA, PBK, PPM1D, QSER1, HELLS, HNRNPU, TRAP, CDC20, MTHFD2, CKS2, DONSON, INSM1, HMHR, GINS2, ARL13B, RRM2, MAD2L1, HNRNPR, HMG2, PRC1, SMC2, TOPBP1, VRRK1, GMNN, POLA2, TACC3, ERLIN1, CDCA5, G2E3, SCML1, CDCA3, PTTG1, H2AFX, SUPT16H, EXO1, CCNE2, ITGB3BP, SMARCA5, MASTL, HNRNPA3, ASCL1, HIST1H4C, CBX3, NCAPH, DTL, HES6, CENPA, SERTAD4, TOP2A, FANCD2, DEPDC1B, NFATC3, RBBP4, RBBP8, FAMI111B, ATAD5, USP1, DHX15, CENPK, RBMX, N4BP2, ZFP36L1, CDCATL, CCDC15, CHEK1, CHAF1B, NUDT1, RDX, HMG1B, CDC6, ZNF43, CDCA2, TMPO, UBE2S, NVL, H2AFX, IGF1BP2, CDC25C, ESCO2, DEK, ZWILCH, TIMELESS, NDC80, CENPH, CEP152, CHEK2, HAUS1, CENPM, SPC25, DSN1, RTKN2, SOAT1, MCM10, KPNA2, GAS2L3, KIF15, PTBPI, MCM2, TMSB15A, FOXM1, HEN1, SMC5, CLSPN, TCF19, WDHD1, PBRM1, NCAPG2, KIF4A, HMGXB4, RFC4, SOX2, CDC25B, CCDC14, WDR34, TPX2, NUF2, HMG1B, CDCA4, CKAP2L, CCNA2, MCM4, BAZ1A, ARL6IP6, CASP8AP2, HDAC2, HAUS6, CCNB2, TYMS, LMNB1, KIF11, CCNB1, CENPF, WDR76, KIF20B, SHCBP1, ODC1, NEK2, NEDD1, C21ORF58, SPAG5, CDKN3, MEST, CDC7, CORO1C, EZH2, CDT1, CDCA8, DIAPH3, AURKB, MKI67, BIRC5, ZWINT, PTAR1, SMC4, ID4, MXD3, BUB1
4	Amygdala.Late.Fetal	2.15E-26	Amygdala.Late.Fetal : ARX, NRG1, SFRP1, NKAIN3, TNC, CA12, ASCL1, PLAGL1, SDCBP, MS11, SOX9, CHRDL1, PSAT1, SOX2, DDIT4, SLC35F5, LHX2, RPS18, MOXD1, SORD, SLC16A1, FABP7, EEPD1, TMTC4, HSPA6, GNG5, SOX6, GPX3, TRAM1, GATM, RPS2, TSPAN6, PTPRZ1, TFAP2C, CPNE3, ABHD3, LOX, SLC1A3, COL11A1, GPC4, LIFR, SLC16A9, LITAF, HMOX1, CDO1, PRSS23, HSPA1B, GNG12, GPR137B, MSN, HOPX, CD164, CDCA7L, ZFP36L2, LRRRC3B, FBP5, CXCR4, PEA15, MFG8, PHLDA1, DMRTA2, FSTL1, TMEM123, MDK, CNN3, LMNB1, KIF11, CCNB1, CENPF, PON2, PDPN, PALLD, LEPROT, TSPO, SDC2, CARHSP1, TAGLN2, TGIF1, VIM, PYGL, NCAN, ZFP36L1
5	Striatum.Late.Infancy	4.57E-38	Striatum.Late.Infancy : RPS29, RPL7, FAU, RPS12, RPS20, RPL35A, RPL35, RPL37, RPS18, COX7C, RPL32, SERF2, RPS27A, MYL6, RPS5, RPL34, PHPT1, DBI, CD63, RPL28, RPL27A, RPL18, RPL31, S100A11, S100A6, RPL12, RPL23A, CLIC1, RPL9, RPS7, RPL24, RPS14, RPS28, RMLN3, RPL7, RPL27, LGALS1, RPL39, RPL11, FTL, RPS23, B2M, LGALS1, RPS15A, RPL30, MT3, RPL26, RPS27, RPS9, RPL36, RPS8
N.SAHA			
0	Cortex.Early.Mid.Feta	0.049	Cortex.Early.Mid.Fetal : TCF4, KLF6, SOX4, SOX11
1	Cortex.Late.Infancy	0.054	Cortex.Late.Infancy : RPL31, SCG3, SNRPG, RPL27, RPL41, GTF3A, C10RF61, RPL9, HSPB11, RPS27, ARC, RPL39, UBL5, UQCRCQ, COX7B, NDUFB6
2	Striatum.Late.Infancy	0.066	Striatum.Late.Infancy : FTL, MT1E
3	Amygdala.Late.Infancy	2.105e-13	Amygdala.Late.Infancy : RPS27L, RPL7, RPS20, RPL35, MT1X, S100B, DBI, SERF2, MT1E, RPL34, SAT1, MT3, PFDN5, RPL31, S100A11, S100A6, RHOC, RPL9, RPS28, RMLN3, RPL7, RPL27, LGALS1, MT2A, RPS27, LGALS3, RPL36
N.MS-275			
0	Cortex2.Early.Mid.Fetal	5.52E-08	Cortex.Early.Mid.Fetal : TCF4, ID2, SLA, MLLT3, RND3, FRMD4B, SOX4, FAMI126A, ARL4D, SOX11
1	Striatum1.Late.Infancy	6.54E-07	Striatum.Late.Infancy : FTL, S100A11, S100A6, IGFBP7, CLDN10, LGALS1, CD63, CST3, TIMP1, MT2A, DBI, SERF2, B2M
2	Cortex1.Early.Mid.Fetal	1.42E-08	Cortex.Late.Fetal : SLA, NELL2, MLLT11, CD24, CCNI, STMN1, PTPN2, MARCKSL1, TUBA1A, MEF2C, TRAF4, PAFAH1B3, CXADR, SRM, CRMP1, NEUROD6, CSRP2, GPM6A, RTN1, RPRM, RAC3, TUBB, RASL11B, PTP4A1, NEUROD2, BZW2, STMN4, STMN2, MAPK8
3	Striatum2.Late.Infancy	1.77E-54	Striatum.Late.Infancy : RPS15A, RPS29, NDUFA4, UQCRB, GSTK1, RPL7, FAU, RPS12, RPS20, RPL35A, RPS27L, RPL35, MT1X, IFITM3, UQCRCQ, COX7C, RPL32, SERF2, RPS27A, MYL6, MT1E, RPS5, RPL34, PHPT1, RPS27, DBI, RPS10, RPL37, RPL23, COX5B, TIMM8B, RPL27A, RPL38, SAT1, RPL18, GUK1, PFDN5, RPL31, S100A11, S100A6, RPL12, RPL23A, RHOC, CLIC1, RPL9, RPS7, RPL24, SNRPD2, RPS14, RPS28, IFI27L2, RPS24, RPLP1, HSPE1, RPS18, CPTM6, FTL, RPL27, RPL11, LGALS1, MT2A, ANAPC11, RPL30, MT3, RPL26, RPS21, MYL12A, RPS9, UBL5, RPL36, RPS8, COX7B
4	Amygdala.Late.Fetal	1.37E-16	Amygdala.Late.Fetal : SFRP1, TNC, CA12, SDCBP, CXCR4, DDIT4, RHOBTB3, LHX2, GPX3, SLC16A1, PSAT1, SOX9, CTBP2, SLC40A1, TRAM1, GATM, F2R, TSPAN6, MEIS2, PTPRZ1, CPNE3, MMP2, ABHD3, LOX, SLC1A3, GPC4, COL11A1, SRP9, LIFR, LITAF, HSPA6, PRSS23, GNG12, GPR137B, CNN3, CD164, CDCA7L, CCND2, ZFP36L1, ARL6IP6, ADD3, PEA15, MFG8, PHLDA1, PTTG1P, FSTL1, TMEM123, MDK, CMTM6, ITGB8, TMEM98, PON2, PALLD, LEPROT, SDC2, SOX2, TGIF1, VIM, NCAN, MOXD1